Fakultät für Mathematik und Naturwissenschaften | RWTH AACHEN UNIVERSITY

From Sunflower Coumarins to Citric Acid: Natural Compounds for Crop Protection

Von der Fakultät für Mathematik und Naturwissenschaften der RWTH Aachen University zur Erlangung des akademischen Grades eines Doktors der Naturwissenschaften genehmigte Dissertation

vorgelegt von

Jakob Friedrich Weber Böhlen

Master of Science (M. Sc.)

aus

Köln

Berichter: Universitätsprofessor Dr. rer. nat. Uwe Conrath

Universitätsprofessor Dr. rer. nat. Joost van Dongen

Tag der mündlichen Prüfung: 17.07.2026

Diese Dissertation ist auf den Internetseiten der Universitätsbibliothek verfügbar.

Abstract

Protecting crops from the increasing pathogen pressure is a major challenge in modern agriculture. Fungal pathogens are predominantly controlled using fungicides, which impose selective pressure and promote the emergence of fungicide insensitive pathogen isolates, thereby attenuating fungicide efficacy and increasing the risk of yield losses. Therefore, sustainable plant protection strategies that complement the narrow spectrum of available synthetic fungicide classes are urgently needed. This dissertation addresses this challenge using soybean rust disease as a model system with high economic relevance. *Phakopsora pachyrhizi*, the causal agent of the disease, is one of the most destructive pathogens of soybean. I characterized a *P. pachyrhizi* isolate that exhibited reduced sensitivity to all three fungicide classes commonly used in soybean cultivation. In contrast, the sunflower-derived coumarins scopoletin and ayapin remained effective against this isolate, highlighting the potential of natural compounds for disease control. Motivated by this finding, I investigated coumarin biosynthesis in sunflower, with a focus on ayapin formation. Screening 196 sunflower genotypes for their coumarin profiles revealed two contrasting lines: RHA857, which is impaired in ayapin accumulation, and SF_170, which accumulates high levels of both ayapin and scopoletin. Time-course analyses of coumarin secretion and feeding experiments with scopoletin indicated that ayapin is directly derived from scopoletin. Transcriptome analysis of $CuCl_2$-elicited leaf tissue from both genotypes identified twelve candidate genes potentially encoding an ayapin synthase. Functional testing of these genes in a heterologous system has so far not identified the enzyme responsible for ayapin formation. To complement the transcriptomic approach, RHA857 and SF_170 were crossed, generating an F_2 population that segregated for ayapin accumulation in a 1:3 ratio, suggesting the ayapin trait is controlled by a single dominant locus. Bulked segregant analysis of contrasting phenotypic pools from this population is in progress and, together with the transcriptomic data, will provide a framework for pinpointing the gene(s) catalyzing the final step of ayapin biosynthesis. To further dissect coumarin biosynthesis in sunflower, a mutant population of RHA857 was screened, leading to the identification of a mutant with enhanced scopoletin accumulation. In addition, transgenic soybean lines expressing a sunflower feruloyl-6′-hydroxylase and an ATP-binding cassette transporter were generated to explore the transfer of the sunflower coumarin pathway and its targeted phylloplane secretion mechanism into soybean. Finally, citric acid was identified as a potential self-inhibitory compound in *P. pachyrhizi* uredospores. Citric acid inhibited spore germination *in vitro* and reduced soybean rust severity *in planta*. Overall, this work demonstrates how biogenic compounds can be identified and exploited for sustainable crop protection.

Zusammenfassung

Eine der größten Herausforderungen der modernen Landwirtschaft ist es, Nutzpflanzen vor dem steigendem Pathogenbefall zu schützen. Pilzkrankheiten werden hauptsächlich durch den Einsatz von Fungiziden kontrolliert, was zu einem starken Selektionsdruck führt und die Entwicklung von fungizid-insensitiven Isolaten der Pathogene vorantreibt. Strategien für nachhaltigen Pflanzenschutz, die das enge Wirkspektrum synthetischer Fungizid-Klassen komplementieren können, sind daher dringend erforderlich. Diese Dissertation beschäftigt sich mit dieser Herausforderung anhand der Pflanzenkrankheit Sojabohnenrost als Modellsystem. *Phakopsora pachyrhizi*, der Erreger des Sojabohnenrosts, zählt zu den wirtschaftlich bedeutendsten Pilzkrankheitserregern im Sojaanbau. Ich habe in dieser Arbeit ein *P. pachyrhizi*-Isolat charakterisiert, das seine reduzierte Sensitivität gegenüber drei Fungizid-Klassen gezeigt hat. Im Gegensatz zu den Fungiziden zeigten die Cumarine der Sonnenblume, Scopoletin und Ayapin, eine Schutzwirkung gegen dieses Isolat, was die Bedeutung von natürlichen Verbindungen für den Pflanzenschutz hervorhebt. Durch diese Ergebnisse motiviert, habe ich, fokussiert auf Ayapin, die Cumarin-Biosynthese in der Sonnenblume genauer untersucht. Beim einem *Screening* der Cumarin-Profile von 196 Sonnenblumen-Genotypen wurden zwei deutlich unterschiedliche Linien identifiziert: RHA857, die in der Ayapin-Akkumulation beeinträchtigt ist, und SF_170, die hohe Mengen sowohl an Ayapin als auch an Scopoletin akkumuliert. Zeitreihenanalysen der Cumarin-Sekretion und Fütterungsexperimente mit Scopoletin deuteten darauf hin, dass Ayapin direkt aus Scopoletin gebildet wird. Eine Transkriptom-Analyse von durch $CuCl_2$ elizitiertem Blattmaterial beider Genotypen identifizierte zwölf Kandidatengene, die potentiell für eine Ayapin-Synthase kodieren könnten. Durch einen Funktionalitätstest dieser Gene in einem heterologen System konnte bislang jedoch kein Enzym identifiziert werden, das für die Bildung von Ayapin verantwortlich ist. Ergänzend zu der Transkriptom-Analyse wurden RHA857 und SF_170 gekreuzt, wodurch eine F_2-Population erzeugt wurde, die im Verhältnis 1:3 (kein Ayapin : Ayapin) segregierte, was darauf hindeutet, dass das Ayapin-Merkmal von einem einzelnen dominanten genetischem Locus kontrolliert wird. Um die Cumarin-Biosynthese in der Sonnenblume noch weiter zu untersuchen, wurde eine Sonnenblumen-Mutante mit erhöhter Scopoletin-Akkumulation identifiziert und analysiert. Außerdem wurden transgene Sojabohnenlinien erzeugt, die Gene überexprimieren, die eine Feruloyl-6′-Hydroxylase und einen Transporter mit ATP-bindender Kassette der Sonnenblume kodieren, um die Übertragung dieses Stoffwechselwegs in Sojabohne zu untersuchen. Außerdem wurde Zitronensäure als potenziell selbstinhibierende Verbindung in *P. pachyrhizi*-Uredosporen identifiziert. Zitronensäure hemmte die Sporenkeimung *in vitro* und verringerte die Sojarost-Symptomatik *in planta*. Diese Arbeit zeigt, wie biogene Verbindungen identifiziert und für einen nachhaltigen Pflanzenschutz erschlossen werden können.

Declaration on oath

I, Jakob Weber Böhlen, declare on oath that this thesis and its contents are my own and have been generated independently as a result of my own original research.

I hereby declare on oath:

1. This thesis has been produced in its entirety as a doctor of this university;
2. If any part of this thesis has previously been used for an academic degree or other qualification at this or any other institution, this has been clearly indicated;
3. If other own or public publications have been used, this has been clearly indicated;
4. If other own or public publications have been used, the source of this has been clearly indicated. This dissertation is entirely my own work, with the exception of such citations;
5. All relevant sources of support have been acknowledged;
6. If any part of this dissertation is based on the collaboration of others, I have clearly indicated what has been worked on by others and what has been worked on by myself;

_____ _____

Place, Date Name

Funding, publications, and contributions

Part of the research for this thesis was funded by German Research Foundation (DFG, grant numbers 415999524 and 528343185) and BASF Plant Science Company GmbH. Parts of this thesis have been published at conferences and in bachelor and master theses of students that I have supervised. Any publication that is not part of this thesis but was prepared while working on this thesis and to which I contributed as an author is listed below.

Publication:

- Weber Böhlen J., Beesley A., Beyer S. F., Schwinges P., Maas A. E., Schultheiss H., Conrath U. and Langenbach C. J. G. (2026), AtMYB72 as a Biotechnological Tool to Overcome Phenylpropanoid Substrate Limitation and Enhance Coumarin Biosynthesis in Plants, *Plant Biotechnology Journal* 24, no. 5: 3009–3011, https://doi.org/10.1111/pbi.70503

Contributions to conferences as oral or poster presentations:

- Weber Böhlen J., Schwinges P., Beesley A., Spencer D., Wanders V., Biermann R., Beyer S.F., Schultheiss H., Langenbach C.J.G., Conrath U., Tailored *in planta* biosynthesis of antifungal coumarins, DPG-Arbeitskreis Host-Parasite-Interactions, Online-Meeting, March 2021 (oral presentation).
- Weber Böhlen J., Schwinges P., Beesley A., Spencer D., Wanders V., Biermann R., Beyer S.F., Schultheiss H., Langenbach C.J.G., Conrath U., *In planta* biosynthesis of antifungal coumarins for crop protection, 3rd Plant BioProTech Symposium, Reims, France, June 2022 (poster presentation - *awarded as best poster of the Plant BioProTech Awards*).
- Weber Böhlen J., Schwinges P., Beesley A., Spencer D., Wanders V., Biermann R., Beyer S.F., Schultheiss H., Langenbach C.J.G., Conrath U., Tailoring coumarin biosynthesis for crop protection, 36th Conference Molecular Biology of Plants, Hennef, Germany, February 2023 (poster presentation).
- Weber Böhlen J., Beesley A., Schwinges P., Spencer D., Beyer S.F., Schultheiss H., Langenbach C.J.G., Conrath U., Engineering isoscopoletin biosynthesis for crop protection, 20th International Reinhardsbrunn Symposium - Modern Fungicides and Antifungal Compounds, Friedrichroda, Germany, April 2023 (oral presentation).

- Weber Böhlen J., Maas A.E., Kleineberg A., Beesley A., Schwinges P., Langenbach C.J.G., Conrath U., Unraveling the biosynthesis of ayapin - an antifungal coumarin of sunflowers, 39th Conference Molecular Biology of Plants, Hennef, Germany, March 2026 (oral presentation).
- Weber Böhlen J., Maas A.E., Kleineberg A., Beesley A., Schwinges P., Langenbach C.J.G., Conrath U., Low-molecular natural compounds counteract multi-class fungicide insensitivity in *Phakopsora pachyrhizi,* 21th International Reinhardsbrunn Symposium - Modern Fungicides and Antifungal Compounds, Friedrichroda, Germany, April 2026 (oral presentation).

Supervised student's theses:

- Elpida Sfantou, *ABC transporter-mediated coumarin secretion in plants*, bachelor thesis, RWTH Aachen University, 2022
- Lisa Sumaila, *Tailored Isoscopoletin Biosynthesis for Crop Protection*, bachelor thesis, Fachhochschule Aachen, Campus Jülich, 2023
- Marieke Moog, *Gelenkte Isoscopoletin-Biosynthese zur Bekämpfung des Asiatischen Sojabohnenrosts*, bachelor thesis, RWTH Aachen University, 2023
- Jannik Hermanns, *Entwicklung und Anwendung von Verfahren zur Steigerung der Krankheitsresistenz von Sonnenblumen*, master thesis, RWTH Aachen University, 2024
- Julia Burkat, *Antimicrobial Proteins from the Sunflower Leaf Surface for Plant Protection*, bachelor thesis, RWTH Aachen University, 2024
- Alina Kruse, *Charakterisierung von Sonnenblumen-Mutanten hinsichtlich ihrer Cumarin-Biosynthese*, bachelor thesis, RWTH Aachen University, 2024
- Alina Maas, *The use of coumarins for plant protection*, master thesis, RWTH Aachen University, 2024
- Anna Kleineberg, *Unraveling the sunflower phylloplane for enhanced crop protection*, master thesis, RWTH Aachen University, 2025

Table of contents

Abstract ..... **III**

Zusammenfassung ..... **IV**

Declaration on oath ..... **V**

Funding, publications, and contributions ..... **VI**

Table of contents ..... **VIII**

List of abbreviations ..... **XI**

List of figures ..... **XIV**

List of tables ..... **XVII**

1. Introduction **1**

1.1. Development of fungicide resistance **2**

1.1.1. Quinone-outside inhibitors 2

1.1.2. Demethylation inhibitors 2

1.1.3. Succinate dehydrogenase inhibitors 3

1.2. A case study of disease management: Soybean versus *P. pachyrhizi* **4**

1.2.1. Soybean pathogens 4

1.2.2. The lifecycle of *P. pachyrhizi* 5

1.2.3. Fungicide resistance in *P. pachyrhizi* isolates 6

1.2.4. Alternative strategies to fight SBR 8

1.3. The sunflower coumarins – scopoletin and ayapin **12**

1.3.1. Simple Coumarins 12

1.3.2. The biosynthesis of coumarins 13

1.3.3. Ayapin 16

1.3.4. The secretion of coumarins 19

1.4. Aim of the study **20**

2. Results **21**

2.1. Fungicide-insensitive isolate of *P. pachyrhizi* is inhibited by sunflower coumarins **21**

2.2. Evaluating ayapin biosynthesis in different sunflower genotypes **27**

2.3. Unravelling the genetic basis of ayapin biosynthesis **32**

2.4. Screening and identifying sunflower mutants that hyperaccumulate scopoletin 44

2.5. Engineering coumarin biosynthesis in soybean plants 48

2.6. Turning the tables – identification of a *P. pachyrhizi* self-inhibitor 51

3. Discussion 59

4. Conclusion 77

5. Material and Methods 78

5.1. Chemicals 78

5.2. Organisms 78

5.2.1. Cultivation and propagation of *H. annuus* in the greenhouse 79

5.2.2. Cultivation of *H. annuus* under field conditions 79

5.2.3. Cultivation of *G. max* 79

5.2.4. Cultivation of *N. benthamiana* 80

5.2.5. Maintenance of *P. pachyrhizi* isolates 80

5.2.6. Cultivation of *E. coli* 80

5.2.7. Cultivation of *A. tumefaciens* 80

5.3. Experimental Procedures 81

5.3.1. Testing sensitivity of *P. pachyrhizi* isolates against synthetic fungicides 81

5.3.2. *In vitro* germination of *P. pachyrhizi* uredospores 81

5.3.3. *In planta* protection of soybean with natural compounds against *P. pachyrhizi* 83

5.3.4. Inducing coumarin biosynthesis in sunflower 83

5.4. Sunflower Field Trials 85

5.4.1. Screening of sunflower core collection (2023) 85

5.4.2. Screening of RHA857-mutant population (2023) 86

5.4.3. Screening of sunflower crosses (2025) 86

5.5. Genetic Modifications 87

5.5.1. Vector maps and cloned constructs 87

5.5.2. Generating transgenic *E. coli* 88

5.5.3. Generating transgenic *A. tumefaciens* 88

5.5.4. Transient transformation of *N. benthamiana* 89

5.5.5. Generating transgenic soybean lines 89

5.5.6. Crossing of sunflower genotypes 90

5.6. Biomolecular Methods 90

5.6.1. RNA isolation of plant material 90
5.6.2. DNA isolation of plant and fungal material 92
5.6.3. Plasmid isolation of *E.coli* 92
5.6.4. cDNA synthesis 92
5.6.5. Polymerase Chain Reaction (PCR) protocols 93
5.6.6. Agarose Gel Electrophoresis and Clean-up of PCR-Products 94
5.6.7. Sanger Sequencing 95
5.6.8. Transcriptome analysis of sunflower samples 95
5.6.9. Bulked segregant analysis (BSA) of sunflower samples 96

5.7. Biochemical Methods 97

5.7.1. Extraction of coumarins from plant material 97
5.7.2. Generating *P. pachyrhizi* wash water for germination assays 97
5.7.3. Generating *P. pachyrhizi* wash water for analytical processes 97
5.7.4. Separation of *P. pachyrhizi* wash water with a 3 mL C18 column 97
5.7.5. High pressure liquid chromatography (HPLC) analysis 98
5.7.6. Nuclear Magnetic Resonance (NMR) analysis 100

5.8. Software and Databases 100

6. Bibliography 101

7. Acknowledgments 121

8. Supplement 122

8.1. Supplemental Figures 122

8.2. Supplemental Tables 141

List of abbreviations

abbreviation	meaning
2-h-cin-CoA	2-hydroxycinnamoyl-CoA
2-h-cou-CoA	2-hydroxycoumaroyl-CoA
2OGD	2-oxoglutarate-dependent dioxygenase family
4CL	4-coumarate:CoA ligase
6-h-caf-CoA	6-hydroxycaffeoyl-CoA
6-h-fer-CoA	6-hydroxyferoloyl-CoA
AA	amino acid
ABC	ATP-binding cassette
ACN	acetonitrile
ACT	actin
ASM	acibenzolar-S-methyl
ATP	adeonsine triphosphate
AySy	ayapin synthase
BC_1	first backcross generation
BC_2	second backcross generation
BGLU	ß-glycosidases
BSA	bulked segregant analysis
C2'H	*p*-coumaroyl-CoA 2'-hydroxylases
C4H	cinnamic acid 4-hydroxylase
CA	citric acid
CCoAOMT	caffeoyl-CoA O-methyltransferases
CDS	coding sequences
COSY	coumarin synthase
CTAB	cetyltrimethylammonium bromide
ctrl	control
CYP	cytochrome P450-dependent monooxygenase
CYTB	cytochrome B
ddH_2O	double distilled water
D_2O	deuterium oxide
DEA	differential expression analysis
DMI	demethylation inhibitor
DMSO	dimethyl sulfoxide
dsRNA	double-stranded RNA
eGFP	enhanced green fluorescent protein
ELSD	evaporative light scattering detector
ES	epidermis specific
F_1	first filial generation (direct progeny of a cross)

abbreviation	meaning
F_2	second filial generation (selfed progeny of F_1)
F6’H1	feruloyl-CoA 6’-hydroxylases
FA	formic acid
FW	fresh weight
H_2DCFDA	2',7'dichlordihydrofluorescein-diacetate
ha	hectare
HaPR1-like	pathogen-related1-like protein
HIGS	host-induces gene silencing
HPLC	high performance liquid chromatography
IR	induced resistance
ISR	induced systemic resistance
$l_2$fc	$\log_2$ fold change
LB	lysogeny broth
M_1	first generation after mutagenesis
M_2	second generation after mutagenesis
MDCA	3,4-(Methylenedioxy)-cinnamic acid
MDP	methylenedioxyphenyl
MES	2-(N-morpholino)ethanesulfonic acid
ML	maternal line
MoA	mode of action
NMR	nuclear magnetic resonance
OE	overexpression
OMT	O-methyltransferase
p_{adj}	adjusted *p*-value
PAL	phenylalanine ammonia lyase
PCA	principal component analysis
PPP	phenylpropanoid pathway
PSM	plant secondary metabolite
qRT-PCR	quantitative real-time polymerase chain reaction
QoI	quinone-outside inhibitor
RFP	red fluorescent protein
RFU	relative fluorescence units
RNAi	RNA interference
ROS	reactive oxygen species
Rpp	resistance to *Phakopsora pachyrhizi*
RS	reduced sensitivity
RT	room temperature
S8H	scopoletin8’-hydroxylase
SAR	system acquired resistance

abbreviation	meaning
SBR	soybean rust
SCN	soybean cyst nematode
SDHI	succinate dehydrogenase inhibitor
SIGS	spray-induces gene silencing
siRNA	small interfering RNA
SL	stock solution
SNP	single-nucleotide polymorphism
T_0	primary transformants regenerated directly from transformed tissue
T_1	first transgenic generation
T_2	second transgenic generation
TCA	tricarboxylic acid
TMV	tobacco mosaic virus
UGT	UDP-glycosyltransferases
VCA	variant calling analysis
WT	wild-type
YEB	yeast extract beef

List of figures

Figure 1. Schematic overview of coumarin biosynthesis in plants. 15

Figure 2. CYPs catalyze methylenedioxy bridge formation in several biosynthetic pathways in plants.....18

Figure 3. *P. pachyrhizi* isolate RS2 is less sensitive to three major fungicide classes.....23

Figure 4. Scopoletin and ayapin inhibit fungal spore germination and protect soybean from the fungicide tolerant *P. pachyrhizi* isolate RS2 in a dose dependent manner.....26

Figure 5. Genotypic variation in coumarin secretion and accumulation in sunflower in response to $CuCl_2$-elicitation. 28

Figure 6. Sunflower genotypes RHA857 and SF_170 differ in their coumarin accumulation and secretion upon $CuCl_2$-elicitation over time.....30

Figure 7. $CuCl_2$-induced ayapin biosynthesis and secretion from sunflower leaf discs is augmented by scopoletin feeding.....32

Figure 8. Local induction of coumarin biosynthesis and secretion from sunflower leaves by $CuCl_2$-droplet application. 34

Figure 9. Variation of gene expression in two sunflower genotypes upon $CuCl_2$-induced stress...35

Figure 10. Transcriptome analysis reveals differential elicitor-induced expression of *CYP* genes in sunflower genotypes with contrasting ayapin biosynthesis capacities 37

Figure 11. Overexpression of *HaAySy* candidates in *N. benthamiana* leaves does not lead to ayapin accumulation.....41

Figure 12. Crossing of sunflower genotype RHA857 and SF_170 leads to segregants with differential $CuCl_2$-induced ayapin accumulation capacity. 43

Figure 13. Distribution of sunflower mutants altered in scopoletin biosynthesis. 45

Figure 14. Mutant 4/626 of RHA857 has increased scopoletin accumulation compared to the maternal line. 47

Figure 15. Transgenic soybean plants co-expressing different coumarin biosynthesis genes constitutively accumulate scopoletin.....49

Figure 16. *P. pachyrhizi* uredospore germination is sensitive to crowding *in vitro.*.....52

Figure 17. *P. pachyrhizi* germination self-inhibition is associated with a non-proteinaceous water-soluble molecule or combination of molecules. 53

Figure 18. Preparative HPLC fractionation of *P. pachyrhizi* uredospore wash water. 55

Figure 19. Fractions F7 and F10 completely inhibit *P. pachyrhizi* spore germination. 56

Figure 20. Chemical structure of F7 and F10. .....- 57 -

Figure 21. Citric acid reduces soybean rust severity when applied to the foliage. 58

Figure 22. Separation scopolin, scopoletin and ayapin by HPLC. 98

Figure S 1. Coumarin accumulation in droplets on sunflower leaves after $CuCl_2$-elicitation.....122

Figure S 2. Expression of *HaF6'H1* in leaf material of RHA857 induced by $CuCl_2$-droplets 123

Figure S 3. Simultaneous treatment of sunflower genotype SF_170 with scopoletin and $CuCl_2$. 123

Figure S 4. Relative expression of *HaAySy* candidate genes in $CuCl_2$-elicted sunflower leaf discs of RHA857 and SF_170. 124

Figure S 5. Work flow for the identification of candidate genes. 126

Figure S 6. Relative fluorescence of field samples of BC_1F_1-individuals of RHA857-MLxM-4/626. 127

Figure S 7. Relative expression of *AtCOSY* in transgenic soybean lines. 127

Figure S 8. Soybean plants transformed with an DNA construct harboring HaF6'H1 accumulate scopoletin. 128

Figure S 9. HSQC spectra of the active HPLC fraction F7. 129

Figure S 10. HMBC spectra of the active HPLC fraction F7. 130

Figure S 11. pH range of *P. pachyrhizi* wash water. 131

Figure S 12. Identification of *P. pachyrhizi* ABC transporters homologous to PstABCG2. 131

Figure S 13. Sequence alignment of *SDHc* from DNA of RS2 isolate compared to reference. ...132

Figure S 14. Sequence alignment of *CYTb* from DNA of RS2 isolate compared to reference. 132

Figure S 15. Sequence alignment of *CYP51* from DNA of RS2 isolate compared to reference...133

Figure S 16. Antioxidative capacity of scopoletin, ayapin and scoparone. 134

Figure S 17. ROS staining of treated *P. pachyrhizi* uredospores. 134

Figure S 18. Protein sequence alignment of CYP719A37 from *Piper nigrum* and CYP81Q from *Sesamum indicum.* 135

Figure S 19. The coding sequence of HaF6′H1 is identical in sunflower genotypes RHA857-ML and M-4/626. 136

Figure S 20. Relative gene expression of *HaF6H1* and *HaPR1-like* in sunflower genotypes RHA857 and SF170. 137

Figure S 21. Relative expression of HaPR1-like in $CuCl_2$-elictated RHA857-ML and M-4/626.138

Figure S 22. Simultaneous treatment of sunflower genotype SF_170 with scopoletin and $CuCl_2$. 138

Figure S 23. A blueprint reveals photoprotective effect of coumarins.....138

Figure S 24. Vector map of a modified pB2GW7 vector used for overexpression constructs. 139

Figure S 25. Vector map of the pB1PES2POE vector used to generate soybean transformation constructs. 139

Figure S 26. Soybean transformation process 140

List of tables

Table 1. Fungicides used for *P. pachyrhizi* sensitivity assays. 22

Table 2. Putative ayapin synthases (AySy) identified by transcriptome analysis of sunflower genotypes RHA857 and SF_170.....39

Table 3. ^{1}H and ^{13}C NMR data of F7 and F10. .....- 57 -

Table 4. List of plants that were examined in this study. 78

Table 5. List of plant pathogens used in this study. 79

Table 6. Plant expression constructs used in this work. 87

Table 7. List of genetically modified plant lines generated in this study. 90

Table 8. Thermal cycling conditions for standard PCR. 93

Table 9. Thermal cycling conditions for proofreading PCR. 94

Table 10. Thermal cycling conditions for qRT-PCR analysis. 94

Table 11. Sample overview and grouping for RNA sequencing and bioinformatic analysis. 96

Table 12. Solvent gradient for separation of coumarins in *H. annuus* samples. 99

Table 13. Solvent gradient for separation of coumarins in *G. max* samples. 99

Table 14. Solvent gradient for separation of coumarins in *N. benthamiana* samples. 99

Table 15. List of software, databases and internet sources used in this study. 100

Table S 1. Coumarin profile of $CuCl_2$-elucidated sunflower genotypes. 141

Table S 2. Dry-weight of fractions of *P. pachyrhizi* spore wash water..... 143

Table S 3. Number of sequenced fragments and bases (RNA). 143

Table S 4. Statistics of mapped fragments (RNA). 144

Table S 5. Statistics of significantly differentially expressed genes in comparison group A vs B. 144

Table S 6. Sequencing primers used in this work. 144

Table S 7. qRT-PCR primers used in this work. 145

Table S 8. Primers used for Gibson Cloning. 146

Table S 9. Differential expression of *CYP* genes in RHA857 (group 2 vs group 1). 148

Table S 10. Differential expression of *CYP* genes in SF_170 (group 4 vs group 3). 149

Table S 11. Differential expression of *CYP* genes between stressed SF_170 and stressed RHA857 (group 4 vs group 2). 150

1. Introduction

From first domesticating wheat during the Neolithic Revolution, which started the Holocene ~11,700 years ago, over the "Green Revolution" in the mid-20th century, humankind has developed increasingly efficient agricultural systems that now feed a growing world's population. However, the need for efficiency and improvement of yield has led to the point where monoculture and excessive use of pesticides have raised concerns that the damage imposed on the environment exceeds the benefits (Kreick et al., 2025). We have learned that pesticides, even though helpful and much needed for plant protection, can also have negative impacts on water quality, biodiversity, and human health (Aktar et al., 2009; Schmidt-Jeffris et al., 2021; Tang et al., 2021). Consequently, these concerns have prompted political action over the past decades, such as the "European Green Deal" and the "Farm to Fork" strategy of the EU that proposes a reduction of agrochemicals used by the year 2030 by 50 %, or the "Sustainable Food Systems Strategy MIDORI" that is pursued by Japan (Flors et al., 2024). This alone already shows the urgency that we need to find alternative, more sustainable crop protection strategies to complement our integrated plant protection measures.

However, next to the environmental concerns, the excessive use of fungicides leads to another challenge that might be even greater to overcome, and that extends beyond the field of crop protection: Pathogens can rapidly adapt to the defense mechanisms imposed on them, as the selective pressure exerted in both medical and agricultural systems is immense (Fisher et al., 2018; van Rhijn and Rhodes, 2025). In clinical settings, this phenomenon is more commonly known from the emergence of multidrug-resistant bacteria, such as the methicillin-resistant *Staphylococcus aureus* (MRSA). Similarly, many fungicide-resistant strains of fungal clinical pathogens have been reported since prophylactic use of respective fungicides increases the selective pressure, thus driving the evolution of resistant isolates (Fisher et al., 2018; Lockhart et al., 2023). For plant pathogens, the mechanism is quite similar. Since the 1960s, a "new generation" of fungicides has been developed with two primary objectives: first, to act systemically within plants, meaning that the fungicides can be taken up by the plant and be distributed in the plant tissue; and second, to target very specific proteins within pathogens. This dual action renders these fungicides highly effective against pathogens while maintaining low phytotoxicity towards host plants (Hahn, 2014). However, the focus on specific target genes within pathogens, combined with agricultural practices such as monocultures of genetically homogeneous plant species, has led to an accelerated evolution of fungicide-resistant isolates (Fisher et al., 2018).

1.1. Development of fungicide resistance

1.1.1. Quinone-outside inhibitors

The big challenge in managing fungicide resistance lies in many different mechanisms of resistance development. The most frequent resistant mechanism of a pathogen is the occurrence of point mutations in the target gene of the respective fungicide (Dorigan et al., 2023; Hahn, 2014; van Rhijn and Rhodes, 2025). This, for example, is the case with quinone-outside inhibitor (QoI) fungicides. A class of fungicides that, by targeting the *CYTOCHROME B* (*CYTB*) gene, disrupts the mitochondrial electron transfer chain of a fungus (Hawkins and Fraaije, 2021; Yin et al., 2023). In QoI-sensitive isolates, this leads to the detrimental blocking of adenosine triphosphate (ATP) synthesis. Yet, a single point mutation, most commonly leading to a substitution of the amino acid glycine for alanine at codon 143 (G143A), modifies the conformation of the interaction site of *CYTB* with QoI fungicides. This results in reduced sensitivity of the mutated isolate (Bartlett et al., 2002; Dorigan et al., 2023). This so-called target-site mutation was first observed in *Erysiphe graminis* f. sp. *tritici* (powdery mildew) in 1998 in the north of Germany (Bartlett et al., 2002). Remarkably, this was only two years after the first QoI fungicide was introduced to the market in 1996 (Ma and Michailides, 2005). By now, resistance to QoIs has been reported in over 43 plant pathogens, with 80% resulting from the G143A amino acid substitution. Another prominent mutation leads to the substitution of phenylalanine for lysine at position 129 (F129L) (Dorigan et al., 2023; van Rhijn and Rhodes, 2025). Since QoI fungicides bind to only one specific pocket in CYTB, modifications to this pocket usually lead to qualitative resistance that confers high levels of resistance (Dorigan et al., 2023).

1.1.2. Demethylation inhibitors

For demethylation inhibitors (DMIs), on the other hand, an occurring resistance is rather quantitative than qualitative. DMIs interact with the fungal 14 α-demethylase (CYP51). CYP51 is involved in ergosterol biosynthesis of the fungus by demethylation of lanosterol (Hawkins and Fraaije, 2021; Yin et al., 2023). By interfering with ergosterol biosynthesis, DMIs destabilize the fungal cell membrane, inevitably leading to cell death of isolates sensitive to DMIs. In many fungal species, two *CYP51* orthologs are present; thus, point mutations only lead to a gradual development of resistance (Dorigan et al., 2023). So far, the most commonly identified target site mutation is the change of tryptophane to phenylalanine at position 137 (Y137F) of the amino acid chain (Hawkins and Fraaije, 2021). However, in total, there are 58 mutations in *CYP51* identified that lead to mutations in over 19 fungal species (Dorigan et al., 2023). Yet, not only target-site mutations confer resistance of pathogens against DMIs, but also mutations in the promoter region of *CYP51* have

been reported. These promoter alterations lead to overexpression of the target gene in resistant pathogen isolates, thus compensating for the inhibition by DMIs with increasing numbers of active enzymes. For example, overexpression of *CYP51* in *Blumeriella jaapii* (causal agent of cherry leaf spot), *Venturia inaequalis* (apple scab), or *Colletotrichum gloeosporioides* (chili anthracnose) led to DMI resistance in respective pathogens (Ma et al., 2006; Villani et al., 2016; Wei et al., 2020). These examples show that such resistance mechanisms are broadly spread in many plant pathogens. Yet, for DMI resistance, there are also off-target site or non-target site mechanisms that have been reported and connected to resistance against this fungicide class (Hu and Chen, 2021). The most prominent example for off-target site resistance mechanisms, is the increased expression of efflux transporters such as the ATP-binding cassette transporter (ABC transporter) that often confer multidrug resistance (Waard et al., 2006). These ABC transporters have a rather low substrate specificity, thus they enable the fungus to detoxify several fungicide classes (Hu and Chen, 2021; Waard et al., 2006). The example of DMI resistances that have evolved in plant pathogens displays how diverse and innovative organisms can adapt (Ma and Michailides, 2005).

1.1.3. Succinate dehydrogenase inhibitors

Since this adaptation is not only diverse but evolving quickly, the rate at which resistances emerge is most likely much faster than the rate at which new fungicide products or new classes of fungicides are introduced for plant protection purposes (Fisher et al., 2018). The currently fastest-growing class of fungicides is the class of succinate dehydrogenase inhibitors (SDHIs; Sierotzki and Scalliet, 2013). And even for the newest subclass of these fungicides, the so-called third-generation SDHIs, there are many reports of pathogens that have already gained resistance towards those fungicides (Beckerman et al., 2023; Yin et al., 2023).

SDHIs are carboxamides that act in the mitochondrial membrane of the target organisms. They – as the name implies – inhibit the activity of the succinate dehydrogenase by binding to its ubiquinone binding site, thus, blocking the two-step reduction of ubiquinone. By that, complex II of the electron transfer chain is brought to a halt, which disrupts ATP-biosynthesis of the fungus, similar to QoIs that inhibit complex III (Scalliet et al., 2012; van Rhijn and Rhodes, 2025). The SDH enzyme consists of four subunits (SDHa-SDHd) of which the SDHb, SDHc, and SDHd subunits form the ubiquinone binding site that is targeted by SDHI fungicides (Scalliet et al., 2012). Thus, target-site mutations that confer resistance towards fungicides can occur in all three of those subunits. Accordingly, resistance towards SDHIs is associated with a relatively high number of at least 83 mutations in *SDHb*, *SDHc,* and *SDHd* genes. SDHIs are structurally more diverse than QoIs or DMIs, resulting in various binding modes of SDHI molecules with the target site. Thus, for many pathogens, contrasting cross-resistance has been reported. The cross-resistance is highly dependent

on the occurring mutation and the respective member of the SDHI class. However, several mutations have been identified that lead to resistance towards all members of the SDHI class (Sierotzki and Scalliet, 2013).

Still, since the risk of resistance towards SDHIs is lower than, e.g., for QoI or DMI fungicides, this class is increasingly important for modern crop protection. However, that we still need to diversify the toolbox for fungal control in agriculture is without question (Fisher et al., 2018). A prominent and demonstrative example where excessive use of fungicides is bearing a major problem, highlighting the need for additional and alternative solutions, is the management of the interaction between soybean (*Glycine max*) and *Phakopsora pachyrhizi*, the causal agent of soybean rust (SBR).

1.2. A case study of disease management: Soybean versus *P. pachyrhizi*

Soybean *(Glycine max* (L.) Merrill) is one of the most valuable crops cultivated worldwide. It is valued not only as animal feed, but also as high-oil and high-protein seed for human diets (Liu, 2008). The worldwide soybean production rose from ~27 million tons (t) in 1961 to over 371 million t in 2023 (FAO, 2025), making it the most intensively crop of the Leguminosae family. Over 70 % of soybeans produced in 2023 came from Brazil (152 million t) and the U.S. (113 million t; FAO 2025). This immense production of soybean is visible in the arable land usage of Brazil: With ~ 45 million hectares (ha), the area used for soybean cultivation was more than twice the area that was used for the second most cultivated crop in Brazil (maize;~20 million ha; Statista, 2024). Soybean yields have risen from 1990 to 2023 from 1.75 t/ha to ~ 3.4 t/ha. In the same time frame, however, the use of pesticides (including fungicides) has risen from <1 kg/ha to >12 kg/ha (FAO, 2025). While these data show the importance of the Brazilian market, they also illustrate a great challenge that Brazil is facing in soybean cultivation. One of the biggest threats to soybean cultivation is a broad range of pathogens that are interacting with soybean plants, which led to an above average estimated crop losses of > 30 % in soybean cultivation for the years 2010-2014 (Savary et al., 2019).

1.2.1. Soybean pathogens

It is estimated that 5.24 % of soybean losses in South Brazil and Argentina can be traced back to plant parasitic cyst nematodes (Savary et al., 2019). The soybean cyst nematode (SCN), *Heterodera glycines* Ichinohe, is widely spread and possesses an effective long-term survival in the absence of its host plant. The problem with SCN is that it often goes undetected until severe densities are reached in the soil, which then leads to yield losses. Those high densities are subsequently difficult to reduce again (Tylka and Marett, 2021).

A pathogen that has come into focus more recently is the ascomycete *Corynespora cassiicola*. The fungus causes target spot that can lead to prematurely leave losses of severely infected soybean. For long, this disease was not considered relevant in soybean cultivation. However, in recent years, yield losses caused by *C. cassiicola* have become more relevant. Due to the over-utilization of high-yielding but susceptible cultivars, the disease can now be found in most soybean growing regions (Edwards Molina et al., 2022; Fortunato et al., 2017; Xavier et al., 2013).

Even though diseases such as target spot gain more relevance, the most severe disease threatening soybean cultivation in Brazil, especially in the south, is caused by *Phakopsora pachyrhizi* Syd. & P. Syd. (Chicowski et al., 2024; Godoy et al., 2016; Savary et al., 2019). The obligate biotrophic basidiomycete causes SBR and was first reported in Brazil in 2001 (Yorinori et al., 2005). Since then, SBR alone is estimated to be responsible for up to 6.65 % loss of soybean yield in South Brazil and Argentina which is classified as high magnitude losses (Savary et al., 2019). In a single field, yield losses can increase up to 90 %, when the field remains untreated, because in a few days the pathogen can cause complete defoliation (Godoy et al., 2015; Goellner et al., 2010). To understand the severity of this disease and how yield losses can occur this fast in that devastating manner, it is helpful to have a closer look at the lifecycle of *P. pachyrhizi*.

1.2.2. The lifecycle of *P. pachyrhizi*

Dispersed by wind, asexual, dikaryotic uredospores of *P. pachyrhizi* land on the leaf surface of soybean and can germinate within several hours under favorable conditions (Goellner et al., 2010). In contrast to uredospore-derived invasion by most rust fungi, the elongating germ tube of *P. pachyrhizi* does not rely on finding a stomata to enter the leaf surface but at the tip of the germ tube an appressorium can form that is able to penetrate the epidermis by building up immense pressure of ~ 50 bar to penetrate the epidermis cell (Goellner et al., 2010; Loehrer et al., 2014). Upon penetration, the cell will collapse, and the fungal penetration hypha is able to grow through the collapsed cell into the intracellular space of the mesophyll cells. Here, a septum forms, separating the emerging primary hypha from the separation hypha. The primary hypha branches into several secondary hyphae. With those, the pathogen is able to invade the mesophyll cells of the host plant to build feeding organs, the so-called haustoria. This biotrophic phase of the fungus starts within the first 24 to 48 hours after the uredospore has landed on the leaf surface (Goellner et al., 2010). Within five to eight days post invasion, uredia are formed at the abaxial site of the leaf, where new uredospores develop on short stalks, which then can be released through small pustules called ostioles (Goellner et al., 2010). To prevent spores from germinating prematurely in the uredia, the spores most likely secrete an endogenous self-inhibiting substance, as it is described for several other rust fungi such as *Puccinia graminis* (causal agent of black rust), *Uromyces phaseoli*

(bean rust), *Puccinia helianthi* (sunflower rust) and *Puccinia coronata* (crown rust) (Allen, 1955; Macko et al., 1970; Macko et al., 1971; Macko et al., 1972; Tsurushima et al., 1984). However, to the best of my knowledge, for *P. pachyrhizi* no such self-inhibitor or a crowding effect has been described so far. Investigating and identifying such a self-inhibitor was, thus, part of this work and will be discussed in later parts of this thesis.

Once the spores are dispersed by wind and land on the host's leaf surface, the cycle starts again. This, the rather fast asexual life cycle, and the ability to directly penetrate the host epidermal cell make *P. pachyrhizi* a relatively aggressive plant pathogen that can lead to severe yield losses through defoliation of the crops (Godoy, 2012). This infection cycle of *P. pachyrhizi* consists only of the asexual reproduction of the fungus. Formation of sexual reproduction organs, called telia, and the production of teliospores has been observed in older lesions, yet germination of those sexual spores has not been reported to occur in natural conditions (Bromfield, 1984; Vittal et al., 2012). Despite the lack of sexual reproduction, however, the pathogen is genetically highly diverse and able to adapt quickly. The mechanism behind this, however, is not fully understood. *In vitro* observations describe parasexual recombination by anastomoses – the fusing of several fungal hyphae – that can lead to recombination events (Vittal et al., 2012). The recently published genome of *P. pachyrhizi* also revealed an intense activity of transposable elements in the uredospores (93 % of the *P. pachyrhizi* genome consists of transposable elements) that can confer to genetic alternations (Gupta et al., 2023). Even though not fully understood, the large genetic variability of the pathogen is the main reason why the fungus is so successful from a pathogen point of view and why it makes disease management of soybean rust so challenging.

1.2.3. Fungicide resistance in *P. pachyrhizi* isolates

So far, no commercial soybean variety is resistant to all isolates of *P. pachyrhizi* (Chicowski et al., 2024; Goellner et al., 2010; Langenbach et al., 2016). Immense breeding efforts and intensive screening of wild *Glycine* species as well as cultivated soybean varieties for resistance genes led to the identification of at least seven resistance loci, called Resistance to *Phakopsora pachyrhizi* 1 (*Rpp1*) to *Rpp7* (Chicowski et al., 2024; Childs et al., 2018b). Still, single gene-mediated resistance is quickly overcome due to the large genetic variability of the pathogen (Ceresini et al., 2024; Childs et al., 2018a; Garcia et al., 2008; Kawashima et al., 2016; Yamaoka, 2014). Additionally, breeding of resistant cultivars while maintaining high yield has proven quite challenging (Childs et al., 2018a). Thus, SBR management is still mainly controlled by synthetic fungicides (Ceresini et al., 2024). However, at the same time that the already mentioned overall usage of pesticides in Brazil is increasing (FAO, 2025), the efficacy of the fungicides used for SBR management is steadily

decreasing (Barro et al., 2021; Dalla Lana et al., 2018). This loss of efficacy can be traced back to an increasing number of isolates showing resistance towards one or more fungicide classes.

The three main fungicide classes that are used to control *P. pachyrhizi* in Brazil are the already mentioned DMIs, QoIs, and SDHIs. The first fungicides for SBR management were introduced in 2001, mainly belonging to the DMI family (Godoy et al., 2016). First insensitivities towards DMI fungicides were identified in isolates collected during the 2009-2010 growing season. This insensitivity is, as in other patho-systems, due to either point mutations in *CYP51* or due to *CYP51*-overexpression (Schmitz et al., 2014). Among those mutations was Y131F, which accounts for Y137F in other fungi - the most common mutation associated with DMI resistance (Fisher et al., 2018). Additionally, other mutations such as F120L, K142R, I145F, and I475T were detected, depending on the region where the isolates were collected (Schmitz et al., 2014). This demonstrates how *P. pachyrhizi* adapted to the selection pressure induced by intensive fungicide usage. With decreasing DMI efficacy, more QoIs were introduced on the market, and a fungicide mixture was used. However, here point mutations in *CYTB* were detected in isolates collected from 2012 to 2014. Only one single-nucleotide polymorphism (SNP) was detected that is responsible for the F129L exchange. Interestingly, the G143A exchange that is widespread for other fungal species was yet not found in *Phakopsora* isolates (Klosowski et al., 2016). Still, Müller et al. (2021) detected the F129L exchange in 90 % of samples collected from 2013-2017.

In response to decreasing efficacy of DMI and QoI, SDHIs (in mixtures with QoIs and DMIs) were introduced to control SBR in Brazil in 2013 (Godoy et al., 2016). In samples collected from the 2016-2017 growing season, a first mutation in *SDHc* was detected that led to the exchange from isoleucine to phenylalanine at amino acid (AA) position 86 (I86F) and could subsequently lead to insensitivities against SDHIs (Müller et al., 2024; Simões et al., 2018). This occurred only three years after the introduction of these new fungicides. A later assessment reported that the frequency of the SNP leading to I86F-exchange in *SDHc* increased from 7 % to 90 % from 2015 to 2019 (Mello et al., 2021). Additionally, there are now reports of *P. pachyrhizi* isolates that have already passed an evolution of fungicide adaptation to SDHIs, QoIs, and especially DMIs and show resistance mutations in the corresponding target genes (Müller et al., 2021; Müller et al., 2024).

The rapid adaptation of *P. pachyrhizi* in response to the high selective pressure caused by intensive fungicide applications per growing season emphasizes the need for alternative methods and strategies to manage SBR in soybean cultivation, especially in Brazil (Chicowski et al., 2024; Langenbach et al., 2016).

1.2.4. Alternative strategies to fight SBR

Alternative strategies to fight pathogens are mostly inspired by plants' endogenous defense systems, including their secondary metabolism, and by interactions with plant-associated microbes. Thus, they are highly diverse and reflect the creativity of researchers worldwide who strive to come up with new ideas to keep pace with an ever-changing nature. Since I focused on the soybean – *P. pachyrhizi* interaction, the following approaches and examples are condensed to this research area. However, the general methods are not only restricted to that patho-system but are mostly applicable to other pathogens of soybean or even other crop – pathogen systems. Also, in most cases, alternative strategies do not aim to make synthetic fungicides dispensable but rather aim to add an additional aspect of protection to decrease fungicide use to the most possible minimum.

Biocontrol agents

One strategy to fight SBR could be to use biocontrol agents such as *Simplicillium lanosoniveum,* an antagonistic fungus, that can colonize the uredia of *P. pachyrhizi* and interferes with the uredinial development (Ward et al., 2012). There are also reports of several *Bacillus* species that seem to suppress *P. pachyrhizi* germination, especially when combined with crude coffee oil (Dorighello et al., 2015). *Bacillus subtilis* treatment even reduced *P. pachyrhizi* sporulation by 90 % in greenhouse experiments and seems, therefore, predestined for the development of a biopesticide (Twizeyimana and Hartman, 2019). These studies exemplify the potential of microbial antagonists for the biological control of SBR.

RNA interference technology

Another approach to a more sustainable soybean protection could be the integration of RNA interference (RNAi) technologies. This strategy relies on the introduction of double-stranded (ds)RNA into the host plant. This dsRNA is then processed to so called small interfering (si)RNA and taken up by the pathogen. In the target organism, siRNA, together with Argonaute proteins, binds to respective RNA targets, promoting its degradation and, thus, leading to posttranscriptional gene silencing in the target organism (Koch and Wassenegger, 2021). Delivering the dsRNA into the host plant can either occur transiently by infection of the plant with recombinant viruses or by engineering transgenic plants that (over-)express the dsRNA constructs. These approaches are termed (virus-mediated) host-induced gene silencing, or (Vm)HIGS. More recently an non-transgenic strategy is gaining more attention: here the host plant is "simply" spray-inoculated with the respective dsRNA, this is referred to as spray-induced gene silencing, short SIGS (Beernink et al., 2024).

So far, there are three reports on HIGS/SIGS methods that show effects against SBR in laboratory/greenhouse environments. Hu et al. (2020) could show that VmHIGS-constructs

targeting three genes that are associated with *P. pachyrhizi* uredospore germination or appressorium formation significantly reduced the number of pustules per cm^2 on infected soybean leaves by ~ 60 - 80 %. They could also reach similar results by spray inoculation of SIGS-constructs targeting the same genes (Hu et al., 2020). Another approach aimed to target fungal *chitin synthase* genes via SIGS. Here, however, a significant reduction of SBR symptoms by ~20 % were only shown for co-inoculation of SIGS-constructs together with *P. pachyrhizi* uredospores (Saito et al., 2022). Although the authors also examined pretreatment of the SIGS constructs, the paper presents no quantitative data beyond a single image of a slightly less infected soybean leaf, and the efficiency of this approach remains to be demonstrated (Saito et al., 2022). Further research on the efficacy of SIGS constructs was reported by Ouyang et al. (2024): With the help of the recently published *P. pachyrhizi* genome (Gupta et al., 2023), the authors were able to identify three apoplastic effector genes in *P. pachyrhizi* that are essential for the infection of the fungus as they suppress the plant's immune responses. Simultaneously silencing these three genes via SIGS reduced SBR infection severity by ~ 60 %. This was also true for plants treated with SIGS-constructs 10 days prior to *P. pachyrhizi* inoculation (Ouyang et al., 2024). Since target gene selection is one of the essential steps towards effective RNAi efficacy for crop protection (Beernink et al., 2024), the study by Ouyang et al. demonstrates the usefulness of the recently revealed genome assembly of *P. pachyrhizi* (Gupta et al., 2023) and how it will probably boost research in this regard in the coming years.

Induced resistance

To strengthen the plant has become increasingly relevant in crop protection methods (Bent, 2016). The basic mechanism is to locally or systemically induce resistance in plants. This is generally termed induced resistance (IR). IR that is conferred by inoculation with necrotizing pathogens (or by treatment with compounds triggering the corresponding pathways) is commonly referred as systemic acquired resistance (SAR, Kesel et al., 2021). SAR is predominantly mediated by salicylic acid and N-hydroxy pipecolic acid (Conrath et al., 2015; Kesel et al., 2021). In addition to pathogen inoculation, IR can also be triggered by non-pathogenic plant growth promoting bacteria, a plethora of chemicals or physical injury (Conrath et al., 2015; Pieterse et al., 2014). Inducing a plant's endogenous defense by elicitors bears great potential for crop protection, and two elicitors are already registered inducers for SBR management in the Brazilian market: Romeo® – a cerevisane-based elicitor – and BioImune® – formulated from *Bacillus subtilis* (Paula et al., 2021). However, inducing the defense response of plants also increases the plant's energy need, regardless of pathogen pressure – a trade-off that has to be considered (Huot et al., 2014; van Hulten et al., 2006). Thus, increasing a plant's readiness for defense, but timing the response to the occurrence of the actual stress, would even be more efficient (Buswell et al., 2018; van Hulten et al., 2006).

This can be achieved by defense priming, an induced physiological state of a plant that enables the plant to respond faster to significantly lower levels of defense stimulus than unprimed plants (Conrath et al., 2015). Two well-studied priming-inducing agents are Acibenzolar-S-methyl (ASM) – a derivative of salicylic acid – and azelaic acid – a fatty acid catabolite that is involved in SAR signaling (Conrath et al., 2015). Both elicitors have also recently been evaluated regarding their protective effects against SBR: ASM is described to show protective effects against SBR with 40 - 85 % disease control in greenhouse trials and 60 % in field trials (Cruz et al., 2014; Paula et al., 2021; Twizeyimana and Hartman, 2019). Azelaic acid showed both, a direct fungistatic effect on *P. pachyrhizi in vitro* as well as a defense-priming effect on soybean *in vivo* (Rodrigues et al., 2023). Such an effect was also described for hexanoic acid in the same study (Rodrigues et al., 2023). Despite the immense potential of priming agents in crop protection, only a few priming agents are commercially available today. The recent introduction of Phytalix® serves as one prominent example of the application of a priming agent in the field (Ascribe Bio, 2025). According to Ascribe Bio, Phytalix® is currently being tested in field trials in Brazil to assess the potential of Phytalix® induced protection of soybean plants against SBR and other pathogens.

Once the plant's endogenous defense system is induced, it triggers a cascade of defense responses, one of which is the accumulation of plant secondary metabolites (PSM) with antimicrobial activity (Piasecka et al., 2015). Hence, those PSM could possibly be directly exploited for crop protection.

Plant secondary metabolites

Plants produce a plethora of PSM. More than 100,000 PSM have been identified, yet many of them have not, or only in part, been characterized (Dixon, 2001; Dixon and Dickinson, 2024). Historically, the term "secondary metabolites" was coined for compounds that were considered non-essential for basic plant growth and development, in contrast to "primary metabolites." However, this terminology can be misleading, as many PSMs are now known to play crucial roles in plant survival, particularly in responses to biotic and abiotic stresses (Ahuja et al., 2012; Dixon, 2001; Dixon and Dickinson, 2024). Many PSM have antimicrobial properties that enable plants to effectively resist diseases (Ahuja et al., 2012; Bennett and Wallsgrove, 1994; Hammerschmidt, 1999; Osbourn, 1996). Making use of such endogenous, but also non-endogenous PSM, many of which are biodegradable, could contribute to sustainable crop protection (Lyubenova et al., 2023). PSM that show activity towards *P. pachyrhizi* could serve as natural fungicides in spray application, or their biosynthesis genes could be used to engineer SBR resistance in transgenic plants (Langenbach et al., 2016).

In soybean, some PSM have been associated with *P. pachyrhizi* attack. For example, the isoflavonoids glyceollin, daidzein, and genistein accumulate upon *P. pachyrhizi* infection (Lygin et

al., 2009). Of those three, however, only glyceollin seems to effectively reduce *P. pachyrhizi* spore germination *in vitro* (Lygin et al., 2009). A more recent study used untargeted metabolomics to identify PSM that accumulate in soybean plants upon *P. pachyrhizi* infection. They include phenylpropanoids, terpenoids, and flavonoids (Silva et al., 2020). Notably, the authors investigated the PSM accumulation of a soybean variety that is susceptible to *P. pachyrhizi* (Silva et al., 2020). This suggests that these metabolites are recruited as part of the defense response, but that their timing and/or abundance may be insufficient to prevent disease. To distinguish PSM associated with ineffective versus effective defense, it could therefore be particularly informative to examine plants that are immune to soybean rust, such as non-host species. For example, Ishiga et al. (2015) demonstrated that in *Medicago truncatula* – a legume that is a non-host for *P. pachyrhizi* – genes involved in phenylpropanoid, flavonoid, and isoflavonoid biosynthesis are activated upon *P. pachyrhizi* inoculation. This correlated with the increased accumulation of PSM, such as medicarpin and ononin, which also inhibit germination of *P. pachyrhizi* uredospores *in vitro* (Ishiga et al., 2015). Interestingly, genes involved in the non-host response of *M. truncatula* were also associated with *Rpp2*-mediated resistance to SBR (Ishiga et al., 2015; Pandey et al., 2011; van de Mortel et al., 2007). However, there are isolates of *P. pachyrhizi* that have broken the *rpp2*-mediated resistance (Chicowski et al., 2024; Garcia et al., 2008). Also, medicarpin was one of the isoflavonoids that was associated with *P. pachyrhizi*-response in the susceptible cultivar investigated by Silva et al. (2020). Additionally, soybean and *M. truncatula* both belong to the *Fabaceae* family of plants. It therefore stands to reason that *P. pachyrhizi* has already come into contact with these specific PSM in the course of an evolutionary arms race and has developed strategies for dealing with these plant defense substances. A promising strategy is thus to focus on PSM that are not present in soybean. Accordingly, our research group investigated the non-host response of *Arabidopsis thaliana* and *Helianthus spec.* belonging to the family of *Brassicaceae* and *Asteraceae*, respectively (Beesley, 2022; Beesley et al., 2023; Beyer et al., 2019; Langenbach et al., 2013; Loehrer et al., 2008; Schwinges, 2019; Spencer, 2022).

One gene involved in the non-host response of *A. thaliana* towards *P. pachyrhizi* is *FERULOYL-COA-6'HYDROXYLASE-1* (*AtF6'H1*) – a gene that encodes the key enzyme in scopoletin biosynthesis (Beyer et al., 2019; Kai et al., 2008). Scopoletin, a PSM that belongs to the group of simple coumarins, displays fungistatic effects on *P. pachyrhizi in vitro* and protects soybean from SBR *in planta* (Beesley, 2022; Beyer, 2019; Beyer et al., 2019; Schwinges, 2019). Inoculating *P. pachyrhizi* spores together with scopoletin reduced SBR severity on soybean plants by ~ 85 % (Beyer et al., 2019). In comparison, treating soybean plants with *P. pachyrhizi* spores and Orkestra® - a commercial fungicide that combines QoI and SDHI – reduced the disease severity by 95 % (Beyer et al., 2019). This shows the potential for scopoletin to be used either as a control agent itself

or as a blueprint for near-to-nature fungicides (Beyer et al., 2019). Additionally, our research group aimed to integrate scopoletin biosynthesis into transgenic soybean. So far, transgenic soybeans that overexpress *AtF6'H1* accumulate scopoletin, but have only shown protective effects against *Fusarium virguliforme*, yet no significant reduction of SBR severity (Beesley et al., 2023; Beyer, 2019). To follow up on this approach and to further investigate scopoletin biosynthesis is part of this study and will be addressed in more detail below.

In addition to being involved in the non-host response in *A. thaliana*, scopoletin can be found on the leaf surface of the common sunflower (*Helianthus annuus*). Notably, among 60 plant species tested in a detached-leaf assay, only two species belonging to the genus *Helianthus* suppressed germination of *P. pachyrhizi* (Schwinges, 2019). Additionally, it was described that the *H. annuus* genotype AMES18925 is more resistant to *Puccinia helianthi* (causal agent of sunflower rust) than two other investigated genotypes (Prats et al., 2002; Prats et al., 2007). This resistance correlated with the presence of scopoletin and ayapin on the leaf surface of respective sunflower cultivars. In his doctoral thesis, Patrick Schwinges reported that ayapin inhibits *P. pachyrhizi* spore germination even more effectively than scopoletin, both *in vitro* and *in planta* (Schwinges, 2019). However, despite its intriguing antifungal properties and the resulting potential for crop protection purposes, to date, not much research has been done on ayapin, including its unknown biosynthetic route(s). A part of the present dissertation further elucidates the biosynthesis of ayapin in sunflower.

1.3. The sunflower coumarins – scopoletin and ayapin

1.3.1. Simple Coumarins

Coumarins are PSM that originate from the phenylpropanoid pathway (PPP). The PPP is a quite fascinating biosynthetic pathway, as only a few intermediates from the shikimate pathway diversify into a broad spectrum of important PSM. The PPP is not only origin to the structure giving polymers lignin, cutin, suberin and sporopollein, but also origin to PSM classes that are involved in plant growth regulation, development and stress adaptation such as flavonoids, anthocyanins, tannins, and coumarins (Fraser and Chapple, 2011; Stringlis et al., 2019; Vogt, 2010). The latter comprise six distinct groups: simple coumarins, furanocoumarins, dihydrofuranocoumarins, pyranocoumarins, phenylcoumarins, and bicoumarins (Venugopala et al., 2013). In this work, only the group of simple coumarins was elucidated and will be referred to hereon as coumarins. They have often been associated with plant defense (Dixon, 2001; Gnonlonfin et al., 2012; Stringlis et al., 2019). For example, the presence of coumarin (the simplest of all coumarins) increases the resistance of apple to the necrotrophic fungus *Cytospora mali* (causal agent of Valsa canker; Du et al., 2023). The content of the coumarin umbelliferone is reported to play a role in defense of

immature Marsh grapefruits against the fungus *Penicillium digitatum* (Afek et al., 1999); And, in chamomile leaves, herniarin and umbelliferone contents are rising when the plant is attacked by thrips (*Echinothrips americanus*; Repčák and Suvák, 2013). In *Citrus* species, scoparone content is higher when the species is resistant to the oomycete *Phytophthora citrophthora* than when it is susceptible (U. Afek and A. Sztejnberg, 1988). The coumarin scopoletin is associated with resistance of rubber trees towards the fungus *Mycrocyclus ulei* and with the stress response of wild tobacco towards *Alternaria alternata* (Garcia et al., 1995; Sun et al., 2014). Scopoletin is also described to have feeding-deterrent effects on the caterpillars of *Spilarctia obliqua* (Tripathi et al., 2011). In sunflower, the accumulation of scopoletin together with ayapin is associated with defense response towards the fungi *Sclerotinia sclerotiorum,* and *P. helianthi* (Prats et al., 2002; Urdangarín et al., 1999). Additionally, sunflower cultivars with resistance towards *Orobanche cernua* – a parasitic plant species – accumulated higher levels of scopoletin and ayapin than susceptible cultivars (Serghini et al., 2001). Both coumarins have also been described to have repelling effects towards the sunflower beetle (Olson and Roseland, 1991). These examples demonstrate the broad range of coumarins and their antimicrobial, herbicidal, and insect repellent activity. But, coumarins can also be involved in abiotic stress responses. For example, the coumarins scopoletin, fraxetin, and sideretin are involved in iron uptake under iron-deficiency stress (Fourcroy et al., 2014; Rajniak et al., 2018; Tsai et al., 2018). Additionally, coumarins are recognized for their crucial roles in mediating plant interactions with their surrounding microbiome (Stassen et al., 2021). Scopoletin, for example, contributes to shaping the root microbiome by selectively influencing the assembly of microbes in the rhizosphere (Stringlis et al., 2018).

These intriguing properties of coumarins have attracted sustained research interest over the past decades (Bourgaud et al., 2006; Stringlis et al., 2019; Wang et al., 2025). Consequently, the biosynthetic pathway of the coumarins been studied extensively and is well understood. However, the biosynthetic route of ayapin in sunflower remained elusive.

1.3.2. The biosynthesis of coumarins

In the model plant *A. thaliana*, the core PPP is well described (Fraser and Chapple, 2011) and appears to be largely conserved across most plant species (Wang et al., 2025). Figure 1 shows a schematic of the core PPP involved in coumarin biosynthesis.

Since coumarins originate from the PPP, the first essential step in their biosynthesis is the deamination of the amino acid phenylalanine to cinnamate, catalyzed by phenylalanine ammonia lyase (PAL; Fraser and Chapple, 2011; Vogt, 2010). Cinnamate can be further hydroxylated at the *para*- and *meta*-position of the phenyl group by activities of cytochrome P450-dependent monooxygenases (CYPs) to form the cinnamates *p*-coumarate (4-hydroxycinnamate) and caffeate

(3,4-dihydroxycinnamate), respectively. Catalyzed by a caffeic acid *O*-methyltransferase, the latter can gain a methyl-group at the *meta* hydroxy group to form ferulate (3-methoxy-4-hydroxycinnamate; Bourgaud et al., 2006; Byeon et al., 2014). Each of the four cinnamates can be converted to its corresponding CoA-thioester by 4-coumarate:CoA ligases (4CLs; Ehlting et al., 1999; Yang et al., 2015). These hydroxycinnamate-CoA-thioesters are not only precursors for coumarin biosynthesis. For example, *p*-coumaroyl-CoA represents also the origin of flavonoid biosynthesis (Dixon and Paiva, 1995). And, feruloyl-CoA is converted to coniferaldehyde at the starting point of lignin biosynthesis (Fraser and Chapple, 2011).

For coumarin biosynthesis, however, the key step is the *ortho*-hydroxylation at the phenyl ring of cinnamoyl-, *p*-coumaroyl-, caffeoyl- or feruloyl-CoA. This reaction is catalyzed by enzymes of the Fe(II)- and 2-oxoglutarate-dependent dioxygenase family (2OGD): *p*-coumaroyl-CoA 2'-hydroxylases (C2'Hs) and feruloyl-CoA 6'-hydroxylases (F6'Hs). When light energy is available, this then enables a spontaneous *trans/cis*-isomerisation and lactonization of the respective *ortho*-hydroxy-cinnamate-CoA-thioesters (Goldenberg et al., 2025; Kai et al., 2008; Shimizu, 2014; Vogt, 2010). In darkness, e.g., in the roots, this reaction can also be catalyzed enzymatically by a BAHD acyltransferase – the coumarin synthase (COSY; Vanholme et al., 2019). The formation of simple coumarins heavily depends on the availability of the respective precursors and the specificity of the respective 2OGDs (compare Figure 1). For example, F6'H1 from *A. thaliana* (AtF6'H1) converts caffeoyl-CoA and feruloyl-CoA to the respective precursors of esculetin and scopoletin, respectively (Kai et al., 2008; Ziegler et al., 2017). In contrast, a C2'H from *Ruta graveolens* is described to accept p-coumaroyl-CoA and feruloyl-CoA as substrates *in vitro. In planta*, however, *p*-coumaroyl-CoA is the main available precursor, leading to the formation of umbelliferone, which in turn serves as a precursor for furanocoumarins such as psoralen (Vialart et al., 2012). Two 2OGD orthologs of sweet potato (*Ipomoea batatas*) have been described to accept all three hydroxy cinnamates as substrates *in vitro* (Matsumoto et al., 2012). Previous work in our research group revealed a broad substrate spectrum of IbF6'H2 in transiently transformed *N. benthamiana* plants that accumulated umbelliferone, esculetin, and scopoletin when overexpressing *IbF6'H2* (Weber Böhlen, 2021). We also showed that a sunflower ortholog, HaF6'H1, leads to the accumulation of esculetin and scopoletin, but not umbelliferone *in planta* (Schwinges, 2019; Weber Böhlen, 2021).

By the activity of UDP-dependent glycosyltransferases (UGTs), coumarins with a free hydroxy group (see black dotted box in Figure 1) can also be inactivated by glycosylation using UDP-glucose. The respective β-D-glucosides are subsequently stored in the plant's vacuole and can be reconverted to their aglycones by β-glucosidases (BGLUs) when required (Ahn et al., 2010; Le Roy et al., 2016; Tsai et al., 2018; Vogt, 2010).

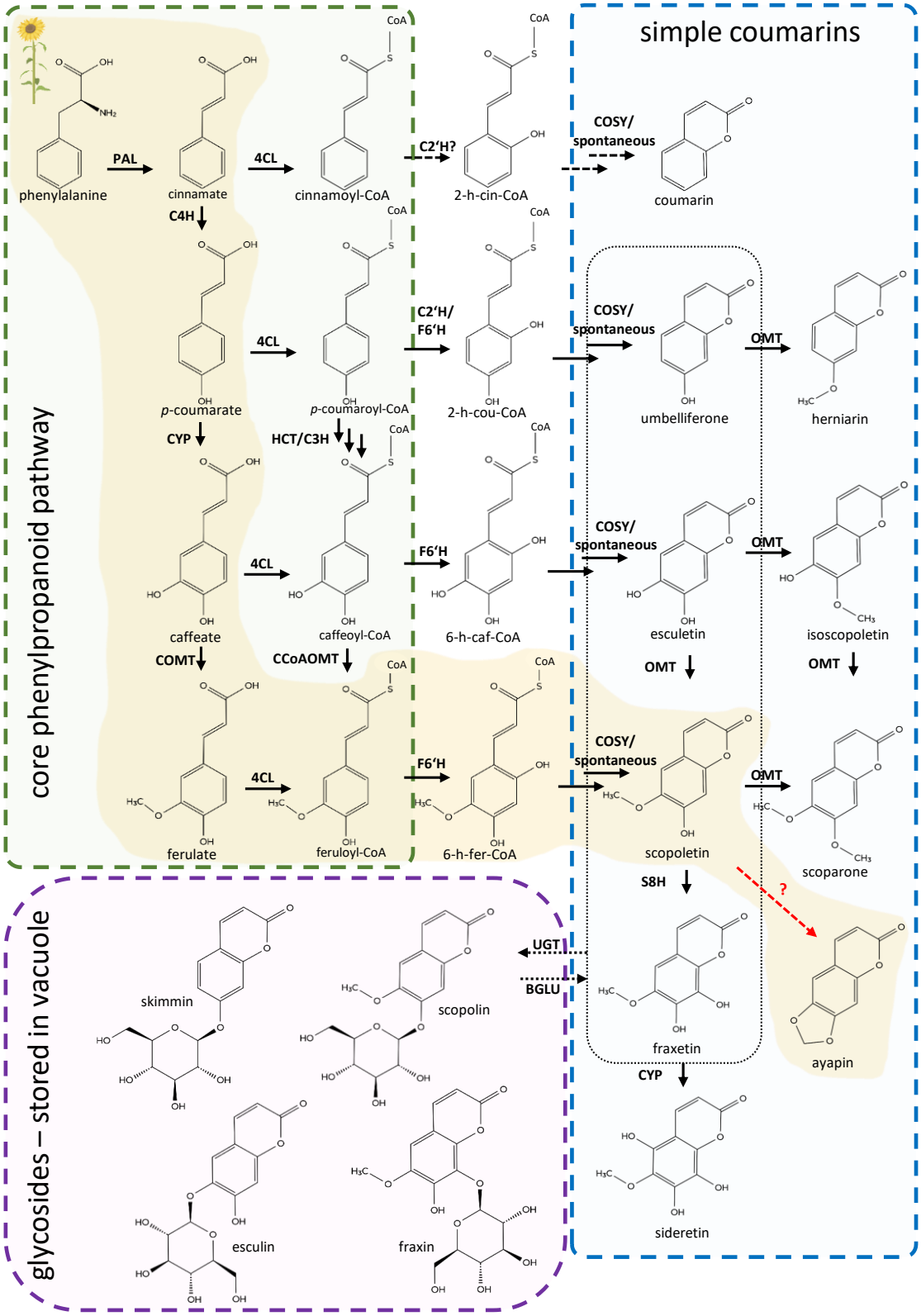

Figure 1. Schematic overview of coumarin biosynthesis in plants. Figure legend appears on the following page.

Figure 1: Simple coumarin biosynthesis in plants originates from the amino acid phenylalanine – the starting point of the core PPP (green box). In a process involving multiple enzymes, the CoA esters cinnamoyl-CoA, coumaroyl-CoA, caffeoyl-CoA, and feruloyl-CoA are synthesized. Involved enzymes are: phenylalanine ammonia lyase (PAL), cinnamic acid 4-hydroxylase

(C4H), cytochrome P450-dependent monooxygenases (CYP), O-methyltransferases (OMT), 4-coumarate-CoA ligases (4CL), and caffeoyl-CoA O-methyltransferases (CCoAOMT). These CoA esters are hydroxylated by Fe(II)- and 2-oxoglutarate-dependent dioxygenases: *p*-coumaroyl CoA 2-hydroxylase (C2'H) and/or feruloyl-CoA 6'-hydroxylases (F6'H). Products are the respective intermediates 2-hydroxycinnamoyl-CoA (2-h-cin-CoA), 2-hydroxycoumaroyl-CoA (2-h-cou-CoA), 6-hydroxycaffeoyl-CoA (6-h-caf-CoA) and 6-hydroxyferoloyl-CoA (6-h-fer-CoA). The ortho-hydroxylation at the 2'/6'-carbon leads to a spontaneous trans/cis-isomerization and lactone ring formation, resulting in the formation of the simple coumarins (blue box): coumarin, umbelliferone, esculetin, and scopoletin. This reaction can also be catalyzed by the enzyme coumarin synthase (COSY). Further modifications of coumarins with free hydroxy groups (black dotted box) include methylation by OMTs or glycosylation by UDP-glycosyltransferases (UGT) and subsequent storage in the vacuole of the plant (violet box). Catalyzed by ß-glycosidases (BGLU), the glycosides can be reconverted to their respective aglycon. Scopoletin can additionally be hydroxylated at position 8' to form fraxetin (catalyzed by scopoletin8'-hydroxylase (S8H)), which can further be hydroxylated to sideretin. The biosynthesis of ayapin remains elusive (indicated by a red arrow). I speculate that ayapin is directly converted from scopoletin, presumably by the activity of a CYP. A potential pathway from phenylalanine to ayapin is indicated by yellow background.

O-methylation can further diversify simple coumarins. For instance, an OMT from poplar catalyzes the methylation of the free hydroxyl group of scopoletin, forming scoparone (6,7-dimethoxycoumarin) *in vitro* (Kim et al., 2006). Additionally, a recent approach comparing metabolomics and transcriptomics in *Artemisia capillaris* revealed an AcOMT that is associated with scoparone biosynthesis. By overexpressing *AcOMT1* together with *AtF6'H1* and *AtCOSY* in *N. benthamiana*, the authors demonstrated scoparone accumulation in transgenic plants (Guo et al., 2025). Consistently, two sunflower OMTs identified by our research group converted esculetin to isoscopoletin and/or (iso-)scopoletin to scoparone *in planta.* By overexpression of *HaOMT1* or *HaOMT3* alongside *IbF6'H2,* transformed *N. benthamiana* plants accumulated isoscopoletin or scoparone, respectively (Weber Böhlen, 2021). It has also been reported that a microbial OMT from *Streptomyces avermitilis* (SaOMT2) can efficiently methylate umbelliferone to herniarin *in vitro* (Chu et al., 2017).

Scopoletin can be hydroxylated at the 8' -position by scopoletin-8'-hydroxylase (S8H) to form fraxetin (7,8-dihydroxy-6-methoxycoumarin), which can then be further hydroxylated by CYP82C4 to yield sideretin (Rajniak et al., 2018; Tsai et al., 2018). These reactions are prominently induced under iron deficiency, and the resulting catecholic coumarins contribute to Fe(III) chelation and reductive mobilisation in the rhizosphere (Rajniak et al., 2018).

These examples illustrate that for most coumarins, at least portions of the respective biosynthetic routes have been reconstructed *in vitro* or *in planta*, enabling enzymatic access to umbelliferone, esculetin, scopoletin, isoscopoletin, herniarin, fraxetin, and scoparone. For ayapin, however, a complete and genetically validated biosynthetic pathway has not yet been elucidated.

1.3.3. Ayapin

Ayapin (6,7-(methylenedioxy)coumarin) was first described in 1936 by Bose and Ghosh. The authors claimed to have isolated a "sky-blue fluorescent" coumarin that is free of methoxy groups but has a methylenedioxy group from leaves of the *Asteraceae Eupatorium ayapana* (now *Ayapana*

triplinervis). Appropriately, they named this coumarin ayapin (Bose and Ghosh, 1936). In contrast to scopoletin, which has been identified in many mono- and dicotyledonous plant families (Gnonlonfin et al., 2012), ayapin has been mainly restricted to the *Asteraceae* family (Bohlmann et al., 1980; Bose and Ghosh, 1936; Debenedetti et al., 1998; Gutiérrez-Mellado et al., 1996; Tal and Robeson, 1985). Outside this family, the presence of ayapin has only been reported in roots of *Dendrobium* species (Liu et al., 2011; Zheng et al., 2000), in leaves of *Cistus laurifolius* (Vogt and Gülz, 1991), and in roots of Bistort (*Polygonum bistorta*; Sun et al., 2007).

However, in most of those plant species, the presence of ayapin has only been documented, whereas the dynamics of its accumulation have been elucidated solely in *Helianthus* species, predominantly in the common sunflower, in which ayapin accumulation was first reported in 1964 in 2,4-D–treated plants (Dieterman et al., 1964). Later, Tal and Robeson (1985) described the induction of scopoletin and ayapin in sunflower plants that were previously treated with the fungal pathogen *Helminthosporium carbonum.* The authors also demonstrated that ayapin inhibited the growth of that pathogen more effectively than scopoletin (Tal and Robeson, 1985). In sunflower, both coumarins seem to accumulate in response to mechanical wounding and insect feeding (Olson and Roseland, 1991) and after treatment with abiotic elicitors such as sucrose and $CuCl_2$ (Gutierrez, 1995). While the coumarin content is described to vary in different cultivars of sunflower (Prats et al., 2006; Prats et al., 2007; Serghini et al., 2001), there are, to the best of my knowledge, no sources explicitly mentioning sunflower cultivars that only accumulate one or none of the two coumarins. Yet, only a few of the many sunflower cultivars available have been elucidated for their coumarin profile so far.

Because of the simultaneous accumulation after treatment and structural similarity (see Figure 1), Tal and Robinson suggested that ayapin is synthesized directly from scopoletin in sunflowers (Tal and Robeson, 1985). And indeed, in feeding experiments with radio-labeled scopoletin, 36% of the labeled molecules were metabolized to ayapin (45% of the labeled scopoletin were recovered, while the remainder of the recovered label was found in a fraction that included scopolin; Tal and Robeson, 1986). However, ~ 10 years later, Cabello-Hurtado et al. fed $CuCl_2$-induced tubers of *H. tuberosus* with radio-labeled scopoletin and were not able to detect labeled ayapin, although the coumarin normally accumulates in such tubers after $CuCl_2$-stress (Cabello-Hurtado et al., 1998). However, Patrick Schwinges further elucidated the accumulation of scopoletin and ayapin in sunflower cultivar AMES 18925 after $CuCl_2$-treatment. He demonstrated that scopoletin in treated sunflower leaves accumulates earlier (peaking at 48 h) than ayapin (peaking at 72h, Schwinges, 2019). Additionally, accumulation of both coumarins was depleted when sunflower leaf discs were treated with prohexadione – a competitive inhibitor of 2OGDs – prior to $CuCl_2$-treatment. Thus, the

inhibition of the sunflower F6'H, responsible for the biosynthesis of scopoletin, also led to the loss of ayapin accumulation (Schwinges, 2019). These results strongly indicate that scopoletin and ayapin are somehow connected, and ayapin appears to be dependent on scopoletin availability. Therefore, it is plausible to hypothesize that scopoletin serves as the direct precursor of ayapin.

If this hypothesis holds true, the formation of a methylenedioxy bridge would be essential for converting scopoletin into ayapin. In plants, this reaction is described as being exclusively conducted by enzymes belonging to the CYP P450 family (Mizutani and Sato, 2011). As depicted in Figure 2, examples of CYPs catalyzing a methylenedioxy bridge formation can be found in sesame, black pepper fruits, or the traditional Chinese medicine plant *Corydalis yanhusuo* (Liu et al., 2023; Ono et al., 2006; Schnabel et al., 2021).

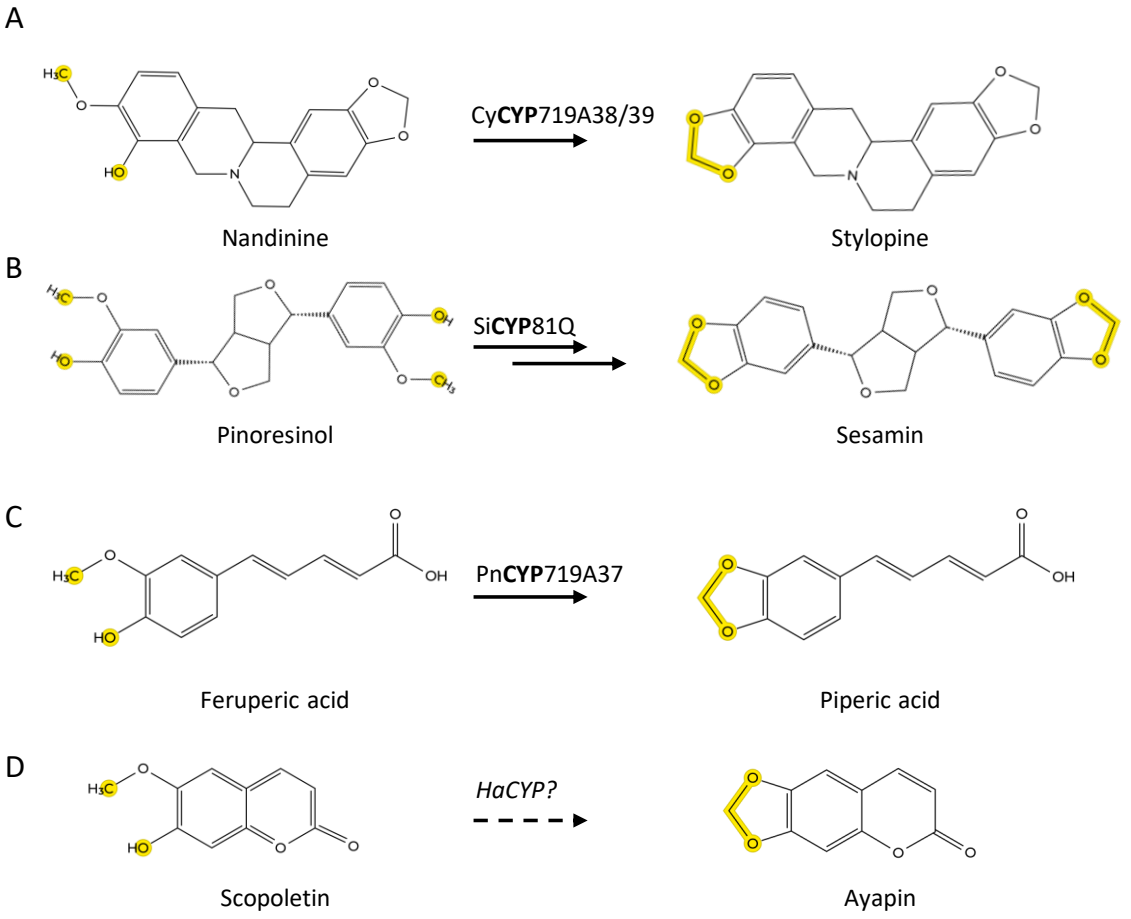

Figure 2. CYPs catalyze methylenedioxy bridge formation in several biosynthetic pathways in plants. (A) CyCYP719A38 and CyCYP719A39 are described to convert the alkaloid nandinine to stylopine in *Corydalis yanhusuo* by catalyzing the formation of a methylenedioxy bridge (Liu et al., 2023). (B) SiCYP81Q is described to convert pinoresinol first to piperitol and then to sesamin by catalyzing the formation of two methylenedioxy bridges in *Sesamum indicum* (Ono et al., 2006). (C) PnCYP719A37 is described to catalyze the methylenedioxy bridge formation of feruperic acid to piperic acid in *Piper nigrum* (Schnabel et al., 2021). (D) Hypothetical formation of a methylenedioxy bridge to convert scopoletin to ayapin in *H. annuus*. (A-D) Respective carbon and oxygen residues that are involved in the reaction and the resulting methylenedioxy bridge are highlighted in yellow.

Identifying a CYP enzyme in sunflower that converts scopoletin to ayapin would provide the missing link in ayapin biosynthesis in plants and provide the opportunity to engineer plants that would gain the function to synthesize ayapin.

Understanding coumarin biosynthesis provides the basis for examining how these metabolites are subsequently secreted and mobilized to sites of plant–microbe interactions. In the context of the *P. pachyrhizi*–soybean interaction, this site corresponds to the leaf surface, on which fungal spores would land and initiate infection (Goellner et al., 2010).

1.3.4. The secretion of coumarins

So far, the secretion mechanism of coumarins has mainly been described for the rhizosphere, in which coumarins are secreted to communicate plant-microbe-interaction or in the event of iron deficiency (Fourcroy et al., 2014; Rajniak et al., 2018; Stringlis et al., 2019; Ziegler et al., 2017). This secretion is mainly associated with ABC-transporters. For example, Fourcroy et al. (2014) describe scopoletin extrusion during iron starvation is mediated by the ATP-binding cassette transporter ABCG37. More recent studies, however, propose that AtABCG37 specifically transports catecholic coumarins such as fraxetin, but not scopoletin (Ziegler et al., 2017). This is also reported for an ABC-transporter from *Nicotiana tabacum* that is involved in secretion of fraxetin or hydroxyfraxetin to the rhizosphere (Lefèvre et al., 2018). However, so far, the mechanism of coumarins secretion to the leaf surface of plants such as sunflowers is poorly understood. During his doctoral studies David Spencer elucidated an ABC-transporter from sunflower, which he named HaABC, regarding its function in coumarin secretion (Spencer, 2022). The accumulation of scopoletin and ayapin on the leaf surface of UV-light-induced sunflowers correlated with the induction of *HaABC* expression in the respective leaf tissue (Spencer, 2022). Additionally, when the *HaABC* was heterologous expressed in tobacco (BY-2) cell cultures, it much increased the extracellular levels of scopoletin compared to cells lacking the transporter (Spencer, 2022). However, whether the coumarin secretion mechanism depends solely on a transporter protein such as HaABC in sunflower remains to be evaluated.

1.4. Aim of the study

This study aims to elucidate coumarin-based and fungal self-inhibitory mechanisms as alternative crop protection strategies against the biotrophic rust fungus *P. pachyrhizi*.

First, I characterize different isolates of *P. pachyrhizi* regarding their tolerance to commercial fungicides. Afterwards, a comparative analysis of one of those isolate's tolerance to natural compounds, with focus on the sunflower coumarins scopoletin and ayapin, is conducted. Then, I examine these coumarins in detail by analyzing the distribution of scopoletin- and ayapin-synthesizing capacity across diverse sunflower genotypes. Next, I investigate scopoletin as a putative metabolic precursor of ayapin and aim to unravel the genetic basis and key biosynthetic steps underlying ayapin formation in sunflower. By screening a sunflower mutant population for lines with increased scopoletin accumulation and secretion, I aim to provide additional entry points to dissect coumarin biosynthesis and to support future breeding or metabolic engineering. Furthermore, this study aims to lay the groundwork for such metabolic engineering by initiating targeted coumarin biosynthesis in transgenic soybean lines by exploiting sunflower and Arabidopsis genes. Finally, I focus on *P. pachyrhizi* itself by investigating whether the fungus exhibits a crowding effect, searching for putative self-inhibitory factor(s), and assessing their potential use as novel tools in soybean protection.

2. Results

Currently, SBR is managed predominantly through intensive applications of conventional fungicides. Our research group focuses on natural alternatives to those fungicides. In this thesis, I emphasize the importance of this topic by first identifying a *P. pachyrhizi* isolate that shows insensitivities to all three fungicide classes that are used in commercial soybean cultivation.

2.1. Fungicide-insensitive isolate of *P. pachyrhizi* is inhibited by sunflower coumarins

To monitor *P. pachyrhizi* biology and development, each season multiple strains are collected at various field sites in Brazil by the Brazilian Agricultural Research Corporation - Embrapa (**Em**presa **Bra**sileira de **P**esquisa **A**gropecuária; Da Rocha et al., 2025). In this study, three *P. pachyrhizi* isolates that were sampled and provided by Embrapa were analyzed regarding their sensitivity to different classes of fungicides. According to Embrapa, two of the three isolates were collected between 2007 and 2008 and the third in 2016. These isolates are hereafter referred to as reduced-sensitivity isolates (RS1–RS3).

Soybean plants were pretreated with fungicides and subsequently inoculated with different *P. pachyrhizi* isolates. Their tolerance or susceptibility to the respective fungicide was compared to our in-house standard *P. pachyrhizi* isolate (br05) that was collected in Brazil in 2005 and has since been maintained in our research group (Beyer et al., 2019). The following fungicides were tested: Proline® - a DMI with the active substance prothioconazole; F500® - a QoI with the active substance pyraclostrobin; Imtrex® - an SDHI with the active substance fluxapyroxad; and Orkestra® - which is a QoI/SDHI-combination of fluxapyroxad and pyraclostrobin. An overview of those fungicides and the concentrations used is listed in Table 1. Upon spray applications of the fungicides and drying, treated trifolia were inoculated with a suspension of 1 mg/mL uredospores of each of the four *P. pachyrhizi* isolates. Eight to twelve days post inoculation, the leaves were harvested, and the percentage area that was covered with rust pustules was evaluated. The relative disease severity was calculated by comparing the percentage of the diseased area of each leaflet to the median of the control treatment within each *P. pachyrhizi* isolate (Figure 3). When plants were pretreated with 100 % of the respective fungicide's stock solution (SL), the infection severity of br05-inoculated plants was reduced by 98-100 % compared to the median of the control treatment (Figure 3). Hence, the br05 isolate of *P. pachyrhizi* was susceptible to all fungicides tested. Consequently, the following analysis focused on significant differences in fungicide sensitivity of the isolates RS1, RS2, and RS3 compared to the br05 isolate at various doses of fungicides.

Soybean leaves that were pretreated with the Proline® (DMI) showed almost no SBR symptoms when inoculated with *P. pachyrhizi* isolates br05 or RS1 (Figure 3A). However, the infection severity was significantly increased when plants were inoculated with RS2 compared to inoculation with br05 (Figure 3A). Plants pretreated with 100 % of the Proline®-SL and then inoculated with the RS2 isolate showed a relative median diseased area of ~5 % that rose to ~25 % for plants pretreated with 6.25 % of the Proline®-SL. For plants inoculated with isolate RS3, this effect was seen with 25 % and more of Proline®-SL (Figure 3A).

Table 1. Fungicides used for *P. pachyrhizi* sensitivity assays. DMI = demethylation inhibitors; QoI = quinone outside inhibitors (QoI); SDHI = succinate dehydrogenase inhibitors. The concentration stated as stock solution equals the concentration that was used as 100 % fungicide solution in the conducted experiments.

commercial fungicide	active ingredient (AI)	fungicide class	AI conc.	stock solution (SL) ≙ 100 %	Conc. AI in SL
Proline®	prothioconazole	DMI	250 g/L	80 µL/L	20 mg/L
F500®	pyraclostrobin	QoI	250 g/L	0.5 g/L	125 mg/L
Imtrex®	fluxapyroxad	SDHI	62.5 g/L	500 µL/L	31.25 mg/L
Orkestra®	fluxapyroxad + pyraclostrobin	SDHI + QoI	167 g/L 333 g/L	62.5 µL/	10.4 mg/L 20.9 mg/L

Soybean leaves that were pretreated with F500® (QoI) showed a slight increase in the infection severity with decreasing fungicide concentration when inoculated with br05, RS1, or RS3 (Figure 3B). For plants pretreated with 100 % of the F500®-SL and inoculated with RS2, the infection severity was significantly stronger, with a median infection severity of ~ 62 % (Figure 3B). At levels of 25 and 12.5 % of F500®-SL, inoculation with RS2 caused infection severity levels similar to those with no fungicide treatment. At these F500 concentrations , inoculation with RS1 and RS3 also led to significantly stronger infection severity when compared to br05 inoculation (median RS1 = ~11-21 %, median RS3 = ~12-15 %, Figure 3B).

Soybean leaves that were pretreated with 12.5 - 100 % of the Imtrex®-SL (SDHI) showed the strongest reduction of disease severity at all concentrations and isolates tested (Figure 3C). Only inoculation with RS2 significantly increased the infection severity when plants were pretreated with 50 or 12.5 % of the SL compared to br05 inoculation (Figure 3C). At 12.5 % of the Imtrex®-SL, RS2 inoculation led to an increase of infection severity of over 50 %, which was also reached for br05 at an Imtrex® concentration of 6.25 %.

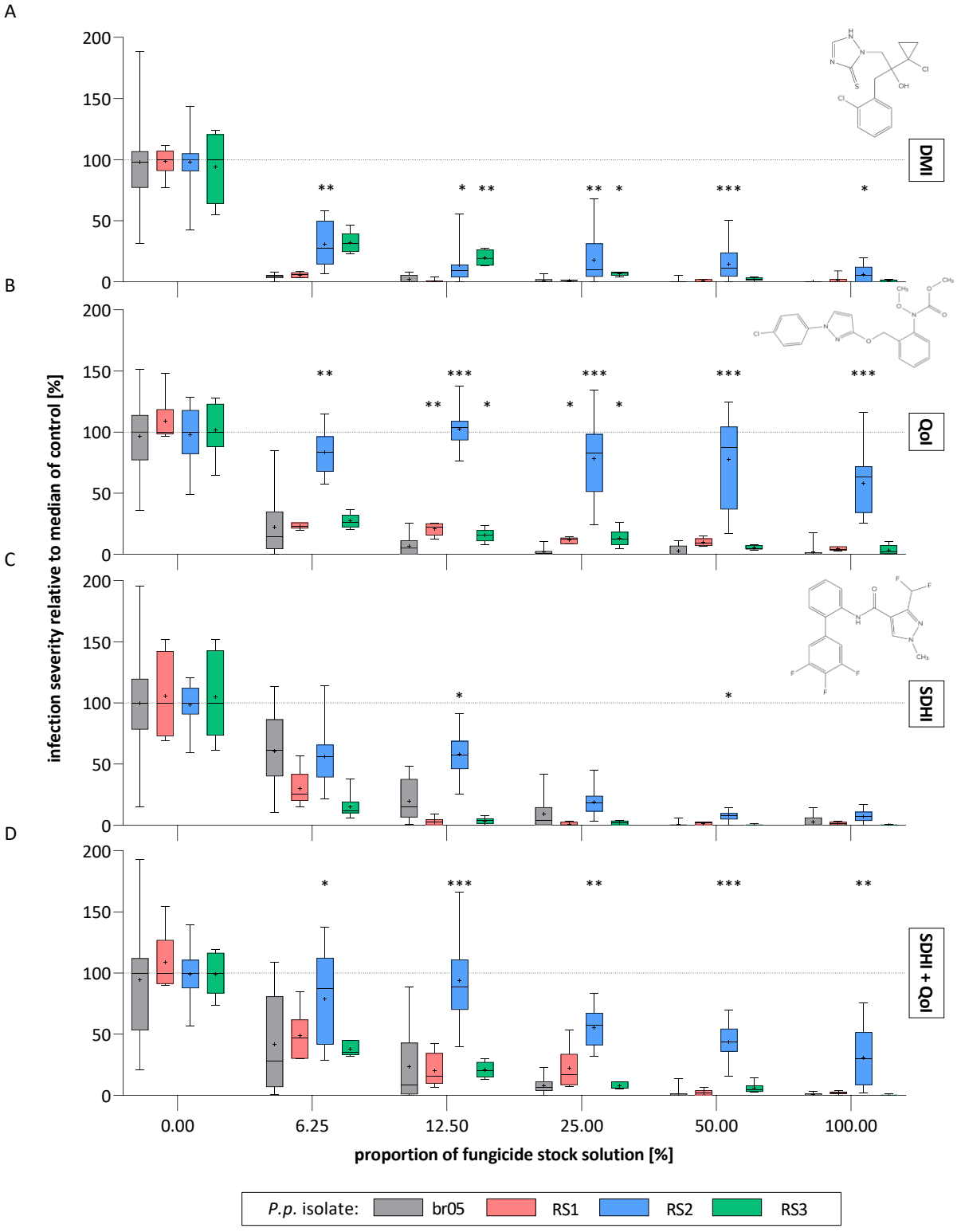

Figure 3. *P. pachyrhizi* isolate RS2 is less sensitive to three major fungicide classes. The reference *P. pachyrhizi* isolate br05 and three isolates (RS1–RS3) were tested for their sensitivity to different fungicide classes. Primary trifolia of three-week-old soybean plants were spray-treated with commercial fungicides of indicated classes 24 h before inoculation with *P. pachyrhizi* spores of isolate br05 (grey), RS1 (red), RS2 (blue), or RS3 (green). For inoculation, 1 mg/mL of uredospores were suspended in ddH_2O supplemented with 0.01 % Tween-20 (v/v). For **de**methylation **i**nhibitors (**DMI**), the commercial fungicide Proline® (active substance: prothioconazole; structure shown in A) was used in a stock concentration of 80 µL/L (**A**).

For **q**uinone **o**utside **i**nhibitors (**QoI**), the commercial fungicide F500® (active substance: pyraclostrobin; structure shown in B) was used in a stock concentration of 0.5 g/L (**B**). For **s**uccinate **de**i**h**ydrogenase **i**nhibitors (**SDHI**), the commercial fungicide Imtrex® (active substance: fluxapyroxad; structure shown in C) was used in a stock concentration of 500 µL/L (**C**). For the combination of **SDHI** and **QoI**, the commercial fungicide Orkestra® (active substances fluxapyroxad and pyraclostrobin) was used in a stock solution of 62.5 µL/L (**D**). After 8-12 days, infection severity was evaluated by scanning the treated leaflets and calculating the diseased area using the software Assess 2.0. The infection severity was calculated relative to the median of the control of each isolate. For RS1 and RS3, data were obtained from 6 leaflets in one experiment with two plants per treatment. Data of RS2- and br05-inoculated plants were acquired from 18 leaflets of three individual experiments with two plants per treatment. Asterisks indicate significant differences in the infection severity of RS1-RS3 compared to the infection severity of the respective br05 treatment based on the Kruskal-Wallis test of multiple comparisons ($p^* \leq 0.03$, $p^{**} \leq 0.002$, $p^{***} \leq 0.0001$). Experiments were performed by Alina Maas (master thesis within the scope of this work).

In case of Orkestra® pretreatment, the inoculation with RS2 led to the strongest increase in infection severity compared to br05 (Figure 3D). At 100 % of the Orkestra®-SL, inoculation with RS2 led to over 30 % infection severity, which is significantly higher than for the other isolates, as plants inoculated with br05, RS1, and RS3 showed almost no symptoms (Figure 3D).

Taken together, plants inoculated with RS2 suffered a significantly stronger infection severity compared to inoculation with br05, regardless of the fungicide used for pretreatment. RS2 showed reduced sensitivity to all three fungicide classes tested (Figure 3) and tolerates the combination of QoI and SDHI when challenged with both fungicide classes at the same time. Because RS2 is less sensitive to the fungicide classes currently used for SBR control, it was selected for further experiments as a multisite-tolerant fungal isolate.

This fungicide tolerance makes RS2 a valuable tool to investigate whether small natural compounds can be used for sustainable SBR control. Our research group has previously shown that coumarins, particularly scopoletin and ayapin, effectively protect soybean against the *P. pachyrhizi* isolate br05 (Beesley et al., 2023; Beyer, 2019; Beyer et al., 2019; Schwinges, 2019). To determine whether this also holds true for RS2, the spore germination of this isolate was elucidated in the presence of scopoletin and ayapin.

For this, fresh uredospores of *P. pachyrhizi* isolates RS2 or br05 (for comparison) were incubated either in double distilled (dd)H_2O supplemented with Tween-20 (v/v, water control), in ddH_2O containing 0.1 % dimethyl sulfoxide (DMSO, solvent control), or in ddH_2O containing 0.1 % DMSO and 25 µM, 50 µM, 75 µM, or 100 µM scopoletin or ayapin. Three hours after incubation, spore germination was evaluated by counting germinated and non-germinated spores (Figure 4A). Scopoletin at 25 µM did not significantly reduce spore germination of either isolate. In contrast, at 50 µM scopoletin and 25 µM of ayapin, the spore germination rate of both tested isolates was significantly reduced by >50 %. Finally, at a concentration of 100 µM of both coumarins, the germination rate of both isolates was significantly reduced to < 10 %. Notably, 100 µM ayapin was

sufficient to completely inhibit the spore germination of isolate RS2, while br05 spores germinated up to a mean of 2.5 % in the presence of 100 µM ayapin (Figure 4A).

To test whether this effect also occurs *in planta*, soybean plants were co-inoculated with coumarins and *P. pachyrhizi* spores of isolate RS2 or br05. A suspension of 1 mg/mL uredospores and either 250 or 500 µM scopoletin or ayapin was supplemented with Tween-20 and sprayed on the first fully developed trifolium of soybean plants. The experimental setup included two controls: an aqueous suspension containing only spores and Tween-20, and a second suspension additionally supplemented with 0.1 % DMSO. Figure 4 B shows an example of the effect of ayapin on the infection severity caused by both *P. pachyrhizi* isolates. The ddH_2O-treated leaves showed the characteristic phenotype of the emerging rust pustules (Figure 4B). For the leaves that were co-inoculated with 500 µM ayapin, only a few isolated pustules were detected for either isolate (Figure 4B). Yet, no prominent differences were observed between the symptoms caused by the two *P. pachyrhizi* isolates.

Quantification of infection severity revealed that both scopoletin and ayapin significantly reduced the infection severity caused by br05 and RS2 (Figure 4C). For plants co-inoculated with br05 and 250 µM of either scopoletin or ayapin, the median infection severity was slightly higher (median ~ 45 %) than for plants co-inoculated with RS2 and the same coumarin concentration (median ~ 30 %). Co-inoculation with 500 µM ayapin caused lower infection severity than co-inoculation with 500 µM scopoletin, regardless of the isolate used for infection. Interestingly, the infection severity of soybean plants co-inoculated with RS2 and 0.1 % DMSO was slightly decreased compared to br05 (Figure 4C).

Overall, both tested coumarins seemed to provide protection against br05 but also against the fungicide tolerant isolate RS2. This makes potential usage of these coumarins for crop protection, whether as single use or as supplement for existing products, highly interesting.

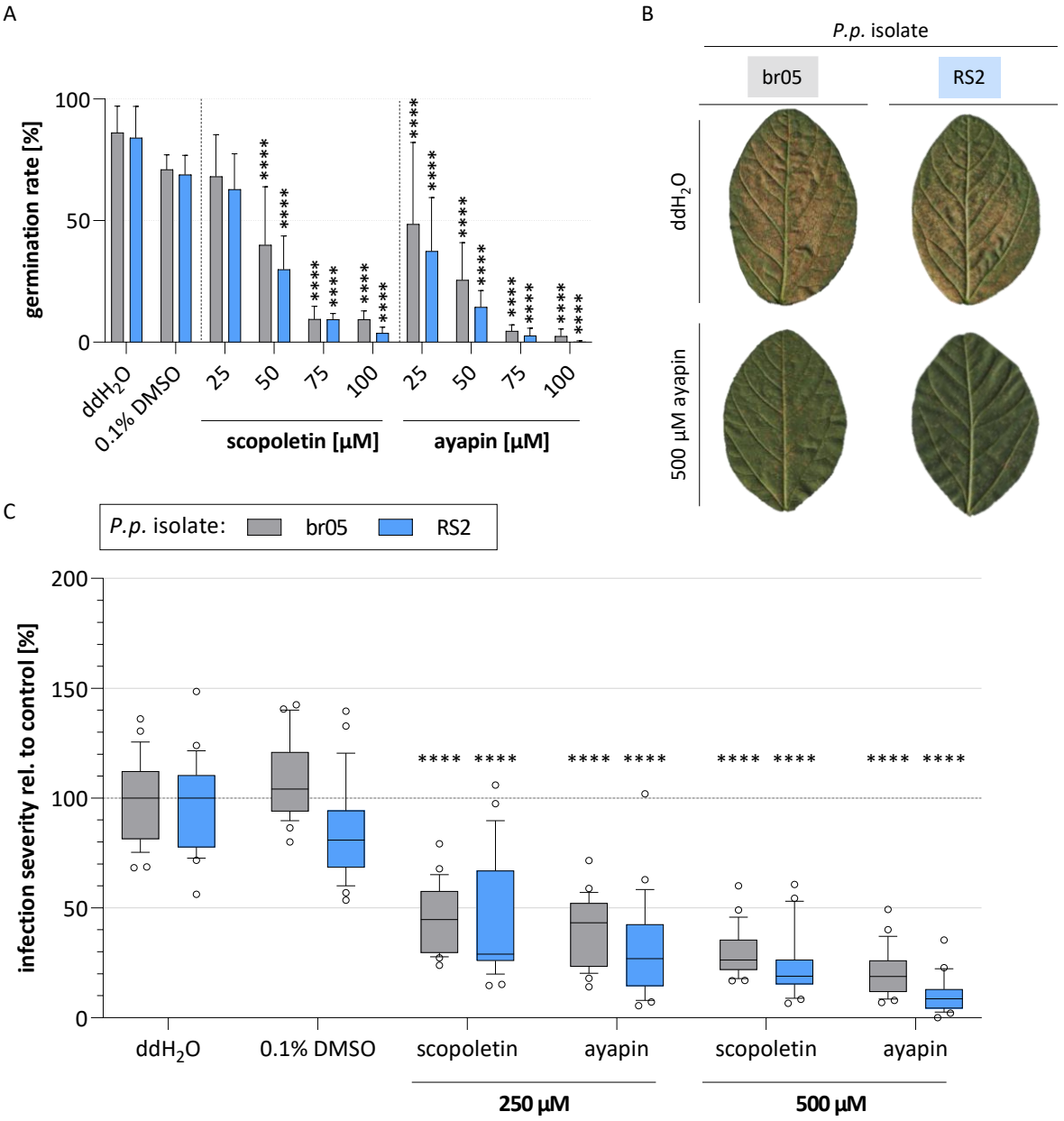

Figure 4. Scopoletin and ayapin inhibit fungal spore germination and protect soybean from the fungicide tolerant *P. pachyrhizi* isolate RS2 in a dose dependent manner. Germination rates of *P. pachyrhizi* isolate br05 (grey) or RS2 (blue) uredospore suspensions were determined microscopically three hours after incubation under rotation. Spore suspensions (1 mg/mL uredospores in ddH_2O with 0.01 % Tween-20 (v/v)) were supplemented with scopoletin or ayapin at the indicated concentrations, or with 0.1% DMSO (solvent control). (**A**). Primary trifolia of three-week-old soybean plants were inoculated with *P. pachyrhizi* spores of isolate br05 or RS2, to test the effect of coumarins against the two isolates *in planta*. 1 mg/mL of uredospores were suspended in 250 or 500 µM scopoletin or ayapin, as indicated. The suspensions were supplemented with 0.01 % Tween-20 prior to spray inoculation. 8-12 days post-co-inoculation, the disease severity was evaluated by assessing the infected leaf area, as exemplified in B. The infected leaf area was calculated relative to the median of the ddH_2O-control treatment (**C**). Box plots show the median of each treatment as black bar and outliers outside of 10-90 % as hollow dots. Data consists of three independent experiments with three plants per treatment (a total of 27 leaflets). Asterisks indicate significant differences of the treatments to the respective control of each isolate according to Dunnett's multiple comparisons test with **** ≙ $p \leq 0.0001$. Note that RS2 – the isolate that was insensitive to tested fungicides – is affected by scopoletin and ayapin in the same severity as isolate br05. Experiments were performed by Alina Maas (master thesis within the scope of this work).

2.2. Evaluating ayapin biosynthesis in different sunflower genotypes

The two coumarins scopoletin and ayapin showed a protective effect against the fungicide tolerant *P. pachyrhizi* isolate RS2 (Figure 4). Hence, those coumarins might be a useful tool in cases where currently used, conventional fungicides lose their efficacy due to emerging insensitivities. To use these compounds for crop protection, they could be applied directly on respective plants. Alternatively, soybean production could make use of transgenic soybean plants that accumulate and secrete coumarins to the leaf surface, mimicking the sunflower phylloplane. For scopoletin, this approach has already been followed by our research group (Beesley et al., 2023; Beyer et al., 2019). Engineering transgenic soybeans that accumulate scopoletin is feasible because the biosynthesis of scopoletin is well understood. This is not the case for ayapin, whose biosynthesis in plants has not yet been fully elucidated. In this thesis, ayapin biosynthesis in sunflower was investigated to gain a better understanding of this pathway.

To get insight of how the ability to synthesize coumarins is spread across *H. annuus*, 196 genotypes of this species were screened in a field trial in 2023 at the Agricultural Experimental Station Eckartsweier in Willstätt, Germany. The plants used for this field trial were kindly provided by Volker Hahn and grown and maintained by his team. Per genotype leaf discs were taken from three plants, and were floated on a $CuCl_2$ solution, which is known to elicit coumarin accumulation in sunflower (Gutierrez, 1995; Schwinges, 2019). The accumulation of coumarins and their secretion in the incubation solution was analyzed by high performance liquid chromatography (HPLC). For a scheme of the experimental set-up, see Figure 5A, and for a photo of the field of various genotypes, see Figure 5C. Figure 5B presents the distribution of secreted scopoletin and ayapin content.

The largest group of genotypes secreted both coumarins to moderate concentrations up to 1 µM of scopoletin/ayapin. A list with name, mean values, and standard deviation of each genotype can be found in Table S 1. The genotype that secreted the highest levels of scopoletin was RHA401, which, interestingly, also belonged to the group of genotypes that did not secrete ayapin. RHA857 also fell into this group; preliminary analyses in our research group had already suggested that this genotype is impaired in ayapin biosynthesis (Spencer, 2022). In contrast, genotypes HA852, SF_317 and RHA463 accumulated both coumarins to relatively high levels, while the genotypes SF_170 and HA393 belonged to a group that almost exclusively secreted ayapin (red dots, Figure 5B). By analyzing the different genotypes with an UV-lamp at night , I detected obvious visible differences in fluorescence quality as shown in Figure 5D. While genotype HA-R8 displayed green

fluorescence, HA393 fluoresced blue. Notably, HA-R8 belonged to the group that only accumulated scopoletin (Figure 5B).

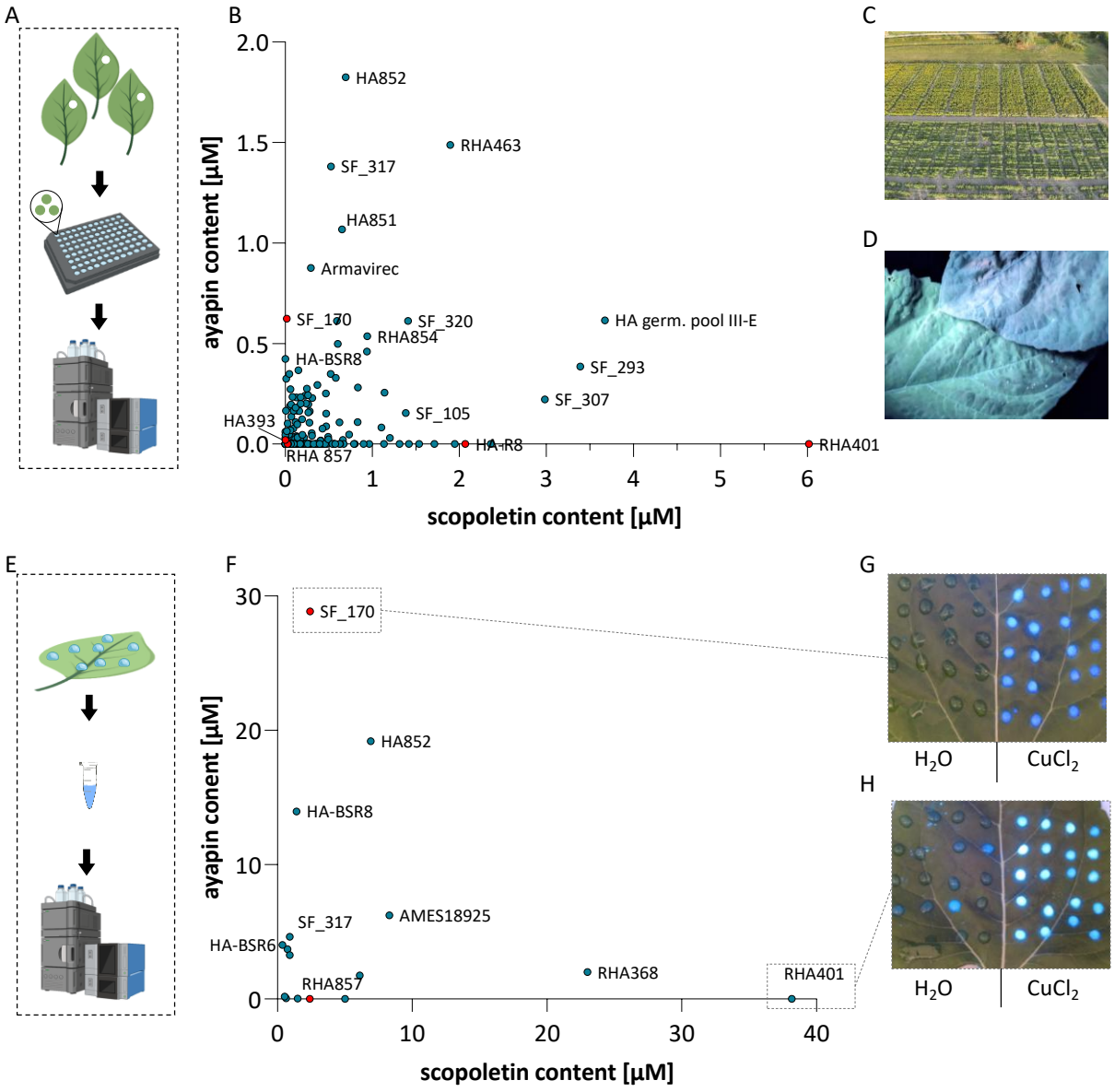

Figure 5. Genotypic variation in coumarin secretion and accumulation in sunflower in response to $CuCl_2$-elicitation. A subset (196 genotypes) of a sunflower core collection (growth stage V-6 to V-10) was sampled in a field trial conducted at the agricultural experimental station Eckartsweier in Willstätt, Germany. As depicted in **A**, three leaf discs per plant were floated on 300 µM $CuCl_2$ solution (200 µL per well) to elicit coumarin accumulation. Incubation time was approx. 48 h. Coumarin content was analyzed via HPLC. Dots represent the mean value of three individual plants per genotype. Red dots highlight genotypes that are further mentioned in this work (**B**). An aerial view of the field with the core collection sown in rows of 12 plants per genotype is shown in **C.** Under UV-light at night, qualitative differences in fluorescence of the adaxial leaf side were observed between genotypes; Ha-R8 (lower left corner) and Ha393 (upper right corner) are shown as examples. (**D**). Note that Ha-R8 did not secrete any ayapin, while HA393 did not secrete any scopoletin (red dots in **B**). A selection of 16 genotypes was further analyzed in the laboratory. As depicted in **E**, 20 µL-droplets of 300 µM $CuCl_2$ were placed on the adaxial leaf side. After 48 h of incubation, droplets were recollected, and the coumarin content was analyzed via HPLC. Dots represent the mean value of two individual plants per genotype. Red dots highlight the two genotypes that were selected for further analysis of the scopoletin/ayapin biosynthesis described in this work (**F**). UV-light revealed the coumarin accumulation in the droplets after $CuCl_2$-elicitation (right; **G**, **H**), compared to the water control (left; **G**, **H**). Here, the two genotypes SF_170 (**G**) and RHA401

(**H**) are shown as examples. Note that $CuCl_2$-droplets on the leaf surface of the SF_170 genotype fluoresce dark blue (**G**, right), while droplets placed on the RHA401 genotype fluoresce bright blue (**H**, right). The field trial (**A**-**D**) was done in cooperation with Volker Hahn and his team (Distribution of the work was as follows: Providing the cultivation area, sowing and maintaining the field was done by Hahn's team. The sampling was done by several members of the AG Conrath under my supervision. Analysis and further processing of the data was performed by me).

Based on the field data, I selected 16 sunflower genotypes for further evaluation in the laboratory and greenhouse. Plants were grown for 28 days before individual leaves were harvested and 20µL-droplets of $CuCl_2$ were transferred on the adaxial side of those leaves. The hydrophobic and hairy surface of sunflower leaves ensures that these droplets keep their integrity and can be recollected after 48 hours of incubation. Subsequently, the content of coumarins that accumulated in the droplets can be evaluated by HPLC. A scheme of the experimental set-up is shown in Figure 5E.

The volume of the droplets (20 µL) was a tenth of the volume used in the floating assay (200 µL). Thus, the total coumarin concentration was ~10-fold higher in the droplets than in the floating medium (compare Figure 5B and F). Still, the genotypes showed a similar distribution pattern of coumarin accumulation. RHA401 was strongly accumulating scopoletin but no ayapin in the droplets (Figure 5F). This resulted in bright, almost white fluorescing droplets on the leaf surface (Figure 5H). In this set-up, no genotype was exclusively accumulating ayapin; however, genotypes such as SF_170 or HA-BSR6 accumulated ~10-fold more ayapin than scopoletin (Figure 5F). These droplets fluoresced dark blue, as exemplarily shown for SF_170 in Figure 5G. Based on these findings, I decided that SF_170 – a genotype that apparently was highly efficient in ayapin biosynthesis and RHA401 – a genotype impaired in ayapin biosynthesis, but highly productive in scopoletin accumulation - would be interesting to compare in further analysis. Unfortunately, at this time, I did not have enough seeds of RHA401 available to ensure a proper experimental set-up, thus I chose to proceed with RHA857 - a genotype also impaired in ayapin biosynthesis.

To further assess the differences between RHA857 and SF_170 regarding their ability to biosynthesize coumarins, leaf discs of at least four-week-old sunflower plants were incubated on $CuCl_2$ to elucidate coumarin accumulation. This experimental set-up enabled not only the analysis of secreted coumarins over time, but also the coumarin content in the leaf discs at the same time points. Frozen aliquots of leaf tissue could additionally be used for transcriptional analysis.

At 24 h time points over four days, leaf discs and their floating medium were separately collected. The coumarin content of leaf-disc extracts and the floating medium were subsequently subjected to HPLC analysis for coumarins (Figure 6). The coumarin content in the leaf extracts was normalized to µg/g fresh weight (FW). As the area of one g of sunflower leaves roughly corresponds to half a

square decimeter, the content of the floating medium was normalized to µg/½ (dm^2). This enabled comparison of the coumarin content in leaves to that in the floating medium.

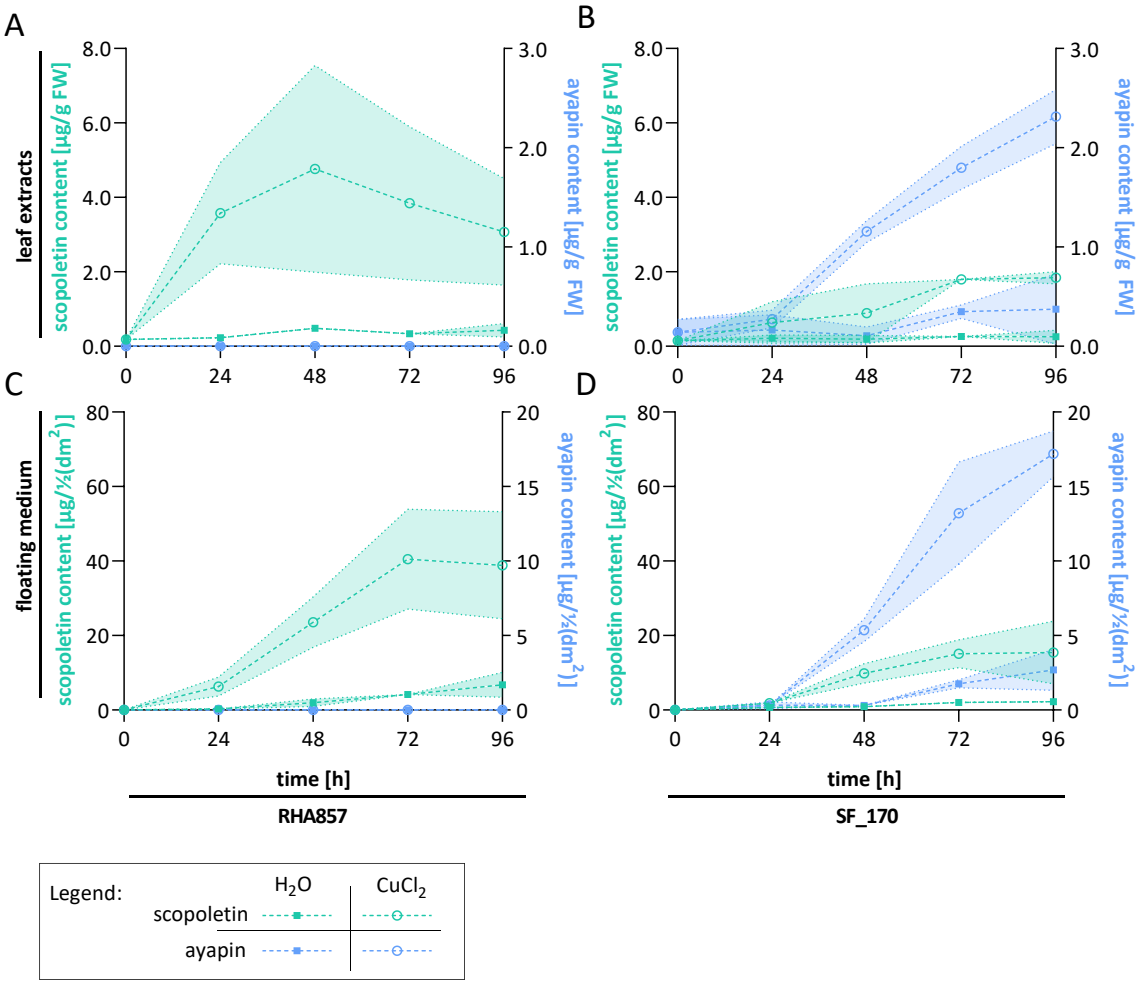

Figure 6. Sunflower genotypes RHA857 and SF_170 differ in their coumarin accumulation and secretion upon $CuCl_2$-elicitation over time. Over the course of 96 h**,** leaf discs of four-week-old sunflower genotypes RHA857 (**A**, **C**) and SF_170 (**B**, **D**) were incubated on either ddH_2O (control, ■) or 300 µM $CuCl_2$ to elicit coumarin biosynthesis (○). The coumarin content of methanolic extracts of the leaf discs (**A**, **B**) and floating medium (**C**, **D**) harvested at the indicated time points was analyzed via HPLC. The scopoletin content (green) is plotted on the left y-axis, while the ayapin content (blue) is plotted on the right y-axis. Shades represent the range of two independent biological replicates. Note that only the SF_170 genotype accumulates and secretes ayapin over the course of 96 h. Experiments were performed by Alina Maas (master thesis within the scope of this work).

In the leaf extracts of RHA857, the scopoletin content peaked at 48 h of $CuCl_2$-induction and slightly decreased afterwards (Figure 6A, left y-axis). No ayapin was detected in this genotype (Figure 6A, right y-axis). Over 72 h, the scopoletin content in the floating medium of RHA857 steadily rose before reaching a plateau from 72 h to 96 h. Again, no ayapin could be detected (Figure 6C). In contrast, ayapin content increased with incubation time in SF_170 leaf discs and floating medium (Figure 6B/D, blue). Scopoletin concentration in the SF_170 extracts and floating medium

was about half of the levels in the respective RHA857 samples. In total, the coumarin content that was secreted to the floating medium was higher by a magnitude of ten compared to the coumarin content from extracted leaf tissue (Figure 6).

Hence, it seemed that a large proportion of the synthesized coumarins were transported to the leaf surface rather than being accumulated in the leaf tissue. Also, the lower levels of scopoletin in the samples from SF_170 compared to RHA857 suggested that scopoletin was presumably converted to ayapin. As it is unknown whether scopoletin is a direct precursor of ayapin, I wanted to further understand the possible biosynthetic connection between the two coumarins. As the structure of scopoletin suggests that a methylenedioxy-bridge-formation is the missing step to ayapin (Figure 7A), I decided to expose sunflower leaves to concentrations of scopoletin that exceeded physiological levels. This was done by floating leaf discs on an aqueous solution containing 500 µM scopoletin. Simultaneously, droplets containing a $CuCl_2$-solution were placed on the surface of the floating leaf discs to enhance coumarin biosynthesis. A scheme of the experimental set-up is shown in Figure 7B. As in previous experiments, the response of the two genotypes RHA857 and SF_170 was compared. 48 h after incubation, the droplets were recollected from the leaf surface, and their coumarin content was quantified. Even when floating on 500 µM scopoletin, no ayapin was detected in RHA857 droplets (Figure 7C). However, scopoletin content was ~ 100-fold increased in the droplets from the RHA857-leaf-discs that floated on scopoletin in contrast to the ones floating on water, regardless of $CuCl_2$-induction. This data implied (i) that sunflower leaf discs, which float on coumarin-containing media, are indeed capable of taking up the coumarins and subsequently delivering the molecules to the leaf surface via their endogenous transport mechanism, and (ii) that RHA857 seems to be impaired in ayapin biosynthesis.

In contrast, ayapin was detected in droplets taken from leaf discs of SF_170. While $CuCl_2$ droplets on the leaf discs floating on water showed a slight increase of ayapin compared to the water droplets, the increase in the $CuCl_2$ droplets placed on the leaf discs floating on 500 µM scopoletin was 10-fold higher compared to the water droplets of the same leaf discs (Figure 7C). Based on this data, scopoletin appears to be directly linked to ayapin biosynthesis, as higher levels of scopoletin associate with increased ayapin accumulation. However, these data also suggest that additional regulatory changes within the leaf tissue are required, as high levels of scopoletin alone were insufficient to increase the ayapin content markedly.

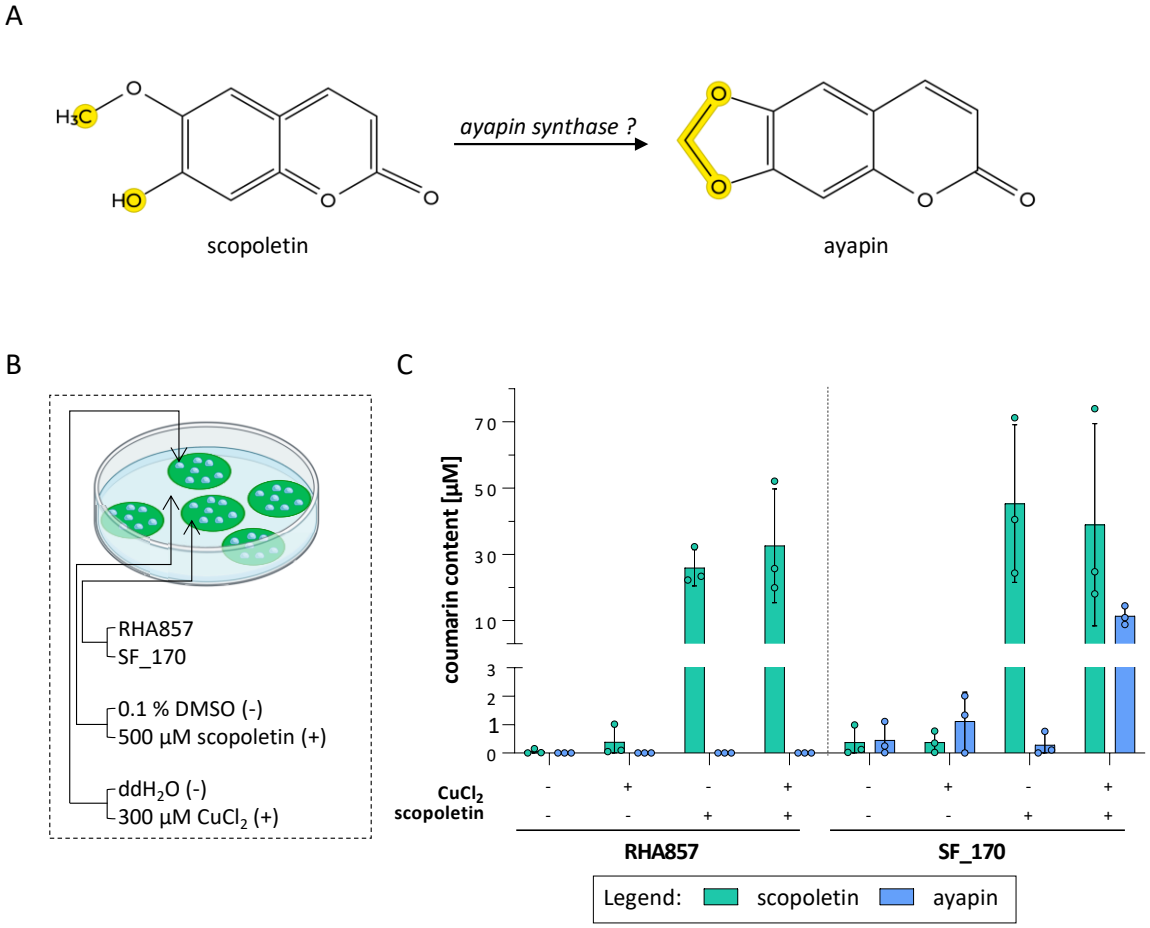

Figure 7. $CuCl_2$-induced ayapin biosynthesis and secretion from sunflower leaf discs is augmented by scopoletin feeding. Panel **A** depicts the proposed one-step enzymatic conversion of scopoletin to ayapin, in which a methylenedioxy bridge is formed between the terminal carbon atom and the hydroxy group. To evaluate whether sunflower leaves convert scopoletin to ayapin, leaf discs of the sunflower genotypes RHA857 (left) and SF_170 (right) were incubated floating on either 0.1 % DMSO (-) or a 500 µM scopoletin (+) solution that contained 0.1 % DMSO. Additionally, ddH_2O-droplets (-; as control) or $CuCl_2$-droplets (+; to induce coumarin biosynthesis) were placed adaxially on the leaf surface (**B**). After incubation of 48 h, droplets were recollected, pooled per treatment, and the scopoletin (green) and ayapin (blue) content was measured via HPLC (**C**). Error bars depict the standard deviation of three replicates with pooled leaf discs of three plants per genotype. Note that ayapin content increases only in the SF_170-samples that were elicited with $CuCl_2$ and incubated on scopoletin. Experiments were performed by Anna Kleineberg (master thesis within the scope of this work).

2.3. Unravelling the genetic basis of ayapin biosynthesis

To identify potential genes involved in ayapin biosynthesis, I used two sunflower genotypes with contrasting responses to $CuCl_2$: SF_170, which reproducibly accumulated ayapin upon $CuCl_2$ treatment, and RHA857, which responded to $CuCl_2$ but was impaired in ayapin accumulation. Previous data indicated that at least one gene required for ayapin biosynthesis is induced by $CuCl_2$-treatment in SF_170 leaves. Therefore, transcriptome analyses were performed on leaf samples from stressed and unstressed SF_170 plants, and $CuCl_2$-induced transcriptional changes were compared between SF_170 and RHA857 to identify candidate genes for ayapin biosynthesis that

are either not induced or carry loss-of-function amino acid substitutions in RHA857. However, it was important to ensure that the leaf tissue used for RNA isolation for the transcriptome analysis was as homogeneous as possible, differing only in the plant's response to $CuCl_2$. Thus, droplets that either contained H_2O or $CuCl_2$ were placed in close proximity to each other on the same leaf of the adequate sunflower genotype. After 48 h of incubation, the characteristic blue fluorescence of the sunflower coumarins was visible only in the $CuCl_2$-droplets (Figure 8A). A time series of pictures taken every six hours also vividly illustrated how the fluorescence starts to emerge over time and subsequently increases (Figure S 1). These droplets were recollected afterwards, and HPLC analysis revealed that the scopoletin content was significantly increased in the $CuCl_2$-droplets for both genotypes, while the ayapin content only increased significantly in $CuCl_2$-droplets placed on the leaf surface of SF_170 (Figure 8B). Again, no ayapin could be detected in droplets placed on RHA857. This data suggested that I succeeded in enforcing a local induction of coumarin secretion in leaves exposed to $CuCl_2$-droplets.

Thus, only the plant material directly beneath the droplets was excised after the droplets were collected, as depicted in Figure 8C. Leaf discs from the same treatment were pooled prior to RNA isolation. Preliminary quantitative real-time polymerase chain reaction (qRT-PCR) analysis of RHA857 plant material showed that expression of *HaF6'H1* – the key enzyme in scopoletin biosynthesis – was induced only in the leaf material beneath the $CuCl_2$-droplets, but not in the leaf tissue beneath the water droplets (Figure S 2). This supported the assumption that the leaves were very locally induced by this method. RNA of three replicates of genotypes RHA857 and SF_170 and treatment with H_2O or $CuCl_2$ was isolated and checked to meet the quality requirements for total transcriptome analysis.

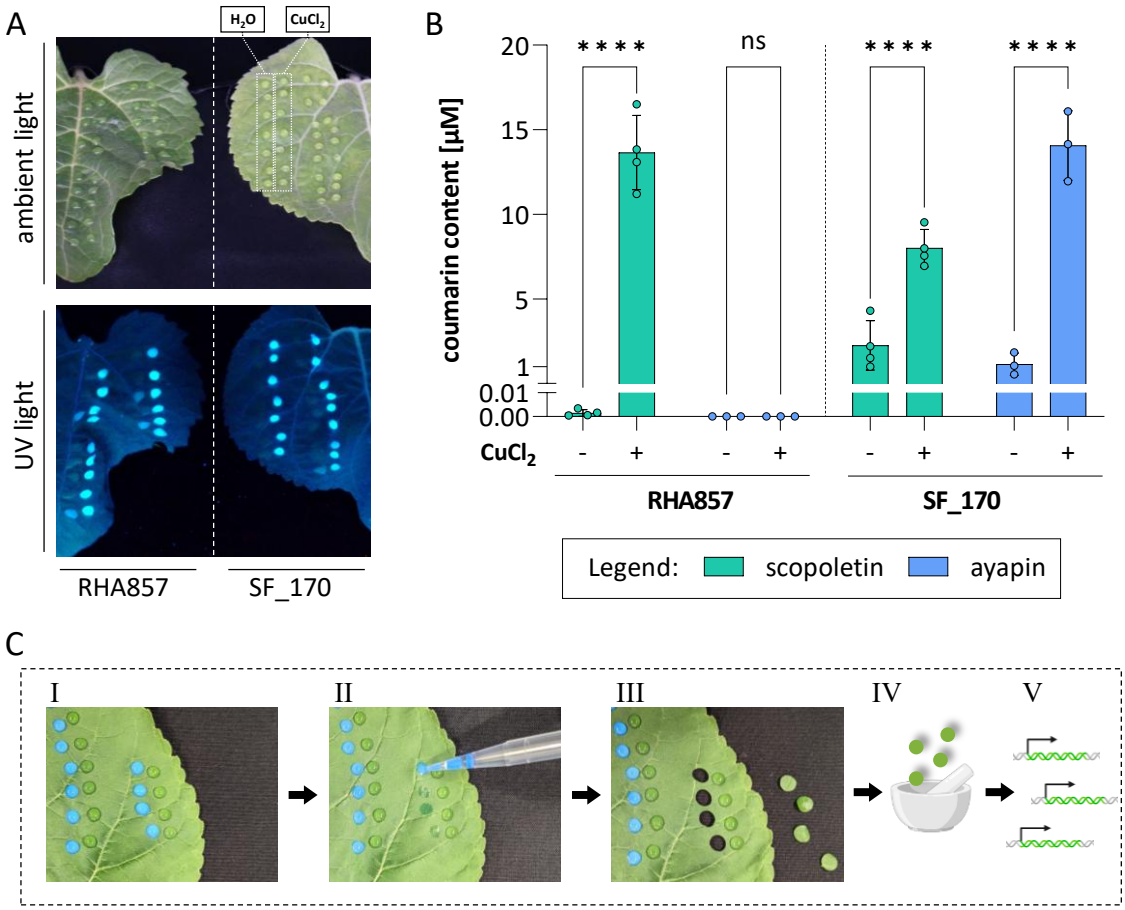

Figure 8. Local induction of coumarin biosynthesis and secretion from sunflower leaves by $CuCl_2$-droplet application. ddH_2O- and $CuCl_2$-droplets were placed on the leaf surface of four-week-old sunflowers (genotype RHA857 (l.) and SF_170 (r.)) in close proximity to each other (left line of each row of droplet pairs consists of ddH_2O, the right line consists of 300 µM $CuCl_2$ solution, as indicated with white boxes). To visualize coumarin accumulation, pictures were taken while the leaves were exposed to UV light after 48 h of incubation. Note that only the respective $CuCl_2$-droplets fluoresce bright blue, while water droplets remain mostly without fluorescence (**A**). Droplets were collected and pooled for each treatment. The coumarin content was quantified via HPLC analysis for samples that were prepared for a transcriptome analysis of the two indicated sunflower genotypes (**B**). Scopoletin (green) and ayapin (blue) content of at least three independent biological replicates is shown. Bars indicate the mean, with the standard deviation indicated by error bars, while dots represent single data points. Asterisks show significant differences between water and $CuCl_2$-treatments for each genotype ($p < 0.0001$, according to Šídák's multiple comparisons test). ns = not significant. To conduct a transcriptome analysis, only leaf material directly beneath the droplets was excised and pooled per genotype and treatment. This experimental procedure is depicted in **C**. Experiments were performed by Alina Maas (master thesis within the scope of this work).

The transcriptome analysis, including RNA library preparation and sequencing, was performed as a custom service by CeGaT (Tübingen, Germany). Principal component analysis (PCA) was carried out on the gene expression data. Genes with a read count of at least two were retained and grouped into four expression clusters (Figure 9). The first principal component, responsible for 87 % of differential gene expression, can be traced to the genotype. RHA857 samples (green) clustered on the negative segment of the x-axis, while SF_170 samples (blue) clustered on the positive segment. The second principal component that separated the data sets can be traced back to the treatment. This was responsible for 9 % of data variation. Control samples (dark colors) clustered on the

positive segment of the y-axis, as stress-induced samples (light colors) clustered on the negative segment of the y-axis.

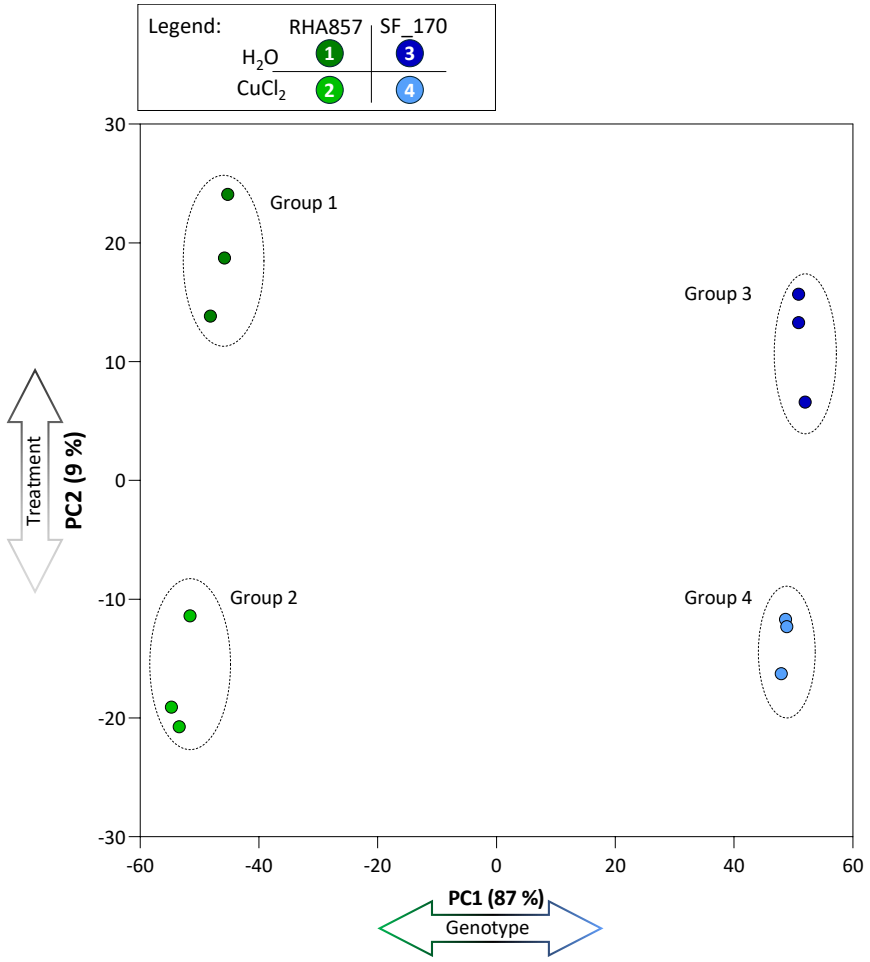

Figure 9. Variation of gene expression in two sunflower genotypes upon $CuCl_2$-induced stress. RNA from leaf discs of sunflower genotypes RHA857 and SF_170 was isolated and subjected to transcriptome analysis. Leaf discs were punched out from areas where ddH_2O- or $CuCl_2$-droplets had been placed for 48 h. Each treatment per genotype was replicated three times, resulting in a total of 12 samples for analysis, with each point in the PCA plot representing one RNA-seq sample. PCA was performed on normalized expression values of genes with at least two reads per sample and clustered the 12 samples into four groups, reflecting differences in genotype (PC1) and treatment (PC2). Group 1 consists of the three samples from the RHA857 that were incubated with the water control (dark green), while Group 2 consists of the RHA857 samples that were stressed by $CuCl_2$ treatment (light green). Groups 3 and 4 consist of the respective SF_170 samples (ddH_2O treatment = dark blue, $CuCl_2$ treatment = light blue).

Custom differential expression analysis (DEA) of the RNA-seq data was performed, comparing treatments within each genotype (group 2 vs. group 1; group 4 vs. group 3) and the $CuCl_2$-induced stress response between both genotypes (group 4 vs. group 2). I manually filtered the data set, retaining only genes with a base-mean value of at least 50 counts and a transcript length greater than 500 bp for further analysis. This yielded > 20,000 genes that were differentially expressed between those groups, shown as grey dots in the volcano plots in Figure 10A–C. Because this number of candidate genes was too high for meaningful, hypothesis-driven candidate selection, I used prior biochemical knowledge about ayapin formation to further restrict the data set. If

scopoletin is indeed the direct precursor of ayapin, its conversion would require formation of a methylenedioxy bridge (Figure 7A). Such methylenedioxy-bridge formations have so far been described exclusively for CYPs (Bourgaud et al., 2006; Liu et al., 2023; Mizutani and Sato, 2011; Ono et al., 2006; Schnabel et al., 2021). On this basis, I limited subsequent analyses to genes annotated as *CYP*s and treated these as primary candidates for a putative ayapin synthase (AySy).

For filtering *CYP* gene candidates, I employed the gene annotation of the reference genome HanXRQr1.0-SUNRISE provided by Badouin et al. (2017). DEA was restricted to CYP-annotated transcripts with a base mean ≥ 50. A *CYP* gene was regarded as differentially expressed when the adjusted *p*-value (p_{adj}) was ≤ 0.5; this deliberately relaxed p_{adj} threshold was chosen to avoid excluding potential candidates at this stage. Genes with a $\log_2$ fold change (l_2fc) > 0 and $p_{adj} \leq 0.5$ were considered induced, and genes with a $l_2fc < 0$ and $p_{adj} \leq 0.5$ were considered repressed. Volcano plots in Figure 10A and B highlight induced (red dots) and repressed (blue dots) *CYP* genes in comparisons of group 2 vs 1 and group 4 vs 3, respectively. Complete lists of differentially expressed *CYP* genes in these comparisons are provided in Table S 9 and Table S 10.

To identify candidate genes for the putative AySy, I focused on *CYP* genes that fulfilled two criteria: (i) they were induced by $CuCl_2$ in SF_170 (4 vs 3), and (ii) they were more strongly expressed in stressed SF_170 than in stressed RHA857 (4 vs 2). Applying criterion (i) yielded 33 CYP genes that were upregulated in SF_170 in response to $CuCl_2$ (Figure 10D, 4 vs 3). Applying criterion (ii), using the same p_{adj} and l_2fc cut-offs, identified 32 CYP genes that were more highly expressed in stressed SF_170 than in stressed RHA857 (Figure 10D, 4 vs 2; Table S11). The intersection of these two sets comprised 11 CYP genes (3 + 8 in Figure 10D; Table 2), which were considered primary AySy candidates. For example, gene *HanXRQChr04g0106751* is upregulated in both comparisons (Figure 10 B/C), and was thus included as an AySy candidate (Table 2).

The expression pattern of these 11 *CYP* genes was validated via qRT-PCR in samples of sunflower leaf discs that were incubated on $CuCl_2$ over time (Figure S 4). Since HaAySy3/5/7/9 were not (differentially) expressed in sunflower samples that were induced with $CuCl_2$ (Figure S 4), they were disregarded. The remaining seven candidates *HaAySy1/2/4/8/10/11/12* (Table 2) were further taken into account.

In addition, I included two further *CYP* genes that did not fully meet these criteria but were of particular interest. HaAySy6 did not pass the p_{adj} threshold in the comparison 4 vs 2 ($p_{adj} = 0.65$), but was retained because it belongs to the same CYP family as the SiCYP that catalyzes methylenedioxy-bridge formation in sesame (Ono et al., 2006). HaAySy14 did not fulfil the $l_2fc > 0$ criterion in the comparison 4 vs 3 ($l_2fc = -0.37$), but was selected because it was induced in two of

the three SF_170 replicates under $CuCl_2$ and showed no detectable expression in RHA857 (Table 2). The same pattern could be confirmed by qRT-PCR with different samples (Figure S 4).

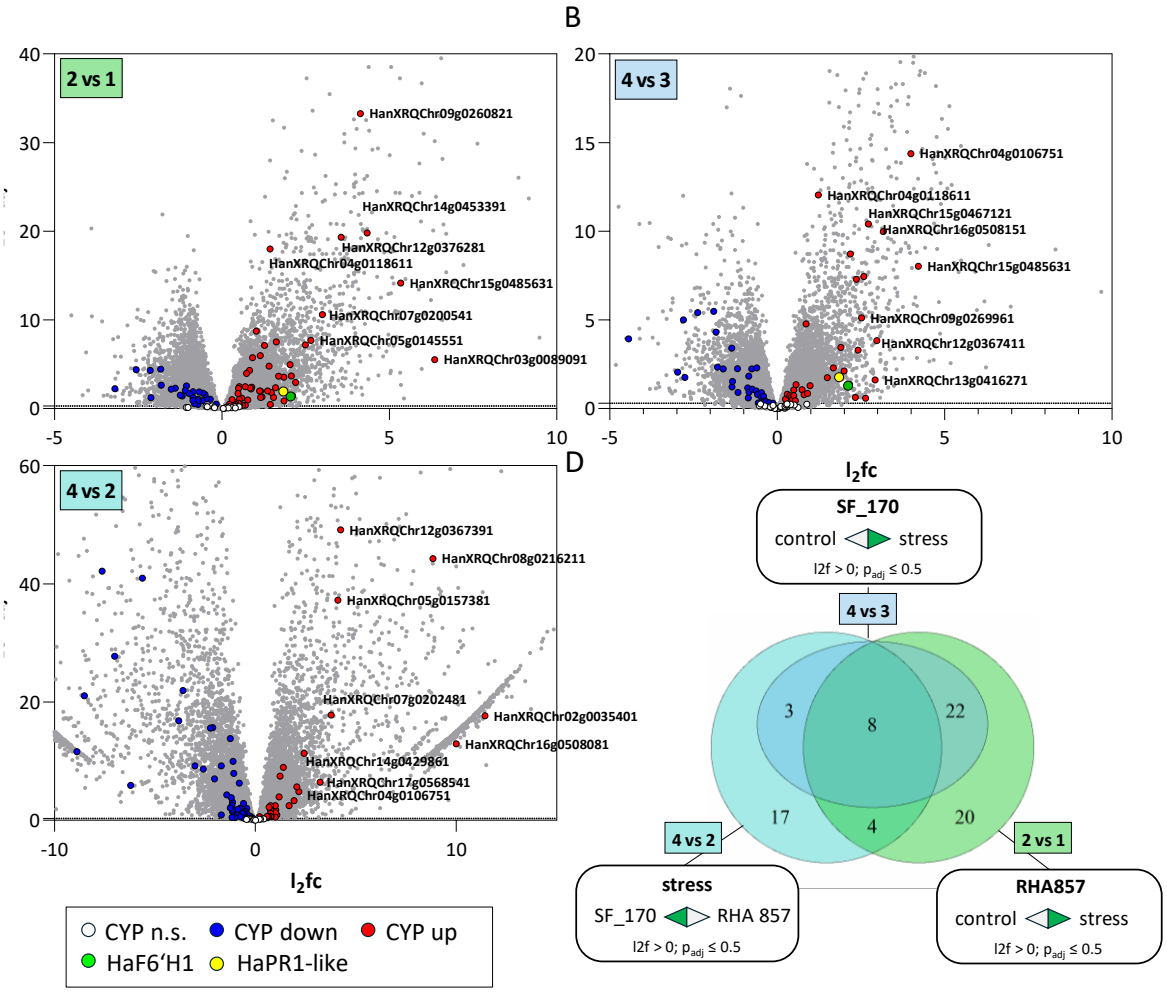

Figure 10. Transcriptome analysis reveals differential elicitor-induced expression of *CYP* genes in sunflower genotypes with contrasting ayapin biosynthesis capacities Transcriptome data of sunflower genotypes RHA857 and SF_170 in control and stress conditions were analyzed regarding the differential expression between the following groups: Group1: Control-treatment RHA857; Group2: Stress-treatment RHA857; Group3: Control-treatment SF_170; Group4: Stress-treatment SF_170. **A** shows differentially expressed genes of RHA857 after stress-treatment *versus* control treatment (2 vs 1). **B** shows the respective comparison of SF_170 samples. **C** shows differentially expressed genes in stressed SF_170 samples *versus* stressed RHA8587 samples (4 vs 2). Grey dots represent transcripts with a base mean value over 50 (**A-C**). Genes annotated as *CYP* are highlighted in blue when they are significantly ($p_{adj} \leq 0.5$) repressed ($l_2fc < 0$) and in red when they are significantly induced ($l_2fc > 0$; **A-C**). White dots are *CYP* genes that are not significantly regulated (n.s.). Green and yellow dots highlight the differential expression gene encoding the feruoyl-6'hydroxylase1 enzyme (*HaF6'H1*) and the pathogen-related1-like protein (*HaPR1-like*), respectively (**A**, **B**). Data presents the mean value of three replicates per group. Note that for **A-C** the negative $\log_{10}$ of the p_{adj}-value is plotted, thus significance is reached for $y = -\log_{10} 0.5 = 0.30103$, indicated by the grey dotted line. $lf_2c = \log_2$ fold-change; p_{adj} = adjusted *p*-value. The Venn diagram shows the number of *CYP* genes that are significantly ($p_{adj} \leq 0.5$) induced ($l_2fc > 0$) in each indicated group comparison (**D**). Note that 11 (3+8) CYPs are both, significantly upregulated in SF_170 samples under stress-conditions (4 vs 3), and upregulated in stressed SF_170 samples compared to stressed RHA857 (4 vs 2) samples.

To identify further candidates that might have been missed by relying solely on explicit "cytochrome P450" annotation, I manually screened genes whose functional annotation indicated CYP-like monooxygenases. Genes annotated as trans-cinnamate 4-monooxygenase, isoflavone 2-hydroxylase, flavonoid 3-monooxygenase, squalene monooxygenase, or geraniol 8-hydroxylase were also considered as candidate genes, because these enzymes belong to the CYP superfamily according to the InterPro database (Blum et al., 2025). Within this group, only HaAySy17, annotated as flavonoid 3-monooxygenase-like, was strongly upregulated in SF_170 and showed only very low read counts in the RHA857 samples, which was consistent with qRT-PCR analysis (Figure S 4).

Additionally, I compared the coding sequences of CYP and CYP-like monooxygenases that were induced in stressed SF_170 samples (4 vs 3) but were not more strongly expressed in SF_170 than in RHA857 under $CuCl_2$ treatment (4 vs 2) between the two genotypes. For this purpose, a variant calling analysis (VCA) was performed to detect SNPs in the respective reads relative to the reference genome.

However, a drawback of this strategy was that due to a lack of seeds from the SF_193 genotype, which was used to assemble the reference genome (Badouin et al., 2017), I could not determine whether the reference genotype is capable of synthesizing ayapin (note that this specific genotype was not among the 196 genotypes analyzed in this work). Thus, I had to consider two possible scenarios: The reference genotype can synthesize ayapin, in which case loss-of-function mutations in the coding sequence in RHA857 would be of interest; or the reference genotype cannot biosynthesize ayapin, in which case SF_170-specific coding mutations could represent gain-of-function changes. Consequently, SNPs in both genotypes were considered potentially relevant. This analysis resulted in two further candidates genes, *HaAySy16* and *HaAySy18*, which were upregulated in both genotypes but carried SF_170-specific coding SNPs predicted to result in 1 and 22 AA changes, respectively (Table 2).

Table 2. Putative ayapin synthases (AySy) identified by transcriptome analysis of sunflower genotypes RHA857 and SF_170. The Gene ID references to the database of heliagene.org. Annotation according to www.heliagene.org. Four groups of three replicates were compared; Group1:H_2O-treatment RHA857; Group2: $CuCl_2$-treatment RHA857; Group3: H_2O-treatment SF_170; Group4: $CuCl_2$-treatment SF_170. Here the log_2-fold-change and adjusted *p*-value (p_{adj}) of indicated group comparisons is shown for respective candidate genes. Reads of each candidate gene was checked for single gene polymorphisms (SNP) compared to the reference genome of SF_193. Occurring SNPs were checked for resulting amino acid (AA) changes in the respective coding sequence.

				4 vs 3		4 vs 2		2 vs 1		AA changes compared to reference	
candidate	**gene ID**	**description**	**base mean**	**l_2fc**	**p_{adj}**	**l_2fc**	**p_{adj}**	**l_2fc**	**p_{adj}**	**RHA857**	**SF_170**
HaAySy1	HanXRQChr04g0106751	cytochrome P450 93A3-like	689.7	3.99	4.2E-15	2.16	1.4E-05	1.60	4.5E-03	-	-
HaAySy2	HanXRQChr09g0269961	cytochrome P450 83B1-like	337.1	2.52	7.8E-06	0.66	2.5E-01	1.20	5.0E-02	5 AA changes	-
HaAySy4	HanXRQChr16g0504851	cytochrome P450 71A22-like	18342.8	2.16	4.3E-02	1.00	3.1E-01	2.11	3.5E-02	-	-
HaAySy6	HanXRQChr02g0040121	cytochrome P450 81E8-like	1070.5	1.90	3.5E-04	0.26	6.5E-01	1.85	2.8E-04	-	-
HaAySy8	HanXRQChr02g0035401	cytochrome P450 71A6-like	174.2	0.91	1.4E-01	11.43	2.1E-18	-1.06	7.4E-01	-	15 AA changes
HaAySy10	HanXRQChr17g0541311	cytochrome P450 CYP72A219-like	5431.8	0.50	9.0E-02	1.24	3.3E-08	1.27	7.2E-08	15 AA changes	-
HaAySy11	HanXRQChr05g0157381	cytochrome P450 CYP82D47-like	383.9	0.46	3.0E-01	4.11	5.6E-38	2.49	6.7E-08	7 AA changes	-
HaAySy12	HanXRQChr16g0527141	cytochrome P450 89A2-like	203.0	0.38	1.9E-01	0.20	2.5E-01	-0.86	1.2E-01	-	10 AA changes
HaAySy14	HanXRQChr08g0216211	cytochrome P450 CYP82D47-like	188.2	-0.37	7.1E-01	9.99	1.2E-13	1.45	3.4E-01	-	9 AA changes
HaAySy16	HanXRQChr07g0204401	cytochrome P450 CYP72A219-like	9669.5	0.42	0.23	-0.24	0.42	0.41	0.22	1 AA change	-
HaAySy17	HanXRQChr03g0088021	flavonoid 3 -monooxygenase-like	1220.7	3.75	1.5E-03	11.16	2.3E-22	3.48	1.0E-01	-	7 AA changes
HaAySy18	HanXRQChr17g0540991	cytochrome P450 CYP72A219-like	1107.6	2.72	4.0E-11	-2.04	9.8E-08	1.13	1.0E-02	22 AA changes	-

For testing the candidate genes listed in Table 2, these were transiently expressed in *N. benthamiana*. To do so, the coding sequence of each respective AySy was amplified via PCR from cDNA of SF_170 RNA samples and cloned in *E. coli*. Plasmids isolated from *E. coli* were then used to transform A. *tumefaciens*. Finally, *A. tumefaciens* harboring the respective coding sequence of the AySy candidates were infiltrated into *N. benthamiana* leaves. Since *N. benthamiana* does not biosynthesize scopoletin in notable concentrations, *A. tumefaciens* harboring *HaF6'H1* and *AtMYB72* were co-infiltrated. The *HaF6'H1* gene was chosen as it encodes one of the key enzymes in scopoletin biosynthesis. The transcription factor AtMYB72 can be used as a tool to boost the early phenylpropanoid pathway to ensure a sufficient precursor supply (Weber Böhlen et al., 2026). The biosynthetic pathway of this approach is briefly depicted in Figure 11A. After 72 hours of incubation, leaves were harvested, and methanolic extracts of the leaves analyzed via HPLC. Even though transiently transformed leaves accumulated high amounts of scopoletin (~5-30 µg/gFW), no ayapin was detected in leaves co-overexpressing the respective transgenes (Figure 11B). The expression of each *HaAySy* in the respective samples was validated via qRT-PCR (Figure S 3).

To further validate the candidate genes that were identified by transcriptome analysis of the two genotypes RHA857 and SF_170 (Table 2), and to potentially identify new candidates, I used a genetic approach by initiating a **b**ulked **s**egregant **a**nalysis (BSA) of the progeny from crossing events of the two genotypes. Thus, RHA857 (the genotype unable to synthesize ayapin) and SF_170 (the genotype that accumulates ayapin) were crossed in cooperation with Volker Hahn. For the crossing, RHA857 was used as the recipient, while the pollen was delivered by SF_170. The F_1-generation was selfed in a greenhouse at RWTH Aachen University. The F_2-generation was grown and maintained at the agricultural experimental station Eckartsweier (Willstätt, Germany) to enable the analysis of a potential segregating phenotype in large scale. For an theoretical overview see Figure 12A. Before selfing the F_1-generation, the progeny of the different crossing events was evaluated for their ability to accumulate and secrete ayapin. Five plants per crossing event were analyzed. For seven of nine events, ayapin was detected in samples of each tested plant (Figure 12B). This confirmed that the crossing was successful for those seven events, since sunflowers grown from seeds derived from RHA857 plants are naturally not able to accumulate ayapin (Figure 6, Figure 7, Figure 8).

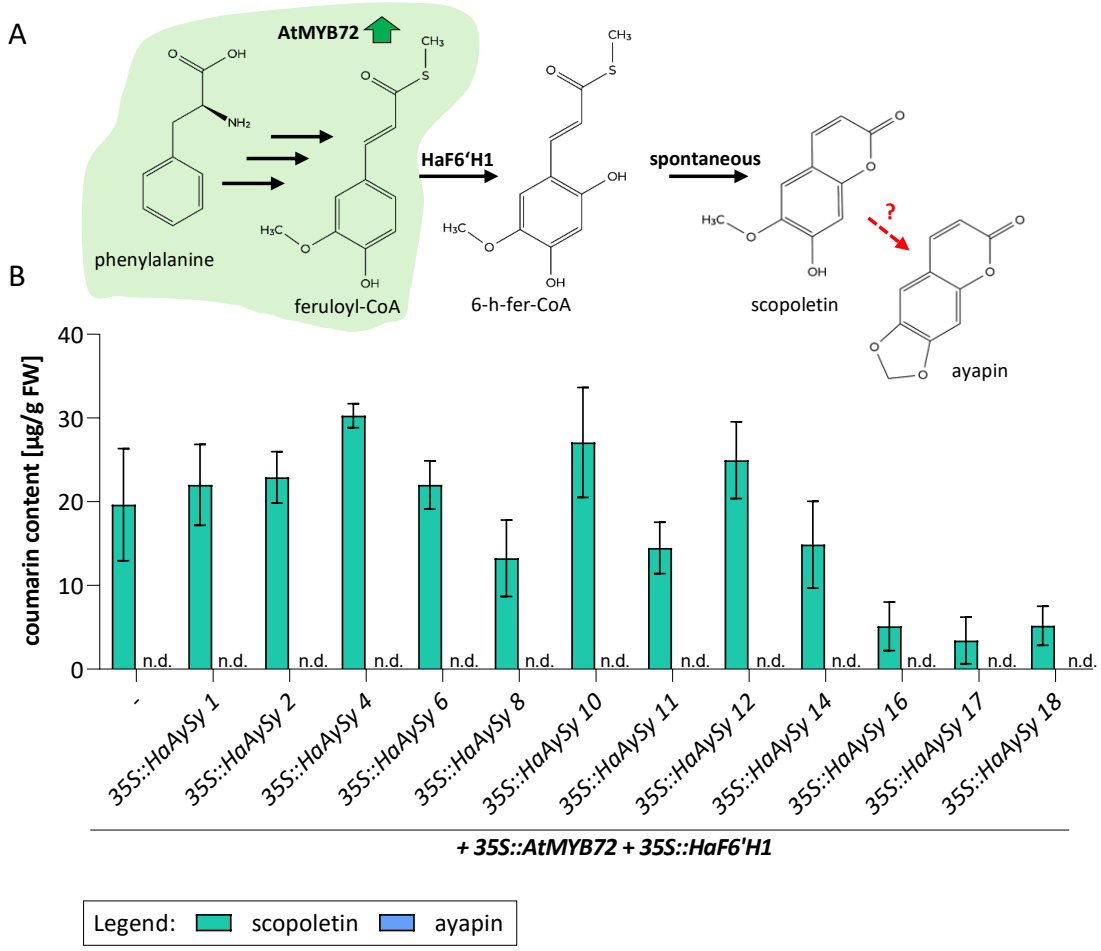

Figure 11. Overexpression of *HaAySy* candidates in *N. benthamiana* leaves does not lead to ayapin accumulation. Four-week-old *N. benthamiana* plants were transiently transformed with *A. tumefaciens* strains carrying overexpression vectors of the indicated genes. (**A**) Schematic representation of the coumarin biosynthetic pathway reconstituted in *N. benthamiana*. The Arabidopsis transcription factor AtMYB72 was included to boost the core PPP (green shading), while the enzyme HaF6'H1 catalyzes the conversion of feruloyl-CoA to 6-h-fer-CoA which is then spontaneously converted to scopoletin. The putative *HaAySy* candidates were co-overexpressed to potentially catalyze ayapin formation from scopoletin. Cultures of the respective *A. tumefaciens* strains were mixed prior to infiltration. To enhance transformation efficiency, an equal volume of an *A. tumefaciens* strain harboring a p19-encoding plasmid was added to each mixture. Transformed plants were cultivated for 72 h under long-day conditions before harvesting the leaf tissue. (**B**) Coumarins were extracted from frozen leaf material and analyzed via HPLC. Scopoletin (green) and ayapin (blue) content was calculated for 1 g fresh weight of the harvested leaf material and is displayed accordingly. "n.d." = non-detectable. Error bars indicate the standard deviation of three biological replicates. Experiments to test candidates HaAySy1-HaAySy14 were conducted by Anna Kleineberg (master thesis within the scope of this work).

The F_1-population was selfed to gain F_2-seeds that, according to Mendel's laws, should segregate in their capability to accumulate ayapin. However, at the time, it was unknown how the segregation pattern would present itself. For BSA, I chose to gather DNA of at least 50 plants that were impaired in ayapin biosynthesis and 50 plants that were not. To find the 50+ samples that would be impaired in ayapin biosynthesis, I aimed to sample at least 1000 plants. Therefore, seeds of the selfed F_1-offspring (Events #1-6, Figure 12B) were sown at the field trial site in Willstätt. From each plant four leaves were harvested and four leaf discs per leaf were excised. HPLC analysis of the floating

medium revealed strong variation across the samples. Some of them accumulated high amounts of ayapin, as shown for RxS_2 in Figure 12C (blue peak at retention time 11 min). Such samples were clearly accumulating and secreting ayapin. However, for samples that did not show such clear peak at the retention time of 11 min, chromatograms were evaluated manually. Adequate samples were considered a "no ayapin" sample only if there clearly was no peak seen, as shown in Figure 12D for sample RxS_1 (black line). All 365 samples that were analyzed accumulated scopoletin in the concentration range from 0.005 µM to 0.3 µM (Figure 12E). However, manual evaluation of samples with ayapin content below 0.01 µM (red shade, Figure 12E) revealed 77 samples for which I did not detect ayapin, as shown for sample RxS_1 (Figure 12D). In sum, 288 plants were found to accumulate ayapin, while 77 plants appeared to be impaired in ayapin biosynthesis (Figure 12F). This resulted in a segregation pattern of ~ 1:3.75, suggesting that the difference in the ability to synthesize ayapin may be influenced by a single gene or a gene cluster that follow the laws of simple Mendelian inheritance. From the group of 288 ayapin-biosynthesizing plants, 50 were randomly chosen for DNA extraction, while from the group of 77 ayapin-impaired plants, the 50 plants that accumulated the most scopoletin were chosen. DNA was isolated, equimolar pooled, and sent for custom BSA. In future work, the results of this analysis will provide the strongest and most promising foundation to clarify the biosynthesis of ayapin in plants.

Figure 12 (see the next page). Crossing of sunflower genotype RHA857 and SF_170 leads to segregants with differential $CuCl_2$-induced ayapin accumulation capacity. For BSA, the two sunflower genotypes RHA857 and SF_170 were crossed by Volker Hahn. As depicted in **A**, RHA857 is impaired in ayapin biosynthesis as represented by a green floral head and the filled, tip-down rectangle. In contrast, SF_170 can biosynthesize ayapin, as represented by a blue floral head and the hollow, tip-up rectangle. The seeds of the crossing events were sown in a greenhouse at the University of Aachen and five four-week-old plants per event were elicited by placing $CuCl_2$-droplets on the leaf surface. After 48 h of incubation, the droplets were harvested and their coumarin content determined by HPLC. **B** shows the ayapin/scopoletin ratio for each sampled plant per event represented as dots, while the floating bar shows the min to max range. Note that for crossing events 1-6 and 8, all plants were able to secrete ayapin into the droplet. Those plants were selfed in the greenhouse. In 2025, T_2-seeds of event 1-6 were randomly sown and maintained by the Hahn team in Willstätt. In a field trial ~1000 F_2-segregants were randomly selected for further processing. Therefore, eight leaf discs of those plants were punched out and separately incubated in 96-well plates filled with 200 µL of a 300 µM $CuCl_2$ solution (Eight further leaf discs were harvested and frozen in dry ice for later DNA extraction). ~48 h after incubation, the $CuCl_2$ floating medium was harvested, pooled for each plant, and analyzed for scopoletin and ayapin content via HPLC. **C** presents an example of three samples as HPLC chromatogram. Peaks that represent scopoletin (retention time: 7.2 min) and ayapin (retention time: 11 min) are indicated by arrows. **D** shows the same chromatograms, but zoomed in. Note that sample RxS_1 (black line) shows no peak at 11 min, indicating that no ayapin was secreted to the medium. The floating medium of 365 plants was measured via HPLC. After automatic annotation and quantification by the HPLC software, every chromatogram with ayapin content below 0.01 µM was manually checked for peaks at 11 min as exemplified in **D**. The distribution of ayapin and scopoletin across all samples is shown in **E**. In total, 77 plants were impaired in their ability to synthesize ayapin (▼) and 288 were not (Δ, **F**).

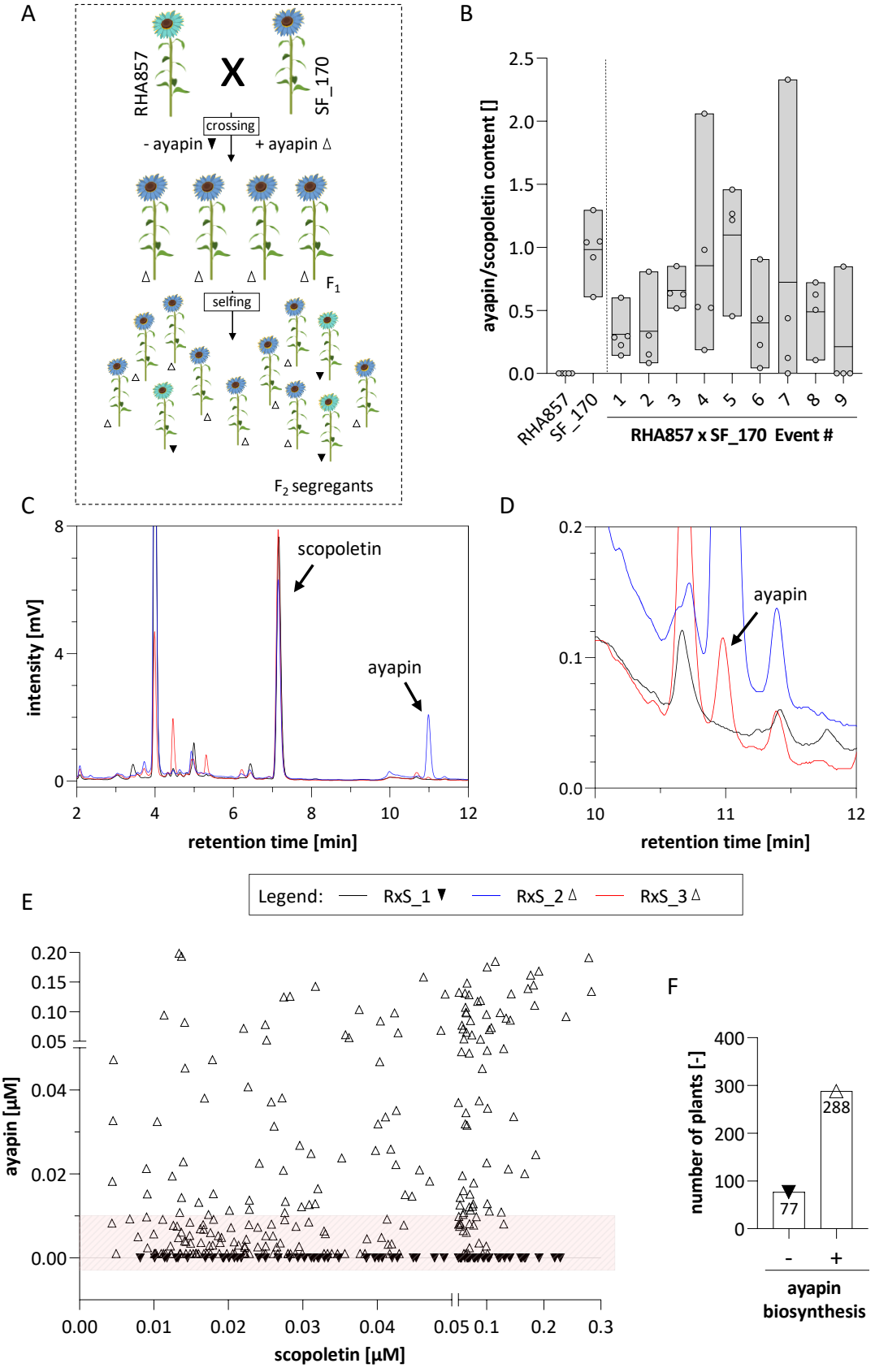

Figure 12. Crossing of sunflower genotype RHA857 and SF_170 leads to segregants with differential $CuCl_2$-induced ayapin accumulation capacity. For the figure caption, see previous page.

2.4. Screening and identifying sunflower mutants that hyperaccumulate scopoletin

Elucidating ayapin biosynthesis in sunflower was primarily driven by the hypothesis that ayapin formation is catalyzed by CYPs. Consequently, the transcriptome analysis was rather targeted and focused on one specific player in the coumarin biosynthesis of sunflowers. In addition, I aimed to include a forward genetic screen in this work for a broader understanding of coumarin biosynthesis and secretion in sunflower.

For this, randomly selected seeds of an M_2-generation of mutagenized RHA857 sunflower plants were sown and maintained at the agricultural experimental station Eckartsweier. The mutagenesis of RHA857 was performed previously as part of another project (Rozhon et al., 2023). Although this particular sunflower line cannot accumulate ayapin, it can potentially inform about other aspects of coumarin biology, such as enhanced biosynthesis or the transport to the leaf surface.

For screening the RHA857 mutants, three leaves per plant were harvested, and one leaf disc from each leaf was incubated on $CuCl_2$ in 96-well microplate. After incubation for 48 h, leaf discs were removed, and the fluorescence of the floating medium was measured. Since noticeable mutants had to be selfed in the field, the time window of analysis was short, as flowerheads had to be sealed before bloom. Consequently, a rapid assessment of the field samples had to be conducted in the laboratory. In total, 4,128 plants were sampled and evaluated regarding the fluorescence of the incubation medium. The variation in fluorescence was high, so the threshold for outliers was set to > 275 % or < 10 % relative fluorescence compared to the mean fluorescence of 47 plants of the maternal line RHA857 (Figure 13A). By doing so, seven mutant plants were identified that produced high fluorescing floating medium, while 27 mutants were identified with low fluorescent medium (Figure 13A). The floating medium of those outliers was additionally measured by HPLC, ruling out mutant (M) 2-1051-11-H7 and M 3-660-7-G12 as the high fluorescence did not correlating with high scopoletin content (Figure 13B). For the remaining samples, high fluorescence correlated with high scopoletin content. Plants that were identified were traced back in the field and selfed to generate F_1-seeds. Selfing, maintaining, and subsequent harvesting of the seeds was again done by the Hahn team. Ripened and dried seeds were then sent back to Aachen for further investigation.

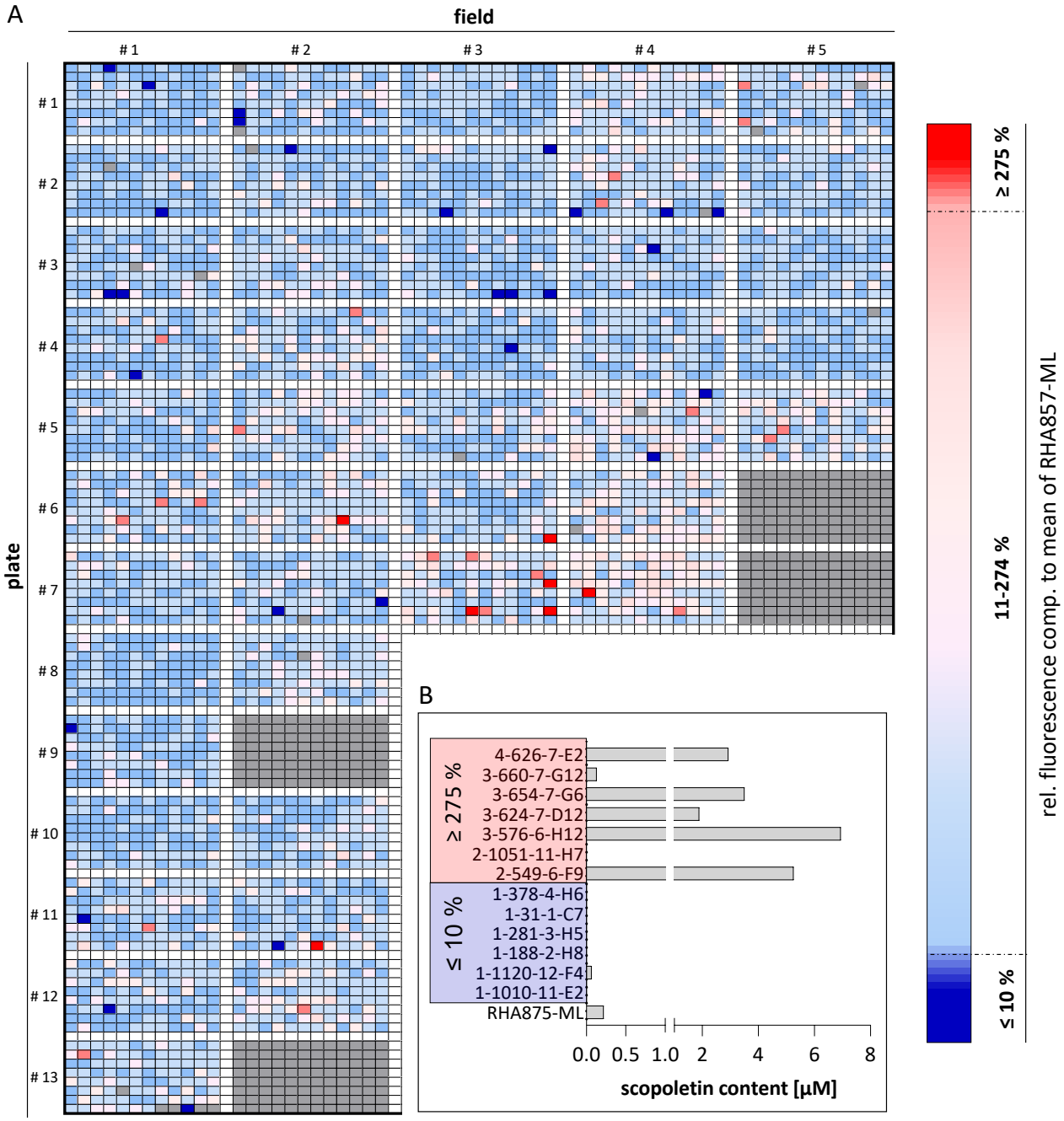

Figure 13. Distribution of sunflower mutants altered in scopoletin biosynthesis. A M_2-progeny of RHA857 was randomly screened for coumarin phenotypes. In total, leaves of 4,128 single mutant plants (growth stages R-3 to R-4) were harvested, and three leaf discs per plant were incubated in a single well of a 96-well plate that contained 200 µL $CuCl_2$. After incubation for 48 h, leaf discs were removed from the plates, and the fluorescence of the floating medium was measured via a microplate reader. The relative fluorescence of each mutant was compared to the mean fluorescence of 47 plants of the RHA857 maternal line (ML; RFU= relative fluorescence units; **A**). Mutants with fluorescence values below 10 % (dark blue) or above 275 % (red) of the maternal-line mean were selected for selfing in the field. Coumarin content of the floating medium of selected mutants was also analyzed via HPLC (**B**). Number codes (e.g. 4-626-7-E2) refer to the position of the plant in the field and to the corresponding sample in the 96-well plate (here: plant 626 in field 4, sample E2 on plate 7).The field trial was conducted in cooperation with Volker Hahn.

Before an in-depth analysis of putative coumarin biosynthesis-mutants, their phenotype had to be confirmed or negated. Of all screened F_1-mutants, only M 4-626-7-E2 (subsequently referred to as M-4/626) showed a reproducible phenotype across several individual plants by hyper-accumulating scopoletin in comparison to the RHA857 maternal line (ML) in response to $CuCl_2$ stress (Figure 14A). This phenotype was robust, as it could also be observed in a field trial, where 15 F_1-plants of M-4/626 were analyzed and compared to 12 plants of RHA857-ML. The median fluorescence was 4-fold increased ($p < 0.0001$) in the mutant line in comparison to the ML (Figure 14B).

To further analyze the dynamics of scopoletin accumulation and secretion in M-4/626, leaf discs of RHA857-ML and M-4/626 were incubated on a $CuCl_2$ solution. Samples were taken every 24 h until 96 h. With mean values of 0.76 µg/g FW (M-4/626) in contrast to 0.17 µg/g FW (RHA857-ML), the scopoletin content in extracts of M-4/626 was over 4-fold higher than in the maternal line after 24 h (Figure 14C). The coumarin content in extracts of M-4/626 slowly decreased in the remaining 72 h, while the content in RHA857-ML extracts rose steadily, leading to 0.62 µg/g FW and 0.47 µg/g FW, respectively. In contrast, the floating medium of M-4/626 samples rose continuously up to 72 h, where it exceeded the scopoletin content of the maternal line by a factor of 5.5 (mean = 25.7 µg/½ [dm^2] and mean = 4.6 µg/½ [dm^2], Figure 14D). In both sunflower lines, scopoletin content in the floating medium decreased after 72 h. Overall, the scopoletin content in the floating medium was at least 10-fold increased, compared to the scopoletin content in the measured extracts.

To check whether the difference in coumarin accumulation and secretion between M-4/626 and RHA857 was due to already known components in coumarin biosynthesis, the expression of the key biosynthesis gene – *HaF6'H1* – and a putative coumarin transporter – *HaABC* – was evaluated *via* qRT-PCR analysis of the leaf disc material. Yet, no differences in the mean relative expression to the housekeeping gene *HaACT* were observed for *HaF6'H1* (Figure 14E). In both lines, expression of *HaF6'H1* was strongly induced by $CuCl_2$. For M-4/626, the maximum in expression was reached after 24 h, while for RHA857-ML, the peak expression was reached after 48 h. The mean relative expression of *HaABC* was more than twice as strong in the samples of M-4/626 (rel. expr. of ~0.14) than RHA857-ML (rel. expr. of ~ 0.06) after 24 h (Figure 14E). Parallel to *HaF6'H1* expression, *HaABC* expression peaked 24 h earlier in M-4/626 compared to RHA857-ML.

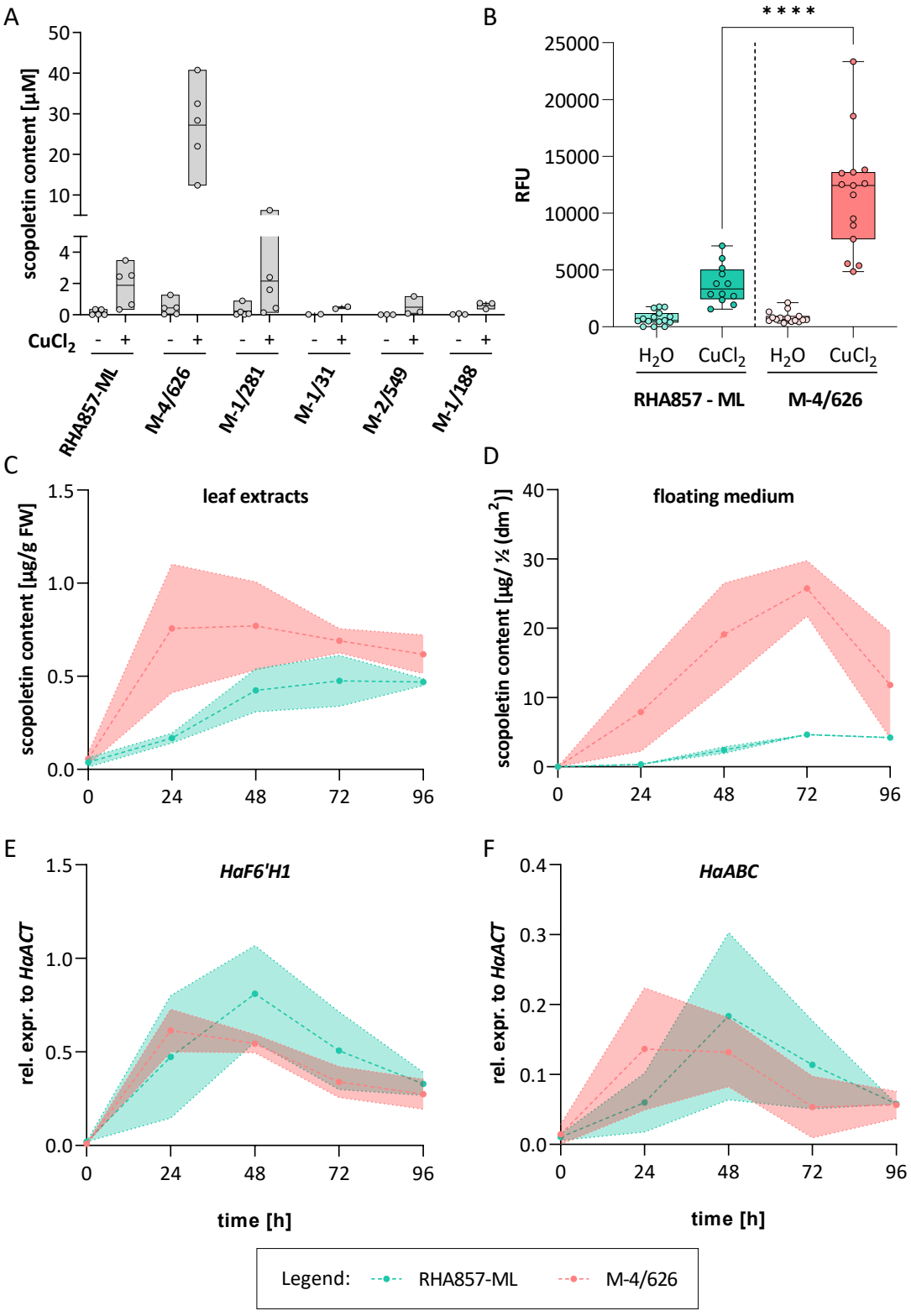

Figure 14. Mutant 4/626 of RHA857 has increased scopoletin accumulation compared to the maternal line. A M_2-population of RHA857 was randomly screened for coumarin phenotypes. Selected mutants were selfed, and the F_1 generation was further analyzed by placing H_2O- or $CuCl_2$-droplets on the leaf surface of four-week-old sunflowers. After incubation for 48 h, the scopoletin content was evaluated via HPLC. Each data point represents pooled droplets from one individual plant per indicated mutant. ML = maternal line (**A**). The F_1-generation of M-4/626 was grown at the agricultural

experimental station Eckartsweier. Eight leaf discs per plant were harvested and incubated floating on either H_2O (as control) or $CuCl_2$ in a 96-well-plate to induce scopoletin biosynthesis. **B** presents the mean fluorescence in RFU of the eight wells of each individual plant after 48 h of incubation. In total, 15 mutant and 12 plants of the RHA857 maternal line are shown. **** = $p<0.0001$ according to Tukey's multiple comparisons test. For further analysis of the M-4/626-line, leaf discs of four-week-old mutant (red) or maternal plants (green) were incubated floating on 300 µM $CuCl_2$ for 96 h in a petri dish. Leaf discs and floating medium were harvested to indicated time points. The scopoletin content of methanolic extracts of the leaf discs (**C**) and of the floating medium (**D**) was analyzed via HPLC. Note that 1 g of sunflower leaf discs has an average area of ~ ½ dm^2, thus the unit of the floating medium was chosen as shown to ensure comparability between extracts (**C**) and floating medium (**D**). From the harvested leaf discs, RNA was isolated and reverse transcribed to cDNA to perform qRT-PCR analysis. The gene expression of *HaF6'H1* (**E**) – encoding the key enzyme for scopoletin biosynthesis – and *HaABC* (**F**)- encoding a potential scopoletin transporter – was analyzed relative to the expression of *HaACT*. Shades in **C-F** represent the range of two biological replicates for RHA857-ML and the standard deviation of four biological replicates for M-4/626. Note that, even though scopoletin content in leaf extracts and the floating medium of the mutant line is increased, there is no major differences between the expression level of the two involved genes. Experiments in **A** and **C-F** were performed by Alina Kruse (bachelor thesis within the scope of this work).

Together, these data suggest that M-4/626 seems to be a mutant that accumulates and secretes significantly higher amounts of scopoletin than RHA857-ML. To enable future analysis of the underlying genetic difference(s), M-4/626 was backcrossed with RHA857-ML. This BC_1F_1-progeny was selfed, and seeds of the resulting BC_1F_2-generation were sown and maintained at the agricultural experimental station Eckartsweier. Plants that exceeded fluorescence levels of RHA857-ML (Figure S 6) were again backcrossed with the maternal line to further dilute background mutations and approximate the original RHA857 genetic background. Seeds of this BC_2F_1-progeny are now valuable for future investigations, including whole-genome analyses.

2.5. Engineering coumarin biosynthesis in soybean plants

The results obtained so far indicate that sunflower coumarins have potential for use in crop protection. Additionally, this work provides a basis to further elucidate aspects of coumarin biosynthesis and secretion in sunflower, such as the synthesis of ayapin or increased accumulation of scopoletin. However, whether and, if so, how these compounds could be applied remained elusive. One possible approach to answer these questions is the provision of transgenic soybean plants that accumulate and secrete the sunflower coumarins.

In the following, I aimed to transfer coumarin biosynthesis genes from sunflower into soybean. Previous work in our research group generated several transgenic soybean lines that overexpressed *AtF6'H1* and accumulated scopoletin. Yet, even though scopoletin shows a protective effect against *P. pachyrhizi in vitro* and *in planta* (Beyer et al., 2019, this work), the transgenic soybean lines did not possess increased resistance to the pathogen (Beyer, 2019). This may be due to scopoletin not being efficiently secreted to the leaf surface. To generate transgenic soybean plants that would secrete scopoletin to the leaf surface, I made use of a sunflower ABC transporter (HaABC) that David Spencer identified and the sunflower F6'H (HaF6'H1) identified by Patrick Schwinges in

their respective doctoral work (Schwinges, 2019; Spencer, 2022). In my work, I designed and cloned DNA constructs for soybean transformation (for an overview see Figure 15A and Figure S 8A).

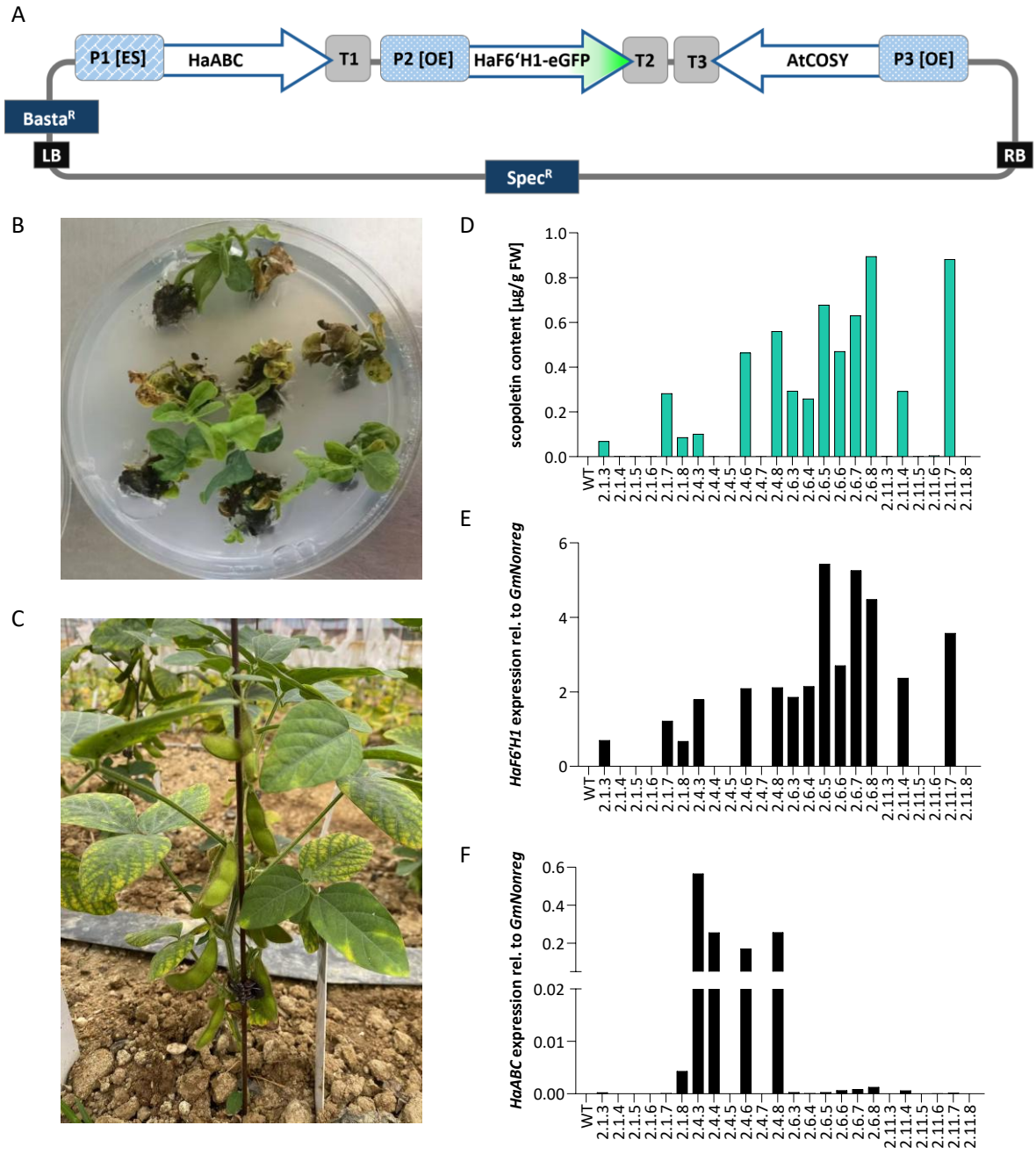

Figure 15. Transgenic soybean plants co-expressing different coumarin biosynthesis genes constitutively accumulate scopoletin. Soybean plants cv. W82 were transformed with the DNA construct shown in **A.** The vector was designed to harbor three coding sequences (CDS). The first promoter sequence (P1), derived from soybean, has been reported to be epidermis-specific, although it has not previously been tested in transgenic soybean. The second and third promoters were proven overexpression (OE) promoters. The CDSs encoded an enhanced green fluorescent protein (*eGFP*) fused to feruloyl 6-hydroxylase 1 from sunflower (*HaF6'H1*), an ATP-binding cassette transporter from sunflower (*HaABC*), and a coumarin synthase from Arabidopsis (*AtCOSY*). For plant selection, a glufosinate resistance cassette (BASTA) was included. Selection in bacteria was mediated via a spectinomycin resistance cassette (Spec^R). **B** shows soybean explants that are selected

on BASTA-containing medium after transformation of soybean seedlings with *A. tumefaciens*. Positive explants were used to generate T_1-seeds. **C** shows a representative T_0-plant transformed with the respective DNA construct. Pictures in **B** and **C** were provided by Lifeasible Inc. The scopoletin content in the leaves of six individuals of selected transformation events was measured via HPLC (**D**). The relative expression of the transgenes *HaF6'H1* (**E**) and *HaABC* (**F**) in the same leaves was determined by qRT-PCR with *GmNREG* as reference gene. Each bar represents the data of one individual plant. In the labels on the x-axis in **D-F**, the second number refers to the transformation event, while the third number refers to the individual plant.

To keep the expression levels of the HaABC transporter moderate and direct its localization to the epidermis, I used a soybean-derived promoter (*p*GmPRP3), which is described to enhance expression in the adaxial epidermis of mature soybean leaves (Wyatt et al., 1992). This promoter was chosen with the aim of restricting transporter activity to the leaf surface and potentially minimizing pleiotropic effects of strong, ubiquitous expression. Also, the transformation vector harbored two further promoter sequences - an ubiquitin promoter derived from parsley (*p*PcUBI) and the 35S promoter from the Cauliflower Mosaic Virus (*p*CaMV35S), both are established and well-researched overexpression promoters used in plant biotechnology (Amack and Antunes, 2020; Kishi-Kaboshi et al., 2019). I placed the coding sequence of the *HaABC* transporter gene under the control of the epidermis-specific promoter *p*GmPRP3, while *HaF6'H1*, C-terminally fused to *eGFP*, was expressed under the control of *p*PcUBI. Expression of *AtCOSY* was driven by the *p*CaMV35S promoter. (Figure 15A). Plasmids containing the respective transformation constructs were used for custom transformation of soybean *cv.* Williams 82 (W82). After transformation, explants were transferred to BASTA-containing selection medium (Figure 15B), and only glufosinate-resistant explants that continued to grow were retained. These resistant ("positive") explants were then induced to form shoots and roots and, finally, transferred to soil to regenerate F_0-plants (Figure 15C). Up to 20 T_1-seeds of each positive transformation event were harvested and provided for further analysis.

In a first screen, the lines of each transformation event were evaluated and selected by eGFP and scopoletin fluorescence. Six T_1-individuals per event were further analyzed as shown in Figure 15D-F. Wild-type (WT) plants neither accumulated any scopoletin nor expressed any of the respective transgenes. The coumarin content in the leaves of transgenic soybeans that accumulated scopoletin ranged from ~0.07 µg/g FW to ~0.9 µg/g FW. Notably, all tested individuals of transformation event #6 accumulated scopoletin to relatively high levels compared to other lines (Figure 15D). This correlates with the expression of *HaF6'H1*. Transcripts of this gene were detected in the leaf material of each plant that accumulated scopoletin. The relative expression levels ranged from ~0.7 to ~5.4 compared to the reference gene (Figure 15E). Transcript levels for *HaABC* were at least 10-fold lower than for *HaF6'H1*, ranging from ~0.00025 to 0.6 compared to the reference gene (Figure 15F). Soybean plants that expressed *HaABC* survived and did not show obvious growth penalties (Figure 15C). All individuals that expressed *HaF6'H1* also expressed

AtCOSY (Figure S 7). From each transformation event, two individuals that accumulated scopoletin and showed the strongest expression of *HaF6'H1*, *HaABC,* and *AtCOSY* were chosen to generate T_2-seeds. This next generation of these transgenic soybean lines will be used to assess the effects of the presence of the HaABC-transporter on scopoletin secretion in soybean and whether the secretion of scopoletin in transgenic soybean leads to a protective effect against *P. pachyrhizi*.

2.6. Turning the tables – identification of a *P. pachyrhizi* self-inhibitor

So far, this work has focused on sunflower-derived coumarins as a promising approach for sustainable protection of soybean. A conceptually different strategy is to exploit intrinsic regulatory mechanisms of *P. pachyrhizi* itself. For several fungal pathogens, it has been shown that spores produce germination inhibitors – compounds capable of suppressing spore germination at high spore densities (Allen, 1955; Macko et al., 1972). These inhibitors are thought to prevent germination in densely packed spore deposits and to promote germination only when spores are dispersed at lower densities, for example on a host leaf surface. In this chapter, I therefore investigated whether *P. pachyrhizi* produces germination self-inhibitors and whether such activity could be harnessed for crop protection.

To elucidate whether *P. pachyrhizi* produces germination self-inhibitors, freshly harvested uredospores were adjusted to different spore densities. At 1 mg/mL, the germination rate was ~ 90 % (Figure 16A). In contrast, at 5 mg/mL germination dropped by more than 80 %, and at 10 mg/mL it was almost completely impaired (Figure 16A). Interestingly, washing the spores with water (supplemented with Tween-20) before the germination assay recovered the germination rate almost completely for suspensions of 5 mg/mL spores and partly for 10 mg/mL spores (Figure 16B). Conversely, incubating spore suspensions of 1 mg/mL together with the wash water obtained from higher-density spore suspensions (as depicted in Figure 16C) decreased the spore germination rate (Figure 16D). For an initial spore density of 10 mg/mL, spore germination was reduced by more than 50 % ($p < 0.0001$) compared to the control treatment (~90 % germination rate, Figure 16D). Wash water from isolate br05 also inhibited spore germination of isolate RS2 to a similar extent as the endogenous wash water from RS2 (Figure 16E). Together, these data suggest that *P. pachyrhizi* spores produce one or more germination self-inhibitory substances.

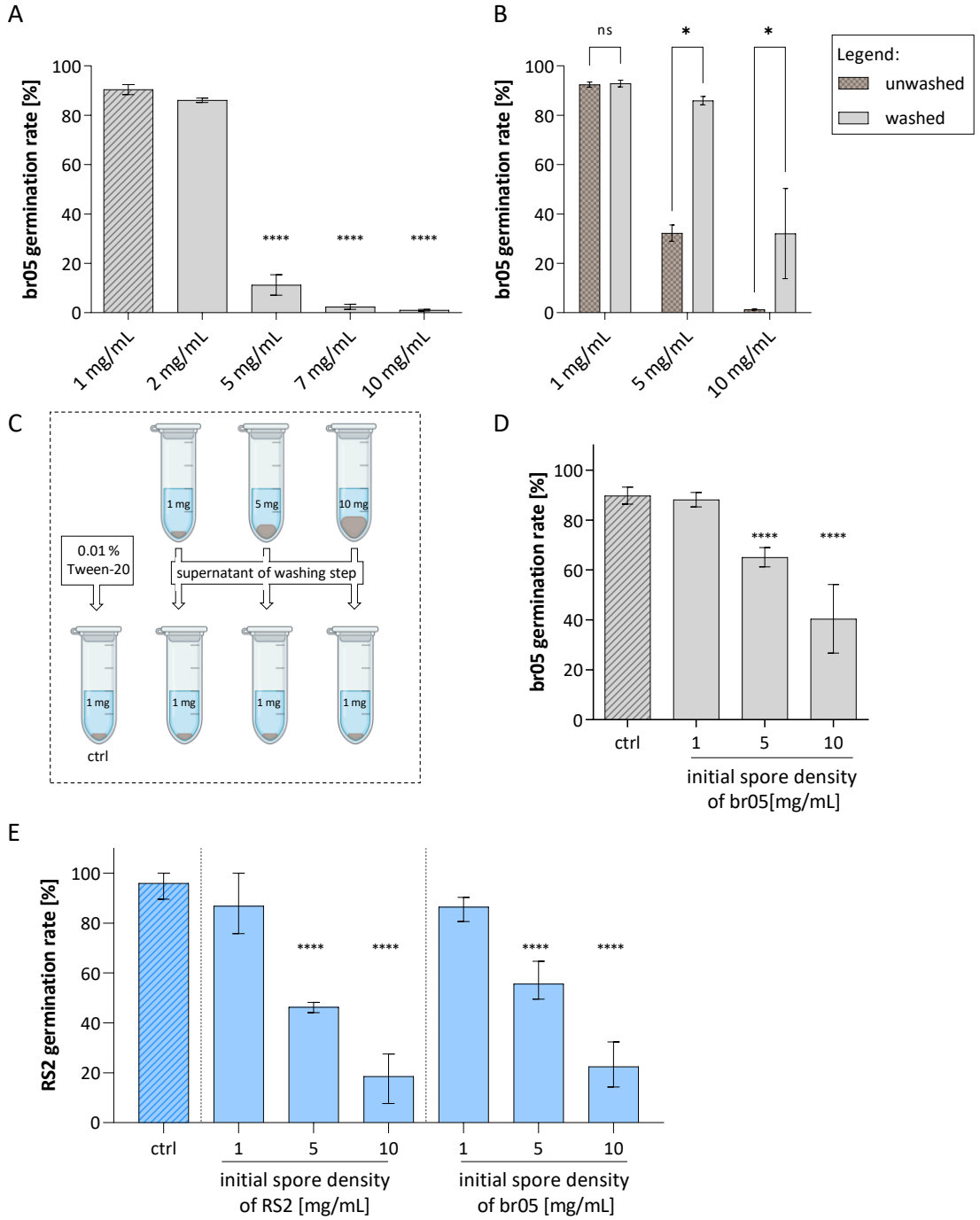

Figure 16. *P. pachyrhizi* uredospore germination is sensitive to crowding *in vitro.* Germination rates of *P. pachyrhizi* uredospore suspensions were determined microscopically after 3 h of incubation under rotation. The germination rate of isolate br05 incubated in indicated spore densities is shown (**A**). Different amounts of *P. pachyrhizi* (br05) uredospores were washed five times with 0.01 % Tween-20 (v/v) in water and subsequently incubated for three hours under rotation (grey bars, **B**). For comparison, unwashed uredospores (brown bars, **B**) were analyzed. As indicated in **C**, uredospores (isolates br05 and RS2, as indicated) were suspended to different densities, and supernatants from these different suspensions were then added to fresh uredospores (1 mg/mL) of isolate br05 (**D**) and isolate RS2 (**E**). All spore suspensions were supplemented with 0.01% (v/v) Tween-20. Mean values and standard deviations were derived from data of three independent experiments. In each experiment, at least 3 × 100 spores were counted per treatment. Asterisks in **A**, **D,** and **E** indicate significant differences to the control evaluated by Dunnett's multiple comparisons test with $p < 0.0001$; Asterisks in **B** indicate significant differences to each respective unwashed control (unpaired *t*-test $p \leq 0.05$). ns = not significant. Experiments in **A**, **B**, and **D** were performed by Steven Dreischhoff during his master thesis (Dreischhoff, 2019).

At this point, the identity of the self-inhibitor(s) remained elusive. As a first step towards its identification, spore washing needed to be scaled up to get the sufficient amounts of wash water needed for further analysis. Spores were collected from infected soybean leaves over time and stored at -80 °C. 900 mg of uredospores were washed together in 45 mL of water. As depicted in Figure 17A, the supernatant was subsequently loaded onto a C18 chromatography column. The flow-through was collected. Afterwards, the column was eluted first with H_2O, then with a 50:50 (v/v) mixture of H_2O and acetonitrile (ACN), and finally, with 100 % ACN. All samples, including the raw supernatant, were split into two halves one of which was treated with proteinase K to digest the vast majority of proteins.

The germination of *P. pachyrhizi* spores in the presence of these fractions was assessed *in vitro*. Spores did not germinate when they were incubated in the raw supernatant, the flow-through, and the H_2O-elution-fraction regardless of proteinase K treatment (Figure 17B). Germination was impaired by ~ 90 % in the eluate with the H_2O/ACN mixture, and the ACN-fraction allowed a germination rate that was similar to the control (Figure 17B). Because proteinase K treatment did not recover spore germination, the self-inhibitory substance(s) did not seem to be or require a protein. The unknown inhibitor(s) were fairly soluble in water and seemed to be relatively polar.

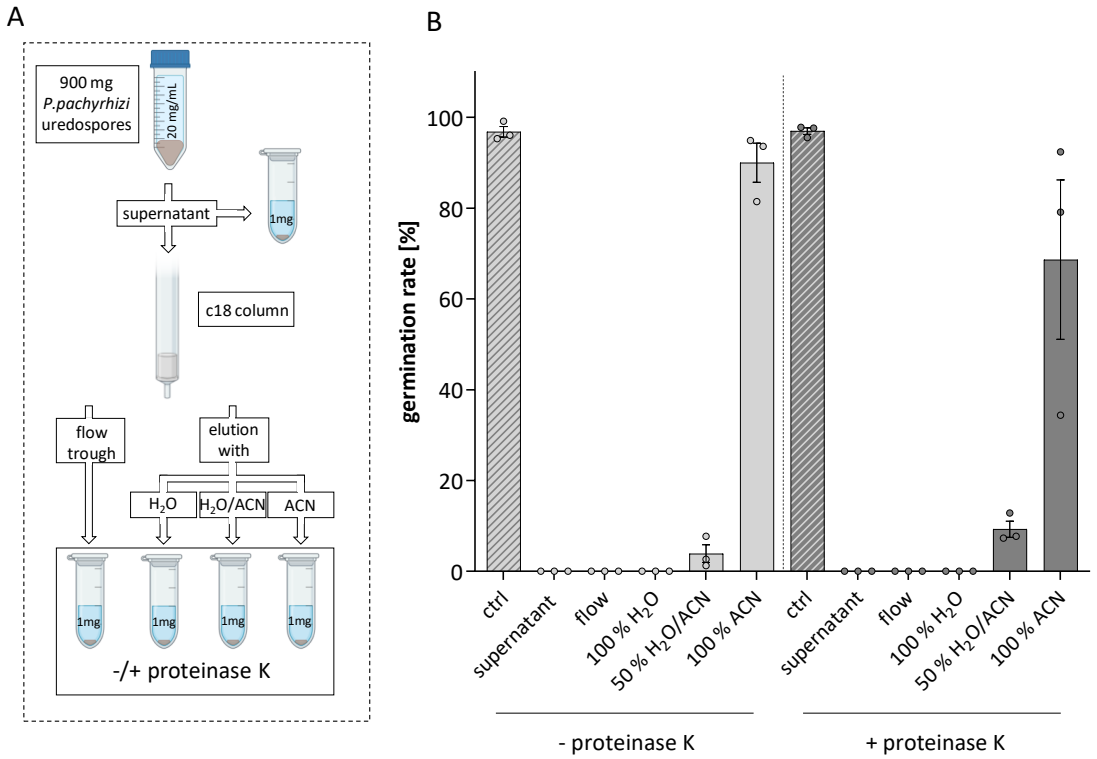

Figure 17. *P. pachyrhizi* germination self-inhibition is associated with a non-proteinaceous water-soluble molecule or combination of molecules. As depicted in **A**, 900 mg uredospores of *P. pachyrhizi* were washed in 45 mL ddH_2O (+ 0.01 % Tween-20), and 10 mL of the supernatant was separated via a 3 mL C18 column (end-capped, CHROMABOND). After loading

the supernatant, the flow-through was collected ("flow"). The column was eluted first with 4 mL 100 % ddH_2O, secondly with 4 mL 50 % ddH_2O/Acetonitrile (ACN, v/v), and lastly with 4 mL 100 % ACN. All three elution solutions were substituted with 1.5 % acetic acid. Samples were evaporated and split into two halves. One half of the samples was treated with proteinase K. 1 mg/mL spore solution was incubated rotating with respective samples for 3 h. The germination rate of the uredospores was evaluated microscopically (**B**). 100 spores were counted three times for each treatment.

As a next step toward identifying the *P. pachyrhizi* uredospore self-germination inhibitor, I fractionated spore wash water by preparative HPLC at the Helmholtz Centre of Infection Research (Braunschweig, Germany). Since previous results suggest that the germination inhibitory substance was well soluble in water, I chose a HPLC column with a polar end-capped C18 stationary phase. The column was stable in 100 % aqueous mobile phase, which was maintained for 25 min before gradually increasing the proportion of ACN. To detect as wide a spectrum of unknown substances as possible, I used an evaporative light scattering detector (ELSD) combined with a UV-detector at wavelengths of 210, 260, 280, and 320 nm. The ELSD allows detection of compounds that do not absorb UV-VIS radiation. Three injections of 40 mg of raw spore extract each were separated, resulting in reproducible chromatograms (Figure 18).

During the 100 % aqueous mobile phase, prominent peaks at $\lambda = 210$ nm appeared at retention times of 2.8, 4.2, 5.4, 6.8, 8.4, 9.2, 15.9, and 16.2 min. However, only the peaks at 2.8, 4.2, 8.4, 15.9, and 16.2 min. showed a corresponding ELSD signal. Fractions corresponding to these peaks were collected individually and tested for the capacity to inhibit *P. pachyrhizi* spore germination. Because the timeframe of my work in Braunschweig was limited, a rapid screening set-up was used to evaluate the activity of each fraction against *P. pachyrhizi*. In a germination assay, the germination of spores was assigned to one of three categories: similar to the water control (not active); reduced to ~20–70 % of the control (semi-active); or reduced to <20 % of the control (active). Fractions belonging to the peaks at 4.2, 8.4, and 9.2 min retention time were classified as active (Figure 18). Fractions corresponding to the peaks at 2.8 and 5.4 min, as well as the fraction collected immediately after the 9.2 min peak, were semi-active, whereas fractions at 6.8, 15.9, and 16.2 min did not reduce germination compared to the water control and were considered inactive. The dry weights of all fractions are summarized in Table S 2. Notably, the two heaviest fractions (0-3 and 3-4 min) were only semi-active, whereas full activity resided in less abundant fractions.

Additionally, to the fractions of the aqueous phase, I collected one fraction from 18 to 45 min that included the substances that were eluted when the solvent became increasingly ACN-rich (less polar). For this fraction, I also detected no spore germination (Figure 18). As previous results pointed to an inhibitor that was fairly soluble in water, I initially focused on the peaks appearing between 0 and 18 min for further evaluation, as these eluted under 100 % aqueous conditions.

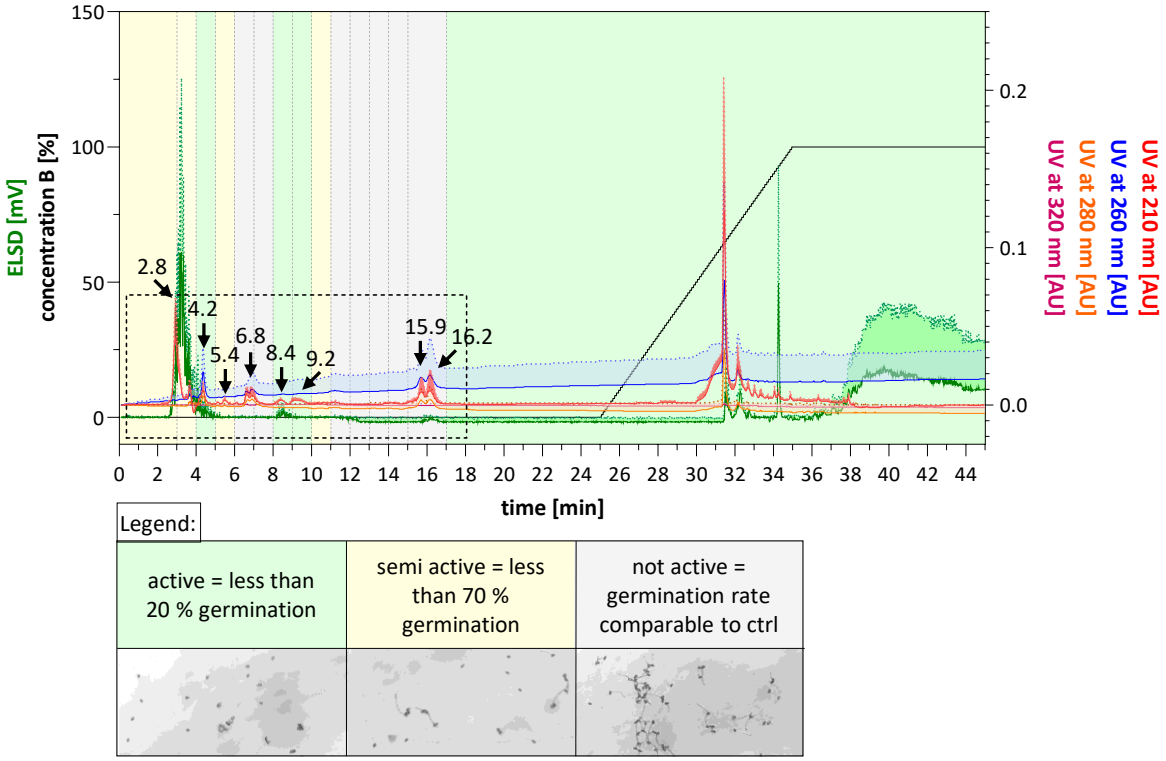

Figure 18. Preparative HPLC fractionation of *P. pachyrhizi* uredospore wash water. 758 mg *P. pachyrhizi* uredospores were washed with 37.5 mL H_2O. The supernatant was lyophilized, yielding 168 mg of raw extract. Three aliquots of 40 mg of this wash-water extract were analyzed by preparative HPLC. For separation, a 4 µm Hydro-RP 80 Å column (250 x 21.2 mm) was used. Signals were detected via an UV detector at indicated wavelengths (right y-axes) and via an evaporative light scattering detector (ELSD, left y-axes). The flow rate was set to 20 mL/min. From 0 to 25 min, the mobile phase consisted of 100 % water (+0.1 % formic acid (FA)). At 25 min acetonitrile (+0.1 % FA) concentration rose gradually for 10 min (solvent B, black line, left y-axes). The plots show mean signal intensities of three runs, with colored shading representing the standard deviation of each signal. Each sample was fractionated as indicated by vertical, grey lines. All fractions were evaporated, weighed, and re-dissolved in 1 mL H_2O. All fractions were roughly estimated for activity against *P. pachyrhizi* germination. Therefore, 100 µL of each fraction was mixed with 900 µL of a uredospore suspension to a final concentration of 1 mg/mL uredospores. After 3 h of rotating incubation, the germination rate was evaluated microscopically. Activity of the fraction was sorted into three groups. An active group; when the germination rate was ~< 20 % (green). A semi-active group; when the germination rate was between ~20 – ~70 % (yellow). And a non-active group; when the germination rate was > ~70 % and ,thus, similar to the control (grey). Note that for these experiments, *P. pachyrhizi* spores had to be used that had been stored at RT, resulting in a reduced overall germination rate.

In the first test, fractions corresponding to peaks at 4.2, 8.4, and 9.2 inhibited *P. pachyrhizi* spore germination completely, even after 1:10 dilution. These active fractions were further separated to isolate the compounds corresponding to each peak. The detailed fractionation is shown in Figure 19A. Those fractions were collected, evaporated, and weighed. A germination assay in which all fractions were set to 0.25 mg/mL revealed that fractions F7 and F10 inhibited spore germination completely (Figure 19B). Those fractions corresponded to the original peaks at 8.4 and 9.2 min. The germination rate of spores incubating in solutions of F8 and F9 was reduced to 20 % and 5 %, respectively. F3, which corresponded to the peak at 4.2 min, reduced spore germination by ~40 % (Figure 19B). Representative micrographs of spores that germinated in water or 0.25 mg/mL of F7

are shown in Figure 19C. While the elongating germ tube of *P. pachyrhizi* uredospores is clearly visible in the control sample (gt, Figure 19C), there was no germ tube formation for spores that were incubated in F7 (sp, Figure 19C).

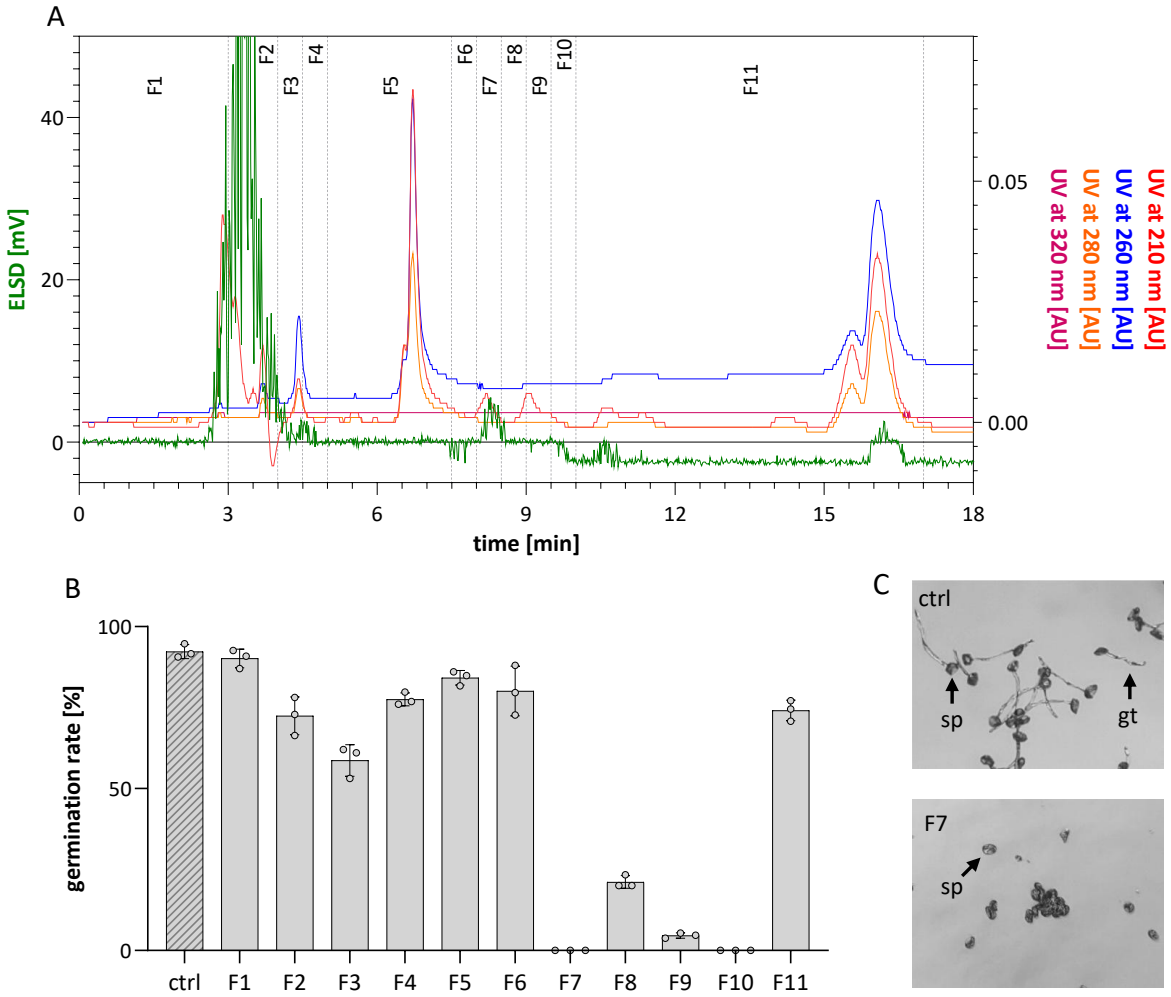

Figure 19. Fractions F7 and F10 completely inhibit *P. pachyrhizi* spore germination. 650 mg of *P. pachyrhizi* uredospores were washed with 32.5 mL H_2O. The supernatant was lyophilized, yielding 145 mg of raw extract. 40 mg of this wash water extract were analyzed by preparative HPLC (**A**). For separation, a 4 µm Hydro-RP 80 Å column (250 x 21.2 mm) was used. Signals were recorded with an UV detector at indicated wavelengths (right y-axes) and with an ELSD (left y-axes). The flow rate was set to 20 mL/min. Elution was carried out with 100 % water containing 0.1 % FA. The sample was fractionated as indicated by grey lines. For better resolution, the left y-axis is cut off at 50 mV. All fractions were evaporated to dryness, weighed and re-dissolved in water to a final concentration of 0.25 mg/mL. 1 mL of each fraction (+ 0.01 % Tween-20) was mixed with 1 mg of fresh *P. pachyrhizi* uredospores. ddH_2O (+0.01 %Tween-20) served as control (ctrl). After 3 h of incubation under rotation, the germination rate of the uredospores was evaluated microscopically (**B**). Because the quantity of substance recovered in each fraction was very low, this experiment was performed only once. Error bars show the standard deviation of three counting events of at least 100 spores each. As exemplified in **C**, F7 and F10, completely inhibited spore germination. sp = uredospore; gt = germ tube.

To identify the active compounds in F7 and F10, fractions of four runs were pooled for each fraction to gain at least 1 mg dry weight per fraction. After accumulating sufficient material, the samples were dissolved in D_2O and subjected to nuclear magnetic resonance (NMR) spectroscopy. The ^1H

and ^{13}C NMR data are summarized in Table 3. Two methylene groups (C_2/C_4; δ_C 43.4, δ_H 2.86 and 3.03 ppm) and three carbonyl signals (C_1/C_5 at δ_C 173.7 ppm and C_6 at δ_C 177.2 ppm) are consistent with a symmetric tricarboxylic acid. Signal assignment was supported by 2D NMR (Figure S 9, Figure S 10). Comparison of these data with reference NMR data deposited for citric acid in the SDBS database (SDBSWeb - No. 1995) revealed that F7 and F10 contain citric acid (Figure 20).

Table 3. ^{1}H and ^{13}C NMR data of F7 and F10. 700 MHz (^{1}H), 176 MHz (^{13}C), solvent D_2O, 298 K. δC/δH in ppm; multiplicity and J (Hz) refer to ^{1}H signals. Atom numbering as in Figure 20.

atom #	δ_C	δ_H
1	173.7	–
2a	43.4	2.86 (d, 15.8)
2b	43.4	3.03 (d, 15.8)
3	73.4	–
4a	43.4	2.86 (d, 15.8)
4b	43.4	3.03 (d, 15.8)
5	173.7	–
6	177.2	–

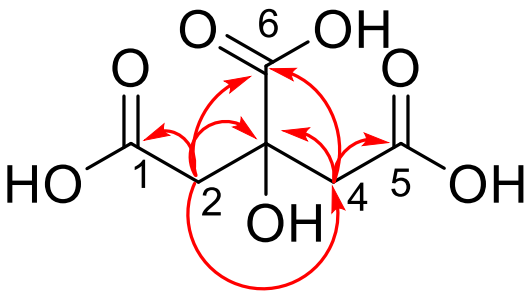

Figure 20. Chemical structure of F7 and F10. NMR analysis disclosed citric acid as a putative germination self-inhibiting substance. The numbering of the carbon atoms (1–6) corresponds to the assignments in Table 3. Red arrows indicate key HMBC correlations. For HMBC spectra see Figure S 10.

After identifying citric acid (CA) as the active compound in fractions F7 and F10, I tested its effect on *P. pachyrhizi* spore germination *in vitro*. Even 62.5 µM CA reduced the germination rate of *P. pachyrhizi* uredospores by ~70 %. At 250 µM CA (pH = 2.1), spore germination was completely inhibited (Figure 21A). In presence of 1 mM MES buffer (pH = 5.0), complete inhibition of spore germination required 75 mM CA, whereas at 18.75 mM CA (+1 mM MES) germination was partly recovered to ~60 %. These data indicate that the effect of CA is largely mediated by acidification of the incubation medium. Notably, the wash water of *P. pachyrhizi* spores had a pH of ~6.0, independent of spore density (Figure S 11).

To test the effect of CA on *P. pachyrhizi in planta*, soybean plants were co-inoculated with buffered (+ 2mM MES) or unbuffered CA and *P. pachyrhizi* spores. Co-inoculation with 10 mM CA visibly reduced the number of rust pustules on treated soybean leaflets (Figure 21B). Quantification of the diseased leaf area revealed that co-inoculation with 1, 5, or 10 mM unbuffered CA significantly reduced the disease severity of treated plants by ~20, 40, or 60 %, respectively (Figure 21C). This effect was attenuated when CA was buffered with 2 mM MES. While co-inoculating 2 mM alone did not lead to any differences in disease severity compared to the control treatment, 1, 5, or 10 mM

CA in the presence of 2 mM MES reduced disease severity by ~7, 12, and 25 %, respectively; only the effect of 10 mM buffered CA was statistically significant ($p \leq 0.0001$).

Taken together, citric acid was identified as a putative *P. pachyrhizi*–derived germination self-inhibitor. External application of CA also reduced rust severity on soybean leaves, indicating that citric acid could be explored as complementary measures for soybean crop protection.

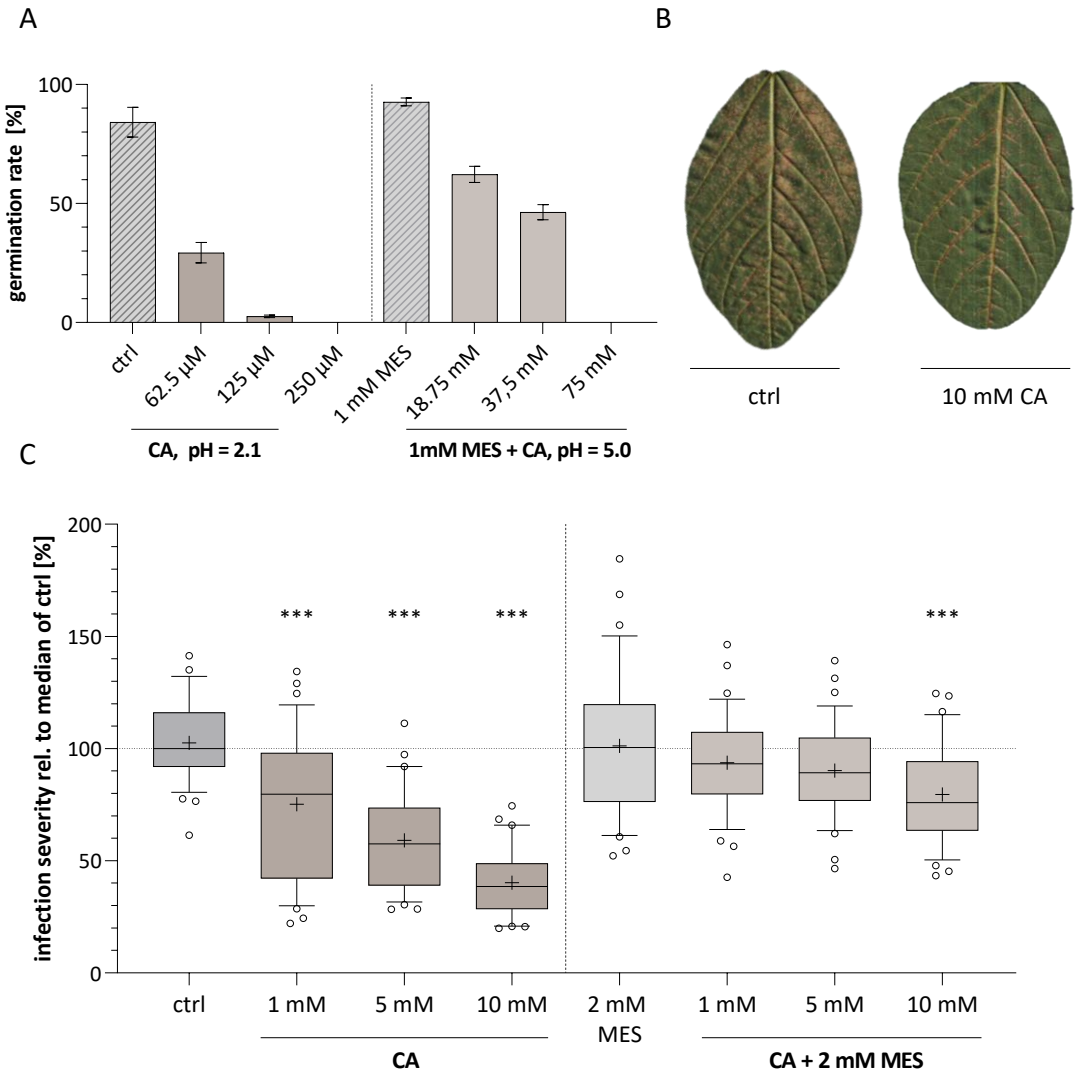

Figure 21. Citric acid reduces soybean rust severity when applied to the foliage. Uredospores of *P. pachyrhizi* were suspended in water (ctrl) or in CA at the indicated concentrations (note in **A** the use of both µM and mM). All suspensions contained 0.01% (v/v) Tween-20. Spores were incubated under rotation for 3 h, after which germination was evaluated microscopically (**A**). Bars show the mean value of a count of over 100 spores, which was repeated three times at different areas of sight. The effect of citric acid *in planta* was evaluated by co-inoculation of citric acid with uredospores onto the first fully developed trifolia of three-week-old soybean plants. After 8-12 days, leaflets were evaluated for disease severity by quantifying the percentage of leaf area covered by rust pustules and comparing it to the control treatment, as exemplified in **B**. In addition to unbuffered CA, a second set of treatments contained 2 mM MES buffer to adjust the pH to 5.8 (**C**). Disease severity of each leaflet was calculated relative to the median value of the ctrl treatment. Box plots show outliers outside the 10–90 % range as hollow dots; the black bar marks the median of each treatment. Data are from three independent biological experiments with at least three plants per experiment; in total, 33 leaflets were evaluated per treatment. Asterisks indicate significant differences to the control treatment (ctrl) according to Dunnett's multiple comparisons test (*** = $p \leq 0.0001$).

3. Discussion

The immense use of fungicides to manage SBR in Brazil has led to an increasing number of *P. pachyrhizi* isolates that adapted to this selective pressure by the development of insensitivities or resistance to single fungicides or whole classes of fungicides (Dalla Lana et al., 2018; Klosowski et al., 2016; Mello et al., 2021; Müller et al., 2021; Müller et al., 2024; Schmitz et al., 2014; Simões et al., 2018). Such adaptation was also demonstrated in this work with *P. pachyrhizi* isolate RS2 being less sensitive to QoI, DMI and SDHI fungicides (Figure 3). Hence, it is plausible that this isolate was originally sampled in 2016 because third-generation SDHI fungicides were only introduced in the Brazilian market for SBR management in 2013 (Godoy et al., 2016). Consequently, the two isolates RS1 and RS3 presumably did not experience any selective pressure regarding SDHI fungicides and, thus, did not show any adaptation regarding SDHIs (compare Figure 3 C,D). The insensitivity of RS2, however, is in line with other isolates collected from the growing season 2016-2017 that posed reduced sensitivity towards SDHI fungicides due to the I86F mutation in *SDHc* (Simões et al., 2018). Sequencing data of RS2 showed a single nucleotide polymorphism (SNP) in the sequence of *SDHc* of RS2 at position 515 (ATT->CTT), leading to the same I86F mutation (Figure S 13). These findings underline the rapid genetic adaptation by *P. pachyrhizi*.

Additionally, the disease severity of soybean plants inoculated with RS2 and pretreated with the QoI-fungicide could not be decreased in a dose-dependent manner (Figure 3B). This hints towards a qualitative resistance of this isolate towards QoIs. This is in line with QoI resistance being conferred by an F129L mutation to *CYTB,* of which *P. pachyrhizi* possesses only one single copy (Schmitz et al., 2014). This is underlined by the sequence data of RS2. Here, a SNP at position 385 (TTT->CTT) leading to the described F129L mutation is present (Figure S 14). The sequence data also confirms the presence of a type I intron directly after the codon that codes for AA 143 in *PpCYTB* (Figure S 14). Due to the presence of this intron, the prominent G143A mutation in CYTB is absent in *P. pachyrhizi* and other rust fungi, because a mutation at this position would disrupt splicing and be lethal for the fungus (Grasso et al., 2006; Klosowski et al., 2016). F129L conferred resistance is described to be relatively weak compared to G143A-conferred resistance (Dorigan et al., 2023). For example, the EC_{50}-dose of QoI fungicides for *Pyricularia grisea* and *Alternaria solani* isolates harboring the F129L mutation is described to be between 0.3 and 4 mg/L *in vitro* (Kim et al., 2003; Leiminger et al., 2014). The RS2 isolate, however, was still able to successfully infect soybean plants at QoI concentrations of 125 mg/L (Figure 3B), hence QoI resistance in *P. pachyrhizi* seems to be much stronger despite being conferred by the “weaker” F129L mutation.

In contrast, RS2 (and RS3) were already affected by the lowest dose (1.25 mg/mL) of Proline® (DMI) tested, despite being less sensitive towards the fungicide than br05 and RS1 (Figure 3A). However, the sensitivity of *P. pachyrhizi* isolates towards DMIs seems to depend on the combination of point mutations in *CYP51* (Stilgenbauer et al., 2023). Next to the combination, there are also six alleles of *CYP51* present in the *P. pachyrhizi* genome (Stilgenbauer et al., 2023), thus leading to a quantitative resistance which is mirrored by the dose-dependent resistance of RS2 and RS3 towards Proline® (Figure 3A). This correlates with the sequencing data of RS2 on *CYP51* (Figure S 15). At positions 441 and 587, the sequence of the RS2-version of *CYP51* is undecisive. Here, the sequencing peaks indicate the presence of both adenine and cytosine (pos. 441) and tyrosine and cytosine (pos. 587). These SNPs lead to the amino acid changes F120L and Y131H, respectively. The variance in the sequence data also underlines that likely just one ortholog of *CYP51* seems to be mutated. These mutations have been associated with DMI resistance in *P. pachyrhizi* before (Schmitz et al., 2014). However, Stilgenbauer et al. reported that prothioconazole is most effective against *P. pachyrhizi* isolates harboring the F120L/Y131H-combination compared to other *CYP51*-mutation combinations and DMI fungicides. In the same work, the authors present that a combination of F120L and Y131H confers cross-resistance to several DMI fungicides, since both mutations are located directly in the binding pocket of the CYP51 enzyme (Stilgenbauer et al., 2023). Other mutations in *CYP51* that have been described by Stilgenbauer et al. (2023) were not present in the RS2 sequence (data not shown). The insensitivity of RS2 could also be further due to the overexpression of *CYP51*. E.g., tandem repeats in the promoter region of a *CYP51* variant of *Venturia inaequalis* lead to overexpression of *CYP51* and result in DMI-resistance (Schnabel and Jones, 2001; Villani et al., 2016). Such overexpression has been described for *P. pachyrhizi* isolates harboring the combination of F120L and Y131H before (Schmitz et al., 2014). More in-depth genetic analysis of RS2 would be necessary to fully elucidate the mechanism behind this multi-fungicide-insensitive *P. pachyrhizi* isolate.

The ability of RS2 to overcome multiple fungicide classes might also be linked to ABC transporters, since multi-drug resistance is often accompanied by alterations of ABC transporters that enable the fungus to detoxify itself by excretion of the fungicide (Waard et al., 2006). However, for rust fungi, there have not been many reports of ABC transporter-mediated multidrug resistance so far. Just one recent study describes PstABCG2 – an ABC transporter of *Puccinia striiformis* f. sp. *tritici* – the c.a. of wheat stripe rust – as being directly associated with resistance towards DMI and SDHI fungicides (Ji et al., 2025). Blasting the protein sequence of the described *PstABCG2* against the recently published *Phakopsora* genome (Gupta et al., 2023), revealed six potential proteins with a

protein identity > 40 % that could be considered for further research to understand multi-drug resistance mechanisms in *P. pachyrhizi* (Figure S 12).

To the best of my knowledge, the analysis of RS2 shown in this work is the first report that experimentally shows that this combination of target site mutations leads to insensitivity of all three fungicide classes in *Phakopsora* isolates. This supports findings by Müller et al. (2021) who described the presence of the respective mutations in monouredinial *Phakopsora* isolates, but only presented reduced sensitivity of those isolates towards DMI and SDHI fungicides. Taken together, the presumably quick adaption of isolate RS2 to fungicide treatments demonstrates why alternative, complementary methods for crop protection are needed.

On the antifungal potential of coumarins

Previous work disclosed a dose-dependent inhibition of *P. pachyrhizi* uredospore germination by the sunflower coumarins scopoletin and ayapin *in vitro* (Beyer et al., 2019; Schwinges, 2019). This study confirms that both coumarins effectively inhibit germination of fungicide-sensitive isolate br05 and, importantly, of isolate RS2 in a similar micromolar range (Figure 4 A). In co-inoculation assays, disease severity on soybean was even more strongly reduced for RS2 than for br05, and 500 µM ayapin decreased RS2-induced rust symptoms by more than 90 % (Figure 4C).

However, there is also an increased infection severity of soybean plants co-inoculated with RS2 and DMSO. Such an effect was not observed for the br05 isolate (Figure 4C). This could indicate that the mutations of RS2 to survive fungicide treatment come with a slight fitness penalty. Such fitness penalties are described to be connected to the I86F mutation in *SDHc* (Claus et al., 2022). Yet, despite these fitness penalties, the *SDHc*-I86F mutation remained stable for 36 generations of fungicide-free propagation (Claus et al., 2022), and the mutation was also detected in *P. pachyrhizi* populations collected from volunteer plants during soybean-free periods (Mello et al., 2021). Hence, the described fitness penalty seems not to be severe enough to be eliminated by evolution and will most likely spread further in *P. pachyrhizi* populations, especially when the selection pressure remains high due to fungicide treatment. On the other hand, these fitness penalties seem to compromise the fungus's ability to cope with the effect of antifungal coumarins (Figure 4). That could be because those coumarins most likely have a more mechanistic mode of action (MoA) compared to the target-side specific fungicides.

One of the MoAs of scopoletin is probably that it has the ability to scavenge reactive oxygen species (ROS, Beyer et al., 2019), which are often required by fungal spores for germination development (Egan et al., 2007). Scopoletin is able to scavenge ROS on the same level as the antioxidant Trolox (Beyer et al., 2019; Figure S 16). Fluorescence microscopy and H_2DCFDA staining shows that

scopoletin also scavenges ROS inside the fungal spore (Beyer et al., 2019; Figure S 17). ROS scavenging may also explain why the presence of the solvent DMSO, relative to untreated controls, decreased *P. pachyrhizi* germination and disease severity on inoculated soybeans (Figure 4). DMSO itself has ROS-scavenging properties as it is oxidized by ROS to dimethyl sulfone (Bansal and Wang, 2024).

In the case of ayapin, however, it is unlikely that germination inhibition could be explained by the reduction of endogenous, fungal ROS, since ayapin does not possess a free hydroxy group (Figure 1). Additionally, previous work by our research group indicates that ayapin does not affect ROS levels in ABTS assays (Figure S 16). Furthermore, H_2DCFDA staining showed that fungal spores that were incubated with 125 µM ayapin did not germinate, but still showed strong fluorescence, which indicates a high endogenous ROS accumulation (Figure S 17). Hence, inhibition of *P. pachyrhizi* spore germination by ayapin must be caused by a complementary MoA.

One possible MoA could be that ayapin inhibits CYP enzymes of the fungus that are involved in germination processes: Unlike other simple coumarins, ayapin bears a methylenedioxy bridge, forming a 1,3-benzodioxole motif fused to the aromatic ring (Figure 1). This structure is also described as methylenedioxyphenyl (MDP). MDPs are known in pharmacology to confer mechanism-based inhibition of CYPs: following initial CYP-mediated oxidation of the methylene carbon, a reactive carbene is generated that forms a metabolic-intermediate complex with the heme iron, leading to quasi-irreversible loss of enzymatic activity (Chi et al., 2024; Kamel and Harriman, 2013; Orr et al., 2012). Such a phenomenon is also described for the synergist effect of MDP substances, piperonyl butoxide, or 2,3-methylenedioxynaphthalene, which enhance insecticide efficacy by inhibiting CYPs in target organisms (Feyereisen, 2015; Sacher et al., 1969). The latter also has structural similarities to ayapin, since both have a second ring structure that is fused to the MDP motif (Sacher et al., 1969).

Notably, piperonylic acid - a small MDP found in the bark of the Paracoto tree and a structural mimic to cinnamic acid – is inhibiting the CYP enzyme C4H of the PPP *in vitro* (Schalk et al., 1998). In the same study, the authors additionally tested several other small MDPs with a similar structure to piperonylic acid. Among the substances tested was ayapin, which significantly inhibited C4H enzyme activity by 13 % (Schalk et al., 1998). This was not as strong as piperonylic acid, but still much stronger than e.g., 3,4-(Methylenedioxy)-cinnamic acid (MDCA; 2 % inhibition) – a known inhibitor of CYPs such as 4CLs (Funk and Brodelius, 1990). This exemplifies that ayapin is indeed able to inhibit CYPs in a biological context Parallel to the plant kingdom, the CYP enzyme superfamily in fungi, especially plant-pathogenic fungi, is large, with many CYPs being

differentially expressed during development of the fungus (Ortiz-Álvarez et al., 2024). Thus, one could argue that ayapin is bioactivated by endogenous CYPs of *P. pachyrhizi* and subsequently inhibits fungal CYPs that are essential for germination processes.

The biochemical properties of ayapin could further support this hypothesis: Due to the absence of free hydroxy groups, ayapin is relatively hydrophobic. This is consistent with ayapin's relatively late retention on a C18 reversed-phase HPLC column, where hydrophobic, low-polarity analytes interact more strongly with the stationary phase and should therefore elute at longer retention times (Figure 22). This hydrophobicity should facilitate membrane permeation. A fact that seems to play a crucial role in the anti-fungal activity of coumarins. For example, esculetin (two free hydroxy groups) shows higher antioxidative activity than scopoletin (one free hydroxy group), yet does not inhibit *P. pachyrhizi* spore germination, most likely due to higher hydrophilicity and thus lesser permeability compared to scopoletin (Beyer, 2019). Notably, scoparone, like ayapin, lacks a free hydroxy group, is relatively hydrophobic, and does not exhibit ROS-scavenging activity (Figure 1, Figure S 16). However, scoparone shows a much weaker protective effect against *P. pachyrhizi in vitro* and in *planta* (Schwinges, 2019; Weber Böhlen, 2021). In this comparison, the only structural difference between scoparone and ayapin is the methylenedioxy bridge in ayapin, supporting the hypothesis that ayapin affects the spores via a distinct mode of action that is connected to this unique chemical moiety. These presumably different MoA of scopoletin and ayapin might be the reason that ayapin is inhibiting *P. pachyrhizi* even more effectively than scopoletin. *In vitro* assays with *Sclerotinia sclerotiorum* revealed a 10-times higher effect of ayapin against the fungus compared to scopoletin (Urdangarín et al., 1999). The authors discuss whether this is due to ayapin being more hydrophobic than scopoletin (Urdangarín et al., 1999).

Overall, next to scopoletin, ayapin seems quite potent for protecting soybean from SBR. Coumarins could be used for crop protection by direct application as biocontrol agents. To obtain sufficient amounts of coumarins for direct application in plant protection, one option could be to extract them from plant species that naturally accumulate relatively high levels of these secondary metabolites. An alternative, and potentially more efficient and sustainable, strategy to the direct application would be to engineer target crops synthesizing, accumulating, and secreting coumarins. To achieve this, it is essential to elucidate the biosynthetic pathway of compounds such as ayapin, thereby providing the genetic basis required for transferring and reconstructing the pathway in other species. As a basis for both approaches – the extraction of ayapin and the elucidation of its biosynthesis – a suitable host plant was needed.

On sunflower as a model for uncovering ayapin biosynthesis

So far, the dynamics of ayapin accumulation are so far only described for sunflowers (Gutierrez, 1995; Gutiérrez-Mellado et al., 1996; Prats et al., 2002; Tal and Robeson, 1986). Hence, in a large field trial almost 200 sunflower genotypes were screened regarding their coumarin secretion (Figure 5). Since the field plants were naturally exposed to several abiotic and arguably biotic stresses, the experimental environment lacks controlled conditions, resulting in high standard deviations between the samples of each genotype (Table S 1). Still, this field data gives a first overview of coumarin secretion in a broad range of sunflower genotypes and may lay the foundation for further studies on coumarins in sunflower.

Deriving from the field data, 16 genotypes with distinct coumarin profiles were selected and re-tested under greenhouse conditions. Despite some quantitative differences in coumarin accumulation, most genotypes showed the same qualitative pattern as they did in field experiments (Figure 5). In this second screening, genotype SF_170 secreted the highest amount of ayapin of all tested genotypes, while simultaneously secreting scopoletin in the same range as RHA857 (Figure 5B). In line with the observations by David Spencer (2022), no traces of ayapin could be found in any RHA857 samples across all experiments during this work (Figure 5-Figure 8 and Figure 12, Figure 14). This strongly suggests that RHA857 is completely impaired in ayapin biosynthesis, while being able to accumulate and secrete scopoletin to average sunflower levels. In contrast, ayapin could be detected in each sample of SF_170 ayapin (Figure 5-Figure 8). Thus, it was intriguing to elucidate coumarin biosynthesis by comparing those two contrasting genotypes more deeply.

At the beginning of this work, I hypothesized that ayapin is directly synthesized from scopoletin *in planta*. This hypothesis is supported by three observations: (i) sunflower genotypes that secreted ayapin at high concentrations (>10 µM) did not exceed scopoletin concentrations of > 10 µM, arguably because scopoletin is converted to ayapin (Figure 5B); (ii) ayapin levels of SF_170 samples during $CuCl_2$-elicitation increased steadily over, whereas scopoletin levels increased up to 24 h and then plateaued (Figure 6); (iii) in samples of the same experiment, *HaF6'H1* expression was similar between the two genotypes (Figure S 20), while scopoletin concentration was much higher in RHA857 samples (Figure 6). Thus, one could assume that a similar HaF6'H1 activity would lead to similar scopoletin levels in both genotypes. Notably, the sum of scopoletin and ayapin in the SF_170 samples is similar to the scopoletin content in RHA857 samples (Figure 6). Interestingly, higher ayapin concentrations of SF_170 leaf discs could only be reached when elicited with $CuCl_2$ (Figure 7 B/C). The induction of ayapin biosynthesis upon stress is in line with earlier

observations in this research group (Schwinges, 2019) and earlier findings (Gutierrez, 1995; Prats et al., 2002; Tal and Robeson, 1985).

Taken together, feeding sunflower stem sections with radiolabeled scopoletin led to the detection of radiolabeled ayapin (Tal and Robeson, 1986); inhibiting scopoletin biosynthesis with prohexadione led to impaired ayapin accumulation (Schwinges, 2019); feeding sunflower plants with high amounts of scopoletin leads to increased accumulation of ayapin (Figure 6, Figure 7C). Thus, together with the structural similarity, it seems plausible that scopoletin is directly converted to ayapin by the formation of a methylenedioxy bridge (Figure 7A). Furthermore the formation of ayapin from scopoletin seems not to occur spontaneously in a physiologically relevant time span. Otherwise, supplying scopoletin in high concentrations should already lead to an increase in ayapin accumulation, regardless of $CuCl_2$-treatment (Figure 7 C). Moreover, this result argues against a scenario in which the genes underlying ayapin biosynthesis are constitutively expressed and present in the plant, with $CuCl_2$ merely increasing precursor availability.

This work demonstrated that placing a drop of $CuCl_2$ onto the leaf surface was sufficient to elicit coumarin accumulation in the leaf surface and in the respective droplet (Figure 8, Figure S 1). This elicitation was highly localized, as nearby H_2O-droplets showed almost no coumarin accumulation. Therefore, this set-up was rated suitable to elucidate plant tissue that was very locally induced and compare it to uninduced tissue from the same leaf or even from the same leaf area (Figure 8). This approach was exploited for a global transcriptome analysis of the sunflower genotypes RHA857 and SF_170 to identify genes that were elicited by $CuCl_2$, and thus might play a role in ayapin biosynthesis. PCA of the transcriptome data identified the variance between the genotypes as the most relevant (PC1) and the variance between treatments as the second most relevant (PC2) cause for occurring differences in the transcriptome data (Figure 9). Biological replicates clustered by genotype and treatment, supporting the robustness of the design and the separation of underlying molecular responses. Within each genotype, the six samples clustered tightly, indicating homogeneous input material. DEA revealed that *HaF6'H1* was significantly upregulated in both genotypes under $CuCl_2$ stress ($l_2fc > 1.5$, yellow dot, Figure 10 A,B). As described for AtF6'H1 in Arabidopsis (Kai et al., 2008), HaF6'H1 is the key enzyme for scopoletin biosynthesis in sunflowers. (Schwinges, 2019). Thus, *HaF6'H1*-expression served as a marker for coumarin biosynthesis activation. Next to this marker, I assumed that the gene responsible for ayapin biosynthesis should also be induced in the SF_170 samples. Additionally, from the previous data, I hypothesized that a putative AySy candidate would be either not expressed or only weakly expressed in RHA857 samples. Conversely, a detectable induction and expression in RHA857

would imply that the respective AySy candidate had lost its biological function, most likely due to mutation.

As already mentioned, in both scenarios I assumed that the gene was belonging to the CYP superfamily, since the formation of methylenedioxy bridges is described to be catalyzed by these enzymes (Bourgaud et al., 2006; Mizutani and Sato, 2011; Ono et al., 2006; Schnabel et al., 2021). Most of these CYPs that are described to catalyze this specific reaction belong to the CYP81 or CYP719 families (Mizutani and Sato, 2011). However, CYP families and subfamilies are classified based only on their respective AA sequence identity. In general, CYPs with an AA sequence identity higher than 40 % are clustered in one family (Nelson, 2006). Notably, the two families described to catalyze methylenedioxy bridge formations are quite heterogeneous. For example, PnCYP719 and SiCYP81, which both catalyze methylenedioxy bridge formation in their respective plant species (compare Figure 2, Ono et al., 2006; Schnabel et al., 2021), only have a 25 % AA sequence identity and less than 50 % AA sequence similarity (Figure S 18). This shows that structurally distinct CYPs from different families can catalyze similar reactions. Conversely, some CYPs with high sequence homology exhibit entirely different substrate specificities and convert different substrates (Otey et al., 2004). Because of this, and since so far no conserved motif that is specific for methylenedioxy bridge formation in CYPs is described, I chose to consider all enzymes belonging to the CYP superfamily as potential candidates for ayapin biosynthesis. In the sunflower genome that was published by Badouin et al. in 2017 and updated in 2020, 322 genes are annotated as "cytochrome P450 monooxygenases" (Badouin et al., 2017). These exclude specific annotations such as isoflavone-hydroxylases or germacrene A oxidases, which also belong to the CYP superfamily. In total, at least 610 genes that are annotated in the sunflower genome could be considered as monooxygenases that could be responsible for ayapin formation. The transcriptome analysis revealed 33 of those CYPs that were significantly upregulated in the leaf tissue of genotype SF_170 that was induced with $CuCl_2$ (Figure 10). By additional criteria, these CYPs were narrowed down to a final 12 candidate genes (Table 2). The decisions that led to the final candidates are described in the results section (2.3) and are depicted in Figure S 5.

While the identification of promising AySy candidates was successful, their subsequent experimental validation introduced additional challenges. Prokaryotic expression systems, such as „simple" overexpression in *E. coli* is not feasible for studying plant-derived CYPs since these enzymes are embedded in the membrane of the endoplasmic reticulum (Bourgaud et al., 2006). Therefore, a eukaryotic test system was needed. The final AySy candidates (Table 2) were tested by transiently overexpressing them in *N. benthamiana*. To provide a sufficient supply of scopoletin, *HaF6'H1*- and *AtMYB72*-constructs were co-infiltrated. Under these conditions, scopoletin content

in transformed leaves reached levels that were notably higher (~5-30 µg/g FW; Figure 11) than scopoletin content in induced sunflower leaf extracts, which are arguably sufficient for ayapin biosynthesis (~1-2 µg/g FW; Figure 6).

In theory, this setup promised several advantages compared to, for example, yeast expression systems: *N. benthamiana* should naturally provide the required cofactors such as heme and NADPH. Moreover, CYP reactions require a cytochrome P450 reductase as a redox partner (Urban et al., 1997). This reductase, however, does not appear to be CYP specific. For example, AtATR1 – a CYP reductase from Arabidopsis – is used in several biotechnological approaches to enhance CYP reaction mechanisms across species (Liu et al., 2023; Schnabel et al., 2021; Urban et al., 1997). Thus, reductases present in *N. benthamiana* should be sufficient for the tested CYP candidates. The test system also provided the opportunity to co-overexpress all candidates or subsets thereof to assess whether a combination of enzymes is required for ayapin biosynthesis. Additionally, testing CYPs in an intact plant environment offers the possibility that, even if scopoletin is not the precursor of ayapin, boosting the PPP in general by overexpressing *AtMYB72* (Weber Böhlen et al., 2026) might nonetheless allow identification of the relevant candidate.

In practice, however, transient overexpression of all AySy candidates in *N. benthamiana* did not lead to detectable ayapin accumulation, despite strongly elevated scopoletin levels (Figure 11) Because this system currently lacks a positive control, it remains unclear whether this reflects the absence of the correct AySy candidate among those tested, insufficient activity of the *N. benthamiana* assay system, or a combination of both. Consequently, additional heterologous test systems will be required to clarify the enzymatic steps of ayapin biosynthesis. Functional analyses of plant CYPs are frequently performed in yeast expression systems combined with microsomal feeding assays (Ono et al., 2006; Schnabel et al., 2021), which therefore represent a logical next step for future work.

Nevertheless, it remains possible that the transcriptome analysis has not yet identified the correct candidate for ayapin biosynthesis. I chose to elucidate the transcriptomic changes at 48 h based on the findings that ayapin levels increase continuously over a period of 96 h (Figure 6). Also, feeding scopoletin in high concentrations led to ~6-fold higher ayapin concentrations in droplets harvested after 48 h compared to 24 h (Figure 7, Figure S 22). And, *HaF6'H1*-expression was also most induced at 24 h and 48 h after elicitation in both sunflower genotypes (Figure 14, Figure S 20). Still, a potential AySy could already be strongly upregulated within the first 24 h and then could have rapidly declined on the transcriptional level. For example, in Arabidopsis, $CuCl_2$-treatment led to induction of pathogenesis-related genes (*PR-1* and *PR-5*) at 8 h post treatment and declined already

after 12 h of treatment (Liu et al., 2015). However, for sunflower, it seemed that the $CuCl_2$-response was slower compared to the response in Arabidopsis, since *HaPR1-like* expression was increasing over 48 h (Figure S 20, Figure S 21) and was still significantly induced in the transcriptome data at this timepoint compared to the water control (Figure 10 A/B, green dot).

Moreover, it is also possible that, even though previous results in the literature point in this direction, CYPs are not the decisive enzymes for these reactions. Other oxygenases, such as Fe^{2+}-dependent dioxygenases or flavin-dependent monooxygenases, could potentially form a methylenedioxy bridge within an enzyme complex. Even though this might be chemically plausible, it remains speculative.

To obtain genetic evidence for the locus (or loci) controlling ayapin formation independently of the CYP-based approach, a BSA was initiated. For this, genotypes SF_170 and RHA857 were crossed. Notably, almost all F_1-individuals were able to accumulate ayapin (Figure 12 B), indicating that the ability to synthesize ayapin behaves as a dominant trait. The segregation pattern of ~1:3 in the F_2-generation additionally showed that this "ayapin-trait" is most likely inherited according to simple Mendelian laws (Figure 12 E/F). Consequently, if several genes are involved in the key step for ayapin synthesis, they would probably be inherited as a cluster. Otherwise, it stands to reason that only one gene is involved to catalyze the last step in ayapin biosynthesis. To identify the genomic region in question, DNA of 50 F_2-individuals that accumulated ayapin was pooled. A second pool (or bulk) consisted of DNA of 50 F_2-individuals that were not able to accumulate ayapin. Both DNA-bulks, together with pooled DNA of each parental line, were chosen for whole genome sequencing. The subsequent BSA, which is being carried out at the time of writing, will hopefully provide further insight into the genetic basis of ayapin biosynthesis and to complement the transcriptomic data.

The attempts to elucidate ayapin biosynthesis represent a rather focused investigation of one individual step within sunflower coumarin metabolism. To uncover additional, potentially previously overlooked aspects of coumarin biosynthesis, a forward genetic screen can be advantageous, as it may enable an initially unbiased assessment of coumarin-related phenotypes. Such a screen revealed sunflower mutant M-4/626 which displayed a robust and heritable phenotype of increased scopoletin accumulation and secretion that was confirmed across independent experiments and in a field setting (Figure 13, Figure 14, Figure S 6).

In the case of the identified mutant M-4/626, the biosynthesis gene *HaF6'H1* was neither significantly altered in transcription nor was any mutation detected in its coding sequence that could account for the higher scopoletin accumulation (Figure 14, Figure S 19). In addition, *HaABC*

transcription showed at most a two-fold increase and accelerated induction in the mutant (Figure 14). This rather subtle transcriptional shift may contribute to the increased secretion of scopoletin, but it seems unlikely that it fully accounts for the several-fold changes in metabolite levels. Hence, additional, yet unidentified, genetic factors could contribute to the M-4/626 phenotype. One of these factors could be a transcription factor that increases the precursor availability in the mutant line, which would subsequently lead to higher scopoletin content, once *HaF6'H1* is induced. A similar mechanism was described by Zamioudis et al. (2014) in Arabidopsis roots. AtMYB72 increases transcription of genes in the core PPP without affecting *AtF6'H1* expression (Beesley, 2022; Weber Böhlen et al., 2026; Zamioudis et al., 2014).

It is also conceivable that the coumarin phenotype simply reflects a more rapid general stress response of the mutant to $CuCl_2$ induction, since $CuCl_2$ is not a coumarin-specific elicitor but a general elicitor that triggers pathogen-associated defense responses in plants, including *PR* gene expression (Liu et al., 2015). Consistent with this, *HaPR1-like* was strongly induced by $CuCl_2$ in the transcriptome analysis of both RHA857 and SF_170 (Figure 10). However, in M-4/626, *HaPR1-like* transcript levels after $CuCl_2$-elicitation were ~2-fold lower than in RHA857-ML (Figure S 21). Thus, a more sensitive response to $CuCl_2$ should rather lead to a stronger transcription of *HaPR1-like* than a weaker transcription, as shown in this work. In future work, it will therefore be necessary to elicit the mutant with different stressors, e.g. UV-light, to determine whether a faster response can be observed in the mutant under other conditions.

Independent of changes in known pathway or stress-responsive genes, leaf surface morphology may also contribute to the M-4/626 phenotype. For example, short glandular trichomes are specialized epidermal structures that accumulate that are described to secrete PSM onto the phylloplane (Glas et al., 2012; Shepherd et al., 2005). A higher density of short glandular trichomes in M-4/626 could therefore enhance scopoletin secretion without major changes in known pathway genes. Hence, a comparative analysis of leaf surface anatomy and trichome density in M-4/626 and RHA857-ML will be part of future work.

To allow further dissection of the phenotype, the mutant has already been back-crossed (BC) in the maternal line in the course of this work. BC_1-plants were evaluated in the field, where some individuals seemed to have kept the scopoletin-hyperaccumulating phenotype (Figure S 6). Positive BC_1-plants again were backcrossed in the RHA857-ML of which BC_2-plants will be selected for the particular phenotype again (Presotto et al., 2011). The BC_2 generation will then be subjected to genomic analysis to find candidate genes that are responsible for the scopoletin-hyperaccumulation trait.

Next to the mutant line of RHA857, the elucidation of the sunflower core collection also revealed genotypes that seem increased in coumarin accumulation. Most prominent was RHA401 – a genotype that accumulated ~ 20-fold more scopoletin than RHA857 (Figure 5B). Because the genetic background of RHA401 is likely more divergent from RHA857 than that of M-4/626, genetic dissection could be more complex. Nevertheless, RHA401 represents a promising resource for identifying additional factors involved in induced coumarin accumulation, for example through comparative transcriptomic or targeted candidate-gene approaches.

Taken together, the identification of the scopoletin-hyperaccumulating mutant M-4/626 provides a powerful genetic entry point to uncover novel regulators and mechanisms controlling coumarin biosynthesis and exudation in sunflower. Furthermore, the combination of the transcriptome analysis and the whole-genome sequencing analysis bears great potential to finally identify the gene or genes that code for the enzyme responsible for the key step in ayapin formation.

On harnessing sunflower coumarins

Building on these genetic insights, an important next step is to explore how sunflower-derived coumarins can be harnessed for practical crop protection and biotechnological applications.

In sunflowers, the accumulation of coumarins has been correlated with various defense responses: increased resistance towards *S. sclerotiorum*, *P. helianthi,* and *Orobanche cernua*, and repelling effects towards the sunflower beetle (Olson and Roseland, 1991; Prats et al., 2002; Rial et al., 2021; Serghini et al., 2001; Urdangarín et al., 1999). Thus, understanding the coumarin biosynthesis in sunflower and identifying a trait that corresponds to high coumarin accumulation could be of interest to sunflower breeders in the search for new defense traits.

Additionally, a high coumarin content in sunflower could not only be interesting for protection of the sunflower itself, but moreover could provide a source for bioeconomic approaches that focus on the multiple valorization of residual streams from agriculture (Kover et al., 2022). Investigating whether a crude extract of the sunflower biomass that is left after harvesting is feasible to be used as a biopesticide, e.g., by simply extracting the soluble contents of sunflower, could potentially provide farmers with an additional source of income. Similar approaches are already suggested for the valorization of the residual biomass from potato and tomato plants (Adebomi et al., 2025). Such an approach would be especially promising when such a high-accumulating genotype would be crossed with a genotype that is able to synthesize ayapin, since ayapin seems to bear an even greater antifungal potential than scopoletin (Figure 4, Schwinges, 2019). However, the effectiveness, formulation, environmental safety, and potential agronomic trade-offs of such biomass-based biopesticides would need to be systematically evaluated.

It has been reported that, among other inducers, coumarin biosynthesis is also induced by UV-light in several plant species (Spencer, 2022; Wang et al., 2025). Thus, based on their structure, scopoletin and ayapin may also be exploited beyond their antimicrobial activity for photoprotective purposes. Such a putative photoprotective effect can be qualitatively visualized using UV-sensitive paper (Figure S 23). Since there is an increasing need for photo protectants of light-sensitive agrochemicals (Deota et al., 2023), the sunflower coumarins could potentially serve as a biodegradable alternative to be added to agrochemicals for UV-protection. Photo protection also plays an important role in SIGS. Here, nanocarriers such as clay nanosheets are used to protect siRNA from UV-degradation (Chen et al., 2025). It would be intriguing to investigate whether coumarins would also be able to photo-protect the RNA when co-applied with it. In light of ongoing efforts to use SIGS to protect soybean from soybean rust (Ouyang et al., 2024), a combined application of SIGS with sunflower coumarins could provide a dual benefit: protection of siRNA from UV radiation and, simultaneously, a direct inhibitory effect on *P. pachyrhizi*, as demonstrated in this work.

Complementary to exogenous application of crude sunflower extracts or isolated coumarins for crop protection, transfer of the coumarin biosynthesis and secretion pathway from sunflower to crops like soybean, which lack this defense mechanism, may contribute to secure crop yield under disease pressure.

This work demonstrates that it is possible to functionally transfer sunflower biosynthesis genes into soybean, as seen in transgenic soybean lines overexpressing *HaF6'H1* and consequently accumulating scopoletin (Figure 15D/E, Figure S 8). Preliminary data in this work indicate that scopoletin levels in these transgenic soybeans are similar to the levels in $CuCl_2$-induced sunflowers leaves (0.5-5 µg/g FW, Figure 6, Figure 15, Figure 14, Figure S 8). However, the scopoletin content will be more extensively evaluated when plants are further selected and propagated in still ongoing work. Even though previous results from this research group gained from work on transgenic soybeans overexpressing *AtF6'H1* did not yet yield success regarding protection against *P. pachyrhizi* (respective plants only had a ~10 % reduction of soybean rust symptoms in field trials in Brazil, Beyer, 2019), accumulating coumarins in soybeans still seems to be a promising approach that needs some minor adjustments. A recent study described that ferulic acid content – a direct precursor of scopoletin – is rising in soybean plants that were inoculated with *P. pachyrhizi* compared to the content in untreated control plants (Silva et al., 2020). This naturally occurring boost of ferulic acid in soybean could likewise lead to a boost of scopoletin upon pathogen attack, when *HaF6'H1* is respectively expressed. However, for sufficient protection of such transgenic soybeans, the antimicrobial coumarins would probably not only need to accumulate in the plant but

also be secreted to the leaf surface, as discussed by Sebastian Beyer and David Spencer in their respective studies (Beyer, 2019; Spencer, 2022). In this regard, David Spencer investigated an ABC transporter from sunflower (HaABC), which seems to play a role in coumarin secretion (Spencer, 2022).

Whether the sunflower secretion mechanism can be transferred to soybean by expressing *HaABC* remains to be determined. The transgenic soybean lines generated in this study were able to grow and reproduce despite *HaABC* expression (Figure 15), which is already a success compared to previous attempts in our research group, where straightforward overexpression of *HaABC* caused detrimental effects on the plants (data not shown). This improvement was likely due to the fact that the relative expression levels of *HaABC* were 10-100 times lower then the levels of overexpressed transgenes *HaF6H1* and *AtCOSY* (Figure 15E/F, Figure S 7). To gain those lower expression levels of *HaABC*, the respective CDS was placed under the control of the promoter sequence of *GmPRP3* – a gene whose mRNA was described to localize in the epidermis of mature soybean leaves (Wyatt et al., 1992). Accordingly, the promoter region of this gene was chosen in this work to restrict transcription of *HaABC* to epidermal cells at the leaf surface. For RNA isolation of the analyzed leaf material, however, whole leaves were homogenized, so the proportion of epidermal cells in the samples was relatively low. In addition, the *p*GmPRP3 sequence had not been tested in transgenic soybean before. To examine its activity and spatial specificity, a second line was generated in which *eGFP* is driven by *p*GmPRP3, while *mRFP* is constitutively expressed (Figure S 8). A first preliminary screen yielded one successful transformation event. Notably, relative *eGFP* expression in this line was ~10-fold lower than relative *HaF6'H1* expression, whose CDS was placed under the control of *p*PcUBI (Figure S 8). In future work, this line can be used to analyze the localization of eGFP in relation to mRFP and thereby provide further insights into the suitability of *p*GmPRP3 for genetic engineering.

The genetic tools have so far been discussed mainly in the context of the soybean–SBR interaction. However, the potential applications of this toolbox extend beyond this patho-system. For example, work in this research group demonstrated that transgenic soybean lines overexpressing *AtF6'H1* showed increased resistance to *F. virguliforme* (Beesley et al., 2023). In addition, recently published studies have shown that overexpressing a cotton *F6'H1* (*GhF6'H1*) led to increased scopoletin levels in *Gossypium hirsutum* (cotton) and enhanced resistance towards *Verticillium dahlia* (Gao et al., 2024). Also, the overexpression of a sweet potato *F6'H* (*IbF6'H2*) in tobacco led to increased scopoletin accumulation and increased resistance towards *F. oxysporum* (Wang et al., 2024).

Even though these examples show a great potential for how plant metabolic engineering could be used for crop protection, there could potentially also be a downside of hyperaccumulation of coumarins such as scopoletin, since high coumarin concentration has also been associated with phytotoxic effects (Le Roy et al., 2016). Recent work in this research group, for example, demonstrated that Arabidopsis that hyperaccumulate scopoletin by simultaneous overexpression of *AtMYB72* and *AtF6'H1* show a dwarfed phenotype. Here, the endogenous detoxification mechanism of the plant by glycosylating scopoletin to its inactive form scopolin, can most likely not overcome the coumarin concentration (Beesley, 2022; Weber Böhlen et al., 2026). Yet, this work also discusses that genetic fine-tuning can overcome such phenotype.

However, all these recently mentioned examples of engineering coumarin biosynthesis in plants have focused on scopoletin. In the future, it would be interesting to expand the coumarin toolbox. This work demonstrated that ayapin might be a potential candidate once the biosynthesis is elucidated. Alexander Beesley demonstrated during his doctoral studies that transgenic soybeans that overexpress the biosynthesis genes necessary for sideretin formation showed a significant reduction of *P. pachyrhizi* infection severity (Beesley, 2022). Moreover several other coumarins, including isoscopoletin, umbelliferone, herniarin, and scoparone show antimicrobial properties (Repčák and Suvák, 2013; Schwinges, 2019; U. Afek and A. Sztejnberg, 1988; Weber Böhlen, 2021), and additionally possess diverse biochemical structures, which lead to different chemical properties (compare Figure 1). Scoparone, for example, parallel to ayapin, lacks free hydroxy groups and thus cannot be glycosylated to an inactive form, whereas isoscopoletin is not degraded when exposed to light and, hence, is potentially longer lasting on the leaf surface (Weber Böhlen, 2021).

Once the in-depth analysis of the transgenic soybean lines generated in this work is completed, they might serve as a blueprint to generate transgenic soybeans that accumulate reasonable high concentrations of a mixture of antifungal compounds on the leaf surface, and once the missing link is found, would allow the generation of soybean plants that accumulate ayapin. In the end, expanding the genetic toolbox and thus diversifying the mix of coumarins that could be added to plants *via* metabolic engineering will be most advantageous regarding crop protection.

On fighting *P. pachyrhizi* with its own weapons

While working with and on *P. pachyrhizi,* it was striking that the spore germination success *in vitro* was highly dependent on the spore density (Figure 16A). Such a crowding effect is already described for several fungal species (Allen, 1955; Chitarra et al., 2005; Leite and Nicholson, 1993; Macko et al., 1972; Tsurushima et al., 1984). In all of these cases, this effect was traced back to so-

called self-inhibitory substances. For *P. pachyrhizi,* there are, so far, no reports on a potential self-inhibitory substance. Yet, the results of this work suggest that such compound or a combination of self inhibitory compounds might also exist for *P. pachyrhizi* (Figure 16-20): First, the density-dependent inhibition can be reversed, when spores are washed with ddH_2O (Figure 16B) and second, the wash water itself can be used to inhibit spore germination at lower density (Figure 16D). This is in line with previous studies where the self-inhibitory substance was also present in the wash fraction (Allen, 1955). Lastly, the supernatant of *P. pachyrhizi* isolate br05 was also inhibiting germination of isolate RS2 (Figure 16E). The fact that the self-inhibitory activity is not isolate-specific, but also affects spores of a different isolate, makes such a compound particularly intriguing for crop protection purposes. Additionally, since a self-inhibitory substance is probably essential for the life cycle and propagation of the fungus, resistance development against such a compound might be a considerable challenge for the pathogen. Hence, isolating and identifying potential self-inhibitory substances of *P. pachyrhizi* could be an inspiration for further nature-based crop protection strategies.

Previously identified self-inhibitory substances are structurally quite diverse, ranging from complex molecules like dihydro-5-hydroxy-5-((8pentyl-2-oxocanyl)-acetyl)-2(3H)-furanone (gloeosporone, Lax A.R. et al., 1985) to rather simple, volatile compounds such as 1-octanol found in *Penicillium camemberti* (Gillot et al., 2016). In rust fungi, especially in the *Puccinia* family, two compounds are predominant: Methyl-ferulate and methyl-3,4-dimethoxycinnamate (Macko et al., 1970; Macko et al., 1972; Tsurushima et al., 1984). Notably, the latter are derivatives of the coumarin precursors cinnamate and ferulate, and are structurally quite similar to scopoletin. Hence, it is quite tempting to speculate that those known self-inhibitory substances act in the same way as scopoletin does (Beyer et al., 2019). Interestingly, for *Puccinia graminis f. sp. tritici* race 126-ANZ-6,7 none of the two substances were identified as an endogenous self-inhibitor (Macko et al., 1972). This also seems to be the case for *P. pachyrhizi*. During this work neither substance could be detected in extracts of *P. pachyrhizi*. However, detailed fractionation of the *P. pachyrhizi* wash water and subsequent NMR analysis revealed the presence of CA in the two highly active fractions of *P. pachyrhizi* wash water (Figure 18-19).

CA is a primary metabolite of most living organisms and a key intermediate in the tricarboxylic acid (TCA) cycle (Berg et al., 2018). Staples and Wynn (1965) report that the TCA cycle is generally active in uredospores of rust fungi. The same authors claim that citric acid was found in extracts of resting uredospores of wheat leaf rust and wheat stem rust to the extent that CA "invariably crystallized from spore extracts" (Staples, 1957; Staples and Wynn, 1965). However, there is no evidence that CA or other TCAs are exported by rust uredospores. So far CA export of

fungal spores is only described for CA-producing species like *Aspergillus niger* during growth phases that include spore germination (Steiger et al., 2019). Thus, the question remains whether CA is actively exported by *P. pachyrhizi* spores or if the presence of CA is only due to metabolic leakage. Based on the fractionation experiments, I calculated that approximately 15-30 µg CA per 1 mg spores were isolated (Table S 2). This accounts for 1.5-3 % of the spore mass, which seems rather high to be only due to metabolic leakage. Yet, to further assess the relation of external and internal CA of *P. pachyrhizi* spores an spore extract could be additionally analyzed.

Reports on citric acid affecting fungal development are rather scarce. Pine and Peacock report in 1958 that the mycelial phase of *Histoplasma capsulatum* – a dimorphic ascomycete – is strongly inhibited by the presence of 1-2 % CA in the media (which corresponds to ~50-100 mM CA). These are rather high, non-physiological concentrations. In the case of *P. pachyrhizi*, the amount of 15-30 µg CA/mg uredospores would theoretically account for a concentration of ~ 0.78-1.56 mM CA in a 10 mg/mL spore suspension, where the self-inhibition of the spores is near 100 % (Figure 16A). To address whether CA could indeed function as such a regulator in *P. pachyrhizi*, I next analyzed the effect of exogenously applied CA on spore germination. 250 µM CA (pH = 2.1) completely inhibited spore germination (Figure 21A). Thus, the CA content would be generally sufficient to potentially be a self-inhibitory substance in the *P. pachyrhizi* wash water. However, buffering CA by adding 1 mM MES, inhibited spore germination only at concentrations of > 37.5 mM (pH = 5; Figure 21A). Yet, in this work, the wash water of *P. pachyrhizi* had a pH of ~ 6, regardless of the spore density (Figure S 11). This suggests that the strong inhibitory activity of CA *in vitro* is largely due to acidification of the medium and not to a specific, pH-independent toxic or signaling effect of the molecule itself. CA might in the end acts as a physicochemical modulator of the environment rather than a dedicated, structurally "tailored" self-inhibitory molecule like gloeosporone, methyl ferulate, or methyl-3,4-dimethoxycinnamate. There is also the possibility that the crowding effect is due to a synergistic effect of several substances, with CA being one of them. Other effects like alternated osmolarity can also not be excluded. In total, ~4.5 mg/mL crude extract was washed of the uredospores (Table S 2).On the one hand, this high content of molecules alone could already affect spore germination. On the other hand, the "heaviest" fractions only had a semi-active effect on spore germination (Figure 18, Table S 2).

Taken together, the question remains whether "the one" self inhibitory substance is present in *P. pachyrhizi* spores or if the crowding effect is rather due to a cocktail of metabolites that are secreted by the pathogen. It is also possible that the crowding effect arises only under the artificial *in vitro* germination conditions and has little relevance for the physiological infection cycle of *P.*

pachyrhizi. In future work, additional analyses of the other active fractions of the uredospore wash water (Figure 18) will be necessary to address these points.

Despite these open mechanistic questions, CA had a protective effect against *P. pachyrhizi in planta*. Even though the effect decreased when CA was buffered, 10 mM CA still provided a significant reduction of the mean disease severity of 20 % (Figure 21B). This is in line with two other organic acids, azelaic acid and hexanoic acid (Rodrigues et al., 2023). Here, the authors describe a protective effect when soybeans were treated with 5-20 mM hexanoic acid or 0.1-1 mM azelaic acid (Rodrigues et al., 2023). However, even though the study demonstrates a direct effect of the acid on the fungal spores, it also states that both acids seem to have a priming effect on the plant itself. Thus, it stands to reason that CA also affected the plant itself.

Interestingly, in Arabidopsis, the TCAs fumarate and citrate are described as a defense priming agent (Balmer et al., 2018). Applying 5-10 mM CA was sufficient to induce the plant's defense response and significantly reduce the disease severity of the bacterial pathogen *Pseudomonas syringae* pv. *tomato* DC3000 without having a direct effect on the bacteria (Balmer et al., 2018). Analyzing the differential transcription of priming marker genes in soybean after CA-treatment would give further insides on a potential priming effect of CA on soybean. Yet, in this work, the CA-experiments on soybean were performed as co-treatment of CA and spores (Figure 21), though it remains the question whether a priming effect is the mechanism that causes the protective effect. Pretreating CA and subsequently inoculating plants with *P. pachyrhizi* will be done in future work to evaluate whether CA or other TCA could be used in a two-way principle: One, to strengthen the plants against pathogen attack, and two, directly challenge the pathogen upon the attack. A similar effect is described by Rodrigues et al. (2023). Moreover CA is produced at large scale by fungal fermentation, which helps to keep its costs low; it is highly water-soluble, readily biodegradable, and regarded as safe for humans and the environment (Ciriminna et al., 2017). In addition, CA is already used extensively in food, pharmaceutical and household products, so its toxicology and handling are well characterized (Ciriminna et al., 2017), suggesting that CA-based plant treatments would likely encounter fewer regulatory hurdles than many new synthetic fungicides.

4. Conclusion

Pathogens continuously evolve mechanisms to overcome fungicide classes, as exemplified by the increased tolerance of *P. pachyrhizi* isolate RS2 towards the three fungicide classes DMI, QoI, and SDHI. Consequently, controlling these pathogens must be approached with equally diversified strategies.

In this work, scopoletin, ayapin and citric acid were disclosed as nature derived compounds with protective activity against *P. pachyrhizi*, and studies with sunflower delineated key genetic and biochemical steps in ayapin biosynthesis and secretion. The identification of candidate genes putatively encoding an ayapin synthase, a coumarin-hyperaccumulating sunflower mutant, and transgenic soybeans expressing sunflower coumarin biosynthetic and transporter genes together provide a framework for exploiting these metabolites in future crop-protection strategies.

Collectively, these findings illustrate how nature-derived compounds and their underlying biosynthetic and secretion pathways can be exploited and engineered for crop protection, while at the same time representing only a small fraction of the biological diversity that could be harnessed for this purpose.

For example, the sunflower coumarins – scopoletin and ayapin – are only two members of the simple coumarins, most of which exhibit antimicrobial activity, and simple coumarins themselves represent just one specialized branch of the phenylpropanoids. Phenylpropanoids are, in turn, only one of many groups of plant secondary metabolites that could potentially be used for crop protection. Moreover, the use of biological substances as antimicrobial agents is only one pillar of plant protection. Inducing a plant's own resistance to biotic and abiotic stresses, or combating pathogens using other innovative approaches e.g. RNA interference technology, further broadens the arsenal to protect plants (or to support plants in protecting themselves). Ultimately, only a combination of strategies and active ingredients, including "classic" fungicide treatments, together with smart, targeted breeding, and good cultural practice will enable the development of efficient and, most importantly, sustainable solutions to the future challenges of crop protection.

5. Material and Methods

5.1. Chemicals

Chemicals used for experimental set-ups were obtained from Carl Roth (Karlsruhe, Germany), AppliChem, or Merck (both located in Darmstadt, Germany), unless stated otherwise. Scopoletin as a reference substance for HPLC calibration was obtained from TCI, Japan, while ayapin was purchased at BLD Pharms, China. Molecular procedures were carried out using double distilled water (ddH_2O), which was processed in an Arium® Ultrapure Water System (Sartorius).

5.2. Organisms

Table 4. List of plants that were examined in this study. Note that a list with all 196 sunflower genotypes that were characterized in field trials can be found in the supplemental data, while this list only shows the genotypes that were further evaluated.

plant species	genotype	reference
Helianthus annuus	RHA857 (R)	University of Hohenheim, V. Hahn
Helianthus annuus	SF_170 (S)	University of Hohenheim, V. Hahn
Helianthus annuus	RHA401	University of Hohenheim, V. Hahn
Helianthus annuus	HA germ. pool III-E	University of Hohenheim, V. Hahn
Helianthus annuus	HA458	University of Hohenheim, V. Hahn
Helianthus annuus	HA851	University of Hohenheim, V. Hahn
Helianthus annuus	HA852	University of Hohenheim, V. Hahn
Helianthus annuus	HA-BSR6	University of Hohenheim, V. Hahn
Helianthus annuus	HA-BSR8	University of Hohenheim, V. Hahn
Helianthus annuus	HA-R8	University of Hohenheim, V. Hahn
Helianthus annuus	RHA368	University of Hohenheim, V. Hahn
Helianthus annuus	RHA426	University of Hohenheim, V. Hahn
Helianthus annuus	SF_234	University of Hohenheim, V. Hahn
Helianthus annuus	SF_317	University of Hohenheim, V. Hahn
Helianthus annuus	SF_320	University of Hohenheim, V. Hahn
Helianthus annuus	AMES18925	USDA: PI 650755
Glycine max	Abelina	Saatbau, Germany
Glycine max	Williams 82	Lifeasable®
Nicothiana benthamiana	-	RWTH Aachen University, U. Commandeur

Table 5. List of plant pathogens used in this study. Isolates RS1, RS2 and RS3 were subjected to single-spore purification on detached soybean leaflets by Embrapa Brazil (Da Rocha et al., 2025).

pathogen	isolate	reference
Phakopsora pachyrhizi	br05	RWTH Aachen University
Phakopsora pachyrhizi	RS1	Embrapa, Brazil
Phakopsora pachyrhizi	RS2	Embrapa, Brazil
Phakopsora pachyrhizi	RS3	Embrapa, Brazil

5.2.1. Cultivation and propagation of *H. annuus* in the greenhouse

Sunflower seeds were kept on moist paper in petri dishes for 72 h under long-day conditions to initiate germination. Germlings were transferred to single pots (Ø 14 cm) containing ED73 soil (Einheitserde®). Seedlings were grown in a greenhouse under long-day conditions (16 h photoperiod) at 20-28 °C with regular watering. Temperature within the greenhouse fluctuated in response to daily changes in outside temperature and the absence of an active cooling system. Plants that were kept for propagation were transferred to larger pots (25x25 cm) and grown until flower heads were developed. To self the mutant or crossing lines, the emerging disc florets were brushed 3-5 times a week with a soft paper tissue to ensure pollination of stigmas. This was repeated until the sunflower flower disc was completely developed. Dry sunflower heads were harvested and fully developed seeds were incubated at 37 °C for at least two weeks to break dormancy.

5.2.2. Cultivation of *H. annuus* under field conditions

The cultivation and propagation of sunflower plants under field conditions were performed and supervised by Volker Hahn and his team (University of Hohenheim). The fields were located at the experimental station Eckartsweier in Willstätt, Germany (Coordinates: 48.521803368018105, 7.871343892834666; Altitude: 141 m above sea level, https://versuchsstation.uni-hohenheim.de/en/qs-eckartsweier-en). In the first two weeks of May, sunflower seeds were directly sawn into the soil and grown according to natural conditions. Data of field trials that are presented in this work, were obtained from plants grown in the 2023 and 2025 growing seasons.

5.2.3. Cultivation of *G. max*

Soybean seeds (cv. Williams 82, cv. Abelina and transgenic soybean lines) were pre-germinated on moist paper in darkness. Pre-germinated seeds were transferred to soil (Einheitserde®, type ED73), lightly covered with loose soil, watered, and grown in a growth chamber under long-day conditions (16 h light at 24 °C, 300 µmol m^{-2} s^{-1} light intensity, followed by 8 h dark at 20 °C) at 75 % relative humidity.

5.2.4. Cultivation of *N. benthamiana*

N. benthamiana seeds were sawn directly on VM soil (Einheitserde®) and cultivated under a hood at long day conditions (5.2.3). After two days the hood was removed, and the seedlings were further incubated for five days. Then single seedlings were transferred to single pots containing ED73 soil (Einheitserde®). For transient expression, plants were four to five weeks old.

5.2.5. Maintenance of *P. pachyrhizi* isolates

To maintain the obligate biotrophic fungus, *P. pachyrhizi* isolate br05 and additional isolates were propagated on susceptible soybean cv. Abelina. Three-week-old plants with fully expanded primary trifoliate leaves were spray-inoculated with a suspension of *P. pachyrhizi* uredospores (1 mg/mL in 0.01% (v/v) Tween20). Immediately after inoculation, plants were placed in an incubation chamber at saturated relative humidity and darkness for ~ 24 h. Subsequently, inoculated plants were cultivated under long-day conditions as described in Section 5.2.3. To prevent cross-contamination between isolates, br05-inoculated plants were kept exclusively in a plant growth chamber, whereas plants inoculated with isolates RS1, RS2, and RS3 were maintained in separate light cabinets. Fresh uredospores were harvested from infected leaves at 10–14 dpi and used either for subsequent plant inoculations or for the respective experiments.

5.2.6. Cultivation of *E. coli*

Liquid cultures of *E. coli* Top10 were incubated shaking at 37 °C at 220 rpm in lysogen broth (LB) medium (Lennox, 20 g/L). To this 1 % (w/v) agar-agar was added for solid media used for *E. coli* incubated on plates. The incubation medium was supplemented with respective antibiotics. For long-term storage, *E. coli* were maintained in glycerol stocks at -80 °C.

5.2.7. Cultivation of *A. tumefaciens*

Liquid cultures of *A. tumefaciens* AGL01 were incubated shaking at 28 °C at 220 rpm in yeast extract beef (YEB) medium (2 g/L yeast extract, 5 g/L beef extract, 5 g/L tryptone-peptone, 5 g/L sucrose). To this 1 % (w/v) agar-agar was added for solid media used for *A. tumefaciens* incubated on plates. The incubation medium was supplemented with respective antibiotics. For long-term storage, *A. tumefaciens* were maintained in glycerol stocks at -80 °C.

5.3. Experimental Procedures

5.3.1. Testing sensitivity of *P. pachyrhizi* isolates against synthetic fungicides

To assess whether the *P. pachyrhizi*. isolates RS1, RS2, and RS3 exhibit reduced sensitivity to one or more fungicide classes, soybean plants (5.2.3) were pretreated with the commercial fungicides listed in Table 1. The used fungicides were Proline® (active substance: prothioconazole; Bayer CropScience), F500® (active substance: pyraclostrobin; BASF), Imtrex® (active substance: fluxapyroxad; BASF), Orkestra® (active substances fluxapyroxad and pyraclostrobin; BASF).

Fully developed primary trifoliolate leaves of 21-day-old soybean plants were sprayed with serial dilutions of each fungicide, starting from the undiluted stock solution (100 %) and proceeding with twofold (1:2) serial dilutions to a final concentration of 6.25 %. All fungicides were diluted in ddH_2O, thus ddH_2O served as the control treatment. On the following day, pretreated soybean plants were randomized, inoculated with uredospores of the respective *P. pachyrhizi* isolate, and cultivated as described in 5.2.5. Depending on the disease severity observed in the control group, inoculated trifoliolate leaves were harvested between 8 and 12 days post inoculation. Leaves showing rust symptoms were scanned from the abaxial side and analyzed using APS Assess 2.0 software. For each plant, the relative infected leaf area was determined and compared to the median value of the corresponding control treatment.

5.3.2. *In vitro* germination of *P. pachyrhizi* uredospores

To elucidate effects of substances on *P. pachyrhizi* uredospore germination, several germination assays were performed.

Germination assay with coumarins

Freshly harvested *P. pachyrhizi* uredospores (5.2.5) were suspended in ddH_2O (+ 0.01 % Tween20) to a final concentration of 1 mg/mL spores. For each sample, 1 mL of suspension was transferred in a 2 mL reaction tube and supplemented with the coumarin of interest in concentration ranging from 25-100 µM. Stock solutions (100 mM) of scopoletin and ayapin were solved in 100 % DMSO. Therefore, a spore suspension containing 0.1 % DMSO served as control. Samples were incubated rotating for 3 hours at RT. To analyze the spore germination, 40 µL of each sample were spread on glass slides and were allowed to dry. The dried slides were evaluated by light microscopy at a 20-fold magnification. Spores were considered as “germinated” when the germ tube was clearly visible (compare Figure 19). The ratio of germinated to ungerminated spores was calculated by counting at least 100 spores per technical replicate. The count was repeated at least three times for each sample.

Germination assay in several spore densities

Freshly harvested *P. pachyrhizi* uredospores (5.2.5) were suspended in ddH_2O (+ 0.01 %Tween20) to a final concentration of 1, 2, 5, 7 or 10 mg/mL spores. Depending on the assay spores were washed five times before being incubated rotating for 3 hours at RT. An unwashed spore density of 1 mg/mL served as control. Germination analysis was done as described above.

Germination assay with crude P. pachyrhizi spore wash water

P. pachyrhizi uredospores (isolate br05 or RS2) were washed according to 5.7.2. Freshly harvested uredospores (isolate br05 or RS2) were then incubated rotating in the wash water substituted with 0.01 % Tween20 in a final concentration of 1 mg/mL. After 3 hours of incubation, the germination analysis was conducted as described above. A scheme of this set-up is depicted in Figure 16 C.

Germination assay with separated fractions of P. pachyrhizi spore wash water

P. pachyrhizi uredospores that were stored at RT for 2-4 days were suspended in ddH_2O (+0.01 %Tween20) to a concentration of 1.1 mg/mL to serve as stock suspension. Of this, 900 µL were mixed with 100 µL of each fraction gained by separating *P. pachyrhizi* spore wash water (5.7.5). Prior to mixing, the fractions were lyophilized, weighed and re-solved in 1 mL ddH_2O. This mix was incubated rotating at room temperature (RT) for 3 h. For a quick-screen analysis the germination rate was scored in three categories: active (germination rate was ~< 20 %), semi-active (germination rate was between ~20 – ~70 %), non-active (germination rate was > ~70 % and comparable to the control). This is visualized in Figure 18. For further analysis of the fractions, 1 mg of freshly harvested *P. pachyrhizi* uredospores was mixed with each fraction (250 µg/mL) and supplemented with 0.01 % Tween20. After 3 hours of incubation, the germination analysis was as described above.

Germination assay with citric acid

Freshly harvested *P. pachyrhizi* uredospores (5.2.5) were suspended in ddH_2O (+ 0.01 %Tween20) to a final concentration of 1 mg/mL spores. A citric acid (CA) stock solution was dissolved in ddH_2O or 1 mM MES buffer (2-(N-morpholino)ethanesulfonic acid). For the buffered CA, the pH was adjusted to 5. Unbuffered CA was added to the spore suspension to a final concentration of 62.5, 125 and 250 µM. For buffered CA, the final concentrations were 18.75, 37.5 and 75 mM. For the buffered CA the control treatment was 1 mM MES (pH = 5). Samples were incubated rotating for 3 hours at RT, and germination was carried out assed as described above.

5.3.3. *In planta* protection of soybean with natural compounds against *P. pachyrhizi*

To assess whether coumarins or citric acid can protect soybean from soybean rust symptoms when they are applied to the leaf surface, the respective compounds were either co-applied with the fungal spores or plants were pretreated prior to inoculation. In both cases, soybean plants were grown as described in 5.2.3 until they were three weeks old and the first trifolia was fully developed. After inoculation, plants were treated and examined as described in 5.3.1.

Co-inoculation of P. pachyrhizi uredospores with natural compounds

The first fully developed trifolia was spray-inoculated with a suspension containing 1 mg/mL of freshly harvested *P. pachyrhizi* uredospores (isolate br05 or RS2) and either scopoletin, ayapin or citric acid in respective concentrations. The suspension was supplemented with 0.01 % Tween20 to ensure sufficient leaf wetting. Control plants were only inoculated with fungal spores suspended in Tween20. In experiments with coumarins, 0.1 % DMSO served as an additional control, since coumarin stock solutions were dissolved in DMSO. In experiments with citric acid, the experiments were performed with and without 2 mM MES to buffer citric acid. Thus, co-inoculation with 2 mM MES served as control for buffered CA-treatments.

Pre-treatment of soybeans with coumarins

For pre-treatment with coumarins, soybean plants were treated with coumarins 72 and 3 h before inoculation. Leaves were sprayed with 250 or 500 µM solutions of the coumarin of interest suspended in 0.01 % Tween20. The respective coumarin stock solutions were solved in 100 % DMSO. Accordingly, 0.1 % DMSO and soybean plants without any pretreatment acted as controls. After pre-treatment, inoculation and evaluation of disease symptoms was done as described above.

5.3.4. Inducing coumarin biosynthesis in sunflower

During the laboratory work on this thesis with sunflowers, four set-ups to elucidate coumarin biosynthesis in sunflowers were used for various research goals. To elicit coumarin accumulation in the plant, for all set-ups a 300 µM $CuCl_2$-solution (solved in ddH_2O) was prepared. The control in these experiments was ddH_2O, respectively. $CuCl_2$ is described to elicit coumarin accumulation (Gutierrez, 1995), and was established as an elicitor in this research group (Schwinges, 2019). Coumarin fluorescence was visualized at 365 nm with a high-intensity-UV-lamp (Blak-Ray® B-100YP High Intensity UV Wafer, UVP).

High-throughput analysis in a microtiter plate format

To screen a large number of sunflower samples, a 96-well microtiter plate (black, Nunc) was filled with 200 µL $CuCl_2$ or ddH_2O. Sunflower leaf discs (⌀ 5 mm) were excised from mature sunflower leaves (21-42 d old). One leaf disc per well was incubated floating at RT for 48 h in the dark (under

field conditions, samples were kept away from sunlight as well as possible). After incubation, the leaf discs were removed from each well to stop coumarin accumulation in the medium. Alternatively, 100 µL of the floating medium were transferred to a new 96-well plate with a multi-channel pipette. Afterwards the plates without leaf discs could be stored at -20 °C until further processing. The fluorescence of the secretion medium was detected using the CLARIOstarPlus plate reader (BMG LABTECH GmbH). The samples were excited at wavelengths between 365 and 415 nm, with emission detected from 460 to 520 nm. For mutant screening (Figure 13), the relative fluorescence was calculated compared to the mean fluorescence of 47 samples of the RHA857 maternal line. For analysis of the sunflower core collection (Figure 5) the incubation medium of each sample was transferred to a 1.5 mL reaction tube and centrifuged at 21,000 g for 5 min. The supernatant was then prepared for HPLC measurement (5.7.5).

Floating assay with sunflower leaf discs

Leaf discs (⌀ 2.6 cm) of four-week-old sunflower genotypes RHA857 and SF_170 were excised, pooled, and leaf discs derived from one plant were randomized. Subsequently, six to eight leaf discs per plant and treatment were incubated on either ddH_2O (control) or 300 µM $CuCl_2$ by floating on 15 mL of the respective medium in a round petri dish. Samples were harvested every 24 hours over the course of 96 hours. Harvesting included collecting, drying, and quick freezing of the leaf discs in liquid nitrogen and transferring 1 mL of the floating medium to a 1.5 mL reaction tube. Leaf samples were ground with ceramic beads and stored at -80 °C until further processing (RNA isolation - 5.6.1, coumarin extraction - 5.7.1). The secretion medium was stored at -20 °C until its coumarin content was quantified by HPLC (5.7.5). The coumarin content in the secretion medium was calculated relative to the leaf area that was in contact with the secretion medium and normalized to µg/½ (dm^2).

Droplet assay on whole sunflower leaves

Fully developed leaves of 24 to 30 days old sunflowers were harvested and placed on moist paper in square petri dishes. 20 µL-droplets were placed on the adaxial leaf surface, while main leaf veins were spared. For evaluation of 16 sunflower genotypes (Figure 5) and selected mutants of RHA857 (Figure 14), droplets containing ddH_2O were placed on one half of the leaf, while droplets containing $CuCl_2$ were placed on the other half. For transcriptome analysis of induced sunflower leaf material, droplets containing ddH_2O or $CuCl_2$ were placed in proximity to each other as depicted in Figure 8 (the distance between the droplets was approx. 3 mm). After incubation in the dark for 48 h, droplets of each treatment per leaf were recollected and pooled. Samples were centrifuged at 21,000 g for 5 min and prepared for HPLC analysis. For the transcriptome analysis, plant material from beneath the respective droplets was excised (leaf discs with a diameter of

5 mm), collected per treatment and leaf, frozen in liquid nitrogen, and homogenized for RNA isolation (5.6.1).

Combination of floating leaf discs and droplet assay

To elucidate whether ayapin biosynthesis was dependent on scopoletin availability, the droplet and floating assay (described above) were combined. For this, leaf discs (⌀ 2.6 cm) of 28-32 days old sunflowers (genotype RHA857 and SF_170) were incubated floating abaxially on 15 mL of a 500 µM scopoletin solution (+ 0.01 % DMSO) or ddH_2O (+ 0.01 % DMSO) as control. Additionally, on the adaxial site of the leaf discs, 20 µL-droplets containing either $CuCl_2$ or ddH_2O were placed. After incubation for 24 or 48 hours in the dark at RT, droplets were recollected and pooled per plant and treatment. Samples were further processed for HPLC measurement (5.7.5). The experimental set-up is depicted in Figure 7.

5.4. Sunflower Field Trials

In this work several field trials were conducted in collaboration with Volker Hahn (University of Hohenheim) and his team. The field site is described in 5.2.2. In both years of the field experiments, I was supported by several members of our research group with the logistics, implementation, and follow-up work of the field experiments.

Because sunflower plants in the field differed markedly in their development due to environmental conditions, sampling time points were defined by phenological growth stages rather than chronological age, using the staging system introduced by Schneiter and Miller (1981).

To induce coumarin accumulation in sunflower samples of the field trials, the microtiter plate format was used as described in 5.3.4. However, for each field trial, the experimental set-up was modified:

5.4.1. Screening of sunflower core collection (2023)

A sub-set of 196 genotypes of the core collection of sunflowers described by Mandel et al. (2011), adapted to local climatic conditions was sawn in short rows with 12 plants per genotype. For sampling, one leaf disc (⌀ 5 mm) of three leaves per plant were excised and incubated together on 300 µM $CuCl_2$ in one well of a 96-well-microtiter plate and processed as described in 5.3.4. Per genotype three individual plants were sampled that were randomly chosen out of the 12 planted plants per genotype. Sampled plants were in the **v**egetative stage and had developed **6-10** mature leaves (stage **V-6 to V1-0**), strongly depending on the genotype and location in the field. A list of the sampled genotypes can be found in Table S 1. To qualitatively assess the fluorescence of the sunflowers, plants were evaluated with a high-intensity-UV-lamp (Blak-Ray® B-100YP High Intensity UV Wafer, UVP) at 365 nm in the dark.

5.4.2. Screening of RHA857-mutant population (2023)

Prior to this work, seeds of the sunflower line RHA857 were mutagenized by exposure to a Cobalt 60 gamma source with 300 Gy (Rhozon et al. 2023). In the 2017 growing season, the seeds were sawn at the agricultural experimental station Eckartsweier in Willstätt, Germany and 2300 M_1-plants were randomly selected for selfing to create M_2-seeds as described in detail by Rozhon et al. (2023). For this work, in 2023, ~25,000 randomly selected M_2-seeds were sawn in Willstätt. Of the respective M_2-plants, 4,128 were randomly selected for sampling. For this, three leaves per plant were harvested and one leaf disc (⌀ 5 mm) per leaf was excised. The resulting three leaf discs were incubated together in one well of a 96-well-microtiter plate on 300 µM $CuCl_2$ and processed as described in 5.3.4. Sampled plants were labeled individually to assure that they could be traced back for further selfing after completed analysis. At the sampling time point, the sunflowers already had reached the reproductive stage (R-3 to R-4) and for some plants the inflorescence was beginning to open. Hence, the samples had to be quickly screened for a potential coumarin phenotype. Samples that exceeded the mean relative fluorescence of the RHA857-ML by 275 % or were below 10 % were considered as interesting candidates. Respective M_2-plants of those samples were selfed and harvested. Those seeds were sent to Aachen and used for in depth-analysis of the respective mutant lines.

5.4.3. Screening of sunflower crosses (2025)

Analysis of F_2-segregants of RHA857xSF_170

For evaluating the biosynthesis of ayapin, sunflower genotypes RHA857 and SF_170 were crossed and successful crossing events were selfed as described in 5.5.6. T_2-seeds of crossing events 1-6 were randomized and 230 g (~5500 kernels) were sawn in Willstätt in spring 2025. ~1000 F_2-segregants (stage R-1) were randomly selected for sampling. For this, four leaves per plant were harvested, and four leaf discs (⌀ 5 mm) were excised from each leaf. Eight of those leaf discs (two per leaf) were pooled in a 1.5 mL reaction tube and immediately stored on dry ice for subsequent DNA isolation (5.6.2). The remaining eight leaf discs were each placed in a separate well of a 96-well microtiter plate and incubated floating on 300 µM $CuCl_2$ for roughly 48 h. After incubation, the floating medium of those eight wells was pooled per plant and coumarin content was measured via HPLC (5.7.5). HPLC analysis was conducted for 365 randomly selected samples.

Analysis of BC_1F_2-progeny of RHA857xM-4/626

Sunflower genotype RHA857 and the mutant line M-4/626 (this work) were backcrossed and selfed as described in 5.5.6. 250 BC_1F_2-seeds of two successful crossing events were randomly sawn in Willstätt in 2025. Of those seeds, only 83 BC_1F_2-plants fully developed (stage R-1) and were sampled accordingly. For control, 12 plants of the RHA857-ML and 15 plants of the M-4/626 were

additionally sampled. The sampling was done similar to the F_2-segregants of RHA857xSF_170 described above and the relative fluorescence was analyzed (5.3.4).

5.5. Genetic Modifications

5.5.1. Vector maps and cloned constructs

To clone overexpression constructs for transient transformation of *N. benthamiana*, the pB2GW7 vector (Karimi et al., 2002) was modified by removing the gateway-cassette and introducing the Ω-enhancer sequence of tobacco mosaic virus (TMV) and a multiple cloning site. The Ω-sequence is described as a translational enhancer in plants (Gallie, 2002). A vector map of this modified pB2GW7 can be found in Figure S 24. For soybean transformation a new vector was designed using the pB2GW7 vector as a backbone. This vector was termed pB1PES2POE and was synthesized via the GeneArt® custom synthesis of ThermoFisher®. A vector map of pB1PES2POE can be found in Figure S 25. The vector consisted of one potentially epidermis specific (ES) promoter (*p*GmPRP3 – analyzed in this work) and two overexpression (OE) promoters (*p*PcUBI and *p*CaMV35S). Each promoter sequence was followed by a translational enhancer and a multiple cloning site. Plant expression vectors that were cloned based on these vectors are listed in Table 6.

Table 6. Plant expression constructs used in this work.
Constructs marked with * were generated in the scope of this work. *[1] was generated by Anna Kleineberg in the course of her master's thesis. For multigene constructs the order of genes is from left to right border on the respective vector.

genes of interest	vector	application
AtMYB72	pB7WG2-D	transient transformation of *N.benthamiana*
*HaF6'H1**	pB2GW7_mod	transient transformation of *N.benthamiana*
*HaAySy1**[1]	pB2GW7_mod	transient transformation of *N.benthamiana*
*HaAySy2**[1]	pB2GW7_mod	transient transformation of *N.benthamiana*
*HaAySy4**[1]	pB2GW7_mod	transient transformation of *N.benthamiana*
*HaAySy6**[1]	pB2GW7_mod	transient transformation of *N.benthamiana*
*HaAySy8**[1]	pB2GW7_mod	transient transformation of *N.benthamiana*
*HaAySy10**[1]	pB2GW7_mod	transient transformation of *N.benthamiana*
*HaAySy11**[1]	pB2GW7_mod	transient transformation of *N.benthamiana*
*HaAySy12**[1]	pB2GW7_mod	transient transformation of *N.benthamiana*
*HaAySy14**[1]	pB2GW7_mod	transient transformation of *N.benthamiana*
*HaAySy16**	pB2GW7_mod	transient transformation of *N.benthamiana*
*HaAySy17**	pB2GW7_mod	transient transformation of *N.benthamiana*
*HaAySy18**	pB2GW7_mod	transient transformation of *N.benthamiana*
*HaABC – HaF6'H1-eGFP – AtCOSY**	pB1PES2POE	stable transformation of *G. max*
*eGFP – HaF6'H1 – mRFP**	pB1PES2POE	stable transformation of *G. max*

5.5.2. Generating transgenic *E. coli*

Gibson assembly and restriction digest

For cloning of the transformation constructs, the Gibson assembly was chosen (Gibson et al., 2009). Plasmids of the vector of interest were linearized using respective Fast Digest® restriction enzymes (ThermoFisher). Restriction was performed by digesting 1 µg of plasmid as described by the manufacturer. The restriction digest was heat inactivated at 80 °C for 10 min. Linearized plasmids were mixed with PCR products of the gene of interests with Gibson-compatible overhangs and incubated with the Gibson Assembly® Master Mix (New England Biolabs) and incubated for 15 min at 50 °C as recommended by the manufacturer. Subsequently, 5 µL of the mixture was used to transform chemically competent *E. coli* Top10 cells.

Transformation of chemically competent E. coli cells

50 µL aliquots of chemically competent *E. coli* Top10 cells were thawed and mixed with 5 µL of plasmid DNA. The mix was incubated on ice for 10-20 minutes in 1.5 mL reaction tubes. After incubation the mixture was incubated at 42 °C for 1 minute to heat-shock the *E. coli* cells. After another 10-minute-incubation on ice, 1 mL liquid LB medium (Lennox, 20 g/L) was added and the cultivation broth was incubated shaking at 37 °C for 30-60 minutes to regenerate the cells. Cells were pelleted and 900 µL of the supernatant was discarded. Cells were resuspended in the remaining 150 µL and spread on LB-Agar-plates with respective antibiotics for selection and incubated for ~24 h at 37 °C. Appearing colonies were validated via PCR-analysis (5.6.5) and positive clones were incubated in liquid LB-medium with respective antibiotics overnight (5.2.6). Of this liquid culture, 800 µL were mixed with 800 µL glycerol and stored at -80 °C, while 2 mL were used for plasmid preparation (5.6.3), subsequent sequencing, and *A. tumefaciens* transformation (5.5.3).

5.5.3. Generating transgenic *A. tumefaciens*

Plasmids of interest used for transformation of *A. tumefaciens* (strain AGL01) were purified from *E. coli* (5.6.3). 2 µL of purified plasmid was mixed with a 50 µL-suspension containing electro-competent *A. tumefaciens* cells. The mix was incubated for 5 min on ice and then transferred to a chilled electroporation cuvette. By use of the MicroPulser (BioRad), the bacteria were exposed to 2.2 kV for 5 ms. Immediately after the electro shock, 1 mL liquid YEB medium (5.2.7) was added to the cuvette and the suspension was transferred to a 1.5 mL reaction tube to be incubated shaking at 28 °C for 2 h to allow the bacteria to generate. Then, 2 µL of the bacteria culture was mixed with 100 µL of sterile ddH_2O and was streaked on agar plates (YEB medium + respective antibiotics for selection). After incubation for two days at 28 °C, the transformation success of emerging colonies was verified via PCR-analysis (5.6.5). Positive clones were transferred to a suspension culture and

incubated overnight (5.2.7). Of this liquid culture, 800 µL were mixed with 800 µL glycerol and stored at -80 °C.

5.5.4. Transient transformation of *N. benthamiana*

For testing potential HaAySy candidates, leaves of *N. benthamiana* were transiently transformed via infiltration of *A. tumefaciens* harboring vectors with the respective gene of interest.

For this, *A. tumefaciens* were cultivated as described in 5.2.7. After incubation for ~24 h, 50 mL of the respective liquid culture was harvested by 15 min of centrifugation at 4,000 g and the incubation medium was discarded. Cell pellets were resuspended in infiltration medium (10 mM MES, 10 mM $MgCl_2$, 150 µM acetosyringone, pH = 5.6) and set to an OD_{600} = 0.5 for *A. tumefaciens* carrying the overexpression constructs and OD_{600} = 1.0 for *A. tumefaciens* carrying the p19-vector. After incubation for at least 3 h, the bacteria were mixed in equal parts for the respective infiltration combination. An equal volume of bacteria carrying the p19-vector was added to each mix to suppress silencing responses of *N. benthamiana* as described by Voinnet et al. (2003). Leaves of three to four week old *N. benthamiana* (5.2.4) were gently incised at the abaxial site with a needle to facilitate infiltration. With the help of a 1 mL syringe, the suspension containing agrobaceria that harbored the constructs of interest was infiltrated in respective leaves with light pressure. Afterwards, plants were placed under regular growing conditions (5.2.4) for three days before being harvested for further analysis (5.6.1 and 5.7.1).

5.5.5. Generating transgenic soybean lines

The transformation constructs for soybean transformation were designed and cloned as described previously (5.5.1 and 5.2.6). The functionality of those constructs was tested by transient transformation of *N. benthamiana*. Plasmids were isolated from *E. coli* (5.6.3) and sent to Lifeasible®, USA for *A. tumefaciens*-mediated soybean transformation. The constructs used for transformation are shown in Figure 15 and Figure S 8. The transformation of the respective *A. tumefaciens* (strain EHA105) and the subsequent soybean transformation was performed by Lifeasible® according to the company's protocol. For each construct, approximately 150 soybean explants were used for transformation and subsequently regenerated on selective media. Putative edited seedlings were transferred to soil and grown to maturity for harvesting T_1-seeds. A short graphic overview of the full transformation process is shown in Figure S 26. About 20 T_1-seeds per transformation event of at least 14 events per construct were transferred back to Aachen (Table 7). Results shown in this thesis are derived from T_1-plants germinated from those seeds. Plants that showed a respective coumarin phenotype were selfed and propagated to generate T_2-seeds that will be further analyzed in future work.

5.5.6. Crossing of sunflower genotypes

Sunflower genotypes were crossed by Volker Hahn and his team in Willstätt, Germany. In all cases, the genotype RHA857 was used as the female receptor line, while genotype SF_170 or mutant M-4/626 served as the pollen donor. In Aachen, F_1-generations (Table 7) of crossed sunflower lines were screened for their respective phenotypes and, in case of successful crossing, selfed to generate T_2-seeds.

Table 7. List of genetically modified plant lines generated in this study.

name	background	genetic modification	# of individual lines
1.x	*G. max cv*. W82	stable transformation*:* *pGmPRP3::eGFP + pPcUBI::HaF6H1 + pCaMV35S::mRFP*	15
2.x	*G. max cv*. W82	stable transformation: *pGmPRP3::HaABC + pPcUBI::HaF6H1-eGFP + pCaMV35S::AtCOSY*	14
RxS	*H. annuus cv.* RHA857 × SF_170	cross: recipient RHA857; pollen of SF_170	7
RxM	*H. annuus cv.* RHA857	backcross: recipient RHA857; pollen of M-4/626	2

5.6. Biomolecular Methods

5.6.1. RNA isolation of plant material

To isolate RNA from plant material, several methods were used depending on the plant species. Regardless of the methods, the concentration of the isolated RNA was photometrically evaluated and the RNA integrity was validated via gel electrophoresis (5.6.6).

H. annuus

To isolate RNA from sunflower plant material, two different methods were used. RNA that was used for the transcriptome analysis (5.6.8) was isolated from ~100 mg plant material using the innuPREP Plant RNA Kit (IST Innuscreen, Germany) following the manufacturer's instruction. Additional to RNA isolation, an enzymatic DNA digestion was integrated using the innuPREP DNase I Digest Kit (IST Innuscreen, Germany). The isolated RNA was suspended in 25 µL ddH_2O and stored at -20 °C.

RNA that was used for cDNA synthesis (5.6.4) was extracted using a rapid cetyltrimethylammonium bromide (CTAB) protocol that was modified from Gambino et al. (2008). As discussed by Patrick Schwinges in his dissertation (2019), this method proved to be sufficient for plant material with high proportion of polyphenolics. For this, ~150 mg of frozen and ground sunflower plant material was mixed with 900 µL of preheated (65 °C) CTAB-extraction buffer (containing 2 % CTAB, 2,5 % PVP-40, 2 M NaCl, 100 mM Tris-HCl pH 8.0, 25 mM EDTA pH 8.0 and 2 % of freshly added β-mercaptoethanol) in a 2 mL reaction tube. The mixture was

incubated for 10 min at 65 °C before 900 µL of chloroform:isoamyl-alcohol (24:1 v/v) were added and the sample was mixed vigorously. The samples were centrifuged (11,000 g) at 4 °C for 10 min and the supernatant was transferred to a fresh 2 mL reaction tube and directly mixed with 900 µL of chloroform:isoamyl-alcohol (24:1 v/v) again. The centrifugation step (11,000 g, 4 °C, 10 min) was repeated and the supernatant was again transferred to a fresh reaction tube, mixed with $LiCl_2$ to a final concentration of 3 M $LiCl_2$, and incubated on ice for at least 30 min to precipitate the RNA. By subsequent centrifugation (21,000 g) at 4 °C for 20 min, precipitated RNA was pelleted and the supernatant could be discarded. The RNA pellet was dissolved by incubation for 10 min in preheated (65 °C) SSTE-buffer (containing 10 mM Tris-HCl pH 8.0, 1 mM EDTA pH 8.0, 1 % SDS, 1 M NaCl) at 65 °C. Next, the sample was mixed with an equal volume of chloroform:isoamyl-alcohol (24:1 v/v) and centrifuged (11,000 g) at 4 °C for 10 min. The supernatant was transferred to a fresh reaction tube containing ice-cold isopropanol (0.7 times the volume of the supernatant) to precipitate the clean RNA. The RNA was pelleted by centrifugation (21,000 g, 4 °C, 15 min) and the supernatant was discarded. Then, the pellet was washed twice with 70 % EtOH, dried, and finally resuspended in 30 µL ddH_2O and stored at -20 °C.

G. max

Total RNA was isolated from soybean leaves by extracting ~100 mg of frozen, homogenized leaf tissue in 555 µL lysis buffer (2 % (w/v) ultrapure SDS, 68 mM trisodium citrate, 132 mM citric acid, 10 mM EDTA, pH = ~3.5). After vigorously mixing the samples, 185 µL protein precipitation buffer (4 M NaCl, 17 mM trisodium citrate, 33 mM citric acid, pH = ~3.5) was added. Then, the samples were briefly mixed and incubated on ice for 5 min, followed by centrifugation (21,000 g) at RT for 5 min. The supernatant was transferred to a fresh 1.5 mL reaction tube, combined with 500 µL isopropanol, and incubated for 15 min at room temperature to precipitate RNA. The RNA was pelleted by centrifugation (21,000 g, RT, 5 min) and subsequently washed with 500 µL 70% ethanol, dried on ice for 10 min, resolved in 30 µL dd_{H2O} and stored at - 20 °C.

N. benthamiana

For expression control of transient transformed *N. benthamiana* plant material, RNA was extracted via a single-step method with Trizol as originally described by Chomczynski and Sacchi (1987). For this, at least 100 mg of plant material was frozen in liquid nitrogen and ground with ceramic beads. The frozen plant material was mixed with 1 mL Trizol (380 mM ammonium-thiocyanate, 780 mM guanidine-thiocyanate, 59 mM NaOAc, 5 % glycerol, 47.5 mL phenol, pH 5.0) in a 2 mL reaction tube, vortexed and incubated at RT for 3 min. Then, samples were centrifuged (21,000 g, 4 °C, 15 min) and 500 µL of the respective supernatant was mixed with 500 µL of isopropanol to precipitate the RNA, which was subsequently pelleted by centrifugation (21,000 g, 4 °C, 10 min).

The pellet was washed two times with 70 % ethanol before being allowed to dry for at least 30 min. To resuspend the pellet, 30 µL ddH_2O were added and the sample was incubated at 55 °C for 10 min. The RNA was stored at – 20 °C.

5.6.2. DNA isolation of plant and fungal material

H. annuus

In preparation of the BSA (5.6.9), genomic DNA was isolated from sunflower samples collected during the field trial of 2025 (5.4.3). For this, the frozen plant material was homogenized with the help of a Precellys® in 1.5 mL reaction tubes using glass beads. From the ground and frozen plant material, DNA was isolated using the NucleoSpin Plant II® Kit (Macherey-Nagel, Germany) according to the manufacturer's instructions. The DNA was resuspended in 50 µL ddH_2O and the concentration was photometrically determined. The DNA was stored at -20 °C until further use.

P. pachyrhizi

To isolate genomic DNA from *P. pachyrhizi* uredospores, freshly harvested fungal spores (5.2.5) were frozen and homogenized. The DNA was extracted as described by Edwards et al. (1991). Extracted DNA was resuspended in 100 µL ddH_2O and stored at -20 °C until being prepared for sequencing (5.6.7).

5.6.3. Plasmid isolation of *E.coli*

Plasmids were purified from 2-4 mL of an over-night culture (5.2.6) of an *E. coli* strain harboring the plasmid of interest using the NucleoSpin Plasmid EasyPure® Kit (Macherey-Nagel, Germany) according to the manufacturer's instructions. Plasmid DNA was stored at -20 °C.

5.6.4. cDNA synthesis

Complimentary DNA (cDNA) was synthesized from total plant RNA (5.6.1) using random primers for qRT-PCR analysis (5.6.5) to generate short, representative cDNA fragments across the entire transcript. For cloning (5.5.1) and sequencing (5.6.7) of the full-length CDS, cDNA was synthesized using oligo(dT) primers to selectively reverse transcribe polyadenylated mRNAs from their 3′ poly(A) tails, enriching for complete transcript ends.

cDNA synthesis for qRT-PCR analysis

1 µg of isolated plant RNA was treated with DNase I (1× buffer, 10 µL reaction; Thermo Scientific) for 30 min at 37 °C followed by heat inactivation at 70 °C for 15 min. For cDNA synthesis, 1 µL of 50 µM random primer and 1 µL of ddH_2O was added, samples were denatured at 70 °C for 5 min and chilled on ice, then supplemented with 4 µL 5× reverse transcriptase buffer (Thermo Scientific), 2 µL 10 mM dNTPs (Invitrogen), 1 µL RevertAid reverse transcriptase (Thermo Scientific), and

1 µL of ddH_2O, followed by incubation at 25 °C for 10 min, 42 °C for 60 min and 70 °C for 10 min; cDNA was stored at -20 °C.

cDNA synthesis of full-length CDS

Full-length cDNA was generated using oligo(dT) primers and the SuperScript IV reverse transcriptase (Thermo Scientific), which was chosen for its high thermostability and processivity, enabling efficient synthesis of long transcripts. For each reaction, 1 µg RNA was mixed with 1 µL 50 µM oligo(dT) primers and 1 µL 100 mM dNTPs, adjusted to 13 µL with ddH_2O, incubated at 65 °C for 5 min and chilled on ice. Then, the samples were supplemented with 4 µL 5× SSIV buffer, 1 µL 100 mM DTT, 1 µL SSIV reverse transcriptase and 1 µL ddH_2O (20 µL final volume, all Thermo Scientific), followed by incubation at 55 °C for 10 min and 80 °C for 10 min; cDNA was stored at -20 °C.

5.6.5. Polymerase Chain Reaction (PCR) protocols

Several types of PCR were used depending on the application. Standard PCR was employed to verify the insertion of plasmid constructs in transformed *E. coli* (5.5.2) and *A. tumefaciens* (5.5.3) colonies, proofreading PCR was used for high-fidelity amplification of DNA fragments for cloning (5.5.1) or sanger sequencing (5.6.7), and quantitative real-time PCR (qRT-PCR) was applied to quantify specific cDNA sequences for transcriptional analysis.

Standard PCR

Standard PCR (without proofreading activity) was performed with the FastGene® Optima HotStart Ready Mix (Nippon Genetics) according to the manufacturer's instructions, using 1 µL of bacterial suspension as template. The PCR conditions are listed in Table 8. The size of the PCR product was examined via gel electrophoresis (5.6.6).

Table 8. Thermal cycling conditions for standard PCR.

phase	temperature [°C]	duration	# of cycles
initial denaturation	95	3 min	1
denaturation	95	15 s	35
primer annealing	55	30 s	35
elongation	72	1 min/kb	35
final elongation	72	10 min	1

Proofreading PCR for cloning

Proofreading PCR was performed for error-minimized amplification of DNA fragments intended for cloning or sequencing. PCR reactions were set up with Phusion® High-Fidelity DNA Polymerase (Thermo Scientific) according to the manufacturer's instructions, using cDNA (5.6.4) or gDNA (5.6.2) as template. Primers used for cloning are listed in Table S 8, while primers used

for generating PCR products for subsequent sanger sequencing (5.6.7) are listed in Table S 6. The cycling protocol is listed in Table 9. Amplification success was verified by agarose gel electrophoresis (5.6.6).

Table 9. Thermal cycling conditions for proofreading PCR.
The annealing temperature (x) depended on the respective primer constitution and was calculated according to the Thermo Scientific's online Tm calculator.

phase	temperature [°C]	duration	# of cycles
initial denaturation	94	30 s	1
denaturation	94	30 s	35
primer annealing	x	30 s	35
elongation	72	30 s/kb	35
final elongation	72	10 min	1

qRT-PCR

Relative expression levels of the genes of interest (GOIs) in plant tissues were determined by qRT-PCR. cDNA was synthesized as described previously (5.6.4) and diluted 1:10 with ddH_2O. 2 µL of diluted cDNA were mixed with 5 µL 2X iTaq™ Universal SYBR® Green Supermix (Bio-Rad), 0.3 µL RT-primer mix (10 µM each, forward and reverse primer), and 2.7 µL ddH_2O in a 384-well microtiter plate (10 µL total volume per reaction). qRT-PCR was performed on a CFX384 Real-Time System (Bio-Rad), under the cycling conditions listed in Table 10. Expression of genes was normalized to the reference genes of the respective plant species. They were *NbActin* (*N. benthamiana*), *HaActin2* (sunflower) or *GmNRG3* (soybean). The used oligonucleotides are listed in Table S 7.

Table 10. Thermal cycling conditions for qRT-PCR analysis.

phase	temperature [°C]	duration	# of cycles
initial denaturation	95	3 min	1
denaturation	95	15 s	39
annealing/elongation	60	60 s	39
melting curve	+0.5 °C/s, starting at 60	70 s	1
cooling	40	30 s	1

5.6.6. Agarose Gel Electrophoresis and Clean-up of PCR-Products

Separation of DNA and RNA was conducted via 1 % (w/v) agarose gels. For this, agarose was dissolved in TAE buffer (40 mM Tris-HCl, 0.1142 % (w/v) acetic acid, 1 mM EDTA pH = 8.0) by heating. Then, after cooling slightly, 0.005 % (v/v) Midori Green (Nippon Genetics) was added to the molten gel. Gels were cast in an electrophoresis chamber and the forming of loading pockets was ensured by adding a plastic comb. The gel was allowed to solidify, placed in a Mupid-One®

gel electrophoresis system, and covered with TAE buffer. Each pocket of the gel was loaded with 7 to 30 µL of the samples. 5 µL of GeneRulerTM 1 kb ladder (Thermo Scientific) was used as reference for determining the size of fragments. After loading the samples, electrophoresis was carried out at 100 V for 20 min. DNA and RNA were visualized under UV light (366 nm). Bands of the respective PCR products of interest were excised and purified using the NucleoSpin® Gel and PCR Clean-up kit (Macherey-Nagel) according to the manufacturer's instructions.

5.6.7. Sanger Sequencing

For sequencing fungal or plant DNA, the sequence of interest was multiplied via proofreading PCR (5.6.5) and PCR-products were isolated via gel-electrophoresis and subsequent clean-up (5.6.6). 10 µL of PCR product was then mixed with 3 µL of the respective primer. Sanger sequencing was performed by Microsynth Seqlab GmbH (Göttingen, Germany). The resulting DNA sequence data was analyzed using SnapGene® software (GSL Biotech LLC).

5.6.8. Transcriptome analysis of sunflower samples

To evaluate the differential gene expression of sunflower genotype RHA857 and SF_170 in stress or control conditions, a transcriptome analysis with total plant RNA was conducted. For this, sunflower plant material was elucidated as described in 5.3.4 and RNA was extracted (5.6.1). In total, RNA of 12 samples was isolated and the RNA quality was checked via the 2100 Bioanalyzer Instrument and Agilent RNA 6000 Nano Kit, with 1 µL per sample analyzed according to the Quick Start Guide (both Agilent Technologies). A list of the samples is presented in Table 11. The transcriptome analysis was performed by CeGaT GmbH (Tübingen, Germany). According to CeGaT, the RNA library for each sample was prepared from 500 ng of RNA by using a Library preparation kit (TruSeq Stranded mRNA - Illumina). Indexed libraries were sequenced on an Illumina NovaSeq 6000 platform in paired-end mode (2 × 101 bp), achieving an overall Q30 value of 92.09%.

Demultiplexing was performed with Illumina bcl2fastq (v2.20), and adapter sequences were removed using Skewer (v0.2.2, Jiang et al., 2014) without additional quality trimming. Statistics on the raw read data can be found in Table S 3.

Subsequently the reads were aligned to the HanXRQr1.0-SUNRISE reference genome (Badouin et al., 2017) using STAR (v2.7.3, Dobin et al., 2013). Statistics of the mapped reads are listed in Table S 4. Differential expression analysis (DEA) between the submitted genotypes and treatments was performed with DESeq2 (version 1.24.0; Love et al., 2014) in R (version 4.0.4). Genes with fewer than two reads across all samples were excluded prior to statistical analysis. DESeq2's size-factor normalization and a negative binomial generalized linear model with Wald test were used to

estimate log_2-fold-changes (l_2fc), and *p*-values were adjusted for multiple testing using the Benjamini–Hochberg method (p_{adj}, Benjamini and Hochberg, 1995). Unless stated otherwise, genes with $p_{adj} < 0.05$ were considered significantly differentially expressed. Statistics on the DEA are listed in Table S 5.

Table 11. Sample overview and grouping for RNA sequencing and bioinformatic analysis.

CeGaT ID	group	genotype	treatment	replicate
S12033Nr1	1	RHA857	control (ddH_2O)	1
S12033Nr2	2		stress ($CuCl_2$)	1
S12033Nr3	1		control (ddH_2O)	2
S12033Nr4	2		stress ($CuCl_2$)	2
S12033Nr5	1		control (ddH_2O)	3
S12033Nr6	2		stress ($CuCl_2$)	3
S12033Nr7	3	SF_170	control (ddH_2O)	1
S12033Nr8	4		stress ($CuCl_2$)	1
S12033Nr9	3		control (ddH_2O)	2
S12033Nr10	4		stress ($CuCl_2$)	2
S12033Nr11	3		control (ddH_2O)	3
S12033Nr12	4		stress ($CuCl_2$)	3

The generated data sets were provided for download by CeGaT and used to compare transcriptional changes between the sunflower genotypes RHA857 and SF_170 in response to $CuCl_2$-induced stress, with a particular focus on genes associated with coumarin biosynthesis. Based on differential expression and pathway annotation, several candidate genes were identified and prioritized for further analysis; the selection and characterization of these candidates are described in detail in the results section (2.3) and are depicted in Figure S 5.

5.6.9. Bulked segregant analysis (BSA) of sunflower samples

A BSA (Michelmore et al., 1991) was conducted to identify genomic regions associated with ayapin accumulation. For this, field-grown F_2 segregants of RHA857×SF_170 were sampled according to section 5.4.3 and analyzed by HPLC (5.7.5) to determine ayapin accumulation. Plants whose samples showed no detectable ayapin were assigned to the no-ayapin bulk. For the ayapin bulk, plants were randomly selected from those in which ayapin was detected by HPLC analysis. Genomic DNA was isolated from 50 plants per bulk and subsequently pooled into two bulked DNA samples (5.6.2). Additionally, DNA was isolated from 20 individuals per parental genotype (RHA857 and SF_170). In total, four DNA samples (two bulks and two parental samples) were submitted to Biomarker Technologies (BMK) GmbH (Münster, Germany) for whole-genome sequencing (Illumina Nova PE150) and subsequent bioinformatic analysis. The target sequencing depth was 20× coverage for each parental sample and 50× coverage for each bulk. The resulting

reads will be mapped to the HanXRQr1.0 SUNRISE reference genome (Badouin et al., 2017) to identify genomic regions associated with the ayapin phenotype.

5.7. Biochemical Methods

5.7.1. Extraction of coumarins from plant material

Leaf material was harvested and placed in 50 mL reaction tubes, sealed and frozen in liquid nitrogen. Plant material was homogenized with ceramic beads. Approximately 500 mg of plant material was weighed and substituted with 2 mL of 90 % methanol and incubated rotating for 24 h at RT without exposure to direct light. Samples were centrifuged at 4,000 g at RT for 15 min. 1.6 mL of the supernatant was transferred to a 2 mL reaction tube and evaporated using an Eppendorf Concentrator Plus®. The resulting pellet was resuspended with 200 µL MeOH and stored at -20 °C until HPLC analysis (5.7.5).

5.7.2. Generating *P. pachyrhizi* wash water for germination assays

Freshly harvested uredospores of *P. pachyrhizi* were weighed in for the required densities (1 mg/mL, 5 mg/mL and 10 mg/mL) and substituted with 0.01 % Tween-20 in ddH_2O. Samples were mixed vigorously for 30 s and afterwards centrifuged for 5 min at 4,000 g. The supernatant was used for subsequent germination assays (5.3.2).

5.7.3. Generating *P. pachyrhizi* wash water for analytical processes

Uredospores of *P. pachyrhizi* were harvested and stored at -80 °C to collect at least 650 mg of spores. Spores were then washed at a concentration of 20 mg/mL with ddH_2O for at least 24 h by incubating on a rotating device. Subsequently, spores were pelleted, the supernatant was lyophilized, and weighed. The dry, crude extract was then re-dissolved to a final concentration of 40 mg/mL. From 500 mg spores one could extract ~ 105 mg of crude extract. Raw extract was stored at -20 °C until further processing.

5.7.4. Separation of *P. pachyrhizi* wash water with a 3 mL C18 column

A 3 mL C18 column (end capped, CHROMABOND®) was primed with ddH_2O, prior being loaded with 10 mL of uredospore wash water (20 mg/mL; 5.7.3). The flow trough was collected ("flow"). Then, the column was eluted first with 4 mL 100 % ddH_2O, secondly with 4 mL ddH_2O/ACN (1:1), and lastly with 4 mL 100 % ACN. Prior to elution each solution was substituted with 1.5 % acetic acid. Each elution solution was separately collected and evaporated and split into two. One half was treated with proteinase K to digest proteins potentially present in the wash water. Each fraction was separately used for germination assays (5.3.2). For clarification, this workflow is also depicted in Figure 17A.

5.7.5. High pressure liquid chromatography (HPLC) analysis

Analytical separation of coumarins in plant extracts and floating medium

For HPLC analysis, samples were centrifuged for at least 5 min at 16,000 g to pellet potential unsolved particles. 30-50 µL of the supernatant were transferred to 1.5 mL glass screw-neck vials with 0.2 mL silanized glass inserts (both MACHEREY-NAGEL®). Glass vials were sealed with a screw closure (N8) with a silicone/PFTE membrane (MACHEREY-NAGEL®). For larger sample sizes, e.g. from field trials (5.4.3), 200 µL of the supernatant were transferred to 96-well-plates (NUNC, ThermoFisher) and sealed with a silicon mat.

Separation of 10 µL per sample occurred on a C18 reverse phase (RP) column (NUCLEODUR 100-5 C18 ec, MACHEREY-NAGEL®). Column temperature was set to 40 °C. Solvents were ddH_2O and ACN both supplemented with 1.5 % acetic acid. Solvent gradients differed for plants extracts of different species to properly separate the coumarins from other extracted PSM. The gradients are listed in detail in Table 13, Table 12, Table 14. Fluorescing compounds were detected in a fluorescence detector (RF-20A; Shimadzu) at 365 nm excitation/470 nm emission for scopolin and scopoletin or 370 nm excitation/440 nm emission for ayapin. Quantification of those coumarins was done with authentic standards (5.1). An exemplary separation of those standards is depicted in Figure 22.

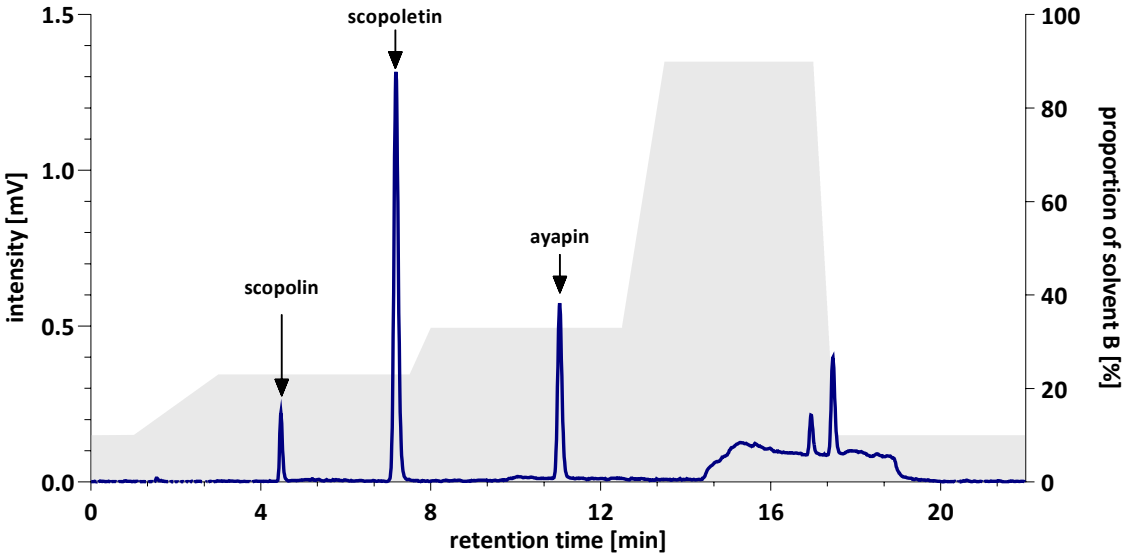

Figure 22. Separation scopolin, scopoletin and ayapin by HPLC. Equimolar standards of the indicated coumarins were separated via a C18 reverse phase (RP) column. Run parameters are listed in table 12. The proportion of solvent B is shown as a grey shade.

Table 12. Solvent gradient for separation of coumarins in *H. annuus* samples.
Solvent A = ddH_2O + 1.5 % acetic acid; solvent B = ACN + 1.5 % acetic acid.

time [min]	flow [mL/min]	solvent A [%]	solvent B [%]
0	1.2	90	10
1	1.2	90	10
3	1.2	77	23
7.5	1.2	77	23
8	1.2	67	33
12.5	1.2	67	33
13.5	1.2	10	90
17	1.2	10	90
17.5	1.2	90	10
22	1.2	90	10

Table 13. Solvent gradient for separation of coumarins in *G. max* samples.
Solvent A = ddH_2O + 1.5 % acetic acid; solvent B = ACN + 1.5 % acetic acid.

time [min]	flow [mL/min]	solvent A [%]	solvent B [%]
0	1.2	90	10
5	1.2	79	21
10	1.2	79	21
11	1.2	10	90
14	1.2	10	90
14,5	1.2	90	10
18	1.2	90	10

Table 14. Solvent gradient for separation of coumarins in *N. benthamiana* samples.
Solvent A = ddH_2O + 1.5 % acetic acid; solvent B = ACN + 1.5 % acetic acid.

time [min]	flow [mL/min]	solvent A [%]	solvent B [%]
0	1.2	90	10
1	1.2	90	10
3	1.2	77	23
10	1.2	77	23
10,5	1.2	67	33
15	1.2	67	33
17	1.2	10	90
20	1.2	10	90
22	1.2	90	10
26	1.2	90	10

Preparational separation of *P. pachyrhizi* wash water

Preparational HPLC analysis was carried out at the facility of the Helmholtz Centre of Infection Research, Braunschweig, Germany. Lyophilized wash-water of *P. pachyrhizi* uredospores (prepared as described in section 5.7.3) was subjected to preparative HPLC using a Büchi Pure C-850 FlashPrep system (Büchi Labortechnik AG, Switzerland). Per run, aliquots of ~ 40 mg wash-water were separated on a 4 µm Synergi® Hydro-RP 80 Å column (250 × 21.2 mm) with a polar end-capped C18 stationary phase (Phenomenex).

The mobile phase consisted of solvent A (ddH_2O + 0.1 % FA) and solvent B (ACN + 0.1 % FA). The column was equilibrated with 100 % solvent A. Separations were carried out at a flow rate of

20 mL/min with a total run time of 45 min using the following gradient: 0-25 min, 100 % A; 25-35 min, linear increase from 0 to 100 % B; 35-45 min, 100 % B. UV signals were recorded at 210, 250, 280, and 320 nm, and an ELSD was used in parallel to detect non-UV-absorbing compounds. Fractions were collected manually according to UV/ELSD peak shape and retention time, evaporated to dryness, and weighed. For rapid assessment of biological activity, each dried fraction was re-dissolved in 1 mL ddH_2O and used in the uredospore germination assay described in section 5.3.2.

5.7.6. Nuclear Magnetic Resonance (NMR) analysis

To elucidate the identity of active fractions separated from *P. pachyrhizi* spore wash water (5.7.3), at least 1 mg of dried substance of the respective fraction (5.7.5) were prepared for NMR analysis by resolving the fractions in deuterium oxide (D_2O). NMR spectra were recorded at 298 K Bruker Avance III 700 spectrometer with a 5 mm TXI cryoprobe (^1H 700 MHz, ^{13}C 175 MHz, Bruker BioSpin GmbH, Ettlingen, Germany) using D_2O as solvent (proton signal was referenced to 4.75 ppm). All NMR measurements were carried out by Hedda Schrey and her team at the facility of the Helmholtz Centre of Infection Research, Braunschweig, Germany.

5.8. Software and Databases

Table 15. List of software, databases and internet sources used in this study.

name	reference
Assess 2.0	American Pathological Society
BioRender	biorender.com
BLASTp/BLASTn	blast.ncbi.nlm.nih.gov/Blast.cgi
CFX ManagerTM Vers. 3.1	Bio-Rad Laboratories Inc.
Citavi 7	Swiss Academic Software GmbH
Clone Manager Professional v.8.0	Sci-Ed
GraphPad Prism V.9.5.1	GraphPad Software, LLC
Heliagene Genome Browser	heliagene.org
Image Lab 4.1	Bio-Rad Laboratories Inc.
InterPro	ebi.ac.uk/interpro/
Microsoft Excel für Office 365	Microsoft
Microsoft Powerpoint für Office 365	Microsoft
Microsoft Word für Office 365	Microsoft
MolView®	Bergwerf Labs
MycoCosm *P. pachyrhizi* Genome Browser	https://mycocosm.jgi.doe.gov/mycocosm/home
NCBI Primer Blast Tool	ncbi.nlm.nih.gov/tools/primer-blast/
RStudio®	Posit Software, PBC
SnapGene®	Shimadzu Corporation

6. Bibliography

Adebomi, J. I., Guo, J. and Niu, C. H. (2025) Extracts of tomatoes and potatoes as biopesticides: a review. *Discover agriculture* **3**, 60.

Afek, U., Orenstein, J., Carmeli, S., Rodov, V. and Joseph, M. B. (1999) Umbelliferone, a phytoalexin associated with resistance of immature Marsh grapefruit to *Penicillium digitatum*. *Phytochemistry* **50**, 1129–1132.

Ahn, Y. O., Shimizu, B., Sakata, K., Gantulga, D., Zhou, C., Bevan, D. R. and Esen, A. (2010) Scopolin-hydrolyzing -glucosidases in roots of Arabidopsis. *Plant and Cell Physiology* **51**, 339.

Ahuja, I., Kissen, R. and Bones, A. M. (2012) Phytoalexins in defense against pathogens. *Trends in plant science* **17**, 73–90.

Aktar, M. W., Sengupta, D. and Chowdhury, A. (2009) Impact of pesticides use in agriculture: their benefits and hazards. *Interdisciplinary toxicology* **2**, 1–12.

Allen, P. J. (1955) The role of a self-inhibitor in the germination of rust uredospores. *Phytopathology* **5**, 259–266.

Amack, S. C. and Antunes, M. S. (2020) CaMV35S promoter – A plant biology and biotechnology workhorse in the era of synthetic biology. *Current Plant Biology* **24**, 100179.

Ascribe Bio (2025). Ascribe Bio's Phytalix® Achieves Breakthrough in Fight Against Bacterial Leaf Blight (BLB) in Rice: *Press Release - March 4, 2025*.

Badouin, H., Gouzy, J., Grassa, C. J., Murat, F., Staton, S. E., Cottret, L., Lelandais-Brière, C., Owens, G. L., Carrère, S., Mayjonade, B., Legrand, L., Gill, N., Kane, N. C., Bowers, J. E., Hubner, S., Bellec, A., Bérard, A., Bergès, H., Blanchet, (…) and Langlade, N. B. (2017) The sunflower genome provides insights into oil metabolism, flowering and Asterid evolution. *Nature* **546**, 148–152.

Balmer, A., Pastor, V., Glauser, G. and Mauch-Mani, B. (2018) Tricarboxylates Induce Defense Priming Against Bacteria in *Arabidopsis thaliana*. *Frontiers in plant science* **9**, 1221.

Bansal, S. and Wang, B. (2024) A critical factor in reactive oxygen species (ROS) studies: the need to understand the chemistry of the solvent used: the case of DMSO. *Chemical science* **15**, 17843–17851.

Barro, J. P., Alves, K. S., Godoy, C. V., Dias, A. R., Forcelini, C. A., Utiamada, C. M., Andrade Júnior, E. R. de, Juliatti, F. C., Grigolli, F. J., Feksa, H. R., Campos, H. D., Chaves, I. C. P. V., Araújo Júnior, I. P., Roy, J. M. T., Nunes Júnior, J., Belufi, L. M. R., Carneiro, L. C., Silva, L. H. C. P., Canteri, (…) and Del Ponte, E. M. (2021) Performance of dual and triple fungicide premixes for managing soybean rust across years and regions in Brazil: A meta ‐ analysis. *Plant Pathology* **70**, 1920–1935.

Bartlett, D. W., Clough, J. M., Godwin, J. R., Hall, A. A., Hamer, M. and Parr-Dobrzanski, B. (2002) The strobilurin fungicides. *Pest management science* **58**, 649–662.

Beckerman, J., Palmer, C., Tedford, E. and Ypema, H. (2023) Fifty Years of Fungicide Development, Deployment, and Future Use. *Phytopathology* **113**, 694–706.

Beernink, B. M., Amanat, N., Li, V. H., Manchur, C. L., Whyard, S. and Belmonte, M. F. (2024) SIGS vs. HIGS: opportunities and challenges of RNAi pest and pathogen control strategies. *Canadian Journal of Plant Pathology* **46**, 675–689.

Beesley, A. (2022). *Tailored coumarin biosynthesis for plant protection*. Dissertation. Aachen, Germany.

Beesley, A., Beyer, S. F., Wanders, V., Levecque, S., Bredenbruch, S., Habash, S. S., Schleker, A. S. S., Gätgens, J., Oldiges, M., Schultheiss, H., Conrath, U. and Langenbach, C. J. G. (2023) Engineered coumarin accumulation reduces mycotoxin-induced oxidative stress and disease susceptibility. *Plant biotechnology journal* **21**, 2490–2506.

Benjamini, Y. and Hochberg, Y. (1995) Controlling the False Discovery Rate: A Practical and Powerful Approach to Multiple Testing. *Journal of the Royal Statistical Society Series B: Statistical Methodology* **57**, 289–300.

Bennett, R. N. and Wallsgrove, R. M. (1994) Secondary metabolites in plant defence mechanisms. *The New phytologist* **127**, 617–633.

Bent, A. (2016) Resistance from relatives. *Nature biotechnology* **34**, 620–621.

Berg, J. M., Tymoczko, J. L., Gatto, G. J. and Stryer, L. (2018) Der Citratzyklus. In: *Stryer Biochemie* (Berg, J.M., Tymoczko, J.L., Gatto, G.J. and Stryer, L., eds), pp. 581–611. Berlin, Heidelberg: Springer Berlin Heidelberg.

Beyer, S. (2019). *Identifizierung und Anwendung von antimykotischen Cumarinen und hormonresponsiven Markergenen für den Pflanzenschutz*. Dissertation. Aachen, Germany.

Beyer, S. F., Beesley, A., Rohmann, P. F. W., Schultheiss, H., Conrath, U. and Langenbach, C. J. G. (2019) The Arabidopsis non-host defence-associated coumarin scopoletin protects soybean from Asian soybean rust. *The Plant journal for cell and molecular biology* **99**, 397–413.

Blum, M., Andreeva, A., Florentino, L. C., Chuguransky, S. R., Grego, T., Hobbs, E., Pinto, B. L., Orr, A., Paysan-Lafosse, T., Ponamareva, I., Salazar, G. A., Bordin, N., Bork, P., Bridge, A., Colwell, L., Gough, J., Haft, D. H., Letunic, I., Llinares-López, F., (…) and Bateman, A. (2025) InterPro: the protein sequence classification resource in 2025. *Nucleic acids research* **53**, D444-D456.

Bohlmann, F., Suwita, A., King, R. M. and Robinson, H. (1980) Neue ent-labdan-derivate aus *Austroeupatorium chaparense*. *Phytochemistry* **19**, 111–114.

Bose, P. K. and Ghosh, S. K. (1936) On the Constitution of Ayapin. *Current Science* **5**, 295.

Bourgaud, F., Hehn, A., Larbat, R., Doerper, S., Gontier, E., Kellner, S. and Matern, U. (2006) Biosynthesis of coumarins in plants: a major pathway still to be unravelled for cytochrome P450 enzymes. *Phytochem Rev* **5**, 293–308.

Bromfield, K.R. (1984). Soybean rust. *American Phytopathological Society*.

Buswell, W., Schwarzenbacher, R. E., Luna, E., Sellwood, M., Chen, B., Flors, V., Pétriacq, P. and Ton, J. (2018) Chemical priming of immunity without costs to plant growth. *New Phytologist* **218**, 1205–1216.

Byeon, Y., Lee, H. Y., Lee, K. and Back, K. (2014) Caffeic acid O-methyltransferase is involved in the synthesis of melatonin by methylating N-acetylserotonin in Arabidopsis. *Journal of pineal research* **57**, 219–227.

Cabello-Hurtado, F., Durst, F., Jorrín, J. V. and Werck-Reichhart, D. (1998) Coumarins in *Helianthus tuberosus* characterization, induced accumulation and biosynthesis. *Phytochemistry* **49**, 1029–1036.

Ceresini, P. C., Silva, T. C., Vicentini, S. N. C., Júnior, R. P. L., Moreira, S. I., Castro-Ríos, K., Garcés-Fiallos, F. R., Krug, L. D., Moura, S. S. de, Da Silva, A. G., Paiva Custódio, A. A. de, May De Mio, L. L., Godoy Gasparoto, M. C. de, Portalanza, D. and Jesus Júnior, W. C. de (2024) Strategies for managing fungicide resistance in the Brazilian tropical agroecosystem: Safeguarding food safety, health, and the environmental quality. *Trop. plant pathol.* **49**, 36–70.

Chen, C., Imran, M., Feng, X., Shen, X. and Sun, Z. (2025) Spray-induced gene silencing for crop protection: recent advances and emerging trends. *Frontiers in plant science* **16**, 1527944.

Chi, Y., Zhu, X., Chen, Y., Li, X., Jiang, Z., Jian, X., Lian, M., Wu, X., Wang, L., Sun, M. and Shi, X. (2024) Metabolic activation and cytochrome P450 inhibition of piperlonguminine mediated by CYP3A4. *International journal of biological macromolecules* **268**, 131502.

Chicowski, A. S., Bredow, M., Utiyama, A. S., Marcelino-Guimarães, F. C. and Whitham, S. A. (2024) Soybean-*Phakopsora pachyrhizi* interactions: towards the development of next-generation disease-resistant plants. *Plant biotechnology journal* **22**, 296–315.

Childs, S. P., Buck, J. W. and Li, Z. (2018a) Breeding soybeans with resistance to soybean rust (*Phakopsora pachyrhizi*). *Plant Breeding* **137**, 250–261.

Childs, S. P., King, Z. R., Walker, D. R., Harris, D. K., Pedley, K. F., Buck, J. W., Boerma, H. R. and Li, Z. (2018b) Discovery of a seventh *Rpp* soybean rust resistance locus in soybean accession PI 605823. *TAG. Theoretical and applied genetics. Theoretische und angewandte Genetik* **131**, 27–41.

Chitarra, G. S., Abee, T., Rombouts, F. M. and Dijksterhuis, J. (2005) 1-Octen-3-ol inhibits conidia germination of *Penicillium paneum* despite of mild effects on membrane permeability, respiration, intracellular pH, and changes the protein composition. *FEMS microbiology ecology* **54**, 67–75.

Chomczynski, P. and Sacchi, N. (1987) Single-step method of RNA isolation by acid guanidinium thiocyanate-phenol-chloroform extraction. *analytical biochemistry* **162**, 156–159.

Chu, L. L., Pandey, R. P., Lim, H. N., Jung, H. J., Thuan, N. H., Kim, T.-S. and Sohng, J. K. (2017) Synthesis of umbelliferone derivatives in *Escherichia coli* and their biological activities. *Journal of biological engineering* **11**, 15.

Ciriminna, R., Meneguzzo, F., Delisi, R. and Pagliaro, M. (2017) Citric acid: emerging applications of key biotechnology industrial product. *Chemistry Central journal* **11**, 22.

Claus, A., Simões, K. and Mio, L. L. M. de (2022) SdhC-I86F Mutation in *Phakopsora pachyrhizi* Is Stable and Can Be Related to Fitness Penalties. *Phytopathology* **112**, 1413–1421.

Conrath, U., Beckers, G. J. M., Langenbach, C. J. G. and Jaskiewicz, M. R. (2015) Priming for enhanced defense. *Annual review of phytopathology* **53**, 97–119.

Cruz, M. F. A., Rodrigues, F. Á., Diniz, A. P. C., Alves Moreira, M. and Barros, E. G. (2014) Soybean Resistance to *Phakopsora pachyrhizi* as Affected by Acibenzolar ‐ S ‐ Methyl, Jasmonic Acid and Silicon. *Journal of Phytopathology* **162**, 133–136.

Da Rocha, V. D., Ferreira, E. G. C., Castanho, F. M., Kuwahara, M. K., Godoy, C. V., Meyer, M. C., Pedley, K. F., Voegele, R. T., Lipzen, A., Barry, K., Grigoriev, I. V., Loehrer, M., Schaffrath, U., Sirven, C., Duplessis, S. and Marcelino-Guimarães, F. C. (2025) Analysis of the genetic diversity of the soybean rust pathogen *Phakopsora pachyrhizi* reveals two major evolutionary lineages. *Fungal genetics and biology FG & B* **179**, 103990.

Dalla Lana, F., Paul, P. A., Godoy, C. V., Utiamada, C. M., da Silva, L. H. C. P., Siqueri, F. V., Forcelini, C. A., Jaccoud-Filho, D. d. S., Miguel-Wruck, D. S., Borges, E. P., Juliatti, F. C., Campos, H. D., Nunes, J., Carneiro, L. C., Canteri, M. G., Ito, M. F., Meyer, M. C., Martins, M. C., Balardin, (…) and Del Ponte, E. M. (2018) Meta-Analytic Modeling of the Decline in Performance of Fungicides for Managing Soybean Rust after a Decade of Use in Brazil. *Plant disease* **102**, 807–817.

Debenedetti, S. L., Nadinic, E. L., Coussio, J. D., Kimpe, N. de and Boeykens, M. (1998) Two 6,7-dioxygenated coumarins from *Pterocaulon virgatum*. *Phytochemistry* **48**, 707–710.

Deota, P. T., Parmar, H. S., Patel, G. M. and Bhatt, G. J. (2023) Impact of ultraviolet-absorbing 2-hydroxy-4-quaternaryammoniumalkoxy benzophenone motif on photodegradation of

disulfoton: a case study. *Environmental science and pollution research international* **30**, 124704–124713.

Dieterman, L. J., Lin, C. Y., Rohrbaugh, L. M. and Wender, S. H. (1964) Accumulation of Ayapin and Scopolin in Sunflower Plants Treated with 2,4-dichlorophenoxyacetic Acid. *Archives of biochemistry and biophysics* **106**, 275–279.

Dixon, R. A. (2001) Natural products and plant disease resistance. *Nature* **411**, 843–847.

Dixon, R. A. and Dickinson, A. J. (2024) A century of studying plant secondary metabolism-From "what?" to "where, how, and why?". *Plant physiology* **195**, 48–66.

Dixon, R. A. and Paiva, N. L. (1995) Stress-Induced Phenylpropanoid Metabolism. *Plant Cell* **7**, 1085–1097.

Dobin, A., Davis, C. A., Schlesinger, F., Drenkow, J., Zaleski, C., Jha, S., Batut, P., Chaisson, M. and Gingeras, T. R. (2013) STAR: ultrafast universal RNA-seq aligner. *Bioinformatics (Oxford, England)* **29**, 15–21.

Dorigan, A. F., Moreira, S. I., da Silva Costa Guimarães, S., Cruz-Magalhães, V. and Alves, E. (2023) Target and non-target site mechanisms of fungicide resistance and their implications for the management of crop pathogens. *Pest management science* **79**, 4731–4753.

Dorighello, D. V., Bettiol, W., Maia, N. B. and Campos Leite, R. M. V. B. de (2015) Controlling Asian soybean rust (*Phakopsora pachyrhizi*) with *Bacillus spp*. and coffee oil. *Crop Protection* **67**, 59–65.

Dreischhoff, S. (2019). *Secondary metabolites for plant protection*. Master Thesis. Aachen, Germany.

Du, Y., Jia, H., Yang, Z., Wang, S., Liu, Y., Ma, H., Liang, X., Wang, B., Zhu, M., Meng, Y., Gleason, M. L., Hsiang, T., Noorin, S., Zhang, R. and Sun, G. (2023) Sufficient coumarin accumulation improves apple resistance to *Cytospora mali* under high-potassium status. *Plant physiology* **192**, 1396–1419.

Edwards, K., Johnstone, C. and Thompson, C. (1991) A simple and rapid method for the preparation of plant genomic DNA for PCR analysis. *Nucleic acids research* **19**, 1349.

Edwards Molina, J. P., Navarro, B. L., Allen, T. W. and Godoy, C. V. (2022) Soybean target spot caused by *Corynespora cassiicola*: a resurgent disease in the Americas. *Trop. plant pathol.* **47**, 315–331.

Egan, M. J., Wang, Z.-Y., Jones, M. A., Smirnoff, N. and Talbot, N. J. (2007) Generation of reactive oxygen species by fungal NADPH oxidases is required for rice blast disease. *Proceedings of the National Academy of Sciences of the United States of America* **104**, 11772–11777.

Ehlting, J., Büttner, D., Wang, Q., Douglas, C. J., Somssich, I. E. and Kombrink, E. (1999) Three 4-coumarate:coenzyme A ligases in *Arabidopsis thaliana* represent two evolutionarily divergent classes in angiosperms. *The Plant Journal* **19**, 9–20.

FAO (2025) Food and Agriculture Organization of the United Nations (2025) - with major processing by Our World in Data. "Soybean production - UN FAO" [dataset]. Food and Agriculture Organization of the United Nations, "Production: Crops and livestock products" [original data]. Retrieved October 23, 2025 from https://archive.ourworldindata.org/20251014-161652/grapher/soybean-production.html (archived on October 14, 2025).

Feyereisen, R. (2015) Insect P450 inhibitors and insecticides: challenges and opportunities. *Pest management science* **71**, 793–800.

Fisher, M. C., Hawkins, N. J., Sanglard, D. and Gurr, S. J. (2018) Worldwide emergence of resistance to antifungal drugs challenges human health and food security. *Science (New York, N.Y.)* **360**, 739–742.

Flors, V., Kyndt, T., Mauch-Mani, B., Pozo, M. J., Ryu, C.-M. and Ton, J. (2024) Enabling sustainable crop protection with induced resistance in plants. *Front Sci* **2**.

Fortunato, A. A., Araujo, L. and Rodrigues, F. Á. (2017) Association of the Production of Phenylpropanoid Compounds at the Infection Sites of *Corynespora cassiicola* with Soybean Resistance against Target Spot. *Journal of Phytopathology* **165**, 131–142.

Fourcroy, P., Sisó-Terraza, P., Sudre, D., Savirón, M., Reyt, G., Gaymard, F., Abadía, A., Abadia, J., Álvarez-Fernández, A. and Briat, J.-F. (2014) Involvement of the ABCG37 transporter in secretion of scopoletin and derivatives by Arabidopsis roots in response to iron deficiency. *The New phytologist* **201**, 155–167.

Fraser, C. M. and Chapple, C. (2011) The phenylpropanoid pathway in Arabidopsis. *The arabidopsis book* **9**, e0152.

Funk, C. and Brodelius, P. E. (1990) Phenylpropanoid Metabolism in Suspension Cultures of *Vanilla planifolia* Andr. II. Effects of Precursor Feeding and Metabolic Inhibitors. *Plant Physiol* **94**, 95–101.

Gallie, D. R. (2002) The 5'-leader of tobacco mosaic virus promotes translation through enhanced recruitment of eIF4F. *Nucleic acids research* **30**, 3401–3411.

Gambino, G., Perrone, I. and Gribaudo, I. (2008) A rapid and effective method for RNA extraction from different tissues of grapevine and other woody plants. *Phytochemical analysis PCA* **19**, 520–525.

Gao, L., Wang, P., Yan, X., Li, J., Ma, L., Hu, M., Ge, X., Li, F. and Hou, Y. (2024) Feruloyl-CoA 6'-hydroxylase-mediated scopoletin accumulation enhances cotton resistance to *Verticillium dahliae*. *Plant Physiol.*

Garcia, A., Calvo, E. S., Souza Kiihl, R. A. de, Harada, A., Hiromoto, D. M. and Vieira, L. G. E. (2008) Molecular mapping of soybean rust (*Phakopsora pachyrhizi*) resistance genes: discovery of a novel locus and alleles. *TAG. Theoretical and applied genetics. Theoretische und angewandte Genetik* **117**, 545–553.

Garcia, D., Sanier, C., Macheix, J. J. and D'Auzac, J. (1995) Accumulation of scopoletin in *Hevea brasiliensis* infected by *Microcyclus ulei* (P. Henn.) V. ARX and evaluation of its fungitoxicity for three leaf pathogens of rubber tree. *Physiological and Molecular Plant Pathology* **47**, 213–223.

Gibson, D. G., Young, L., Chuang, R.-Y., Venter, J. C., Hutchison, C. A. and Smith, H. O. (2009) Enzymatic assembly of DNA molecules up to several hundred kilobases. *Nature methods* **6**, 343–345.

Gillot, G., Decourcelle, N., Dauer, G., Barbier, G., Coton, E., Delmail, D. and Mounier, J. (2016) 1-Octanol, a self-inhibitor of spore germination in *Penicillium camemberti*. *Food microbiology* **57**, 1–7.

Glas, J. J., Schimmel, B. C. J., Alba, J. M., Escobar-Bravo, R., Schuurink, R. C. and Kant, M. R. (2012) Plant glandular trichomes as targets for breeding or engineering of resistance to herbivores. *International journal of molecular sciences* **13**, 17077–17103.

Gnonlonfin, G. J. B., Sanni, A. and Brimer, L. (2012) Review Scopoletin – A Coumarin Phytoalexin with Medicinal Properties. *Critical Reviews in Plant Sciences* **31**, 47–56.

Godoy, C. V. (2012) Risk and management of fungicide resistance in the Asian soybean rust fungus *Phakopsora pachyrhizi*. In: *Fungicide resistance in crop protection: risk and management* (Thind, T.S., ed), pp. 87–95. UK: CABI.

Godoy, C. V., Bueno, A. d. F. and Gazziero, D. L. P. (2015) Brazilian Soybean Pest Management and Threats to its Sustainability. *Outlook Pest Man* **26**, 113–117.

Godoy, C. V., Seixas, C. D. S., Soares, R. M., Marcelino-Guimarães, F. C., Meyer, M. C. and Costamilan, L. M. (2016) Asian soybean rust in Brazil: past, present, and future. *Pesq. agropec. bras.* **51**, 407–421.

Goellner, K., Loehrer, M., Langenbach, C., Conrath, U., Koch, E. and Schaffrath, U. (2010) *Phakopsora pachyrhizi*, the causal agent of Asian soybean rust. *Molecular plant pathology* **11**, 169-177.

Goldenberg, L., Ghuge, S. A., Doron-Faigenboim, A., Carmeli-Weissberg, M., Shaya, F., Rozen, A., Dahan, Y., Plesser, E., Kelly, G., Yaniv, Y., Arad, T., Ophir, R., Sherman, A., Carmi, N. and Eyal, Y. (2025) A 2OGD multi-gene cluster encompasses functional and tissue specificity that direct furanocoumarin and pyranocoumarin biosynthesis in citrus. *The New phytologist* **245**, 1547–1562.

Grasso, V., Palermo, S., Sierotzki, H., Garibaldi, A. and Gisi, U. (2006) Cytochrome b gene structure and consequences for resistance to Qo inhibitor fungicides in plant pathogens. *Pest management science* **62**, 465–472.

Guo, F., Zhou, H., Yan, F., Chen, J., Zhu, Q., Tan, Y., Guo, Y., Lai, X., Li, Z., Zhang, M., Ni, Y., Klakong, M., Yu, J., Yang, L., Li, S. and Ding, W. (2025) A Comprehensive Multiomics Approach Illuminates the Biosynthetic Mechanism of Scoparone in *Artemisia capillaris*. *Plant biotechnology journal*.

Gupta, Y. K., Marcelino-Guimarães, F. C., Lorrain, C., Farmer, A., Haridas, S., Ferreira, E. G. C., Lopes-Caitar, V. S., Oliveira, L. S., Morin, E., Widdison, S., Cameron, C., Inoue, Y., Thor, K., Robinson, K., Drula, E., Henrissat, B., LaButti, K., Bini, A. M. R., Paget, E., (…) and van Esse, H. P. (2023) Major proliferation of transposable elements shaped the genome of the soybean rust pathogen Phakopsora pachyrhizi. *Nature communications* **14**, 1835.

Gutierrez, M. (1995) Abiotic elicitation of coumarin phytoalexins in sunflower. *Phytochemistry* **38**, 1185–1191.

Gutiérrez-Mellado, M.-C., Edwards, R., Tena, M., Cabello, F., Serghini, K. and Jorrín, J. (1996) The production of coumarin phytoalexins in different plant organs of sunflower (*Helianthus annuus* L.). *Journal of Plant Physiology* **149**, 261–266.

Hahn, M. (2014) The rising threat of fungicide resistance in plant pathogenic fungi: Botrytis as a case study. *Journal of chemical biology* **7**, 133–141.

Hammerschmidt, R. (1999) Phytoalexins: What Have We Learned After 60 Years? *Annual review of phytopathology* **37**, 285–306.

Hawkins, N. J. and Fraaije, B. A. (2021) Contrasting levels of genetic predictability in the evolution of resistance to major classes of fungicides. *Molecular ecology* **30**, 5318–5327.

Hu, D., Chen, Z.-Y., Zhang, C. and Ganiger, M. (2020) Reduction of *Phakopsora pachyrhizi* infection on soybean through host- and spray-induced gene silencing. *Molecular plant pathology* **21**, 794–807.

Hu, M. and Chen, S. (2021) Non-Target Site Mechanisms of Fungicide Resistance in Crop Pathogens: A Review. *Microorganisms* **9**.

Huot, B., Yao, J., Montgomery, B. L. and He, S. Y. (2014) Growth-defense tradeoffs in plants: a balancing act to optimize fitness. *Molecular plant* **7**, 1267–1287.

Ishiga, Y., Uppalapati, S. R., Gill, U. S., Huhman, D., Tang, Y. and Mysore, K. S. (2015) Transcriptomic and metabolomic analyses identify a role for chlorophyll catabolism and phytoalexin during *Medicago* nonhost resistance against Asian soybean rust. *Sci Rep* **5**, 13061.

Ji, F., Gao, X. P., Liu, Y. N., Li, Y., Huang, L. L., Guo, J., Kang, Z. S. and Zhan, G. (2025) ABCG transporter gene PstABCG2 contributes to multidrug resistance in *Puccinia striiformis*. *J. Agric. Food Chem.* **74**, 500–515.

Jiang, H., Lei, R., Ding, S.-W. and Zhu, S. (2014) Skewer: a fast and accurate adapter trimmer for next-generation sequencing paired-end reads. *BMC bioinformatics* **15**, 182.

Kai, K., Mizutani, M., Kawamura, N., Yamamoto, R., Tamai, M., Yamaguchi, H., Sakata, K. and Shimizu, B. (2008) Scopoletin is biosynthesized via ortho-hydroxylation of feruloyl CoA by a 2-oxoglutarate-dependent dioxygenase in *Arabidopsis thaliana*. *The Plant Journal* **55**, 989–999.

Kamel, A. and Harriman, S. (2013) Inhibition of cytochrome P450 enzymes and biochemical aspects of mechanism-based inactivation (MBI). *Drug discovery today. Technologies* **10**, e177-89.

Karimi, M., Inzé, D. and Depicker, A. (2002) GATEWAY vectors for *Agrobacterium*-mediated plant transformation. *Trends in plant science* **7**, 193–195.

Kawashima, C. G., Guimarães, G. A., Nogueira, S. R., MacLean, D., Cook, D. R., Steuernagel, B., Baek, J., Bouyioukos, C., Melo, B. d. V. A., Tristão, G., Oliveira, J. C. de, Rauscher, G., Mittal, S., Panichelli, L., Bacot, K., Johnson, E., Iyer, G., Tabor, G., Wulff, B. B. H., (…) and Brommonschenkel, S. H. (2016) A pigeonpea gene confers resistance to Asian soybean rust in soybean. *Nature biotechnology* **34**, 661–665.

Kesel, J. de, Conrath, U., Flors, V., Luna, E., Mageroy, M. H., Mauch-Mani, B., Pastor, V., Pozo, M. J., Pieterse, C. M., Ton, J. and Kyndt, T. (2021) The Induced Resistance Lexicon: Do's and Don'ts. *Trends in plant science* **26**, 685–691.

Kim, B. G., Lee, Y., Hur, H.-G., Lim, Y. and Ahn, J.-H. (2006) Production of three O-methhylated esculetins with *Escherichia coli* expressing O-methyltransferase from poplar. *Bioscience, biotechnology, and biochemistry* **70**, 1269–1272.

Kim, Y.-S., Dixon, E. W., Vincelli, P. and Farman, M. L. (2003) Field Resistance to Strobilurin (Q(o)I) Fungicides in *Pyricularia grisea* Caused by Mutations in the Mitochondrial Cytochrome b Gene. *Phytopathology* **93**, 891–900.

Kishi-Kaboshi, M., Aida, R. and Sasaki, K. (2019) Parsley ubiquitin promoter displays higher activity than the CaMV 35S promoter and the chrysanthemum actin 2 promoter for productive,

constitutive, and durable expression of a transgene in *Chrysanthemum morifolium*. *Breeding science* **69**, 536–544.

Klosowski, A. C., May De Mio, L. L., Miessner, S., Rodrigues, R. and Stammler, G. (2016) Detection of the F129L mutation in the cytochrome b gene in *Phakopsora pachyrhizi*. *Pest management science* **72**, 1211–1215.

Koch, A. and Wassenegger, M. (2021) Host-induced gene silencing - mechanisms and applications. *New Phytologist* **231**, 54–59.

Kover, A., Kraljić, D., Marinaro, R. and Rene, E. R. (2022) Processes for the valorization of food and agricultural wastes to value-added products: recent practices and perspectives. *Syst Microbiol and Biomanuf* **2**, 50–66.

Kreick, L., Magarey, R. D., Love, M. and Carley, D. S. (2025) Can we resolve the pesticide quandary with eco-efficiency metrics? *Front. Agron.* **7**.

Langenbach, C., Campe, R., Beyer, S. F., Mueller, A. N. and Conrath, U. (2016) Fighting Asian Soybean Rust. *Frontiers in plant science* **7**, 797.

Langenbach, C., Campe, R., Schaffrath, U., Goellner, K. and Conrath, U. (2013) UDP-glucosyltransferase UGT84A2/BRT1 is required for Arabidopsis nonhost resistance to the Asian soybean rust pathogen *Phakopsora pachyrhizi*. *New Phytologist* **198**, 536–545.

Lax A.R., Templeton G.E. and Meyer W.L. (1985) Isolation, purification, and biological activity of a self-inhibitor from conidia of *Colletotrichum gloeosporioides*. *Phytopathology* **75**.

Le Roy, J., Huss, B., Creach, A., Hawkins, S. and Neutelings, G. (2016) Glycosylation Is a Major Regulator of Phenylpropanoid Availability and Biological Activity in Plants. *Frontiers in plant science* **7**, 735.

Lefèvre, F., Fourmeau, J., Pottier, M., Baijot, A., Cornet, T., Abadía, J., Álvarez-Fernández, A. and Boutry, M. (2018) The *Nicotiana tabacum* ABC transporter NtPDR3 secretes O-methylated coumarins in response to iron deficiency. *Journal of experimental botany* **69**, 4419–4431.

Leiminger, J. H., Adolf, B. and Hausladen, H. (2014) Occurrence of the F 129 L mutation in *Alternaria solani* populations in Germany in response to QoI application, and its effect on sensitivity. *Plant Pathology* **63**, 640–650.

Leite, B. and Nicholson, R. L. (1993) A Volatile Self-Inhibitor from *Colletotrichum graminicola*. *Mycologia* **85**, 945–951.

Liu, H., Zhang, B., Wu, T., Ding, Y., Ding, X. and Chu, Z. (2015) Copper Ion Elicits Defense Response in *Arabidopsis thaliana* by Activating Salicylate- and Ethylene-Dependent Signaling Pathways. *Molecular plant* **8**, 1550–1553.

Liu, K. (2008) Food Use of Whole Soybeans. In: *Soybeans*, pp. 441–481: Elsevier.

Liu, X., Jiao, X., Cheng, Y., Ma, Y., Bu, J., Jin, B., Li, Q., Hu, Z., Tang, J., Lai, C., Wang, J., Cui, G., Chen, Y., Guo, J. and Huang, L. (2023) Structure-function analysis of CYP719As involved in methylenedioxy bridge-formation in the biosynthesis of benzylisoquinoline alkaloids and its *de novo* production. *Microbial cell factories* **22**, 23.

Liu, Y.-Y., Yu, H. and Chen, Y.-G. (2011) Chemical constituents of *Dendrobium thyrsiflorum*. *Chem Nat Compd* **47**, 275–276.

Lockhart, S. R., Chowdhary, A. and Gold, J. A. W. (2023) The rapid emergence of antifungal-resistant human-pathogenic fungi. *Nature reviews. Microbiology* **21**, 818–832.

Loehrer, M., Botterweck, J., Jahnke, J., Mahlmann, D. M., Gaetgens, J., Oldiges, M., Horbach, R., Deising, H. and Schaffrath, U. (2014) In vivo assessment by Mach-Zehnder double-beam interferometry of the invasive force exerted by the Asian soybean rust fungus (*Phakopsora pachyrhizi*). *New Phytologist* **203**, 620–631.

Loehrer, M., Langenbach, C., Goellner, K., Conrath, U. and Schaffrath, U. (2008) Characterization of nonhost resistance of Arabidopsis to the Asian soybean rust. *Molecular plant-microbe interactions MPMI* **21**, 1421–1430.

Love, M. I., Huber, W. and Anders, S. (2014) Moderated estimation of fold change and dispersion for RNA-seq data with DESeq2. *Genome biology* **15**, 550.

Lygin, A. V., Li, S., Vittal, R., Widholm, J. M., Hartman, G. L. and Lozovaya, V. V. (2009) The importance of phenolic metabolism to limit the growth of *Phakopsora pachyrhizi*. *Phytopathology* **99**, 1412–1420.

Lyubenova, A., Georgieva, L. and Antonova, V. (2023) Utilization of plant secondary metabolites for plant protection. *Biotechnology & Biotechnological Equipment* **37**.

Ma, Z. and Michailides, T. J. (2005) Advances in understanding molecular mechanisms of fungicide resistance and molecular detection of resistant genotypes in phytopathogenic fungi. *Crop Protection* **24**, 853–863.

Ma, Z., Proffer, T. J., Jacobs, J. L. and Sundin, G. W. (2006) Overexpression of the 14alpha-demethylase target gene (*CYP51*) mediates fungicide resistance in *Blumeriella jaapii*. *Applied and environmental microbiology* **72**, 2581–2585.

Macko, V., Staples, R. C., Allen, P. J. and Renwick, J. A. (1971) Identification of the germination self-inhibitor from wheat stem rust uredospores. *Science (New York, N.Y.)* **173**, 835–836.

Macko, V., Staples, R. C., Gershon, H. and Renwick, J. A. (1970) Self-inhibitor of bean rust uredospores: methyl 3,4-dimethoxycinnamate. *Science (New York, N.Y.)* **170**, 539–540.

Macko, V., Staples, R. C., Renwick, J. and Pirone, J. (1972) Germination self-inhibitors of rust uredospores. *Physiological Plant Pathology* **2**, 347–355.

Mandel, J. R., Dechaine, J. M., Marek, L. F. and Burke, J. M. (2011) Genetic diversity and population structure in cultivated sunflower and a comparison to its wild progenitor, *Helianthus annuus* L. *TAG. Theoretical and applied genetics. Theoretische und angewandte Genetik* **123**, 693–704.

Matsumoto, S., Mizutani, M., Sakata, K. and Shimizu, B. (2012) Molecular cloning and functional analysis of the ortho-hydroxylases of p-coumaroyl coenzyme A/feruloyl coenzyme A involved in formation of umbelliferone and scopoletin in sweet potato, *Ipomoea batatas* (L.) Lam. *Phytochemistry* **74**, 49–57.

Mello, F. E. de, Mathioni, S. M., Fantin, L. H., Rosa, D. D., Antunes, R. F. D., Filho, N. R. C., Duvaresch, D. L. and Canteri, M. G. (2021) Sensitivity assessment and SDHC-I86F mutation frequency of *Phakopsora pachyrhizi* populations to benzovindiflupyr and fluxapyroxad fungicides from 2015 to 2019 in Brazil. *Pest management science* **77**, 4331–4339.

Michelmore, R. W., Paran, I. and Kesseli, R. V. (1991) Identification of markers linked to disease-resistance genes by bulked segregant analysis: a rapid method to detect markers in specific genomic regions by using segregating populations. *Proceedings of the National Academy of Sciences of the United States of America* **88**, 9828–9832.

Mizutani, M. and Sato, F. (2011) Unusual P450 reactions in plant secondary metabolism. *Archives of biochemistry and biophysics* **507**, 194–203.

Müller, M. A., Stammler, G. and May De Mio, L. L. (2021) Multiple resistance to DMI, QoI and SDHI fungicides in field isolates of *Phakopsora pachyrhizi*. *Crop Protection* **145**, 105618.

Müller, M.A., Simões, K., Kochinski, E.G., Prestes, S.J.N., Stammler, G. and Mio, L.L.M. (2024). Selection of *Phakopsora pachyrhizi*-resistant isolates by fungicide applications in the field within the same season. *Journal of Plant Diseases and Protection* **131**.

Nelson, D. R. (2006) Cytochrome P450 nomenclature, 2004. *Methods in molecular biology (Clifton, N.J.)* **320**, 1–10.

Olson, M. M. and Roseland, C. R. (1991) Induction of the Coumarins Scopoletin and Ayapin in Sunflower by Insect–Feeding Stress and Effects of Coumarins on the Feeding of Sunflower Beetle (*Coleoptera: Chrysomelidae*). *Environmental Entomology* **20**, 1166–1172.

Ono, E., Nakai, M., Fukui, Y., Tomimori, N., Fukuchi-Mizutani, M., Saito, M., Satake, H., Tanaka, T., Katsuta, M., Umezawa, T. and Tanaka, Y. (2006) Formation of two methylenedioxy bridges by a *Sesamum* CYP81Q protein yielding a furofuran lignan, (+)-sesamin. *Proceedings of the National Academy of Sciences of the United States of America* **103**, 10116–10121.

Orr, S. T. M., Ripp, S. L., Ballard, T. E., Henderson, J. L., Scott, D. O., Obach, R. S., Sun, H. and Kalgutkar, A. S. (2012) Mechanism-based inactivation (MBI) of cytochrome P450 enzymes:

structure-activity relationships and discovery strategies to mitigate drug-drug interaction risks. *Journal of medicinal chemistry* **55**, 4896–4933.

Ortiz-Álvarez, J., Becerra, S., Baroncelli, R., Hernández-Rodríguez, C., Sukno, S. A. and Thon, M. R. (2024) Evolutionary history of the cytochrome P450s from *Colletotrichum* species and prediction of their putative functional roles during host-pathogen interactions. *BMC genomics* **25**, 56.

Osbourn, A. E. (1996) Preformed Antimicrobial Compounds and Plant Defense against Fungal Attack. *Plant Cell* **8**, 1821–1831.

Otey, C. R., Silberg, J. J., Voigt, C. A., Endelman, J. B., Bandara, G. and Arnold, F. H. (2004) Functional evolution and structural conservation in chimeric cytochromes p450: calibrating a structure-guided approach. *Chemistry & biology* **11**, 309–318.

Ouyang, H., Sun, G., Li, K., Wang, R., Lv, X., Zhang, Z., Zhao, R., Wang, Y., Shu, H., Jiang, H., Zhang, S., Wu, J., Zhang, Q., Chen, X., Liu, T., Ye, W., Wang, Y. and Wang, Y. (2024) Profiling of *Phakopsora pachyrhizi* transcriptome revealed co-expressed virulence effectors as prospective RNA interference targets for soybean rust management. *Journal of integrative plant biology* **66**, 2543–2560.

Pandey, A. K., Yang, C., Zhang, C., Graham, M. A., Horstman, H. D., Lee, Y., Zabotina, O. A., Hill, J. H., Pedley, K. F. and Whitham, S. A. (2011) Functional analysis of the Asian soybean rust resistance pathway mediated by *Rpp2*. *Molecular plant-microbe interactions MPMI* **24**, 194–206.

Paula, S. de, Holz, S., Souza, D. H. G. and Pascholati, S. F. (2021) Potential of resistance inducers for soybean rust management. *Canadian Journal of Plant Pathology* **43**, 298-307.

Piasecka, A., Jedrzejczak-Rey, N. and Bednarek, P. (2015) Secondary metabolites in plant innate immunity: conserved function of divergent chemicals. *New Phytologist* **206**, 948–964.

Pieterse, C. M. J., Zamioudis, C., Berendsen, R. L., Weller, D. M., van Wees, S. C. M. and Bakker, P. A. H. M. (2014) Induced systemic resistance by beneficial microbes. *Annual review of phytopathology* **52**, 347–375.

Pine, L. and Peacock, C. L. (1958) Studies on the growth of *Histoplasma capsulatum*. IV. Factors influencing conversion of the mycelial phase to the yeast phase. *Journal of bacteriology* **75**, 167–174.

Prats, E., Bazzalo, M. E., León, A. and Jorrín, J. V. (2006) Fungitoxic effect of scopolin and related coumarins on *Sclerotinia sclerotiorum*. A way to overcome sunflower head rot. *Euphytica* **147**, 451–460.

Prats, E., Llamas, M. J., Jorrin, J. and Rubiales, D. (2007) Constitutive Coumarin Accumulation on Sunflower Leaf Surface Prevents Rust Germ Tube Growth and Appressorium Differentiation. *Crop Sci.* **47**, 1119–1124.

Prats, E., Rubiales, D. and JorrÍn, J. (2002) Acibenzolar-S-methyl-induced resistance to sunflower rust (*Puccinia helianthi*) is associated with an enhancement of coumarins on foliar surface. *Physiological and Molecular Plant Pathology* **60**, 155–162.

Presotto, A., Fernández-Moroni, I., Poverene, M. and Cantamutto, M. (2011) Sunflower crop-wild hybrids: Identification and risks. *Crop Protection* **30**, 611–616.

Rajniak, J., Giehl, R. F. H., Chang, E., Murgia, I., Wirén, N. von and Sattely, E. S. (2018) Biosynthesis of redox-active metabolites in response to iron deficiency in plants. *Nature chemical biology* **14**, 442–450.

Repčák, M. and Suvák, M. (2013) Methyl jasmonate and *Echinothrips americanus* regulate coumarin accumulation in leaves of *Matricaria chamomilla*. *Biochemical Systematics and Ecology* **47**, 38–41.

Rial, C., Varela, R. M., Molinillo, J. M., Peralta, S. and Macías, F. A. (2021) Sunflower Metabolites Involved in Resistance Mechanisms against Broomrape. *Agronomy* **11**, 501.

Rodrigues, F. C. T., Silveira, P. R., Cacique, I. S., Oliveira, L. M. and Rodrigues, F. A. (2023) Azelaic and hexanoic acids ‐ inducing resistance in soybean against *Phakopsora pachyrhizi* infection. *Plant Pathology* **72**, 1034–1047.

Rozhon, W., Ramirez, V. E., Wieckhorst, S., Hahn, V. and Poppenberger, B. (2023) Generation of high oleic acid sunflower lines using gamma radiation mutagenesis and high-throughput fatty acid profiling. *Frontiers in plant science* **14**, 1138603.

Sacher, R. M., Metcalf, R. L. and Fukuto, T. R. (1969) Selectivity of carbaryl-2,3-methylenedioxynaphthalene combination. Metabolism of the synergist in two strains of houseflies and in mice. *J. Agric. Food Chem.* **17**, 551–557.

Saito, H., Sakata, N., Ishiga, T. and Ishiga, Y. (2022) Efficacy of RNA-spray-induced silencing of *Phakopsora pachyrhizi* chitin synthase genes to control soybean rust. *J Gen Plant Pathol* **88**, 203–206.

Savary, S., Willocquet, L., Pethybridge, S. J., Esker, P., McRoberts, N. and Nelson, A. (2019) The global burden of pathogens and pests on major food crops. *Nat Ecol Evol* **3**, 430–439.

Scalliet, G., Bowler, J., Luksch, T., Kirchhofer-Allan, L., Steinhauer, D., Ward, K., Niklaus, M., Verras, A., Csukai, M., Daina, A. and Fonné-Pfister, R. (2012) Mutagenesis and functional studies with succinate dehydrogenase inhibitors in the wheat pathogen *Mycosphaerella graminicola*. *PloS one* **7**, e35429.

Schalk, M., Cabello-Hurtado, F., Pierrel, M. A., Atanossova, R., Saindrenan, P. and Werck-Reichhart, D. (1998) Piperonylic acid, a selective, mechanism-based inactivator of the trans-cinnamate 4-hydroxylase: A new tool to control the flux of metabolites in the phenylpropanoid pathway. *Plant Physiol.* **118**, 209–218.

Schmidt-Jeffris, R. A., Beers, E. H. and Sater, C. (2021) Meta-analysis and review of pesticide non-target effects on phytoseiids, key biological control agents. *Pest management science* **77**, 4848–4862.

Schmitz, H. K., Medeiros, C.-A., Craig, I. R. and Stammler, G. (2014) Sensitivity of *Phakopsora pachyrhizi* towards quinone-outside-inhibitors and demethylation-inhibitors, and corresponding resistance mechanisms. *Pest management science* **70**, 378–388.

Schnabel, A., Cotinguiba, F., Athmer, B. and Vogt, T. (2021) *Piper nigrum* CYP719A37 Catalyzes the Decisive Methylenedioxy Bridge Formation in Piperine Biosynthesis. *Plants (Basel, Switzerland)* **10**.

Schnabel, G. and Jones, A. L. (2001) The 14alpha-Demethylasse(*CYP51A1*) Gene is Overexpressed in *Venturia inaequalis* Strains Resistant to Myclobutanil. *Phytopathology* **91**, 102–110.

Schneiter, A. A. and Miller, J. F. (1981) Description of Sunflower Growth Stages 1. *Crop Sci.* **21**, 901–903.

Schwinges, P. (2019). *Alternative Strategien für den Pflanzenschutz*. Dissertation. Aachen, Germany.

SDBSWeb - National Institute of Advanced Industrial Science and Technology: Database for Organic Compounds. https://sdbs.db.aist.go.jp (accessed 25 February 2026).

Serghini, K., Pérez de Luque, A., Castejón-Muñoz, M., García-Torres, L. and Jorrín, J. V. (2001) Sunflower (*Helianthus annuus* L.) response to broomrape (*Orobanche cernua* Loefl.) parasitism: induced synthesis and excretion of 7-hydroxylated simple coumarins. *Journal of experimental botany* **52**, 2227–2234.

Shepherd, R. W., Bass, W. T., Houtz, R. L. and Wagner, G. J. (2005) Phylloplanins of tobacco are defensive proteins deployed on aerial surfaces by short glandular trichomes. *The Plant cell* **17**, 1851–1861.

Shimizu, B. (2014) 2-Oxoglutarate-dependent dioxygenases in the biosynthesis of simple coumarins. *Frontiers in plant science* **5**, 549.

Sierotzki, H. and Scalliet, G. (2013) A review of current knowledge of resistance aspects for the next-generation succinate dehydrogenase inhibitor fungicides. *Phytopathology* **103**, 880–887.

Silva, E., Da Graça, J. P., Porto, C., Martin do Prado, R., Hoffmann-Campo, C. B., Meyer, M. C., Oliveira Nunes, E. de and Pilau, E. J. (2020) Unraveling Asian Soybean Rust metabolomics using mass spectrometry and Molecular Networking approach. *Scientific reports* **10**, 138.

Simões, K., Hawlik, A., Rehfus, A., Gava, F. and Stammler, G. (2018) First detection of a SDH variant with reduced SDHI sensitivity in *Phakopsora pachyrhizi*. *J Plant Dis Prot* **125**, 21–26.

Spencer, D. (2022). *A Genetic Apporach to Crop Protection: Ein genetischer Ansatz für den Pflanzenschutz*. Dissertation. Aachen, Germany.

Staples, R. C. (1957) The organic acid composition and succinoxidase activity of the uredospore of the leaf and stem rust fungi. *Contribs. Boyce Thompson Inst.* **19**, 19–31.

Staples, R.C. and Wynn, W.K. (1965). The physiology of uredospores of the rust fungi. *The Botanical Review* **31**, 537–564.

Stassen, M. J. J., Hsu, S.-H., Pieterse, C. M. J. and Stringlis, I. A. (2021) Coumarin Communication Along the Microbiome-Root-Shoot Axis. *Trends in plant science* **26**, 169–183.

Statista (2024) Area planted with grain crops by type in Brazil| Statista. https://www.statista.com/statistics/740069/area-planted-grain-crops-type-brazil/#statisticContainer (accessed 23 October 2025).

Steiger, M. G., Rassinger, A., Mattanovich, D. and Sauer, M. (2019) Engineering of the citrate exporter protein enables high citric acid production in *Aspergillus niger*. *Metabolic engineering* **52**, 224–231.

Stilgenbauer, S., Simões, K., Craig, I. R., Brahm, L., Steiner, U. and Stammler, G. (2023) New CYP51-genotypes in *Phakopsora pachyrhizi* have different effects on DMI sensitivity. *J Plant Dis Prot* **130**, 973–983.

Stringlis, I. A., Jonge, R. de and Pieterse, C. M. J. (2019) The Age of Coumarins in Plant-Microbe Interactions. *Plant & cell physiology* **60**, 1405–1419.

Stringlis, I. A., Yu, K., Feussner, K., Jonge, R. de, van Bentum, S., van Verk, M. C., Berendsen, R. L., Bakker, P. A. H. M., Feussner, I. and Pieterse, C. M. J. (2018) MYB72-dependent coumarin exudation shapes root microbiome assembly to promote plant health. *Proceedings of the National Academy of Sciences of the United States of America* **115**, E5213-E5222.

Sun, H., Wang, L., Zhang, B., Ma, J., Hettenhausen, C., Cao, G., Sun, G., Wu, J. and Wu, J. (2014) Scopoletin is a phytoalexin against *Alternaria alternata* in wild tobacco dependent on jasmonate signalling. *Journal of experimental botany* **65**, 4305–4315.

Sun, X.-B., Zhao, P.-H., Xu, Y.-J., Sun, L.-M., Cao, M.-A. and Yuan, C.-S. (2007) Chemical constituents from the roots of *Polygonum bistorta*. *Chem Nat Compd* **43**, 563–566.

Tal, B. and Robeson, D. J. (1985) The induction, by fungal inoculation, of ayapin and scopoletin biosynthesis in *Helianthus annuus*. *Phytochemistry* **25**, 77–79.

Tal, B. and Robeson, D. J. (1986) The metabolism of sunflower phytoalexins ayapin and scopoletin: plant-fungus interactions. *Plant Physiol* **82**, 167–172.

Tang, F. H. M., Lenzen, M., McBratney, A. and Maggi, F. (2021) Risk of pesticide pollution at the global scale. *Nat. Geosci.* **14**, 206–210.

Tripathi, A. K., Bhakuni, R. S., Upadhyay, S. and Gaur, R. (2011) Insect feeding deterrent and growth inhibitory activities of scopoletin isolated from *Artemisia annua* against *Spilarctia obliqua* (*Lepidoptera: Noctuidae*). *Insect Science* **18**, 189–194.

Tsai, H.-H., Rodríguez-Celma, J., Lan, P., Wu, Y.-C., Vélez-Bermúdez, I. C. and Schmidt, W. (2018) Scopoletin 8-Hydroxylase-Mediated Fraxetin Production Is Crucial for Iron Mobilization. *Plant Physiol.* **177**, 194–207.

Tsurushima, T., Ueno, T., Fukami, H., Mayama, S. and Tani, T. (1984) Identification of the Germination Self-inhibitor from Uredospores of the Oat Crown Rust Fungus. *Agricultural and Biological Chemistry* **48**, 2009–2015.

Twizeyimana, M. and Hartman, G. L. (2019) Effect of Selected Biopesticides in Reducing Soybean Rust (*Phakopsora pachyrhizi*) Development. *Plant disease* **103**, 2460–2466.

Tylka, G. L. and Marett, C. C. (2021) Known Distribution of the Soybean Cyst Nematode, *Heterodera glycines* in the United States and Canada in 2020. *Plant Health Progress* **22**, 72–74.

U. Afek and A. Sztejnberg (1988) Accumulation of scoparone, a phytoalexin associated with resistance of Citrus to *Phytophthora citrophthora*. *Phytopathology.*

Urban, P., Mignotte, C., Kazmaier, M., Delorme, F. and Pompon, D. (1997) Cloning, yeast expression, and characterization of the coupling of two distantly related *Arabidopsis thaliana* NADPH-cytochrome P450 reductases with P450 CYP73A5. *The Journal of biological chemistry* **272**, 19176–19186.

Urdangarín, C., Regente, M. C., JorrÍn, J. and La Canal, L. de (1999) Sunflower Coumarin Phytoalexins Inhibit the Growth of the Virulent Pathogen *Sclerotinia sclerotiorum*. *Journal of Phytopathology* **147**, 441–443.

van de Mortel, M., Recknor, J. C., Graham, M. A., Nettleton, D., Dittman, J. D., Nelson, R. T., Godoy, C. V., Abdelnoor, R. V., Almeida, A. M. R., Baum, T. J. and Whitham, S. A. (2007) Distinct biphasic mRNA changes in response to Asian soybean rust infection. *Molecular plant-microbe interactions MPMI* **20**, 887–899.

van Hulten, M., Pelser, M., van Loon, L. C., Pieterse, C. M. J. and Ton, J. (2006) Costs and benefits of priming for defense in Arabidopsis. *Proceedings of the National Academy of Sciences of the United States of America* **103**, 5602–5607.

van Rhijn, N. and Rhodes, J. (2025) Evolution of antifungal resistance in the environment. *Nature microbiology* **10**, 1804–1815.

Vanholme, R., Sundin, L., Seetso, K. C., Kim, H., Liu, X., Li, J., Meester, B. de, Hoengenaert, L., Goeminne, G., Morreel, K., Haustraete, J., Tsai, H.-H., Schmidt, W., Vanholme, B., Ralph, J. and Boerjan, W. (2019) COSY catalyses trans-cis isomerization and lactonization in the biosynthesis of coumarins. *Nature plants* **5**, 1066–1075.

Venugopala, K. N., Rashmi, V. and Odhav, B. (2013) Review on Natural Coumarin Lead Compounds for Their Pharmacological Activity. *BioMed Research International* **2013**, 1–14.

Vialart, G., Hehn, A., Olry, A., Ito, K., Krieger, C., Larbat, R., Paris, C., Shimizu, B., Sugimoto, Y., Mizutani, M. and Bourgaud, F. (2012) A 2-oxoglutarate-dependent dioxygenase from *Ruta graveolens* L. exhibits p-coumaroyl CoA 2'-hydroxylase activity (C2'H): a missing step in the synthesis of umbelliferone in plants. *The Plant Journal* **70**, 460–470.

Villani, S. M., Hulvey, J., Hily, J.-M. and Cox, K. D. (2016) Overexpression of the *CYP51A1* Gene and Repeated Elements are Associated with Differential Sensitivity to DMI Fungicides in *Venturia inaequalis*. *Phytopathology* **106**, 562–571.

Vittal, R., Yang, H.-C. and Hartman, G. L. (2012) Anastomosis of germ tubes and migration of nuclei in germ tube networks of the soybean rust pathogen, *Phakopsora pachyrhizi*. *Eur J Plant Pathol* **132**, 163–167.

Vogt, T. (2010) Phenylpropanoid biosynthesis. *Molecular plant* **3**, 2–20.

Vogt, T. and Gülz, P.-G. (1991) Isocratic column liquid chromatographic separation of a complex mixture of epicuticular flavonoid aglycones and intracellular flavonol glycosides from *Cistus laufifolius* L. *Journal of Chromatography A* **537**, 453–459.

Voinnet, O., Rivas, S., Mestre, P. and Baulcombe, D. (2003) An enhanced transient expression system in plants based on suppression of gene silencing by the p19 protein of tomato bushy stunt virus. *The Plant journal for cell and molecular biology* **33**, 949–956.

Waard, M. A. de, Andrade, A. C., Hayashi, K., Schoonbeek, H.-J., Stergiopoulos, I. and Zwiers, L.-H. (2006) Impact of fungal drug transporters on fungicide sensitivity, multidrug resistance and virulence. *Pest management science* **62**, 195–207.

Wanders, V. (2019). *Zum Wirkmechanismus von Scopoletin, einem natürlichen Fungizid*. Master Thesis. Aachen, Germany.

Wang, J., Chen, P., Zhao, T., Huang, X., Zong, J., Luo, Q., Peng, C., Wu, X., Qiu, F., Zhao, D., Xiang, L., Zhang, Y., Yang, C., Zhang, F., Liao, Z., Fu, Y. and Zeng, J. (2024) Biosynthesis of Scopoletin in Sweet Potato Confers Resistance against *Fusarium oxysporum*. *Journal of agricultural and food chemistry* **72**, 7749–7764.

Wang, Y., Guan, T., Yue, X., Yang, J., Zhao, X., Chang, A., Yang, C., Fan, Z., Liu, K. and Li, Y. (2025) The biosynthetic pathway of coumarin and its genetic regulation in response to biotic and abiotic stresses. *Frontiers in plant science* **16**, 1599591.

Ward, N. A., Robertson, C. L., Chanda, A. K. and Schneider, R. W. (2012) Effects of *Simplicillium lanosoniveum* on *Phakopsora pachyrhizi*, the soybean rust pathogen, and its use as a biological control agent. *Phytopathology* **102**, 749–760.

Weber Böhlen, J. (2021). *Exploiting sunflower O-methyltransferases for tailored coumarin production in plants*. Master Thesis. Aachen, Germany.

Weber Böhlen, J., Beesley, A., Beyer, S. F., Schwinges, P., Maas, A. E., Schultheiss, H., Conrath, U. and Langenbach, C. J. G. (2026) AtMYB72 as a Biotechnological Tool to Overcome Phenylpropanoid Substrate Limitation and Enhance Coumarin Biosynthesis in Plants. *Plant biotechnology journal*.

Wei, L.-L., Chen, W.-C., Zhao, W.-C., Wang, J., Wang, B.-R., Li, F.-J., Wei, M., Guo, J., Chen, C.-J., Zheng, J.-Q. and Wang, K. (2020) Mutations and Overexpression of *CYP51* Associated with DMI-Resistance in *Colletotrichum gloeosporioides* from Chili. *Plant disease* **104**, 668–676.

Wyatt, R. E., Nagao, R. T. and Key, J. L. (1992) Patterns of soybean proline-rich protein gene expression. *The Plant cell* **4**, 99–110.

Xavier, S. A., Canteri, M. G., Barros, D. C. M. and Godoy, C. V. (2013) Sensitivity of *Corynespora cassiicola* from soybean to carbendazim and prothioconazole. *Trop. plant pathol.* **38**, 431–435.

Yamaoka, Y. (2014) Recent outbreaks of rust diseases and the importance of basic biological research for controlling rusts. *J Gen Plant Pathol* **80**, 375–388.

Yang, S.-M., Shim, G. Y., Kim, B.-G. and Ahn, J.-H. (2015) Biological synthesis of coumarins in *Escherichia coli*. *Microbial cell factories* **14**, 65.

Yin, Y., Miao, J., Shao, W., Liu, X., Zhao, Y. and Ma, Z. (2023) Fungicide Resistance: Progress in Understanding Mechanism, Monitoring, and Management. *Phytopathology* **113**, 707–718.

Yorinori, J. T., Paiva, W. M., Frederick, R. D., Costamilan, L. M., Bertagnolli, P. F., Hartman, G. E., Godoy, C. V. and Nunes, J. (2005) Epidemics of Soybean Rust (*Phakopsora pachyrhizi*) in Brazil and Paraguay from 2001 to 2003. *Plant disease* **89**, 675–677.

Zamioudis, C., Hanson, J. and Pieterse, C. M. J. (2014) β-Glucosidase BGLU42 is a MYB72-dependent key regulator of rhizobacteria-induced systemic resistance and modulates iron deficiency responses in Arabidopsis roots. *The New phytologist* **204**, 368–379.

Zheng, W. P., Tang, Y. P., Zhi, F. and Lou, F. C. (2000) Dihydroayapin, a new coumarin compound from *Dendrobium densiflorum*. *Journal of Asian natural products research* **2**, 301–304.

Ziegler, J., Schmidt, S., Strehmel, N., Scheel, D. and Abel, S. (2017) Arabidopsis Transporter ABCG37/PDR9 contributes primarily highly oxygenated Coumarins to Root Exudation. *Scientific reports* **7**, 3704.

7. Acknowledgments

First of all, I want to thank Prof. Dr. Uwe Conrath for not only giving me the opportunity to work on this project in his lab, but also for many discussions and for trusting me and, thus, giving me the freedom to explore many aspects of plant biology. I also want to thank Prof. Dr. Joost van Dongen for taking the time to evaluate this thesis and for lively discussions, e.g. during excursions to the *Tagebau Hambach.* I thank Prof. Dr. Ulrich Schaffrath for acting as third examiner and Prof. Dr. Stefan Schillberg for chairing the examination.

Next, I want to express my deepest gratitude to Caspar and Patrick for mentoring, supporting, and motivating me throughout many years. I truly enjoyed exploring the world of coumarins with you. Thank you, Caspar, for your enthusiasm, creativity and your positive mindset. I was definitely inspired by that. Thank you, Patrick, for helping me stay focused and for always finding my "roten Faden" and showing me how to tell the story.

A big thank you goes to Dr. Volker Hahn and his team (especially Regina Bauer) for giving us the opportunity to conduct three sunflower field trials and for endless sunflower selfing, crossing and harvesting. Conducting those field trials was truly a valuable experience. I also want to thank Volker for all his advice regarding sunflowers.

Also, I want to express my gratitude to Prof. Dr. Marc Stadler for giving me the opportunity to work on the *P. pachyrhizi* self-inhibitory story in his lab at the Helmholtz Institute in Braunschweig. There, I was greatly supported and supervised by Dr. Hedda Schrey. To her and her doctoral student Hao, I want to say "thank you". I want to also thank Hedda for many (online) meetings and discussions.

A special thank you goes to Alina, whom I had the honor to first supervise during her Master's studies and then to work with as colleagues. It is always a true pleasure to work, discuss and laugh with you. Thanks for always having my back. Additionally, I want to also say thank you to the rest of the "AG WeBö", Anna and Marieke! I really enjoyed first supervising you and then working with you.

Also, to the rest of the students I supervised, I want to express my gratitude: Thank you, Alina, Elpida, Lisa, Julia and Jannik.

Thanks to the many members of the Conrath group I had the pleasure to work with during my time in this lab. Thank you, Linda, PEB, Gerold, Tina, Rico, Sabine, Andrea, Marcella, Verena, Sebi, Franz and Kathrin. A special thanks goes to the coumarin team Alex and David for greatly supporting me, especially at the beginning of this journey. I would also like to thank AG Schaffrath, Marco, Florencia, Louisa and Alex in particular, for many discussions and their support.

Finally, I would like to thank my friends and family for always believing in me and giving me strength outside of the scientific bubble. And last but not least, I would like to thank Clara for her tireless support, the many conversations we have had, for helping me through difficult times over the years, yet also for sharing the good times with me. I couldn't have done it without you.

8. Supplement

8.1. Supplemental Figures

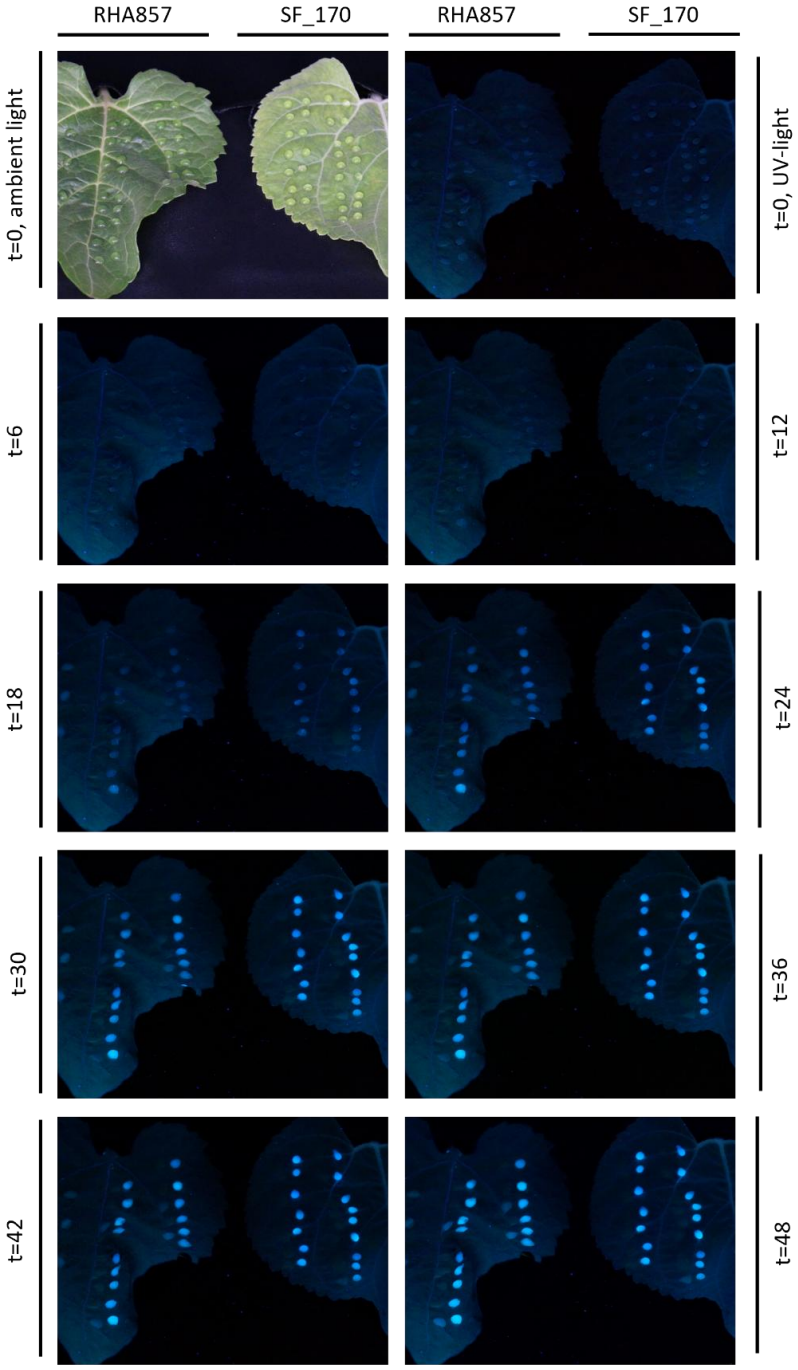

Figure S 1. Coumarin accumulation in droplets on sunflower leaves after $CuCl_2$-elicitation. Droplets of 20 µL ddH_2O (on the left of each double row of droplets) or 300 µM $CuCl_2$ (on the right of each double row of droplets) were applied on sunflower leaves of genotype RHA857 (left in each image) and SF_170 (right in each image). Under UV light, the characteristic blue fluorescence of scopoletin and ayapin was observed in $CuCl_2$-droplets over the course of 48 h, while an image was automatically taken every 6 h. The experiment was conducted with 28-days-old sunflowers by Alina Maas (master thesis within the scope of this work).

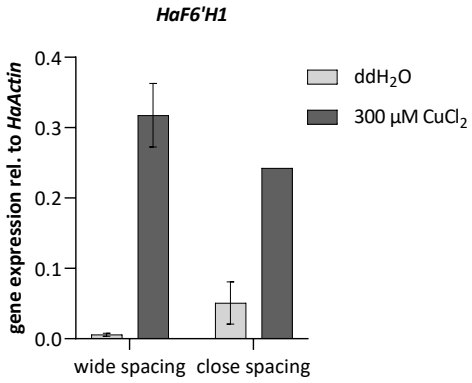

Figure S 2. Expression of *HaF6'H1* in leaf material of RHA857 induced by $CuCl_2$-droplets $CuCl_2$-elicited local stress induction in RHA857 leaves assessed by a droplet assay. Droplets (20 µL) of 300 µM $CuCl_2$ or ddH_2O were applied in either wide or close spacing to the leaf surface. After 48 h, the underlying leaf tissue was harvested, and gene expression was quantified by qRT-PCR. Expression of *HaF6'H1* was normalized to the reference gene *HaActin*. Data derived from two 28-day-old RHA857 plants, with error bars indicating the range. Experiments were performed by Alina Maas (master thesis within the scope of this work).

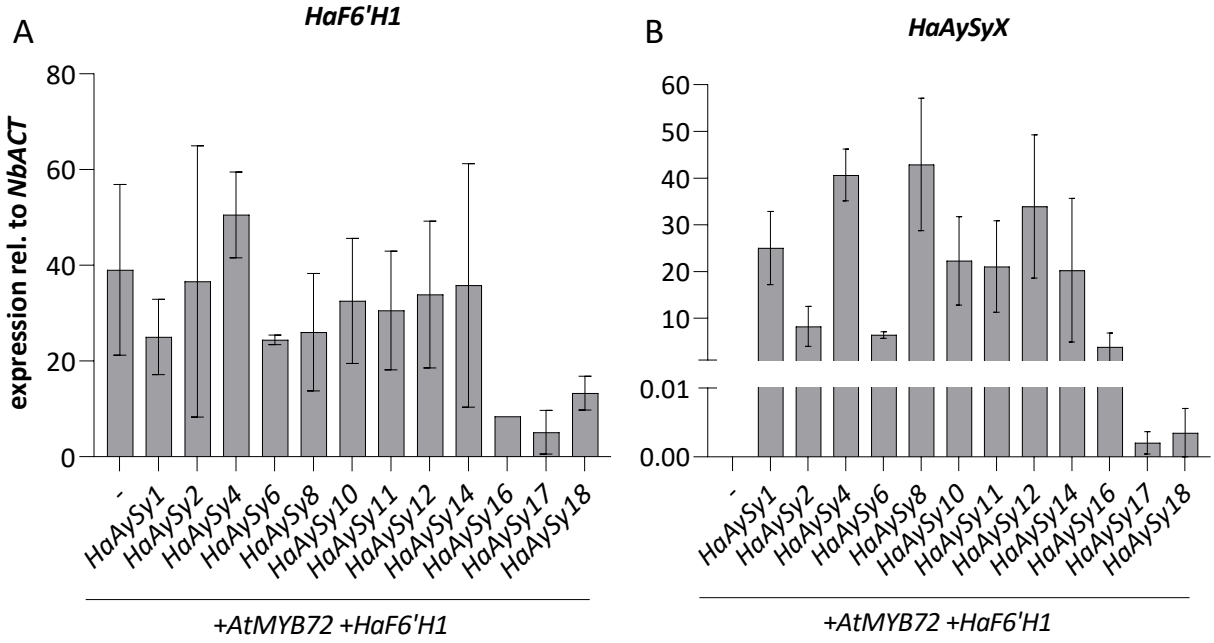

Figure S 3. Simultaneous treatment of sunflower genotype SF_170 with scopoletin and $CuCl_2$. Four-week-old *N. benthamiana* plants were transiently transformed with *A. tumefaciens* strains carrying overexpression vectors of the indicated genes. Cultures of the respective *A. tumefaciens* strains were mixed prior to infiltration. Transformed plants were cultivated for 72 h under long-day conditions before harvesting the leaf tissue. RNA were extracted from frozen leaf material and reverse transcribed to cDNA to perform qRT-PCR analysis. The expression of the transgenes *HaF6'H1* (**A**) and the respective *HaAySy* gene (**B**) was determined relative to reference gene *NbACT*. Error bars indicate the standard deviation of three biological replicates. Experiments to test candidates HaAySy1-HaAySy14 were conducted by Anna Kleineberg (master thesis within the scope of this work).

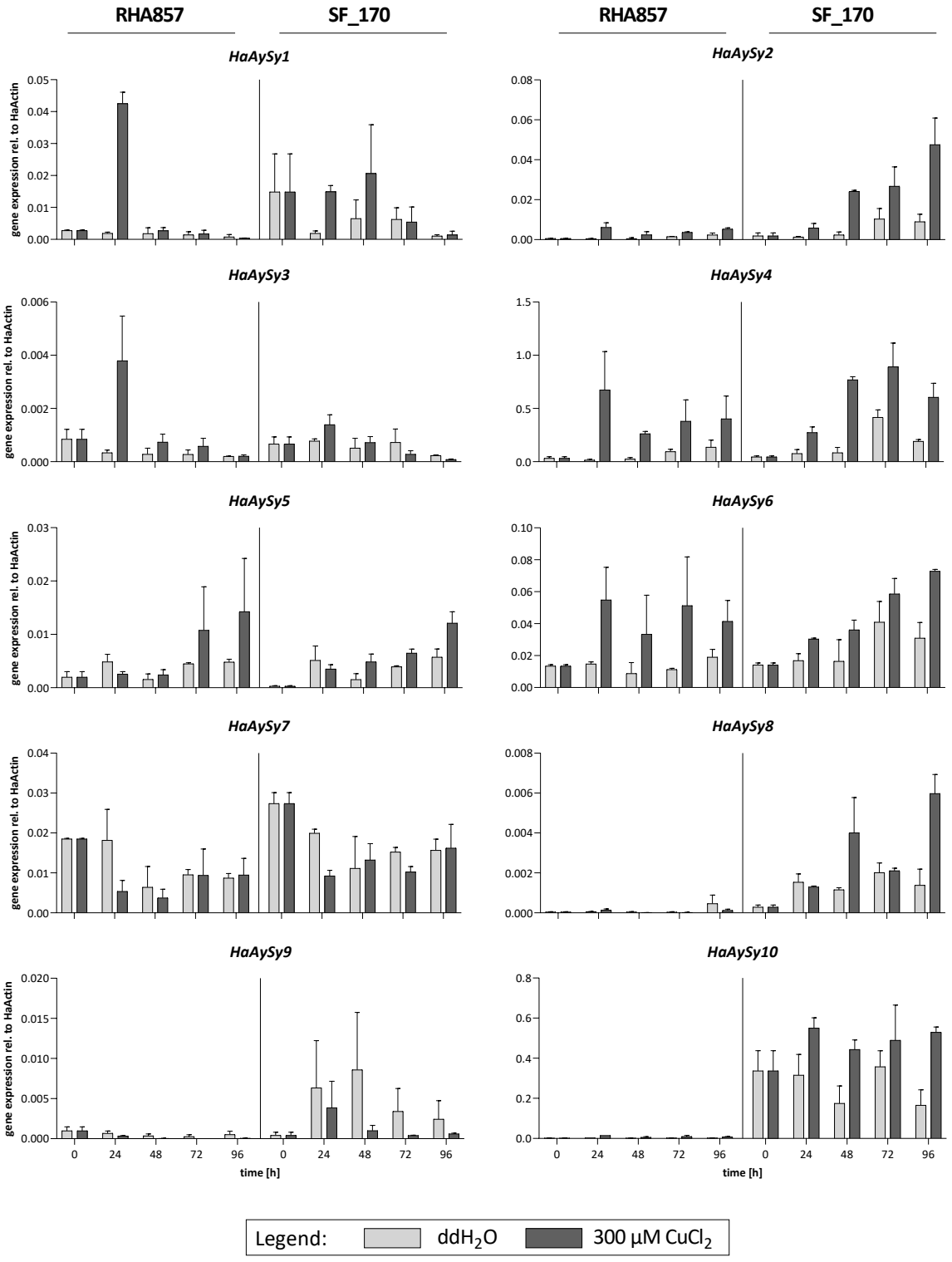

Figure S 4. Relative expression of *HaAySy* candidate genes in $CuCl_2$-elicted sunflower leaf discs of RHA857 and SF_170.This figure continues on the following page.

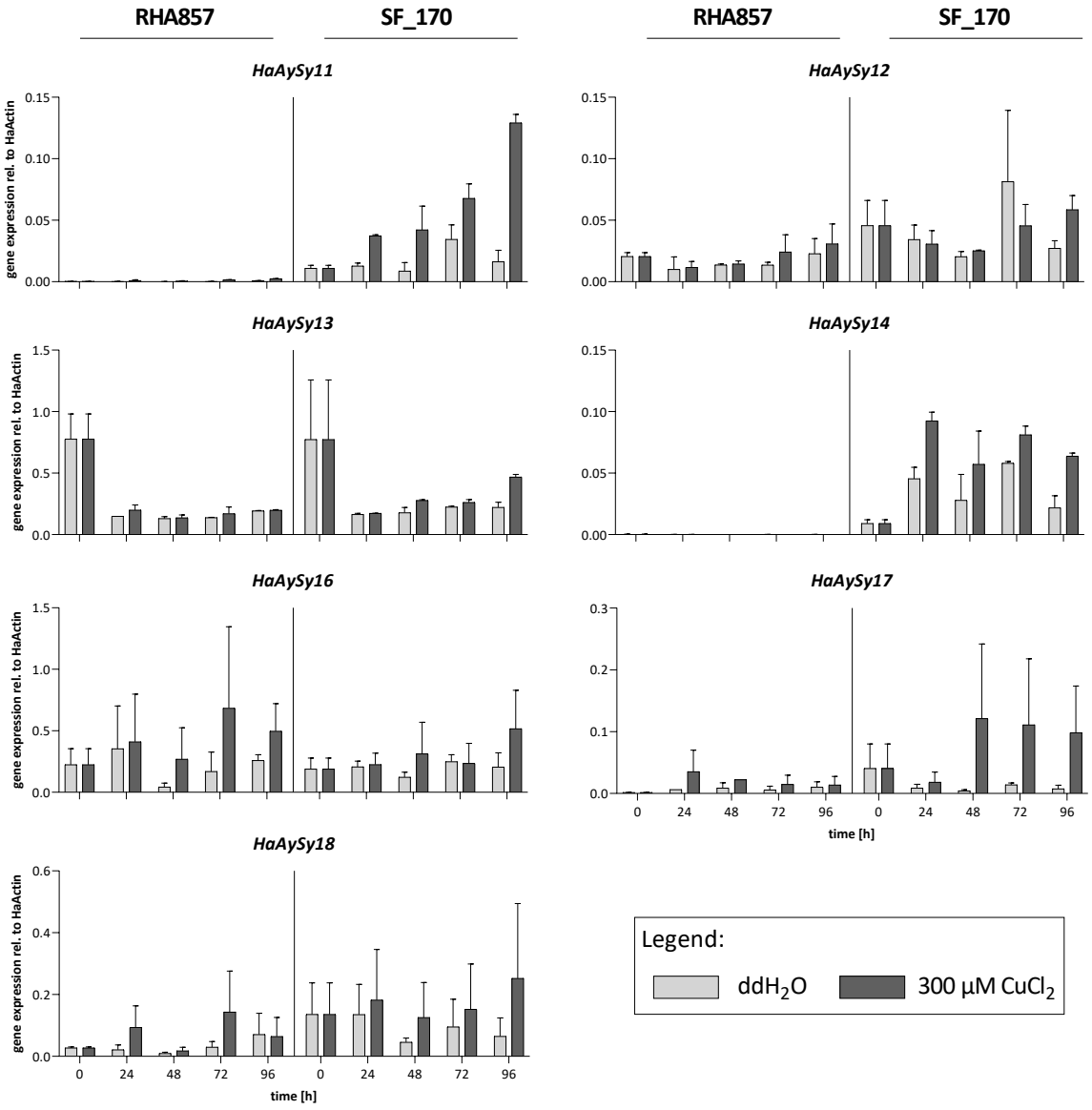

Figure S 4 -continued. Relative expression of *HaAySy* candidate genes in CuCl2-elicted sunflower leaf discs of RHA857 and SF_170. Leaf discs of four-week-old sunflower genotypes RHA857 (left) and SF_170 (right) were incubated on ddH_2O (light grey) or 300 µM $CuCl_2$ solution (dark grey) for the indicated times. Expression of candidates genes *HaAySy1-14* and *HaAySy16-18* was quantified by qRT-PCR and normalized to the reference gene *HaActin*. Error bars indicate range of two biological replicates. Experiments were performed by Alina Maas (master thesis within the scope of this work).

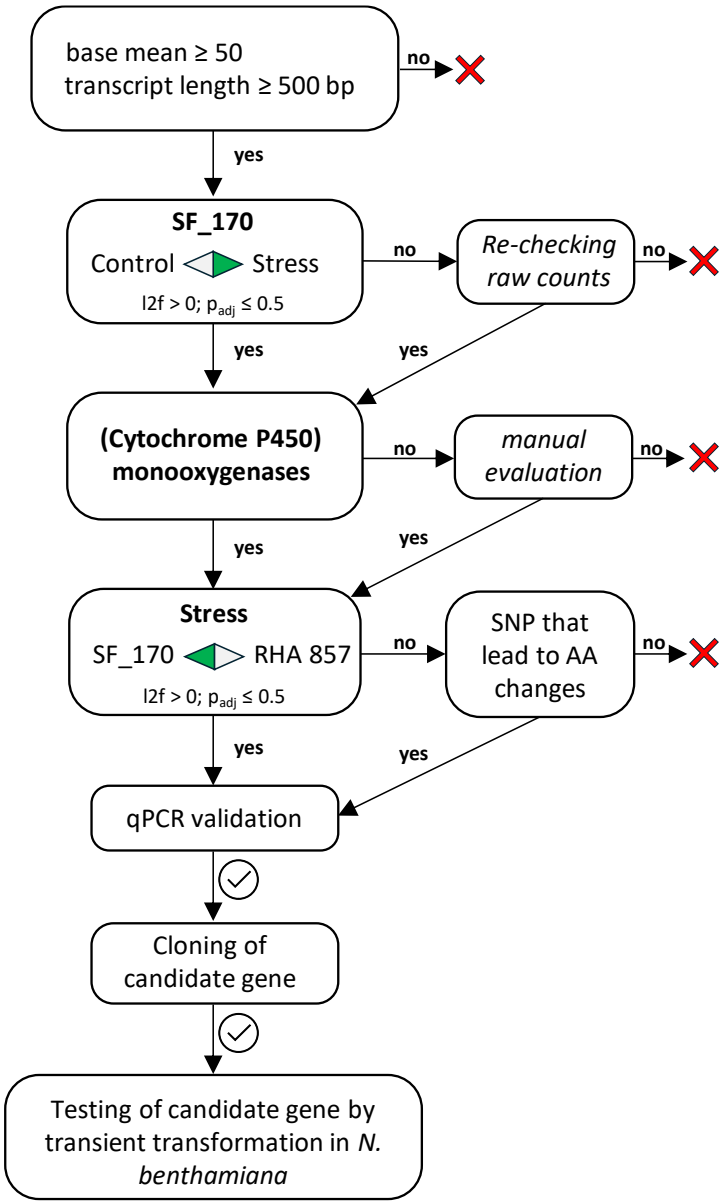

Figure S 5. Work flow for the identification of candidate genes. Differential expression analysis (DEA) data was first trimmed via R for transcripts that showed a base mean > 50 and a transcript length of at least 500 base pairs (bp). After trimming, transcripts that were significantly upregulated in the SF_170 genotype after $CuCl_2$-elicitation were filtered by setting the log2-fold-change (l2f) = > 0 and the adjusted p-value (padj) ≤ 0.5. Out of this group, data was filtered for gene annotations of "Cytochrome P450" and/or "monooxygenases". As some CYP P450 monooxygenases were only annotated by their hypothetical function, the list of upregulated genes in SF_170 was additionally manually screened for further interesting candidates, that also function as CYP, here for example isoflavone 2 -hydroxylase-like or geraniol 8-hydroxylase-like were also considered fur further analysis. Candidates were then filtered for genes that were significantly stronger transcribed in the SF_170 genotype than the RHA857 genotype comparing both $CuCl_2$-stressed samples (l2f > 0; padj ≤ 0.5). Positive hits were then validated via qRT-PCR analysis of sunflower samples that were induced with $CuCl_2$ over the course of 96 h. Genes with no differential expression between the two genotypes or stronger transcription in the RHA857 genotype were checked for single nucleotide polymorphisms (SNP) that lead to AA-changes in the coding sequence. When AA changes occurred, genes were further analyzed along with positive hits. The coding sequence of candidate genes was then cloned from cDNA of the SF_170 genotype and tested by transient transformation in *N. benthamiana* together with genes for scopoletin biosynthesis.

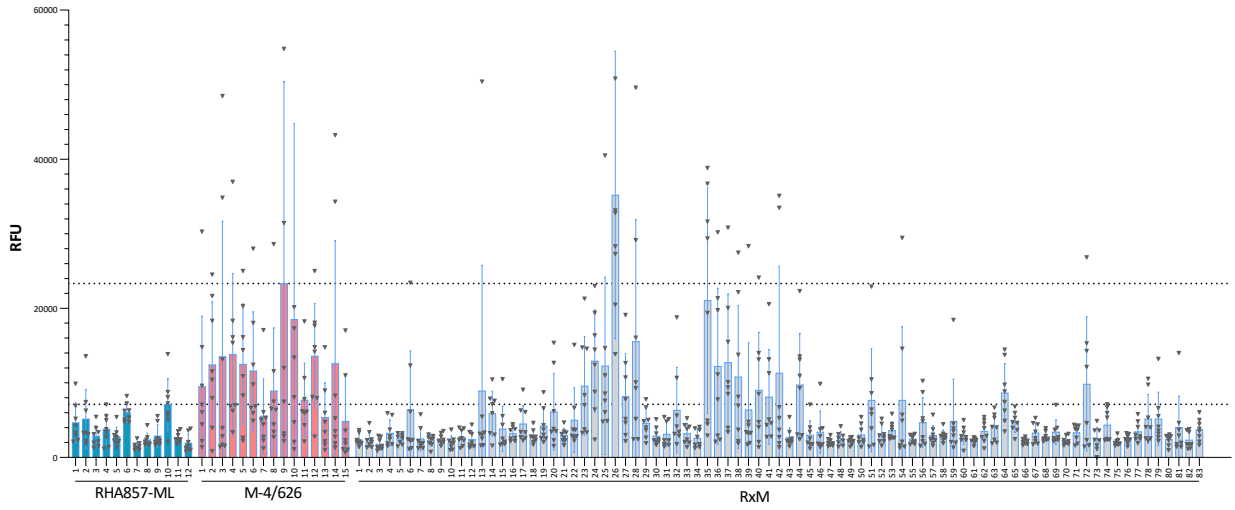

Figure S 6. Relative fluorescence of field samples of BC_1F_1-individuals of RHA857-MLxM-4/626. 12 RHA857-ML and 15 F1-plants of M-4/626 and the BC_1F_1 progeny of RHA857xM-4/626 (RxM, 83 plants in total) were grown at the agricultural experimental station Eckartsweier. Eight leaf discs per plant were harvested and incubated floating on a $CuCl_2$ solution in a 96-well-plate to induce scopoletin biosynthesis. The bars show the mean fluorescence in RFU of the eight wells of each individual plant after 48 h of incubation. Grey triangles represent the relative fluorescence of a single well. RxM individuals whose mean fluorescence exceeded the max mean fluorescence of the RHA857-ML were chosen to be selfed and backcrossed again (BC_2) into the ML. This work was done in cooperation with the Hahn Team.

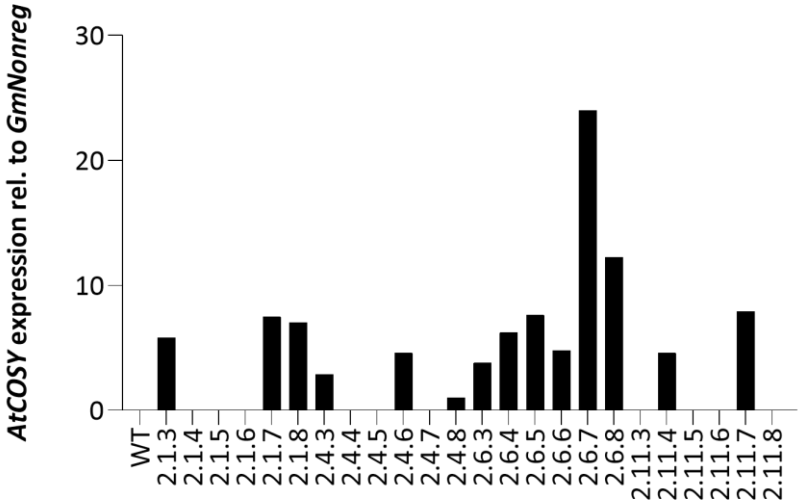

Figure S 7. Relative expression of *AtCOSY* in transgenic soybean lines. The relative expression of the transgene *AtCOSY* in leaf samples of transgenic soybean plants was determined by qRT-PCR with *GmNREG* as reference gene. Each bar represents the data of one individual plant. In the labels on the x-axis, the second number refers to the transformation event, while the third number refers to the individual plant.

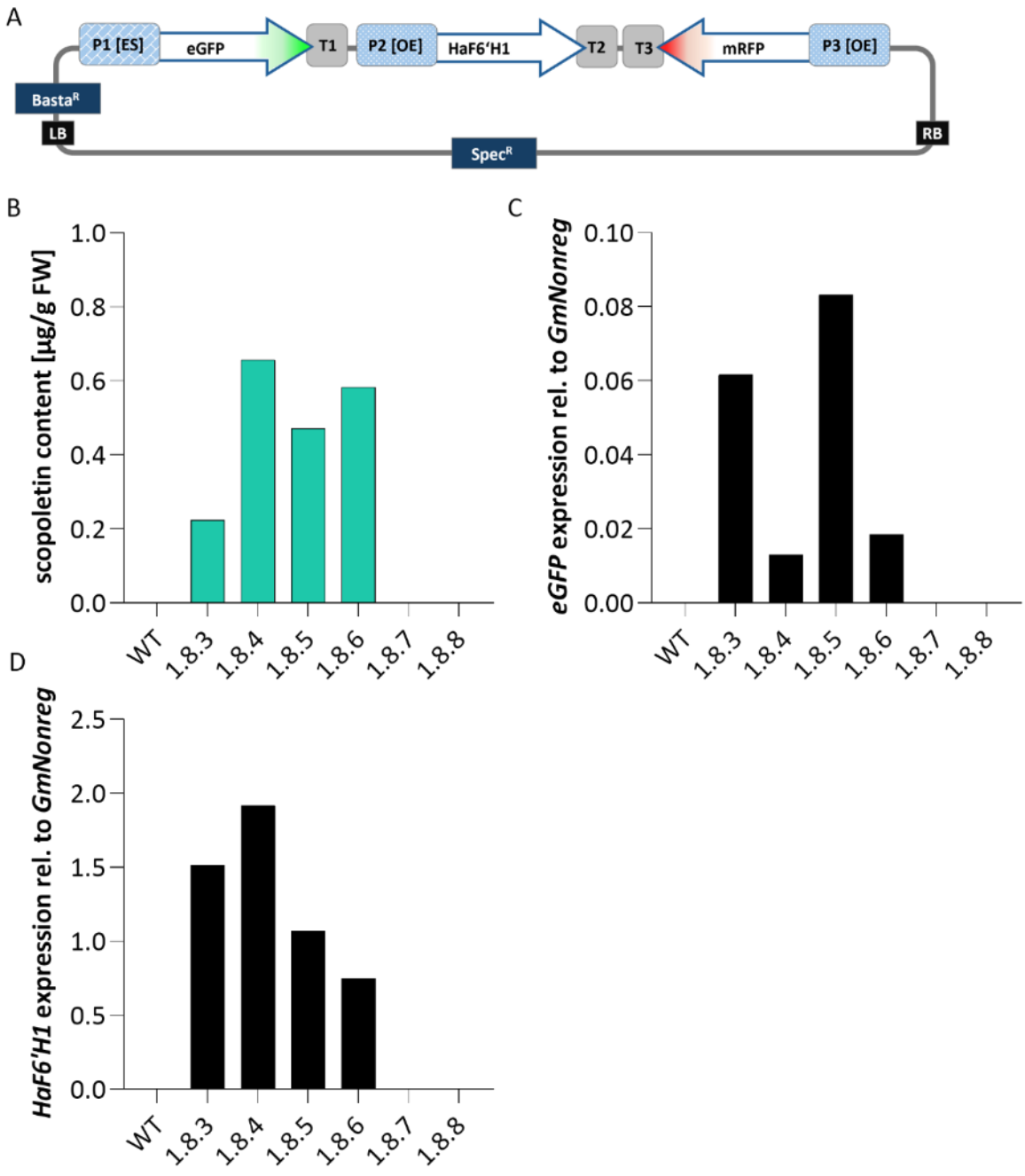

Figure S 8. Soybean plants transformed with an DNA construct harboring HaF6'H1 accumulate scopoletin. Soybean plants cv. W82 were transformed with the DNA construct shown in A. The vector was designed to harbour three coding sequences (CDS). The first promoter sequence (P1), derived from soybean, has been reported to be epidermis-specific. The second and third promoters were proven overexpression (OE) promoters. The CDSs encoded an enhanced green fluorescent protein (*eGFP*), a feruloyl 6-hydroxylase 1 from sunflower (*HaF6'H1*), and a red fluorescent protein (*mRFP*). For plant selection, a glufosinate resistance cassette (BASTA) was included. Selection in bacteria was mediated via a spectinomycin resistance cassette ($Spec^R$). Scopoletin content in the leaves of six individual plants of transformation event #1.8 was measured via HPLC (B). The relative expression of the transgenes *eGFP* (C) and *HaF6'H1* (D) in the same leaves was determined by qRT-PCR with *GmNREG* as reference gene.

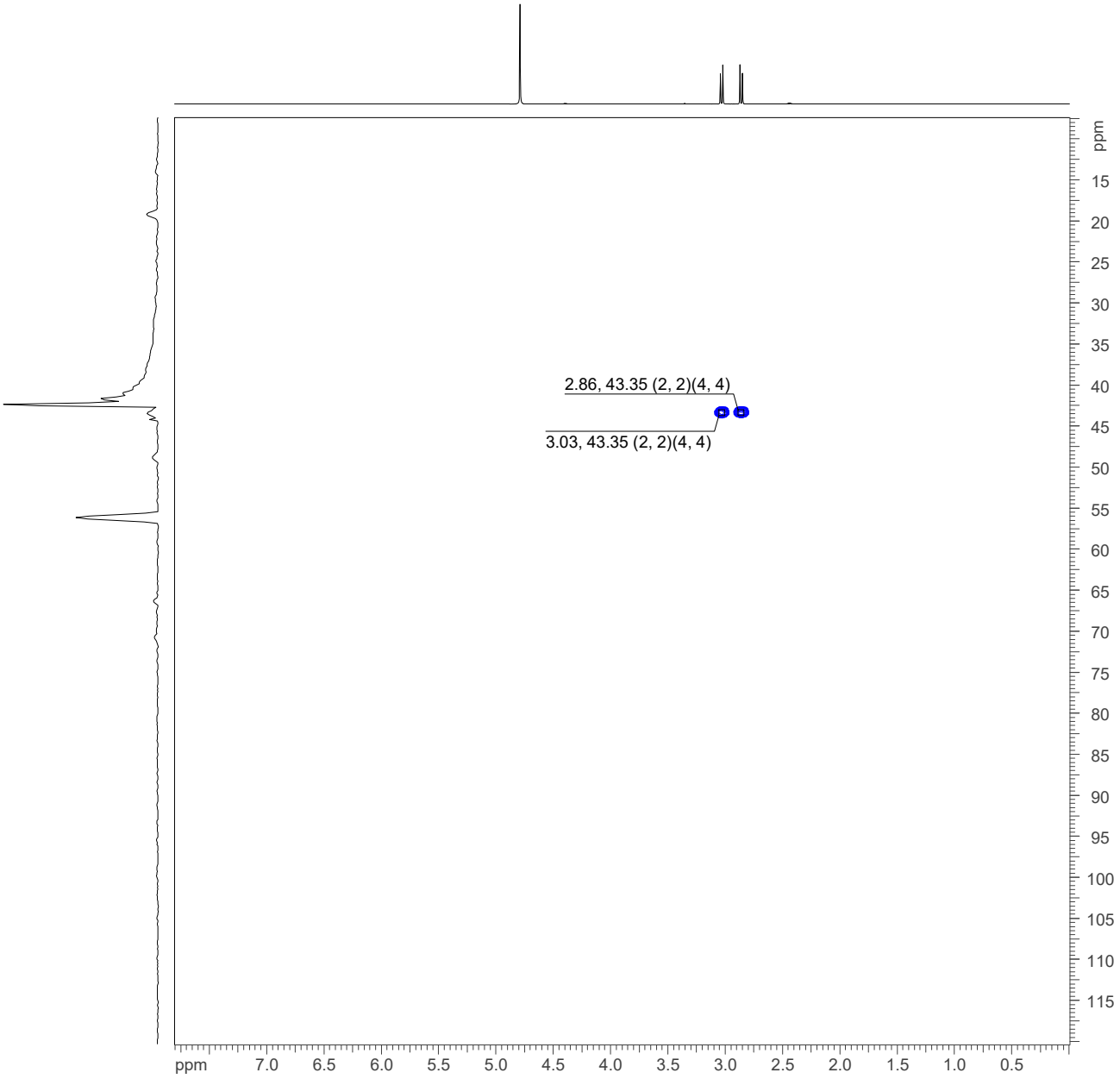

Figure S 9. HSQC spectra of the active HPLC fraction F7. Two-dimensional ^{1}H–^{13}C HSQC spectrum of the compound isolated from HPLC fraction F7 in D_2O at 298 K (700/176 MHz). NMR analyses were performed by Hedda Schrey and her team at the Helmholtz Centre for Infection Research (Braunschweig, Germany).

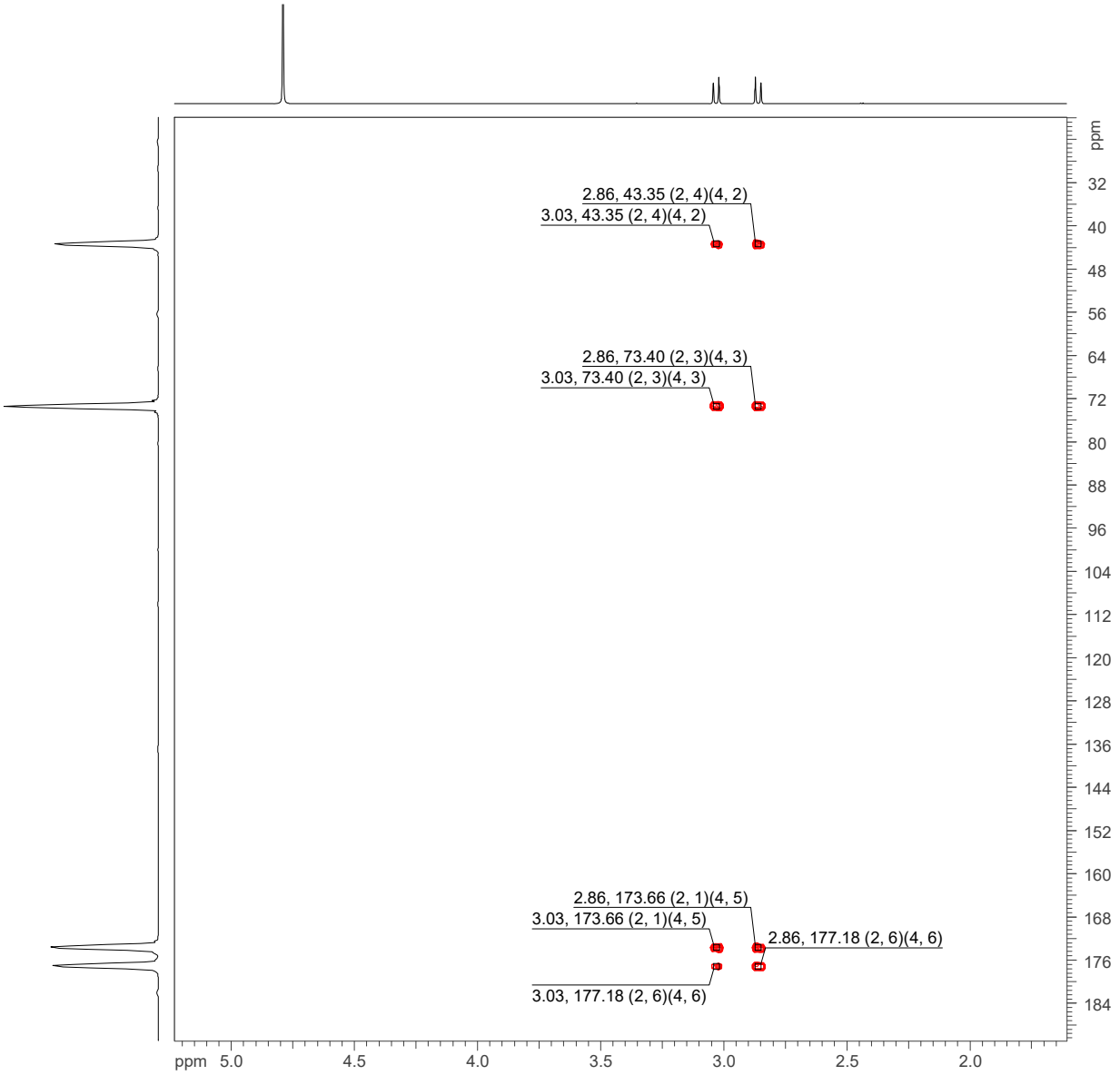

Figure S 10. HMBC spectra of the active HPLC fraction F7. Two-dimensional ^{1}H–^{13}C HMBC spectrum of the compound isolated from HPLC fraction F7, showing long-range heteronuclear correlations between hydrogen and carbon nuclei. NMR analyses were performed by Hedda Schrey and her team at the Helmholtz Centre for Infection Research (Braunschweig, Germany).

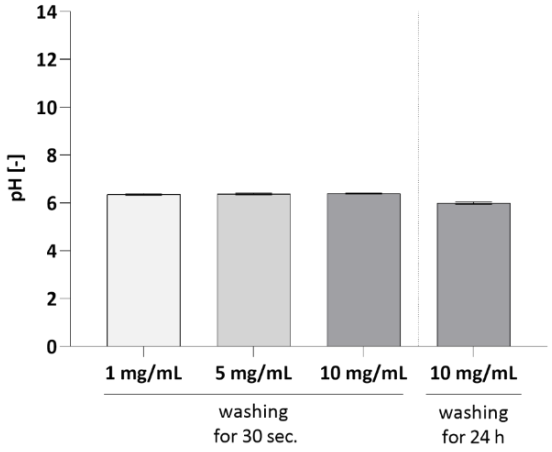

Figure S 11. pH range of *P. pachyrhizi* wash water. *P. pachyrhizi* (isolate br05) uredospores were washed with ddH_2O. The spore density varied from 1-10 mg/mL as indicated. To wash the spores, the spore suspension was incubated rotating for either 30 seconds or 24 hours, as indicated. The pH of the respective supernatant was measured. Bars represent the mean, while error bars indicate the range of two independent replicates.

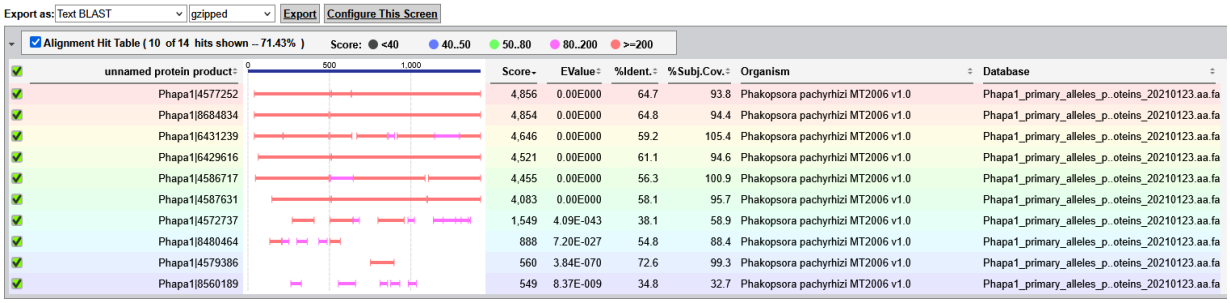
Export as: Text BLAST gzipped Export Configure This Screen

Alignment Hit Table (10 of 14 hits shown -- 71.43%) Score: <40 40..50 50..80 80..200 >=200

unnamed protein product	Score	EValue	%Ident.	%Subj.Cov.	Organism	Database
Phapa1|4577252	4,856	0.00E000	64.7	93.8	Phakopsora pachyrhizi MT2006 v1.0	Phapa1_primary_alleles_p..oteins_20210123.aa.fa
Phapa1|8684834	4,854	0.00E000	64.8	94.4	Phakopsora pachyrhizi MT2006 v1.0	Phapa1_primary_alleles_p..oteins_20210123.aa.fa
Phapa1|6431239	4,646	0.00E000	59.2	105.4	Phakopsora pachyrhizi MT2006 v1.0	Phapa1_primary_alleles_p..oteins_20210123.aa.fa
Phapa1|6429616	4,521	0.00E000	61.1	94.6	Phakopsora pachyrhizi MT2006 v1.0	Phapa1_primary_alleles_p..oteins_20210123.aa.fa
Phapa1|4586717	4,455	0.00E000	56.3	100.9	Phakopsora pachyrhizi MT2006 v1.0	Phapa1_primary_alleles_p..oteins_20210123.aa.fa
Phapa1|4587631	4,083	0.00E000	58.1	95.7	Phakopsora pachyrhizi MT2006 v1.0	Phapa1_primary_alleles_p..oteins_20210123.aa.fa
Phapa1|4572737	1,549	4.09E-043	38.1	58.9	Phakopsora pachyrhizi MT2006 v1.0	Phapa1_primary_alleles_p..oteins_20210123.aa.fa
Phapa1|8480464	888	7.20E-027	54.8	88.4	Phakopsora pachyrhizi MT2006 v1.0	Phapa1_primary_alleles_p..oteins_20210123.aa.fa
Phapa1|4579386	560	3.84E-070	72.6	99.3	Phakopsora pachyrhizi MT2006 v1.0	Phapa1_primary_alleles_p..oteins_20210123.aa.fa
Phapa1|8560189	549	8.37E-009	34.8	32.7	Phakopsora pachyrhizi MT2006 v1.0	Phapa1_primary_alleles_p..oteins_20210123.aa.fa

Figure S 12. Identification of *P. pachyrhizi* ABC transporters homologous to PstABCG2. Protein–protein BLAST using the PstABCG2 protein sequence (XM_047943360.1) as query against the predicted proteome of *P. pachyrhizi* from the genome published by Gupta et al. (2023) on the JGI MycoCosm portal (https://mycocosm.jgi.doe.gov).

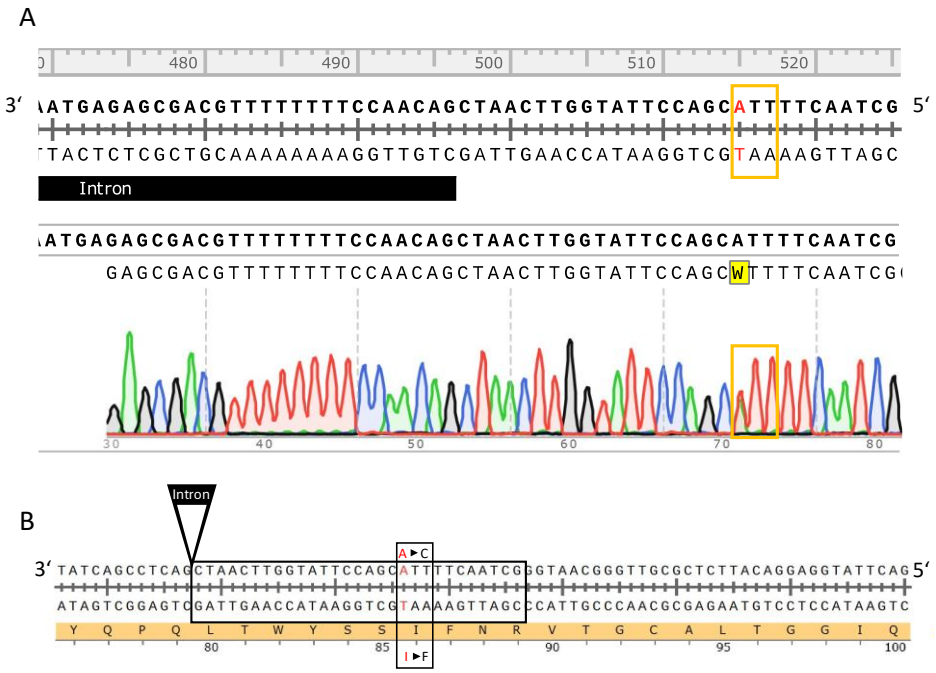

Figure S 13. Sequence alignment of *SDHc* from DNA of RS2 isolate compared to reference. (**A**) Sanger sequencing was performed on *P. pachyrhizi* gDNA of isolate RS2 with primers listed in Table S 6. In the sequencing chromatogram A, C, G, and T are shown in green, blue, black, and red, respectively. W indicates an ambiguous base call (A or T) at this position. Sequence was aligned with the reference *SDHc* sequence according to the *P. pachyrhizi* genome that was published by Gupta et al. (2023). (**B**) AA sequence (beige) that is encoded by the sequenced DNA shown in panel A (horizontal black box). The vertical black box marks the codon encoding isoleucine (I) at position 86 in the reference sequence. An A -> C SNP at this position changes the codon so that it encodes phenylalanine (F). The alignment was done with SnapGene®.

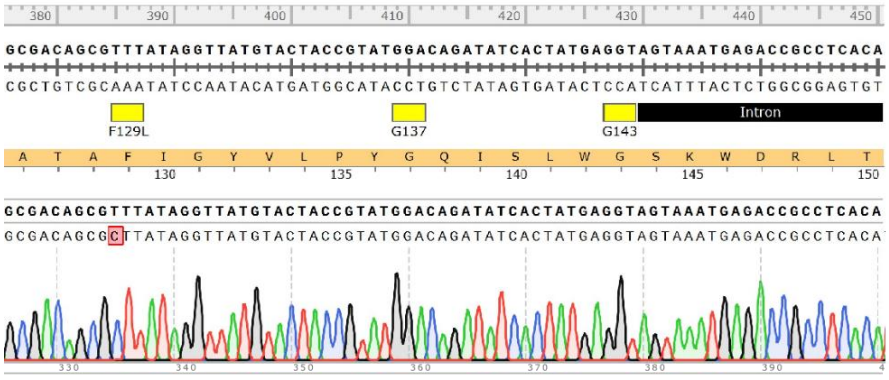

Figure S 14. Sequence alignment of *CYTb* from DNA of RS2 isolate compared to reference. Sanger sequencing was performed on *P. pachyrhizi* gDNA of isolate RS2 with primers listed in Table S 6. In the sequencing chromatogram A, C, G, and T are shown in green, blue, black, and red, respectively. Sequence was aligned with the reference *CYTb* sequence according to the *P. pachyrhizi* genome that was published by Gupta et al. (2023). The AA sequence is shown in beige. Yellow boxes mark codons that, when mutated, are described to confer QoI resistance in *P. pachyrhizi*. Note that the sequence of RS2 shows a T -> C SNP at the codon position that encodes phenylalanine at position 129 in the reference sequence, resulting in a codon encoding leucine (L) at this position in RS2. Experiments were performed by Alina Maas (master thesis within the scope of this work).

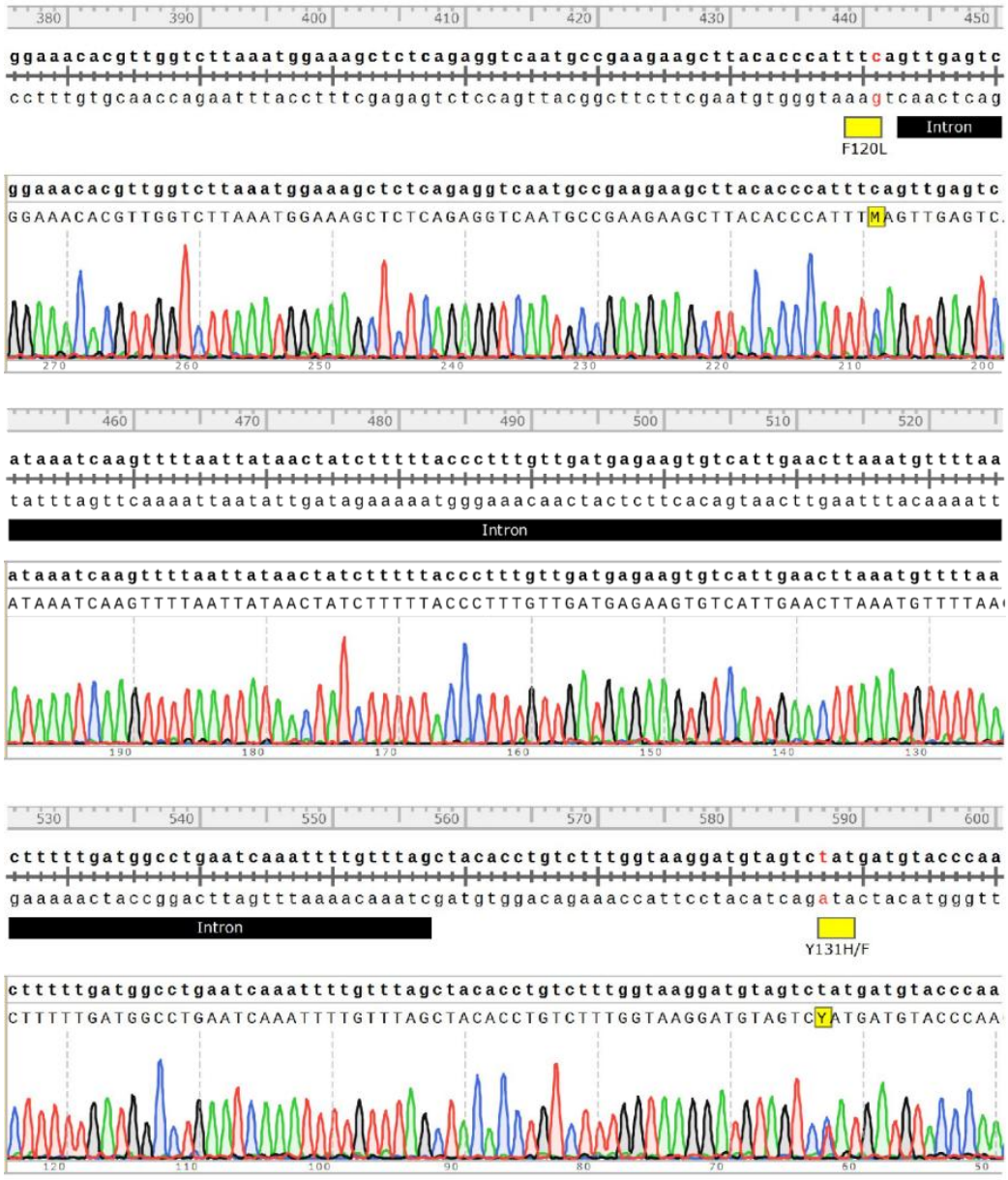

Figure S 15. Sequence alignment of *CYP51* from DNA of RS2 isolate compared to reference. Sanger sequencing was performed on *P. pachyrhizi* gDNA of isolate RS2 with primers listed in Table S 6. In the sequencing chromatogram A, C, G, and T are shown in green, blue, black, and red, respectively. M and Y indicate an ambiguous base calls (M = A or C; Y = C or T) at this position.Sequence was aligned with the reference *CYP51* sequence according to the *P. pachyrhizi* genome that was published by Gupta et al. (2023). Yellow boxes mark codons that, when mutated, are described to confer DMI resistance in *P. pachyrhizi*. Experiments were performed by Alina Maas (master thesis within the scope of this work).

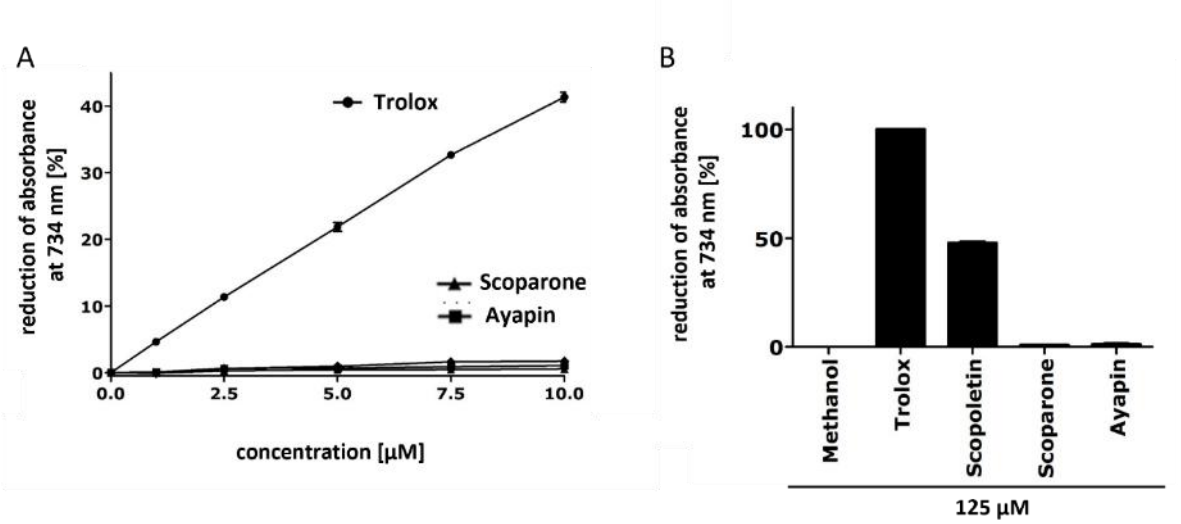

Figure S 16. Antioxidative capacity of scopoletin, ayapin and scoparone. Trolox served as a positive control and methanol as a negative control. The reduction in absorption was measured as a function of concentration. (A) Measurements were taken for trolox, scoparone and ayapin in a concentration range from 0 µM to 10 µM. (B) shows the reduction in absorption using 125 µM of Trolox, scopoletin, scoparone or ayapin. The dots/bars show the mean ± SEM of the measured absorption reduction [%] of an experiment with three technical replicates. Experiments were performed by Verena Wanders during her master thesis, the figure is adapted from her thesis (Wanders, 2019).

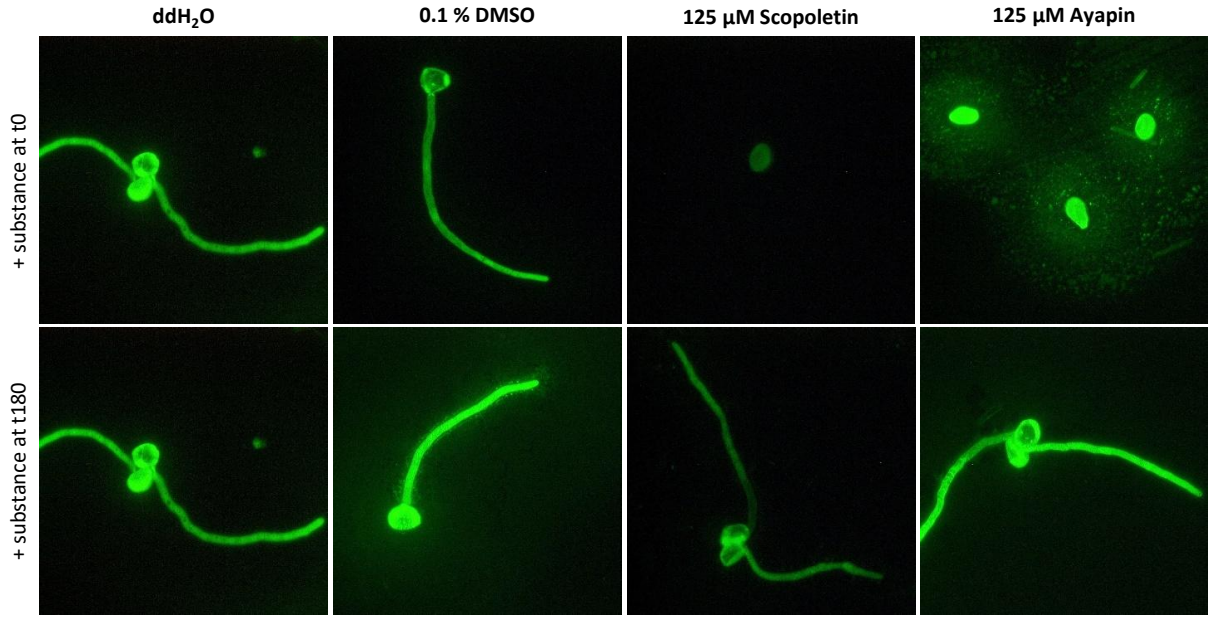

Figure S 17. ROS staining of treated *P. pachyrhizi* uredospores. 1 mg/ml *P. pachyrhizi* uredospores were suspended in 0.01 % Tween 20 ddH_2O and incubated for 4 h with rotation in a reaction vessel at RT. The spores were mixed with substances as indicated. After a total of 240 min, 180 µL of the spore suspension was removed and supplemented with H_2DCFDA to a final concentration of 2.5 mg/mL and incubated for 30 min. ROS accumulation was analyzed by monitoring the fluorescence intensity upon H_2DCFDA staining in a confocal laser scanning microscope (488 nm excitation and 500–550 nm emission). The scale bar corresponds to 50 µm. Representative images from one experiment are shown. Experiments were performed by Verena Wanders during her master thesis, the figure is adapted from her thesis (Wanders, 2019).

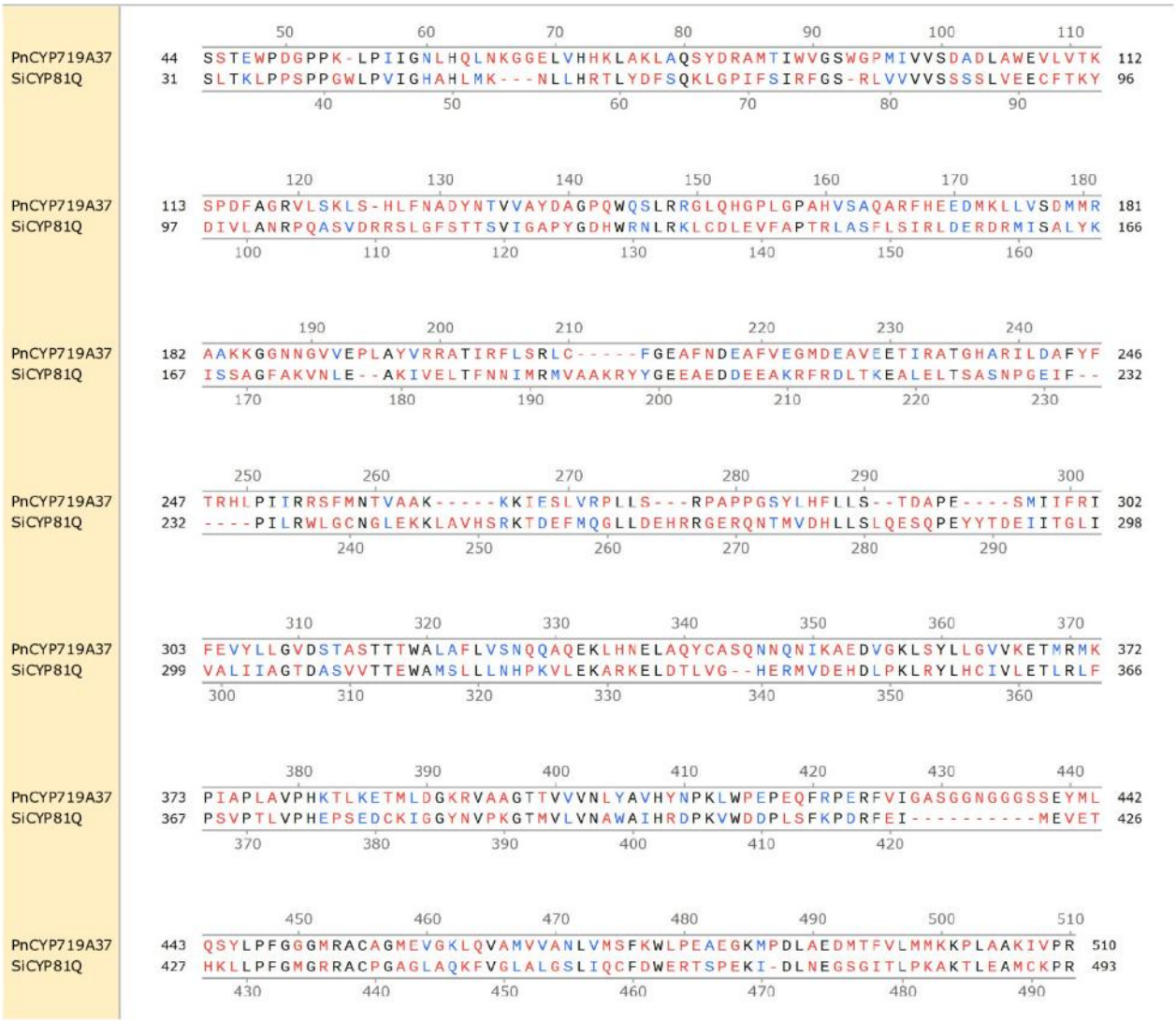

Figure S 18. Protein sequence alignment of CYP719A37 from *Piper nigrum* and CYP81Q from *Sesamum indicum.* The local alignment was done with SnapGene according to the Smith-Waterman algorithm. Identical AA are marked black, chemical similar AA are marked blue, different AA are marked red. The sequence identity was 25.61 %, the similarity was 43.03 % Both sequences were downloaded from **www.uniprot.org**.

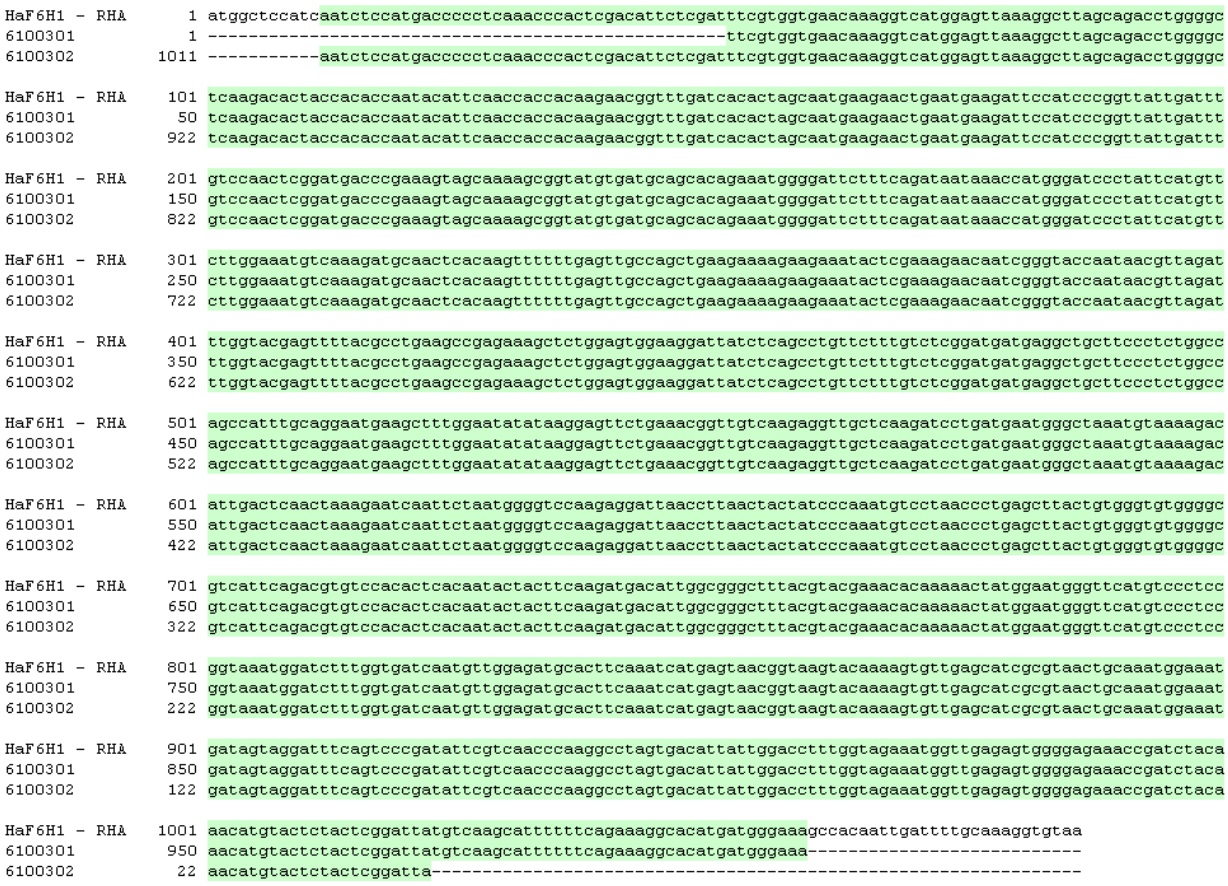

Figure S 19. The coding sequence of HaF6′H1 is identical in sunflower genotypes RHA857-ML and M-4/626. Sanger sequencing was performed on cDNA synthesized from RNA isolated from $CuCl_2$-induced leaf tissue of the sunflower mutant M-4/626. Primers used for sequencing are listed in Table S7. The numbers 6100301 and 6100302 denote sequencing runs with forward and reverse primers of the HaF6′H1 coding sequence, respectively. The resulting sequences were globally aligned to the HaF6′H1 coding sequence of RHA857-ML. Alignment was done with CloneManager. Experiments were performed by Alina Kruse (master thesis within the scope of this work).

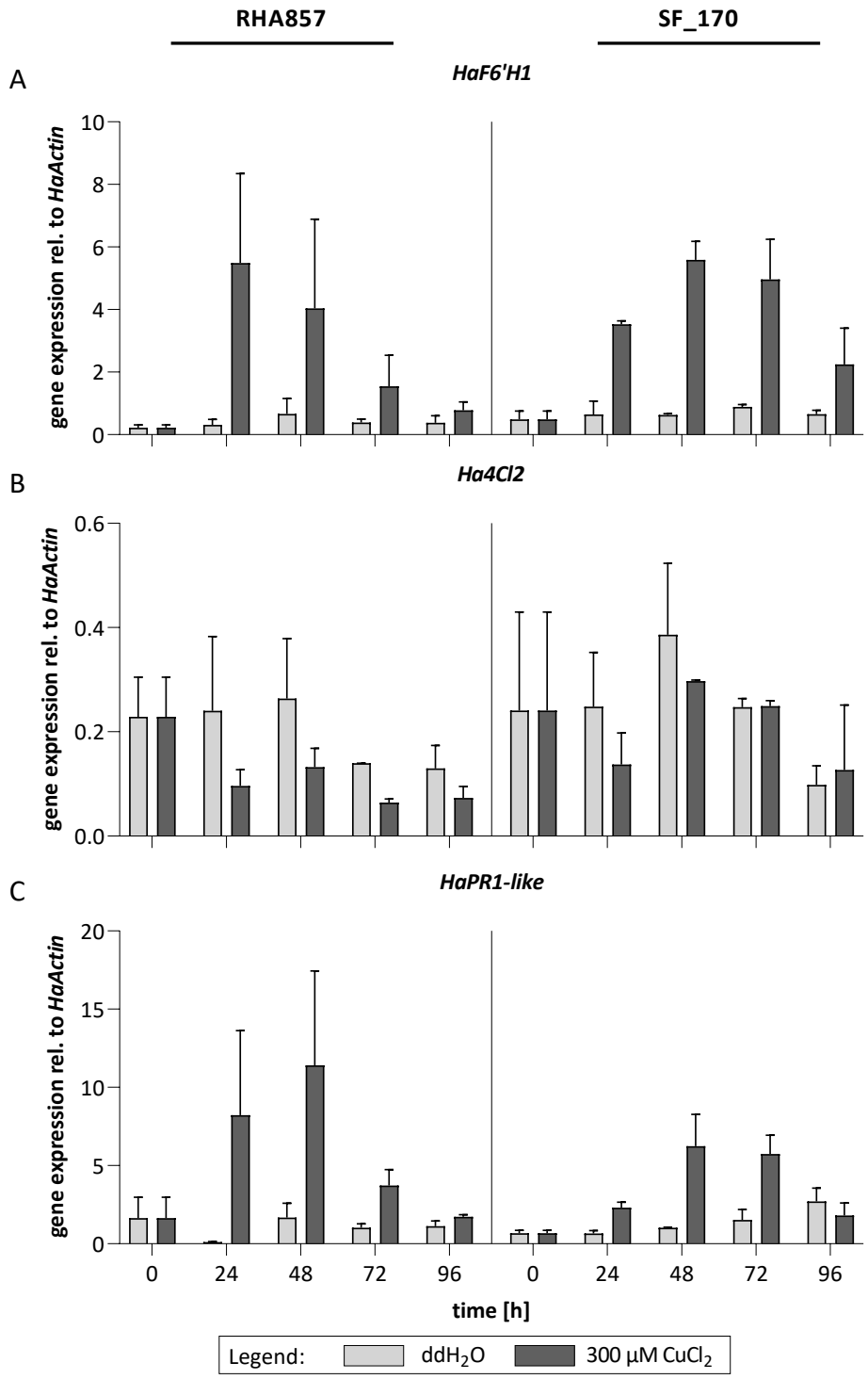

Figure S 20. Relative gene expression of *HaF6H1* and *HaPR1-like* in sunflower genotypes RHA857 and SF170. Sunflower leaf disks of the genotypes RHA857 (left) or SF_170 (right) were incubated on ddH_2O or 300 µM $CuCl_2$ solution for the indicated time. Gene expression of *HaF6'H1* (A), *Ha4Cl2* (B) and *HaPR1-like* (C) was evaluated via qRT-PCR relative to the reference gene *HaActin*. Error bars indicate range of two biological replicates. Experiments were performed by Alina Maas (master thesis within the scope of this work).

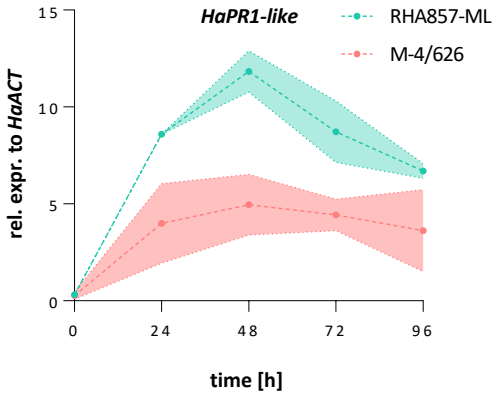

Figure S 21. Relative expression of HaPR1-like in $CuCl_2$-elictated RHA857-ML and M-4/626. Leaf discs of four-week-old M-4/626 mutant (red) or maternal plants (green) were incubated floating on 300 µM $CuCl_2$ for 96 h in a petri dish. Leaf discs were harvested to indicated time points to isolate RNA which was reverse transcribed to cDNA to perform qRT-PCR analysis. The gene expression of *HaPR1-like* was analyzed relative to the expression of *HaACT*. Shades represent the range of two biological replicates for RHA857-ML and the standard deviation of four biological replicates for M-4/626. Experiments performed by Alina Kruse (bachelor thesis within the scope of this work).

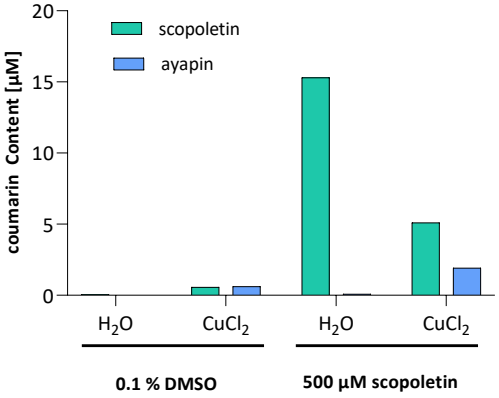

Figure S 22. Simultaneous treatment of sunflower genotype SF_170 with scopoletin and $CuCl_2$. Leaf discs of the sunflower genotype SF_170 were incubated floating on either 0.1 % DMSO or a 500 µM scopoletin solution that contained 0.1 % DMSO. Additionally, ddH_2O-droplets (as control) or $CuCl_2$-droplets (to induce coumarin biosynthesis) were placed adaxially on the leave surface. After incubation of 24 h, droplets were recollected, pooled per treatment and the scopoletin (green) and ayapin (blue) content was measured via HPLC. Bars show the coumarin content of one biological replicate.

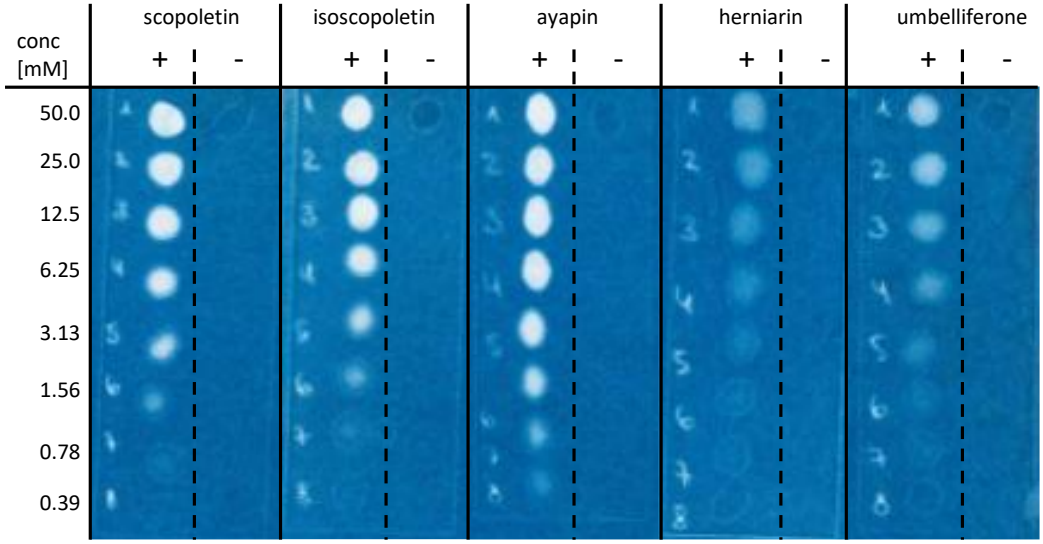

Figure S 23. A blueprint reveals photoprotective effect of coumarins. 20 µL of scopoletin, isoscopoletin, ayapin, herniarin or umbelliferone were placed on a glass slide in indicated concentrations (+). Since the 50 mM solution of each coumarin contained 0.1 % DMSO, 0.1 % DMSO served as negative control (-). Glas slides were placed on commercial solar-sensitive paper and incubated with UV-light for 120 s. Irradiation with UV light induces a photochemical reduction of Fe^{3+} to Fe^{2+}, and the resulting Fe^{2+}-species forms a water-insoluble complex. In the non-exposed areas of the paper, a water-soluble iron compound remains that is subsequently removed during rinsing with water. Note, that in this so-called "blueprint" the areas of the paper that were irradiated by UV rays stayed dark blue, while protected areas turned white.

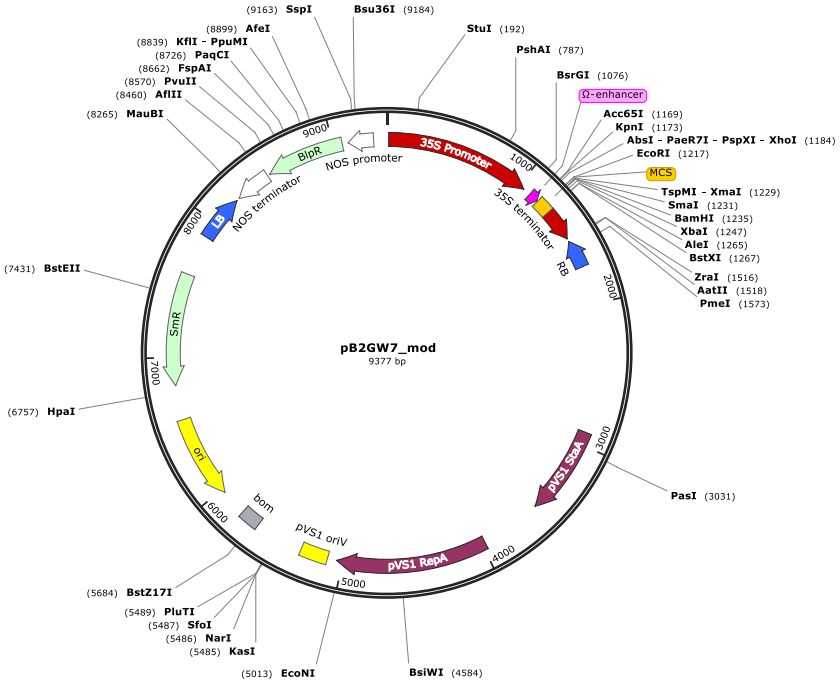

Figure S 24. Vector map of a modified pB2GW7 vector used for overexpression constructs. The vector map was visualised using SnapGene®.

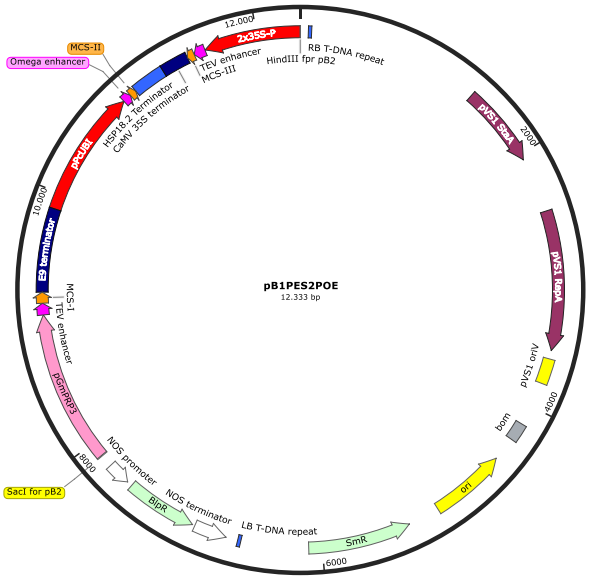

Figure S 25. Vector map of the pB1PES2POE vector used to generate soybean transformation constructs. The vector was designed during this work and synthesized by GeneArt® ThermoFisher, Germany. The vector map was visualised using SnapGene®.

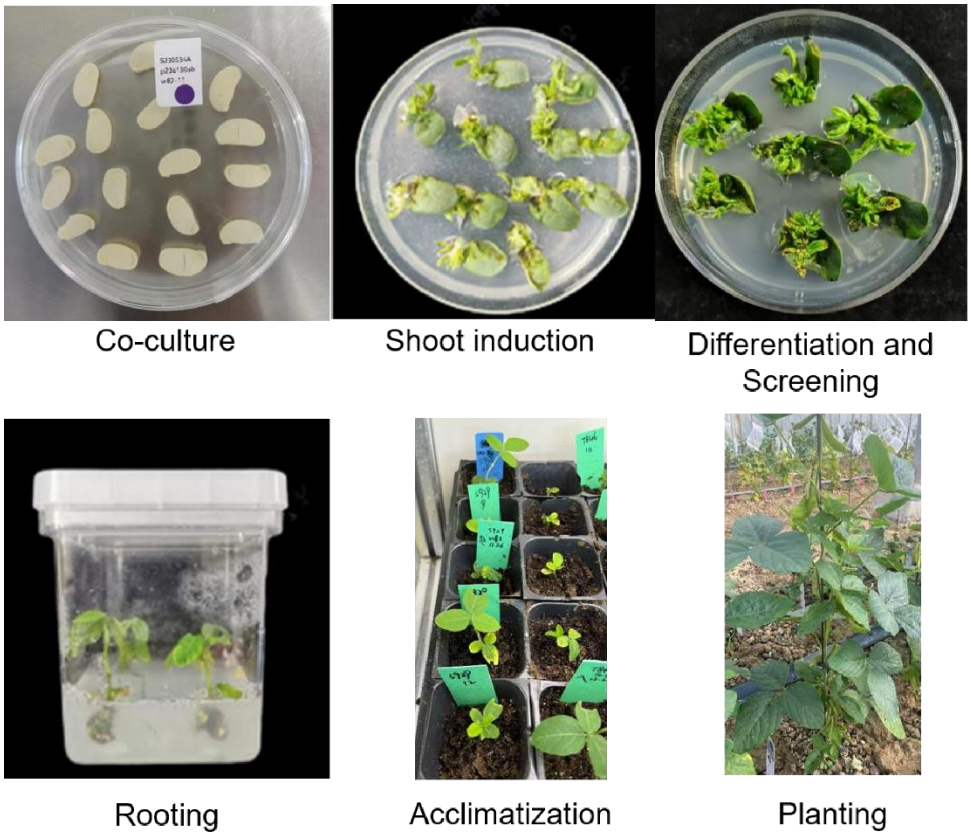

Figure S 26. Soybean transformation process A graphic overview of the *A. tumefaciens*- mediated soybean transformation process. The graphic was provided by Lifeasible® in course of the company's project report.

8.2. Supplemental Tables

Table S 1. Coumarin profile of $CuCl_2$-elucidated sunflower genotypes. A subset (196 genotypes) of a sunflower core collection (growth stage V-6 to V-10) was sampled in a field trial conducted at the agricultural experimental station Eckartsweier in Willstätt, Germany. Three leaf discs per plant were floated on 300 µM $CuCl_2$ solution (200 µL per well) to elicit coumarin accumulation. Incubation time was approx. 48 h. Coumarin content was analyzed by HPLC. The standard deviation of 3 plants per genotype is shown (+/-). Continued on the following page.

Pedigree	Scopoletin [µM]			Ayapin [µM]			Pedigree	Scopoletin [µM]			Ayapin [µM]		
1972R	0.328	+/-	0.345	0.000	+/-	0.000	HA458	0.011	+/-	0.015	0.325	+/-	0.460
ARG1575-2	0.066	+/-	0.093	0.197	+/-	0.144	HA465	0.085	+/-	0.065	0.235	+/-	0.169
Armavirec	0.294	+/-	0.213	0.876	+/-	1.039	HA466	0.120	+/-	0.095	0.038	+/-	0.053
BE96-009	0.198	+/-	0.029	0.046	+/-	0.065	HA467	1.313	+/-	1.168	0.000	+/-	0.000
BRS-1	0.130	+/-	0.093	0.000	+/-	0.000	HA481	0.105	+/-	0.097	0.022	+/-	0.031
BRS-3	0.345	+/-	0.293	0.000	+/-	0.000	HA61	0.522	+/-	0.548	0.349	+/-	0.162
CM447	0.219	+/-	0.169	0.000	+/-	0.000	HA851	0.653	+/-	0.513	1.068	+/-	1.284
DM-3	0.097	+/-	0.138	0.165	+/-	0.077	HA852	0.694	+/-	0.672	1.824	+/-	2.580
Guayacan	0.308	+/-	0.199	0.041	+/-	0.058	HA89	0.059	+/-	0.083	0.273	+/-	0.242
H52B	0.022	+/-	0.031	0.000	+/-	0.000	HA-BSR2	0.238	+/-	0.174	0.203	+/-	0.187
HA germ. pool II	0.250	+/-	0.245	0.276	+/-	0.390	HA-BSR3	0.280	+/-	0.280	0.106	+/-	0.106
HA germ. pool III-A	0.257	+/-	0.192	0.000	+/-	0.000	HA-BSR4	0.010	+/-	0.014	0.166	+/-	0.235
HA germ. pool III-C	0.156	+/-	0.098	0.028	+/-	0.040	HA-BSR5	0.192	+/-	0.114	0.000	+/-	0.000
HA germ. pool III-D	0.000	+/-	0.000	0.061	+/-	0.087	HA-BSR6	0.049	+/-	0.022	0.349	+/-	0.248
HA germ. pool III-E	3.674	+/-	4.410	0.615	+/-	0.729	HA-BSR8	0.000	+/-	0.000	0.423	+/-	0.225
HA germ. pool III-G	0.413	+/-	0.250	0.000	+/-	0.000	HAGPP V-2	0.114	+/-	0.023	0.026	+/-	0.037
HA germ. pool III-J	0.625	+/-	0.460	0.000	+/-	0.000	HA-R2	0.432	+/-	0.319	0.000	+/-	0.000
HA germ. pool III-N	0.081	+/-	0.057	0.000	+/-	0.000	HA-R3	0.044	+/-	0.032	0.047	+/-	0.067
HA germ. pool III-R	0.469	+/-	0.412	0.089	+/-	0.066	HA-R4	0.000	+/-	0.000	0.000	+/-	0.000
HA germ. pool V-1I	0.162	+/-	0.067	0.000	+/-	0.000	HA-R5	0.092	+/-	0.130	0.000	+/-	0.000
HA germ. pool VII	0.624	+/-	0.311	0.108	+/-	0.152	HA-R7	0.494	+/-	0.407	0.036	+/-	0.051
HA germ. pool VII S6	1.201	+/-	0.990	0.030	+/-	0.043	HA-R8	2.068	+/-	1.044	0.000	+/-	0.000
HA1	0.162	+/-	0.230	0.165	+/-	0.130	Hemus	0.468	+/-	0.206	0.252	+/-	0.071
HA133	0.540	+/-	0.059	0.000	+/-	0.000	HIR1734-2	0.083	+/-	0.068	0.000	+/-	0.000
HA208	0.835	+/-	0.572	0.282	+/-	0.336	IMISUN-2	0.045	+/-	0.038	0.000	+/-	0.000
HA234	0.262	+/-	0.156	0.243	+/-	0.344	IMISUN-3	0.102	+/-	0.060	0.000	+/-	0.000
HA246	0.092	+/-	0.077	0.077	+/-	0.058	IMISUN-4	0.372	+/-	0.140	0.000	+/-	0.000
HA250	0.114	+/-	0.100	0.000	+/-	0.000	Jumbo	0.264	+/-	0.207	0.157	+/-	0.223
HA289	0.017	+/-	0.024	0.000	+/-	0.000	KHC14611	0.266	+/-	0.089	0.198	+/-	0.121
HA290	0.053	+/-	0.043	0.000	+/-	0.000	Mammoth	0.581	+/-	0.619	0.328	+/-	0.369
HA315	0.370	+/-	0.255	0.294	+/-	0.291	Manchurian	0.408	+/-	0.428	0.018	+/-	0.026
HA341	0.220	+/-	0.124	0.000	+/-	0.000	NDBLOS	0.065	+/-	0.071	0.000	+/-	0.000
HA369	0.192	+/-	0.121	0.124	+/-	0.126	ND-BLOS	0.476	+/-	0.207	0.000	+/-	0.000
HA372	0.070	+/-	0.028	0.136	+/-	0.119	ND-LBLYS	1.420	+/-	0.069	0.000	+/-	0.000
HA379	0.171	+/-	0.046	0.022	+/-	0.031	ND-LRLYS	0.000	+/-	0.000	0.000	+/-	0.000
HA382	0.054	+/-	0.039	0.188	+/-	0.190	ND-RL0S	0.085	+/-	0.067	0.000	+/-	0.000
HA384	0.029	+/-	0.022	0.101	+/-	0.144	PEREDOVIK304	0.663	+/-	0.587	0.020	+/-	0.029
HA393	0.000	+/-	0.000	0.021	+/-	0.030	R-188	0.042	+/-	0.018	0.000	+/-	0.000
HA403	0.098	+/-	0.139	0.000	+/-	0.000	R-207	0.158	+/-	0.208	0.026	+/-	0.037
HA404	0.150	+/-	0.178	0.368	+/-	0.256	RE320	0.734	+/-	0.265	0.047	+/-	0.067
HA405	0.470	+/-	0.239	0.152	+/-	0.060	RF98-020	0.132	+/-	0.187	0.039	+/-	0.029
HA412HO	0.079	+/-	0.111	0.000	+/-	0.000	RG97-025	0.053	+/-	0.076	0.000	+/-	0.000
HA422	0.120	+/-	0.085	0.109	+/-	0.154	RHA265	0.108	+/-	0.078	0.000	+/-	0.000
HA430	0.143	+/-	0.127	0.033	+/-	0.047	RHA274	0.211	+/-	0.127	0.000	+/-	0.000
HA432	0.044	+/-	0.062	0.000	+/-	0.000	RHA279	0.899	+/-	0.160	0.000	+/-	0.000
HA433	0.427	+/-	0.547	0.076	+/-	0.108	RHA280	1.134	+/-	0.252	0.000	+/-	0.000
HA442	0.100	+/-	0.142	0.000	+/-	0.000	RHA298	0.217	+/-	0.121	0.000	+/-	0.000
HA445	0.226	+/-	0.153	0.240	+/-	0.223	RHA299	0.240	+/-	0.080	0.000	+/-	0.000
HA451	0.159	+/-	0.061	0.000	+/-	0.000	RHA311	0.142	+/-	0.075	0.166	+/-	0.234
HA452	0.142	+/-	0.080	0.181	+/-	0.256	RHA324	0.940	+/-	0.940	0.460	+/-	0.460

Pedigree	Scopoletin [µM]			Ayapin [µM]			Pedigree	Scopoletin [µM]			Ayapin [µM]		
RHA325	0.119	+/-	0.133	0.181	+/-	0.256	SF_212	0.088	+/-	0.124	0.000	+/-	0.000
RHA328	0.353	+/-	0.126	0.000	+/-	0.000	SF_214	0.021	+/-	0.030	0.000	+/-	0.000
RHA329	0.063	+/-	0.023	0.000	+/-	0.000	SF_221	0.282	+/-	0.368	0.000	+/-	0.000
RHA331	0.671	+/-	0.638	0.000	+/-	0.000	SF_230	0.094	+/-	0.133	0.033	+/-	0.047
RHA332	1.949	+/-	1.517	0.000	+/-	0.000	SF_234	2.363	+/-	0.974	0.000	+/-	0.000
RHA334	0.170	+/-	0.126	0.000	+/-	0.000	SF_25	0.564	+/-	0.754	0.000	+/-	0.000
RHA355	0.304	+/-	0.337	0.054	+/-	0.076	SF_263	0.440	+/-	0.247	0.000	+/-	0.000
RHA358	0.224	+/-	0.128	0.000	+/-	0.000	SF_28	0.629	+/-	0.463	0.000	+/-	0.000
RHA363	0.148	+/-	0.069	0.000	+/-	0.000	SF_281	0.084	+/-	0.084	0.000	+/-	0.000
RHA364	0.072	+/-	0.102	0.000	+/-	0.000	SF_293	3.388	+/-	1.781	0.385	+/-	0.365
RHA376	0.789	+/-	0.415	0.000	+/-	0.000	SF_295	0.061	+/-	0.086	0.068	+/-	0.096
RHA386	0.158	+/-	0.129	0.000	+/-	0.000	SF_296	0.833	+/-	0.700	0.110	+/-	0.155
RHA397	1.714	+/-	1.939	0.000	+/-	0.000	SF_306	0.056	+/-	0.064	0.000	+/-	0.000
RHA399	0.099	+/-	0.140	0.000	+/-	0.000	SF_307	2.981	+/-	2.302	0.222	+/-	0.314
RHA400	0.296	+/-	0.284	0.000	+/-	0.000	SF_308	0.026	+/-	0.037	0.000	+/-	0.000
RHA401	6.017	+/-	2.904	0.000	+/-	0.000	SF_310	0.595	+/-	0.466	0.612	+/-	0.627
RHA408	0.032	+/-	0.045	0.000	+/-	0.000	SF_315	0.168	+/-	0.126	0.000	+/-	0.000
RHA418	0.404	+/-	0.086	0.016	+/-	0.023	SF_317	0.524	+/-	0.499	1.380	+/-	0.976
RHA419	0.126	+/-	0.052	0.000	+/-	0.000	SF_320	1.411	+/-	0.522	0.613	+/-	0.169
RHA426	0.000	+/-	0.000	0.000	+/-	0.000	SF_322	0.065	+/-	0.046	0.000	+/-	0.000
RHA428	0.387	+/-	0.422	0.000	+/-	0.000	SF_332	0.066	+/-	0.093	0.000	+/-	0.000
RHA436	0.152	+/-	0.037	0.000	+/-	0.000	SF_334	0.108	+/-	0.076	0.000	+/-	0.000
RHA437	0.038	+/-	0.053	0.000	+/-	0.000	SF_56	0.126	+/-	0.144	0.037	+/-	0.052
RHA443	0.459	+/-	0.487	0.000	+/-	0.000	SF_63	0.965	+/-	0.808	0.000	+/-	0.000
RHA447	0.497	+/-	0.661	0.023	+/-	0.033	SF_70	0.129	+/-	0.149	0.232	+/-	0.171
RHA454	1.104	+/-	0.508	0.083	+/-	0.117	SF_74	0.155	+/-	0.040	0.000	+/-	0.000
RHA461	0.148	+/-	0.107	0.016	+/-	0.023	SF_75	0.281	+/-	0.210	0.163	+/-	0.231
RHA462	0.259	+/-	0.105	0.000	+/-	0.000	SF_80	0.146	+/-	0.207	0.000	+/-	0.000
RHA463	1.895	+/-	2.424	1.488	+/-	1.791	SF_85	0.000	+/-	0.000	0.031	+/-	0.044
RHA464	0.033	+/-	0.046	0.000	+/-	0.000	SF_92	0.262	+/-	0.158	0.000	+/-	0.000
RHA468	0.557	+/-	0.212	0.000	+/-	0.000	SF_95	0.273	+/-	0.193	0.000	+/-	0.000
RHA479	1.139	+/-	0.362	0.255	+/-	0.283	Sputnik	0.010	+/-	0.014	0.000	+/-	0.000
RHA480	0.312	+/-	0.168	0.229	+/-	0.106	Stepnyak	0.113	+/-	0.026	0.000	+/-	0.000
RHA854	0.942	+/-	0.656	0.536	+/-	0.759	SUN48-0003	0.604	+/-	0.333	0.498	+/-	0.353
RHA855	0.165	+/-	0.145	0.000	+/-	0.000	SUN48-0036	0.177	+/-	0.151	0.202	+/-	0.285
RHA857	0.029	+/-	0.040	0.000	+/-	0.000	SUN48-0037	0.041	+/-	0.004	0.000	+/-	0.000
RHA858	0.799	+/-	0.544	0.000	+/-	0.000	SUN48-0038	0.000	+/-	0.000	0.000	+/-	0.000
RHA859	0.195	+/-	0.138	0.000	+/-	0.000	SUN48-0050	0.176	+/-	0.109	0.000	+/-	0.000
SF_19	0.015	+/-	0.021	0.000	+/-	0.000	Sundak	0.053	+/-	0.038	0.000	+/-	0.000
SF_105	1.385	+/-	0.794	0.154	+/-	0.109	USSR-VNIIMK-8931	0.095	+/-	0.134	0.166	+/-	0.234
SF_107	0.013	+/-	0.019	0.000	+/-	0.000	VK-47	0.094	+/-	0.118	0.031	+/-	0.044
SF_110	0.011	+/-	0.016	0.000	+/-	0.000	RHA479	1.139	+/-	0.362	0.255	+/-	0.283
SF_12	0.034	+/-	0.003	0.000	+/-	0.000	HA-BSR3	0.280	+/-	0.280	0.106	+/-	0.106
SF_130	0.178	+/-	0.060	0.000	+/-	0.000	NDBLOS	0.065	+/-	0.071	0.000	+/-	0.000
SF_137	0.216	+/-	0.123	0.031	+/-	0.044	SF_12	0.034	+/-	0.003	0.000	+/-	0.000
SF_142	0.050	+/-	0.071	0.000	+/-	0.000	BE96-009	0.198	+/-	0.029	0.046	+/-	0.065
SF_152	0.363	+/-	0.085	0.000	+/-	0.000							
SF_170	0.017	+/-	0.024	0.623	+/-	0.745							
SF_175	0.140	+/-	0.069	0.098	+/-	0.071							
SF_179	0.000	+/-	0.000	0.046	+/-	0.066							

Table S 2. Dry-weight of fractions of *P. pachyrhizi* spore wash water. 758 mg *P. pachyrhizi* uredospores were washed with 37,5 mL H_2O. The supernatant was lyophilized leading to 168 mg of raw extract. 40 mg of this wash water extract was analyzed via a preparative HPLC. All fractions were evaporated, weighed and resolved in 1 mL H_2O. All fractions were roughly estimated for activity against *P. pachyrhizi* germination. Fractions were classified as active (<20 % germination, green), semi-active (~20–70 %, yellow), or inactive (>70 %, comparable to the control, grey) as depicted in Figure 18.

interval [min]	tube#	weight flask empty [g]	weight flask + fractions [g]	dry-weight fraction [mg]
0-3	1-8	4.79174	4.80510	13.36
3-4	9-12	5.07735	5.10358	26.23
4-5	13-15	4.83407	4.83539	1.32
5-6	16-17	4.80387	4.80420	0.33
6-7	18-19	4.76679	4.76706	0.27
7-8	20-21	5.02918	5.02952	0.34
8-9	22-23	5.02177	5.02389	2.12
9-10	24-25	4.85599	4.85659	0.60
10-11	26-27	4.97085	4.97104	0.19
11-12	28-29	4.73141	4.73182	0.41
12-13	30-31	4.75019	4.75028	0.09
13-14	32-33	4.87280	4.87295	0.15
14-15	34-35	4.85012	4.85027	0.15
15-17	36-39	4.83805	4.83895	0.90
17-end	40-end	4.73185	4.73660	4.75

Table S 3. Number of sequenced fragments and bases (RNA). The transcriptome analysis of sunflower samples was performed by CeGaT GmbH (Germany). Sample ID is explained in Table 11.

CeGaT ID	# of fragments (in million)	# of bases (Gb)
S12033Nr1	43.447	8.763
S12033Nr2	38.799	7.825
S12033Nr3	35.209	7.101
S12033Nr4	66.104	13.333
S12033Nr5	30.939	6.240
S12033Nr6	37.212	7.505
S12033Nr7	28.557	5.760
S12033Nr8	46.633	9.406
S12033Nr9	34.303	6.917
S12033Nr10	35.463	7.153
S12033Nr11	33.541	6.758
S12033Nr12	46.475	9.369

Table S 4. Statistics of mapped fragments (RNA). The transcriptome analysis of sunflower samples was performed by CeGaT GmbH (Germany). Sample ID is explained in Table 11.

CeGaT ID	# of mapped fragments (in million)	Proportion of sequenced fragments (in %)	# of fragments used for expression quantification (in million)	Proportion of fragments used for expression quantification (in %)
S12033Nr1	40.215	92.6	36.677	91.2
S12033Nr2	36.295	93.5	32.887	90.6
S12033Nr3	32.861	93.3	30.370	92.4
S12033Nr4	57.575	87.1	52.170	90.6
S12033Nr5	27.068	87.5	24.496	90.5
S12033Nr6	32.255	86.7	29.158	90.4
S12033Nr7	25.273	88.5	22.971	90.9
S12033Nr8	43.284	92.8	38.554	89.1
S12033Nr9	32.455	94.6	29.915	92.2
S12033Nr10	31.486	88.8	28.586	90.8
S12033Nr11	29.392	87.6	27.088	92.2
S12033Nr12	39.646	85.3	36.133	91.1

Table S 5. Statistics of significantly differentially expressed genes in comparison group A vs B. The transcriptome analysis of sunflower samples was performed by CeGaT GmbH (Germany). Groups are explained in Table 11.

group A	group B	# of significant genes (p_{adj}<0.05)
group 2	group 1	6.917
group 4	group 3	7.153
group 4	group 2	6.758
group 3	group 1	9.369

Table S 6. Sequencing primers used in this work.

primer name	sequence 5'-3'	reference
PpSDHc_F	ATGATGGCCTCAACAATAGCAG	Simões et al. (2018)
PpSDHc_R	TACATTCAGTTATTACCTTCAAAAAAGTAG	
PpCYP51_CDS_F	ATGTCTTCCAGCGTTATAATCGATC	this work
PpCYP51_CDS_R	TTAATTTCTTCTAGTAAACTTCACAGTTGT	
PpCYTB_Gene_F	ATGAGAAATTTCAAGACGCATCCAA	this work
PpCYTB_Gene_R	CTAAGCTGATCATATTATGTTCTTACTACTCTCTA	
HaF6H1_Start_CDS_F	ATGGCTCCATCAATCTCCATGACC	this work
HaF6H1_End_CDS_R	TTACACCTTTGCAAAATCAATTGTGGCTTTCC	

Table S 7. qRT-PCR primers used in this work.

primer name	sequence 5'-3'	reference
NbACT_RT_F	CGAGCGGGAAATTGTTAGG	Beesley (2022)
NbACT_RT_R	ACGGATGAGCTGGTCTTTG	
AtMYB72_RT_F	TTGCTGGATTGTTGAGATGTG	Beesley (2022)
AtMYB72_RT_R	AGGGTTTGATGGTAGTGAATG	
HaActin_RT_F	GGTAACATCGTGCTCAGTGGTGG	Schwinges (2019)
HaActin_RT_R	AACCACCTTGATCTTCATGCTGC	
HaPR1-like_RT_F	GGGCGTTGGAGGAATGGTAT	this work
HaPR1-like_RT_R	CTGAGAATGCGCCAGTACCT	
HaF6'H1_RT_F	CTCCATGACCCCCTCAAACC	this work
HaF6'H1_RT_R	GTGGTAGTGTCTTGAGCCCC	
HaAySy1_RT_F	CTTGTTGAGTACAACCTCAGCTCT	this work
HaAySy1_RT_R	CGAAATGGGCTTGGTGGAAG	
HaAySy2_RT_F	AGGTCGCATGAGGATGAGGA	this work
HaAySy2_RT_R	TAGTATCAGTCCCCGCAGCA	
HaAySy3_RT_F	GGATGGGTGCGGAAATGAGA	this work
HaAySy3_RT_R	GGCAGTTAAAGCCTCGGTCA	
HaAySy4_RT_F	TTATCCCAGAAGCTCGGTGG	this work
HaAySy4_RT_R	GGCTGATGAGACCACAAGGG	
HaAySy5_RT_F	CAGCTAACCTCCAAGCCCC	this work
HaAySy5_RT_R	AGGAAGAACTTTGGGCGGTC	
HaAySy6_RT_F	TGCGATAGGTTTTCGCAGAAATTG	this work
HaAySy6_RT_R	GTGTCTGTCCCCGCTTGTAG	
HaAySy7_RT_F	TGCATGGGCTATAGGCAGAG	this work
HaAySy7_RT_R	TGTAACACGCGTTGTGCGA	
HaAySy8_RT_F	TTGGGTAGGAAGCATGGTGG	this work
HaAySy8_RT_R	GGAGGTAATCGCCAACGCTA	
HaAySy9_RT_F	TAACACATAACCCTCGCGCA	this work
HaAySy9_RT_R	GTAAGTCCAGCCTTCGGGTT	
HaAySy10_RT_F	TGCACGTAACAGAACCTCCG	this work
HaAySy10_RT_R	GGATTCCCTCCTCTTGGCTTT	
HaAySy11_RT_F	GGCTGCATTGTTATCCGCTG	this work
HaAySy11_RT_R	GTTTTCAAGCTCCTGTTGGGC	
HaAySy12_RT_F	CCATACCTGAAAGCGGTGGT	this work
HaAySy12_RT_R	GCACCCTGTGGAATCGTGTA	
HaAySy13_RT_F	CTCGATCTGGTGACTGCGTT	this work
HaAySy13_RT_R	CATCGCTATCGTCATCGGCA	
HaAySy14_RT_F	GCAGCCGGAAAAGATACCCT	this work
HaAySy14_RT_R	TCTACGGCTGGGTTTCTAGC	
HaAySy15_RT_F	CTTGGCTTGCATGGGTTGAC	this work
HaAySy15_RT_R	CGCCTTCGATTGATCCCTCA	
HaAySy16_RT_F	TGTTCTTGGAGTAGCTGTAGCA	this work
HaAySy16_RT_R	ACGGGGTACCCTTGATTCCT	
HaAySy17_RT_F	CGGTTGAAGAAGACGGAAGGA	this work
HaAySy17_RT_R	GGCAACTATGACGTCCATCAACT	
HaAySy18_RT_F	TTCTTCACCTGGTTGGGGC	this work
HaAySy18_RT_R	CCCATTGATCTCCATCAGCACT	
HaABC_RT_F	ACAACGATGGTCGTACTGGC	this work
HaABC_RT_R	GAGGCACGCTGCATACATTG	
GmNREG_RT_F	TCCTGGCTGCTAACTACTTG	Beyer (2019)
GmNREG_RT_R	GGTCTTGCGAATTTCCTCTG	

Table S 8. Primers used for Gibson Cloning.

primer name	sequence 5'-3'	destination vector
eGFP_GBSN_F	AGCAATTTAAATCATTTCTCCAAATGGTGAGCAAGGGCG	pB1PES1POE2
eGFP_GBSN_R	ATACGAACGAAAGCTGTTTCACTTGTACAGCTCGTCCAT	
HaF6H1_GBSN_F	TTACAGGGGCCCGATCCCATGGCTCCATCAATCTCCATG	pB1PES1POE2
HaF6H1_GBSN_R	CATCTTCATATTCATTACTGGTACTTACACCTTTGCAAAA TCAATTGTGG	
mRFP_GBSN_F	GCGCCTCTCGCGATTAATATGGCGATCATCAAAGAGTTT ATGAGA	pB1PES1POE2
mRFP_GBSN_R	GATTTTTGCGGACGCGATCTATTTGTATAATTCGTCCATT CCACCTG	
HaF6H1-eGFP_GBSN_F	TTACAGGGGCCCGATCCCATGGCTCCATCAATCTCCATGA CC	pB1PES1POE2
HaF6H1-eGFP_GBSN_R	CATCTTCATATTCATTACTGGTACTCACTTGTACAGCTCG TCCATG	
AtCOSY_GBSN_F	GCGCCTCTCGCGATTAATATGGCGACACTTGAAATTACC G	pB1PES1POE2
AtCOSY_GBSN_R	GATTTTTGCGGACGCGATTCAAGACAGGGCAAATTCACC TT	
HaABC_GBSN_F	AGCAATTTAAATCATTTCTCCAAATGGATGGAAGTGACA TATACAAAGC	pB1PES1POE2
HaABC_GBSN_R	ATACGAACGAAAGCTGTTCTATCTTTTCTGGAAATTGAAG GATCGAATG	
pB2HaF6H1_GBSN_F	TATTTACAATTACAATTACCGGTACATGGCTCCATCAATC TCCATGAC	pB2GW7_mod
pB2HaF6H1_GBSN_R	GCTTATCGATACCGTCGACCTTACACCTTTGCAAAATCAA TTGTGGCT	
HaAySy1_GBSN_F	CCGGTACCGGGCCCCCCCATGTCATGCATGATTAGACATT TCAACC	pB2GW7_mod
HaAySy1_GBSN_R	ACCGCGGTGGCGGCCGCTCTAATTTATTGATAATAGTGTT GGATCAAGTCGC	
HaAySy2_GBSN_F	CCGGTACCGGGCCCCCCCATGGAACTACTTTTCATGTTTC TTCTTTTGT	pB2GW7_mod
HaAySy2_GBSN_R	ACCGCGGTGGCGGCCGCTCTATGGTTTTTTGCTTGATTTT GTAGCC	
HaAySy4_GBSN_F	CCGGTACCGGGCCCCCCCATGATTCCTTTGGTGTATGTTC TTGC	pB2GW7_mod
HaAySy4_GBSN_R	ACCGCGGTGGCGGCCGCTTTAAACAGAAAATGGCTTCGC AGTAAC	
HaAySy6_GBSN_F	CCGGTACCGGGCCCCCCCATGGATGAAACTCATCTTTTCT TCATTTCT	pB2GW7_mod
HaAySy6_GBSN_R	ACCGCGGTGGCGGCCGCTTCATATTTCTTTCAGAATATGA CCCATTCTCTG	
HaAySy8_GBSN_F	CCGGTACCGGGCCCCCCCATGGTGTTTATCTTTCCCTTAT TCATTTTGT	pB2GW7_mod
HaAySy8_GBSN_R	ACCGCGGTGGCGGCCGCTTCACTTATATGGAGTTGCCAC CACT	
HaAySy10_GBSN_F	CCGGTACCGGGCCCCCCCATGGAAGTGATGAGCATGAGC	pB2GW7_mod
HaAySy10_GBSN_R	ACCGCGGTGGCGGCCGCTTCAAAGCTCACTCAAAATCAA TTGAGC	

primer name	sequence 5'-3'	destination vector
HaAySy11_GBSN_F	CCGGTACCGGGCCCCCCCATGGATTTACTTTTATTAATCATTATCTTTGTATCCAGC	pB2GW7_mod
HaAySy11_GBSN_R	ACCGCGGTGGCGGCCGCTCTATGAATATACATGTGACAGTAGTCGAGG	
HaAySy12_GBSN_F	CCGGTACCGGGCCCCCCCATGGAGACGTGGTTCATCAT	pB2GW7_mod
HaAySy12_GBSN_R	ACCGCGGTGGCGGCCGCTTCATTCTTGAGCCCGAGAAGAAAC	
HaAySy14_GBSN_F	CCGGTACCGGGCCCCCCCATGATACCGGGGATTCTTGTAAACG	pB2GW7_mod
HaAySy14_GBSN_R	ACCGCGGTGGCGGCCGCTTTAGTTGAGTTCGCTTCTTCTACTTAATCTG	
HaAySy16_GBSN_F	GTACCGGGCCCCCCCATGGATATCACTACACTTTCTTGTGT	pB2GW7_mod
HaAySy16_GBSN_R	GCGGTGGCGGCCGCTTTAAATTTTACGTAGAATCAAGTGAGCCCCAAATTGAG	
HaAySy17_GBSN_F	GTACCGGGCCCCCCCATGATATCAGTACTTCGATATAAAATTTACCTCAAAATGACC	pB2GW7_mod
HaAySy17_GBSN_R	GCGGTGGCGGCCGCTTCATCCCATGTAAAGTGTTTTGTCAGATAACC	
HaAySy18_GBSN_F	GTACCGGGCCCCCCCATGGAAGTGATAAGCGTGAGCAT	pB2GW7_mod
HaAySy18_GBSN_R	GCGGTGGCGGCCGCTTCAAAGCTCACTCAAAATCAATTGAGCAC	

Table S 9. Differential expression of *CYP* genes in RHA857 (group 2 vs group 1). DEA of sunflower genotype RHA857 comparing $CuCl_2$-treated samples (group 2) to control samples (group 1) as shown in Figure 10A. Listed are CYP-annotated transcripts with baseMean ≥ 50. Genes with $p_{adj} \leq 0.5$ and $l_2fc < 0$ are marked as repressed (blue), and genes with $p_{adj} \leq 0.5$ and $l_2fc > 0$ as induced (red).

gene_id	description	baseMean	l_2fc	p-value	p_{adj}
HanXRQChr03g0089091	cytochrome P450 87A3	94.4	6.36	1.29E-07	3.11E-06
HanXRQChr01g0014491	cytochrome P450 CYP94A1 family	696.6	5.62	1.32E-52	6.48E-49
HanXRQChr15g0485631	cytochrome P450 CYP82D47-like	86.3	5.34	4.77E-17	7.06E-15
HanXRQChr14g0453391	cytochrome P450	598.5	4.34	4.88E-23	1.62E-20
HanXRQChr09g0260821	cytochrome P450 84A1-like	4975.1	4.14	3.84E-37	5.50E-34
HanXRQChr16g0527151	cytochrome P450 89A2-like	62.6	3.56	1.56E-22	4.73E-20
HanXRQChr09g0272621	cytochrome P450 71A22-like	6119.0	3.00	2.95E-13	2.45E-11
HanXRQChr05g0145551	cytochrome P450 71A22-like	572.6	2.66	4.58E-10	2.00E-08
HanXRQChr05g0157381	cytochrome P450 CYP82D47-like	383.9	2.49	1.72E-09	6.68E-08
HanXRQChr05g0136041	cytochrome P450 86A1	134.7	2.20	1.20E-04	1.14E-03
HanXRQChr16g0504851	cytochrome P450 71A22-like	18342.8	2.11	7.74E-03	3.48E-02
HanXRQChr02g0040011	cytochrome P450	98.4	2.08	1.63E-05	2.08E-04
HanXRQChr09g0268211	cytochrome P450 CYP82D47-like	5667.6	2.03	5.43E-07	1.09E-05
HanXRQChr13g0416271	cytochrome P450 CYP82D47-like	79.8	1.86	4.68E-02	1.39E-01
HanXRQChr02g0040121	cytochrome P450 81E8-like	1070.5	1.85	2.31E-05	2.82E-04
HanXRQChr05g0161391	cytochrome P450 93A3-like	68.5	1.69	1.72E-05	2.18E-04
HanXRQChr12g0380411	cytochrome P450 98A2	1650.2	1.62	7.34E-10	3.07E-08
HanXRQChr04g0106751	cytochrome P450 93A3-like	689.7	1.60	6.17E-04	4.50E-03
HanXRQChr09g0252641	cytochrome P450 CYP82D47-like	152.3	1.54	1.42E-02	5.62E-02
HanXRQChr09g0269921	cytochrome P450 83B1-like	374.6	1.47	2.78E-03	1.53E-02
HanXRQChr08g0216211	cytochrome P450 86B1-like	547.1	1.45	1.62E-01	3.41E-01
HanXRQChr04g0118611	cytochrome P450 710A1-like	498.1	1.44	4.24E-21	1.00E-18
HanXRQChr16g0527111	cytochrome P450 89A2-like	95.8	1.41	8.77E-07	1.67E-05
HanXRQChr11g0351431	cytochrome P450 94C1-like	57.9	1.36	1.62E-03	9.92E-03
HanXRQChr17g0541311	cytochrome P450 CYP72A219-like	5431.7	1.27	1.88E-09	7.24E-08
HanXRQChr09g0269961	cytochrome P450 83B1-like	337.1	1.20	1.21E-02	4.95E-02
HanXRQChr13g0399951	cytochrome P450 76A2-like	4784.3	1.16	1.45E-02	5.71E-02
HanXRQChr05g0132541	cytochrome P450 CYP72A219-like	2656.3	1.15	1.85E-03	1.10E-02
HanXRQChr03g0072731	cytochrome P450 CYP72A219-like	2032.6	1.15	3.93E-08	1.09E-06
HanXRQChr17g0540991	cytochrome P450 CYP72A219-like	1107.6	1.13	1.68E-03	1.02E-02
HanXRQChr03g0072721	cytochrome P450 CYP72A219-like	402.4	1.03	3.23E-11	1.78E-09
HanXRQChr05g0142991	cytochrome P450 reductase	4189.6	0.91	7.06E-08	1.83E-06
HanXRQChr09g0269761	cytochrome P450 83B1-like	424.0	0.89	5.05E-04	3.80E-03
HanXRQChr12g0367531	cytochrome P450 CYP72A219-like	2167.5	0.87	9.01E-04	6.13E-03
HanXRQChr06g0170831	cytochrome P450 CYP72A219-like	1625.8	0.84	6.39E-04	4.63E-03
HanXRQChr04g0128391	cytochrome P450 82C4, isoform 2	581.3	0.83	3.14E-06	5.04E-05
HanXRQChr09g0268181	cytochrome P450 CYP82D47-like	6745.9	0.77	3.22E-02	1.05E-01
HanXRQChr03g0093261	cytochrome P450	527.1	0.74	7.37E-06	1.05E-04
HanXRQChr12g0367521	cytochrome P450 CYP72A219-like	136.6	0.70	4.40E-04	3.39E-03
HanXRQChr16g0527101	cytochrome P450 89A2-like	53.8	0.70	2.21E-01	4.22E-01
HanXRQChr16g0530291	cytochrome P450 90B1	629.6	0.61	2.28E-01	4.31E-01
HanXRQChr14g0461901	cytochrome P450 704C1-like	2429.7	0.60	1.85E-02	6.90E-02
HanXRQChr04g0101261	cytochrome P450 71A6-like	386.9	0.53	2.59E-01	4.68E-01
HanXRQChr15g0496251	cytochrome P450 90A1	1626.8	0.52	2.63E-02	9.04E-02
HanXRQChr08g0223031	cytochrome P450 714A1-like	67.6	0.52	2.02E-01	3.96E-01
HanXRQChr09g0254451	cytochrome P450 reductase	7834.6	0.52	4.44E-04	3.42E-03
HanXRQChr09g0244761	cytochrome P450 reductase	4689.3	0.50	7.77E-04	5.44E-03
HanXRQChr16g0506081	cytochrome P450 82C4, isoform 2	80.7	0.49	1.04E-01	2.49E-01
HanXRQChr05g0131711	cytochrome P450 94A1-like	387.4	0.49	3.63E-03	1.90E-02
HanXRQChr07g0204401	cytochrome P450 CYP72A219-like	9669.5	0.41	8.58E-02	2.17E-01
HanXRQChr02g0040131	cytochrome P450 81E8-like	6415.8	0.40	1.67E-01	3.48E-01
HanXRQChr07g0204371	cytochrome P450 CYP72A219-like	70.9	0.35	2.04E-01	4.00E-01
HanXRQChr13g0423061	cytochrome P450	312.6	0.30	2.93E-02	9.83E-02
HanXRQChr03g0086101	cytochrome P450 CYP82D47-like	2146.3	0.22	1.65E-01	3.45E-01
HanXRQChr01g0025791	cytochrome P450 97B2, chloroplastic	334.2	-0.17	1.48E-01	3.19E-01
HanXRQChr04g0105501	cytochrome P450 734A1-like	215.0	-0.34	2.47E-02	8.64E-02
HanXRQChr17g0541331	cytochrome P450 CYP72A219-like	344.8	-0.45	2.00E-02	7.32E-02
HanXRQChr17g0541341	cytochrome P450 family	294.9	-0.50	5.18E-03	2.54E-02
HanXRQChr16g0527081	cytochrome P450 CYP749A22-like	136.3	-0.56	3.53E-03	1.86E-02
HanXRQChr12g0367391	cytochrome P450 CYP72A219-like	628.9	-0.59	4.38E-02	1.32E-01
HanXRQChr16g0527091	cytochrome P450 89A2-like	357.9	-0.68	2.34E-03	1.33E-02
HanXRQChr16g0527161	cytochrome P450 89A2-like	743.0	-0.71	2.41E-02	8.48E-02
HanXRQChr03g0071571	cytochrome P450,	517.8	-0.71	1.69E-01	3.51E-01
HanXRQChr16g0505931	cytochrome P450 87A3	92.8	-0.71	4.16E-02	1.27E-01
HanXRQChr04g0101921	cytochrome P450 71A6-like	145.5	-0.82	1.25E-01	2.84E-01
HanXRQChr07g0206621	cytochrome P450 704C1-like	1032.3	-0.86	1.35E-02	5.40E-02
HanXRQChr16g0527141	cytochrome P450 89A2-like	203.0	-0.86	3.80E-02	1.19E-01
HanXRQChr05g0142791	cytochrome P450 734A1	126.4	-0.86	2.10E-03	1.22E-02
HanXRQChr08g0231441	cytochrome P450	346.7	-0.98	3.63E-03	1.90E-02
HanXRQChr08g0228731	cytochrome P450	128.4	-1.05	3.52E-04	2.83E-03
HanXRQChr16g0527061	cytochrome P450 CYP749A22-like	92.8	-1.08	4.14E-04	3.23E-03
HanXRQChr03g0084371	cytochrome P450 87A3	80.4	-1.10	1.43E-03	8.97E-03
HanXRQChr16g0502491	cytochrome P450 78A5	303.3	-1.18	8.43E-03	3.72E-02
HanXRQChr17g0546501	cytochrome P450 85A	61.5	-1.24	6.83E-03	3.15E-02
HanXRQChr07g0207181	cytochrome P450 711A1	105.0	-1.39	7.11E-04	5.05E-03
HanXRQChr16g0522911	cytochrome P450	5079.0	-1.51	9.56E-04	6.43E-03
HanXRQChr16g0523711	cytochrome P450	4013.4	-1.81	2.68E-04	2.25E-03
HanXRQChr04g0101901	cytochrome P450 71A6-like	247.8	-1.83	2.14E-06	3.64E-05
HanXRQChr15g0471161	cytochrome P450 716B1-like	58.5	-2.12	1.45E-02	5.73E-02
HanXRQChr11g0325721	cytochrome P450 84A1-like	195.1	-2.14	3.08E-06	4.96E-05
HanXRQChr04g0120371	cytochrome P450 78A3p family	147.1	-2.56	2.43E-06	4.04E-05
HanXRQChr06g0164821	cytochrome P450,	910.3	-3.20	8.39E-04	5.79E-03

Table S 10. Differential expression of *CYP* genes in SF_170 (group 4 vs group 3). DEA of sunflower genotype SF_170 comparing $CuCl_2$-treated samples (group 4) to control samples (group 3) as shown in Figure 10B. Listed are CYP-annotated transcripts with baseMean ≥ 50. Genes with $p_{adj} \leq 0.5$ and $l_2fc < 0$ are marked as repressed (blue), and genes with $p_{adj} \leq 0.5$ and $l_2fc > 0$ as induced (red).

gene_id	description	baseMean	$l_2$fc	p-value	p_{adj}
HanXRQChr15g0485631	cytochrome P450 CYP82D47-like	86.30	4.22	9.37E-11	9.58E-09
HanXRQChr04g0106751	cytochrome P450 93A3-like	689.69	3.99	1.43E-17	4.24E-15
HanXRQChr14g0453391	cytochrome P450	598.55	3.17	6.72E-13	1.04E-10
HanXRQChr09g0252641	cytochrome P450 CYP82D47-like	152.34	2.98	4.93E-06	1.48E-04
HanXRQChr13g0416271	cytochrome P450 CYP82D47-like	79.84	2.93	2.96E-03	2.42E-02
HanXRQChr17g0540991	cytochrome P450 CYP72A219-like	1107.59	2.72	2.35E-13	3.96E-11
HanXRQChr03g0089091	cytochrome P450 87A3	94.38	2.64	9.24E-02	2.60E-01
HanXRQChr09g0272621	cytochrome P450 71A22-like	6118.97	2.59	3.76E-10	3.54E-08
HanXRQChr09g0269961	cytochrome P450 83B1-like	337.08	2.52	1.64E-07	7.77E-06
HanXRQChr05g0136041	cytochrome P450 86A1	134.67	2.42	2.15E-05	5.02E-04
HanXRQChr01g0014491	cytochrome P450 CYP94A1 family	696.62	2.37	5.81E-10	5.13E-08
HanXRQChr16g0527111	cytochrome P450 89A2-like	95.82	2.34	7.81E-02	2.33E-01
HanXRQChr09g0260821	cytochrome P450 84A1-like	4975.06	2.19	1.68E-11	1.95E-09
HanXRQChr16g0504851	cytochrome P450 71A22-like	18342.80	2.16	6.44E-03	4.28E-02
HanXRQChr16g0527101	cytochrome P450 89A2-like	53.78	2.00	6.31E-04	7.56E-03
HanXRQChr02g0040121	cytochrome P450 81E8-like	1070.50	1.90	1.39E-05	3.50E-04
HanXRQChr13g0399951	cytochrome P450 76A2-like	4784.32	1.68	3.80E-04	5.07E-03
HanXRQChr02g0040011	cytochrome P450	98.40	1.50	2.00E-03	1.80E-02
HanXRQChr04g0118611	cytochrome P450 710A1-like	498.11	1.23	4.24E-15	9.00E-13
HanXRQChr05g0132541	cytochrome P450 CYP72A219-like	2656.29	0.98	8.04E-03	5.04E-02
HanXRQChr02g0035401	cytochrome P450 71A6-like	174.19	0.91	3.69E-02	1.41E-01
HanXRQChr05g0142991	cytochrome P450 reductase	4189.60	0.86	3.87E-07	1.66E-05
HanXRQChr09g0268211	cytochrome P450 CYP82D47-like	5667.58	0.81	4.70E-02	1.66E-01
HanXRQChr03g0084371	cytochrome P450 87A3	80.40	0.74	1.76E-02	8.67E-02
HanXRQChr03g0072731	cytochrome P450 CYP72A219-like	2032.55	0.57	6.98E-03	4.54E-02
HanXRQChr05g0161391	cytochrome P450 93A3-like	68.46	0.54	1.55E-01	3.58E-01
HanXRQChr12g0380411	cytochrome P450 98A2	1650.17	0.50	5.71E-02	1.89E-01
HanXRQChr17g0541311	cytochrome P450 CYP72A219-like	5431.75	0.50	1.86E-02	9.00E-02
HanXRQChr05g0157381	cytochrome P450 CYP82D47-like	383.85	0.46	1.15E-01	2.98E-01
HanXRQChr07g0204401	cytochrome P450 CYP72A219-like	9669.51	0.42	7.64E-02	2.29E-01
HanXRQChr16g0527141	cytochrome P450 89A2-like	203.00	0.38	5.68E-02	1.88E-01
HanXRQChr09g0254451	cytochrome P450 reductase	7834.64	0.30	4.12E-02	1.52E-01
HanXRQChr03g0086101	cytochrome P450 CYP82D47-like	2146.32	0.25	1.16E-01	2.99E-01
HanXRQChr01g0025791	cytochrome P450 97B2, chloroplastic	334.20	-0.13	2.64E-01	4.96E-01
HanXRQChr16g0527081	cytochrome P450 CYP749A22-like	136.30	-0.25	2.40E-01	4.68E-01
HanXRQChr12g0367391	cytochrome P450 CYP72A219-like	628.87	-0.34	1.97E-01	4.15E-01
HanXRQChr17g0547051	cytochrome P450 CYP82D47-like	2018.05	-0.36	1.63E-01	3.70E-01
HanXRQChr16g0506081	Cytochrome P450 82C4, isoform 2	80.68	-0.39	2.26E-01	4.52E-01
HanXRQChr16g0527091	cytochrome P450 89A2-like	357.90	-0.41	6.32E-02	2.02E-01
HanXRQChr10g0312591	cytochrome P450 71A1-like	7468.76	-0.47	3.14E-02	1.27E-01
HanXRQChr12g0367531	cytochrome P450 CYP72A219-like	2167.45	-0.47	7.09E-02	2.18E-01
HanXRQChr04g0101261	cytochrome P450 71A6-like	386.92	-0.56	2.32E-01	4.60E-01
HanXRQChr09g0269921	cytochrome P450 83B1-like	374.59	-0.57	2.48E-01	4.79E-01
HanXRQChr16g0527061	cytochrome P450 CYP749A22-like	92.83	-0.59	4.46E-02	1.60E-01
HanXRQChr04g0105501	cytochrome P450 734A1-like	215.00	-0.61	3.85E-04	5.13E-03
HanXRQChr05g0142791	cytochrome P450 734A1	126.43	-0.62	2.29E-02	1.03E-01
HanXRQChr08g0228731	Cytochrome P450	128.45	-0.74	1.60E-02	8.14E-02
HanXRQChr03g0072711	cytochrome P450 CYP72A219	863.42	-0.75	4.50E-04	5.79E-03
HanXRQChr07g0207181	cytochrome P450 711A1	105.05	-0.84	2.88E-02	1.20E-01
HanXRQChr17g0546501	Cytochrome P450 85A	61.50	-0.85	1.53E-03	1.48E-02
HanXRQChr14g0437471	cytochrome P450 71A4-like	125.93	-0.86	8.98E-02	2.55E-01
HanXRQChr16g0505931	Cytochrome P450 87A3	92.84	-0.88	1.25E-02	6.90E-02
HanXRQChr04g0101921	cytochrome P450 71A6-like	145.51	-1.17	3.00E-02	1.23E-01
HanXRQChr08g0231441	cytochrome P450	346.74	-1.19	4.25E-04	5.53E-03
HanXRQChr11g0325721	cytochrome P450 84A1-like	195.06	-1.33	3.89E-03	2.97E-02
HanXRQChr08g0232631	cytochrome P450 82G1-like	3169.87	-1.35	1.02E-02	5.96E-02
HanXRQChr16g0527161	cytochrome P450 89A2-like	742.98	-1.36	1.59E-05	3.94E-04
HanXRQChr16g0522911	cytochrome P450	5079.04	-1.61	4.48E-04	5.78E-03
HanXRQChr16g0523711	cytochrome P450	4013.43	-1.78	3.40E-04	4.66E-03
HanXRQChr04g0101901	cytochrome P450 71A6-like	247.84	-1.83	1.35E-06	4.94E-05
HanXRQChr07g0206621	cytochrome P450 704C1-like	1032.35	-1.90	6.10E-08	3.27E-06
HanXRQChr16g0502491	cytochrome P450 78A5	303.32	-2.38	7.48E-08	3.91E-06
HanXRQChr15g0471161	cytochrome P450 716B1-like	58.53	-2.75	1.89E-03	1.72E-02
HanXRQChr04g0120371	cytochrome P450 78A3p family	147.15	-2.80	2.21E-07	1.00E-05
HanXRQChr02g0051171	cytochrome P450 78A5-like	91.64	-2.97	7.82E-04	8.86E-03
HanXRQChr06g0164821	Cytochrome P450,	910.26	-4.44	3.78E-06	1.18E-04

Table S 11. Differential expression of *CYP* genes between stressed SF_170 and stressed RHA857 (group 4 vs group 2). DEA of sunflower genotypes SF_170 and RHA857 comparing $CuCl_2$-treated samples of SF_170 (group 4) to $CuCl_2$-treated samples of RHA857 (group 2), as shown in Figure 10C. Listed are CYP-annotated transcripts with baseMean ≥ 50. Genes with $p_{adj} \leq 0.5$ and $l_2fc < 0$ (higher in RHA857) are colored blue; genes with $p_{adj} \leq 0.5$ and $l_2fc > 0$ (higher in SF_170) are colored red.

gene_id	description	baseMean	$l_2$fc	p-value	p_{adj}
HanXRQChr02g0035401	cytochrome P450 71A6-like	174.2	11.43	8.39E-20	2.13E-18
HanXRQChr16g0508081	cytochrome P450 CYP82D47-like	188.2	9.99	8.48E-15	1.21E-13
HanXRQChr08g0216211	cytochrome P450 86B1-like	547.1	8.84	3.97E-47	5.39E-45
HanXRQChr16g0527141	cytochrome P450 89A2-like	203.0	5.97	4.82E-65	1.32E-62
HanXRQChr12g0367391	cytochrome P450 CYP72A219-like	628.9	4.25	4.44E-52	7.38E-50
HanXRQChr05g0157381	cytochrome P450 CYP82D47-like	383.9	4.11	5.85E-40	5.64E-38
HanXRQChr17g0546501	Cytochrome P450 85A	61.5	3.78	6.18E-20	1.59E-18
HanXRQChr09g0268221	cytochrome P450 CYP82D47-like	1567.3	3.23	5.78E-08	3.54E-07
HanXRQChr03g0084371	cytochrome P450 87A3	80.4	2.42	4.23E-13	4.92E-12
HanXRQChr04g0106751	cytochrome P450 93A3-like	689.7	2.16	2.99E-06	1.42E-05
HanXRQChr07g0207181	cytochrome P450 711A1	105.0	2.06	4.12E-07	2.23E-06
HanXRQChr16g0530291	cytochrome P450 90B1	629.6	1.93	1.39E-04	4.94E-04
HanXRQChr03g0071571	cytochrome P450,	517.8	1.68	1.12E-03	3.26E-03
HanXRQChr10g0312591	cytochrome P450 71A1-like	7468.8	1.40	1.30E-10	1.13E-09
HanXRQChr17g0541311	cytochrome P450 CYP72A219-like	5431.7	1.24	4.64E-09	3.29E-08
HanXRQChr01g0007601	cytochrome P450 98A2-like	8801.6	1.17	2.71E-05	1.10E-04
HanXRQChr02g0035481	cytochrome P450 71A4-like	64.2	1.06	6.84E-02	1.22E-01
HanXRQChr04g0101901	cytochrome P450 71A6-like	247.8	1.02	8.33E-03	1.97E-02
HanXRQChr16g0502491	cytochrome P450 78A5	303.3	1.01	2.46E-02	5.07E-02
HanXRQChr16g0504851	cytochrome P450 71A22-like	18342.8	1.00	2.09E-01	3.05E-01
HanXRQChr16g0527061	cytochrome P450 CYP749A22-like	92.8	0.99	1.20E-03	3.49E-03
HanXRQChr05g0136041	cytochrome P450 86A1	134.7	0.80	1.52E-01	2.36E-01
HanXRQChr05g0142791	cytochrome P450 734A1	126.4	0.76	6.90E-03	1.67E-02
HanXRQChr07g0190211	cytochrome P450 CYP72A219-like	13178.9	0.76	3.49E-02	6.85E-02
HanXRQChr15g0496251	cytochrome P450 90A1	1626.8	0.76	1.19E-03	3.46E-03
HanXRQChr14g0437471	cytochrome P450 71A4-like	125.9	0.75	1.41E-01	2.22E-01
HanXRQChr16g0527091	cytochrome P450 89A2-like	357.9	0.68	2.24E-03	6.13E-03
HanXRQChr09g0269961	cytochrome P450 83B1-like	337.1	0.66	1.64E-01	2.51E-01
HanXRQChr16g0523711	cytochrome P450	4013.4	0.65	1.92E-01	2.86E-01
HanXRQChr13g0399951	cytochrome P450 76A2-like	4784.3	0.59	2.15E-01	3.11E-01
HanXRQChr08g0223031	cytochrome P450 714A1-like	67.6	0.58	1.44E-01	2.26E-01
HanXRQChr09g0254451	cytochrome P450 reductase	7834.6	0.20	1.64E-01	2.52E-01
HanXRQChr13g0423061	Cytochrome P450	312.6	-0.14	3.14E-01	4.21E-01
HanXRQChr05g0142991	cytochrome P450 reductase	4189.6	-0.18	2.98E-01	4.04E-01
HanXRQChr03g0093261	Cytochrome P450	527.1	-0.24	1.44E-01	2.26E-01
HanXRQChr07g0204401	cytochrome P450 CYP72A219-like	9669.5	-0.24	3.08E-01	4.15E-01
HanXRQChr03g0072731	cytochrome P450 CYP72A219-like	2032.6	-0.41	5.04E-02	9.38E-02
HanXRQChr04g0118611	cytochrome P450 710A1-like	498.1	-0.43	3.72E-03	9.63E-03
HanXRQChr09g0269921	cytochrome P450 83B1-like	374.6	-0.45	3.64E-01	4.72E-01
HanXRQChr05g0132541	cytochrome P450 CYP72A219-like	2656.3	-0.48	1.97E-01	2.91E-01
HanXRQChr16g0527081	cytochrome P450 CYP749A22-like	136.3	-0.50	1.35E-02	3.01E-02
HanXRQChr14g0461901	cytochrome P450 704C1-like	2429.7	-0.56	2.76E-02	5.61E-02
HanXRQChr05g0131711	cytochrome P450 94A1-like	387.4	-0.59	4.54E-04	1.45E-03
HanXRQChr09g0252641	cytochrome P450 CYP82D47-like	152.3	-0.59	3.48E-01	4.56E-01
HanXRQChr08g0228731	Cytochrome P450	128.4	-0.65	3.31E-02	6.56E-02
HanXRQChr04g0101921	cytochrome P450 71A6-like	145.5	-0.75	1.66E-01	2.54E-01
HanXRQChr12g0367531	cytochrome P450 CYP72A219-like	2167.5	-0.76	3.54E-03	9.20E-03
HanXRQChr09g0244761	cytochrome P450 reductase	4689.3	-0.80	8.30E-08	4.97E-07
HanXRQChr16g0527161	cytochrome P450 89A2-like	743.0	-0.87	5.59E-03	1.39E-02
HanXRQChr15g0485631	cytochrome P450 CYP82D47-like	86.3	-1.01	6.13E-02	1.11E-01
HanXRQChr15g0471161	cytochrome P450 716B1-like	58.5	-1.03	2.50E-01	3.51E-01
HanXRQChr04g0128391	Cytochrome P450 82C4, isoform 2	581.3	-1.08	1.45E-09	1.10E-08
HanXRQChr04g0105501	cytochrome P450 734A1-like	215.0	-1.12	1.06E-11	1.05E-10
HanXRQChr04g0101261	cytochrome P450 71A6-like	386.9	-1.13	1.63E-02	3.56E-02
HanXRQChr16g0506081	Cytochrome P450 82C4, isoform 2	80.7	-1.14	2.61E-04	8.82E-04
HanXRQChr14g0453391	cytochrome P450	598.5	-1.16	7.16E-03	1.73E-02
HanXRQChr07g0206621	cytochrome P450 704C1-like	1032.3	-1.16	9.70E-04	2.89E-03
HanXRQChr06g0164821	Cytochrome P450,	910.3	-1.16	2.26E-01	3.25E-01
HanXRQChr16g0527151	cytochrome P450 89A2-like	62.6	-1.20	3.77E-05	1.49E-04
HanXRQChr09g0268641	cytochrome P450 CYP82D47-like	1038.1	-1.25	3.08E-03	8.14E-03
HanXRQChr03g0072721	cytochrome P450 CYP72A219-like	402.4	-1.25	8.77E-16	1.43E-14
HanXRQChr09g0260821	cytochrome P450 84A1-like	4975.1	-1.42	1.13E-05	4.90E-05
HanXRQChr13g0416271	cytochrome P450 CYP82D47-like	79.8	-1.70	6.93E-02	1.23E-01
HanXRQChr17g0547051	cytochrome P450 CYP82D47-like	2018.0	-1.70	6.54E-11	5.91E-10
HanXRQChr17g0540991	cytochrome P450 CYP72A219-like	1107.6	-2.04	1.49E-08	9.80E-08
HanXRQChr06g0170831	cytochrome P450 CYP72A219-like	1625.8	-2.12	9.68E-18	1.96E-16
HanXRQChr09g0269761	cytochrome P450 83B1-like	424.0	-2.23	1.21E-17	2.42E-16
HanXRQChr09g0272621	cytochrome P450 71A22-like	6119.0	-2.60	2.53E-10	2.13E-09
HanXRQChr11g0351431	cytochrome P450 94C1-like	57.9	-3.00	6.69E-11	6.04E-10
HanXRQChr01g0014491	cytochrome P450 CYP94A1 family	696.6	-3.60	2.88E-24	1.10E-22
HanXRQChr05g0145551	cytochrome P450 71A22-like	572.6	-3.82	6.57E-19	1.52E-17
HanXRQChr08g0222171	cytochrome P450 704C1-like	163.8	-5.62	9.13E-44	1.07E-41
HanXRQChr03g0089091	cytochrome P450 87A3	94.4	-6.21	2.12E-07	1.20E-06
HanXRQChr16g0527111	cytochrome P450 89A2-like	95.8	-7.01	2.95E-30	1.69E-28
HanXRQChr17g0541331	cytochrome P450 CYP72A219-like	344.8	-7.07	2.94E-60	6.61E-58
HanXRQChr17g0541341	cytochrome P450 family	294.9	-7.63	5.57E-45	6.88E-43
HanXRQChr12g0367521	cytochrome P450 CYP72A219-like	136.6	-8.51	2.45E-23	8.66E-22
HanXRQChr07g0204371	cytochrome P450 CYP72A219-like	70.9	-8.89	1.90E-13	2.30E-12
HanXRQChr07g0196331	cytochrome P450 82C4-like	319.1	-10.78	5.83E-18	1.22E-16